SURFACE ENHANCED RAMAN SCATTERING OF MERCAPTOPYRIDINE AND PYRAZINAMIDE AND THE FABRICATION OF A METAL-ION SENSOR

by

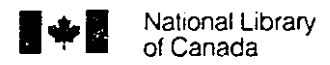
Jean A. Baldwin

A thesis submitted to the Faculty of Graduate Studies and Research in partial fulfillment of the requirements of the degree of

Doctor of Philosophy

July 1996
Department of Chemistry
McGill University
Montreal, Quebec, Canada

©Jean A. Baldwin, 1996



Acquisitions and Bibliographic Services Branch

395 Wellington Street Ottawa, Ontario K1A 0N4 Bibliothèque nationale du Canada

Direction des acquisitions et des services bibliographiques

395, rue Wellington Ottawa (Ontario) K1A 0N4

Your life Votre reférence

Our tile Notre reference

The author has granted an irrevocable non-exclusive licence allowing the National Library of Canada to reproduce, loan, distribute or sell copies of his/her thesis by any means and in any form or format, making this thesis available to interested persons.

L'auteur a accordé une licence irrévocable et non exclusive Bibliothèque permettant à la dи Canada nationale reproduire, prêter, distribuer ou vendre des copies de sa thèse de quelque manière et sous quelque forme que ce soit pour mettre des exemplaires de cette disposition thèse la des personnes intéressées.

The author retains ownership of the copyright in his/her thesis. Neither the thesis nor substantial extracts from it may be printed or otherwise reproduced without his/her permission. L'auteur conserve la propriété du droit d'auteur qui protège sa thèse. Ni la thèse ni des extraits substantiels de celle-ci ne doivent être imprimés ou autrement reproduits sans son autorisation.

ISBN 0-612-19707-7

Canadä

Dedicated to my parents

Margaret and Eugene Baldwin

for their unconditional support

go a mile maith agat

ABSTRACT

Surface Enhanced Raman Scattering (SERS) is a process by which molecules near certain special metal surfaces exhibit Raman scattering that is measurably more intense than is the normal Raman scattering exhibited by molecules in the absence of the surface. The majority of SERS-active metal substrates, such as roughened electrodes and colloidal sols, are fabricated from coinage metals, Au, Ag and Cu. The principal subject of this thesis is the surface enhanced Raman spectroscopic study of the adsorbates; pyrazinamide, 2- and 4mercaptopyridine. A range of SERS-active Ag substrates was used, viz., Ag colloids, metal liquid-like films (MELLFs), and roughened Ag electrodes. In addition, an original technique that encompasses both SERS and waveguide Raman spectroscopy (WRS), known as integrated optics, evanescent wave, surface enhanced Raman spectroscopy (IOEW-SERS) was developed. For this technique, a waveguide heterostructure was fabricated on nano-scale dimensions by self-assembly of silver colloidal particles on thin glass slides. The unique optical behaviors of both SERS and WRS systems are combined such that optically guided light propagates in the thin film with an evanescent wave and couples with surface plasmon modes of metal particles. A comparative SERS study of 2and 4-mercaptopyridine (MPy) was undertaken using all of the above methods. The purpose of this comparison was to determine the similarities between IOEW-SERS and other Ag SERS-active systems. These studies were extended by using a 4-MPy modified SERS-active optical waveguide as a thin film chemical sensor. Intermolecular interactions between probe ions, Cu2+ and H+, with 4-MPy were observed by vibrational perturbations to the IOEW-SERS spectrum. X-ray photoelectron spectroscopy (XPS) allowed a layer-by-layer examination of the 4-MPy derivatized waveguide from the substrate to the Cu²⁺ ion. A potential dependent SERS study of 4-MPy modified Ag electrodes, including the interaction with Cu2+ ions, was undertaken to complement the IOEW-SERS experiment. Additional studies describing the preparation and SERS of MELLFs of pyrazinamide, and 2- and 4-MPy were undertaken. The deposited films were characterized by Transmission Electron Microscopy (TEM) and Surface Plasmon Absorption (SPA).

RÉSUMÉ

La diffusion Raman de type Surface Enhanced (SERS) est un processus selon lequel les molécules situées à proximité de surfaces métalliques spéciales présentent une diffusion Raman qui est plus intense que la diffusion Raman normale manifestée par les molécules en absence de telles surfaces. La majorité des substrats métalliques actifs en SERS, tels les électrodes dépolies et les solutions colloïdales, sont fabriqués à partir de métaux de frappe tels l'or, l'argent et le cuivre. Le sujet principal de cette thèse est l'étude spectroscopique SERS d'adsorbats: pyrazinamide, 2- et 4mercaptopyridine. Une gamme de substrats d'Ag actifs en SERS a été utilisée, comme par exemple des colloïdes d'Ag, des films de métaux à caractère liquide (MELLFs), ainsi que des électrodes d'Ag dépolies. De plus, une technique originale qui comprend à la fois les spectroscopies SERS et Raman de guide d'ondes (WRS) a été développée et est connue sous le nom de SERS d'onde évanescente à optique intégrée (IOEW-SERS). Pour cette technique, une hétérostructure de guide d'ondes a été fabriquée à une échelle nanoscopique par l'auto-assemblage de particules d'argent colloïdales sur de fines lamelles de verre. Les comportements optiques uniques des systèmes SERS et WRS sont combinés de sorte que la lumière guidée par optique puisse se propager dans la couche mince avec une onde évanescente and puisse alors se coupler au modes plasmons de surface des particules métalliques. Une étude SERS comparative du 2- et du 4- mercatopyridine (Mpy) a été entreprise en utilisant toutes les méthodes ci-haut. La raison-d'être de cette comparaison était de déterminer les similitudes entre les systèmes IOEW-SERS et d'autres systèmes d'Ag actifs en SERS. Ces études furent étendues en utilisant un guide d'ondes optique actif en SERS de 4-Mpy modifié comme senseur chimique en couche mince. Les interactions intermoléculaires entre les ions sondes, Cu²⁺ et H⁺ et le 4-Mpy ont été observées par des perturbation vibrationnelles au spectre IOEW-SERS. La spectroscopie photoélectronique des rayons-X (XPS) a permis une interprétation couche par couche du guide d'ondes de 4-MPy dérivé du substrat jusqu'à l'ion Cu²⁺. Une étude SERS, dépendante du potentiel, d'électrodes d'Ag modifiée par 4-MPy, incluant l'interaction avec les ions Cu²⁺ a été entreprise comme complément à l'expérience IOEW-SERS. Des études additionnelles décrivant la préparation ainsi que la SERS de MELLFs des molécules de pyrazinamide, 2- et 4-MPy, ont été entreprises. Les films déposés ont été caractérisés par microscopie de transmission d'électron (TEM) et par adsorption de plasmon de surface (SPA).

FOREWORD

The thesis was prepared in accordance with article B2 of the Guidelines

Concerning Thesis Preparation of McGill University. This article reads as follows:

- "Candidates have the option of including, as part of the thesis, the text of a paper(s) submitted or to be submitted for publication, or the clearly-duplicated text of a published paper(s). These texts must be bound as an integral part of the thesis.
- -If this option is chosen, connecting texts that provide logical bridges between the papers are mandatory. The thesis must be written in such a way that it is more than a mere collection of manuscripts; in other words, results of a series of papers must be integrated.
- -The thesis must still conform to all other requirements of the "Guidelines for Thesis Preparation". The thesis must include: A Table of Contents, an abstract in English and French, an introduction which clearly states the rationale and objectives of the study, a comprehensive review of the literature, a final conclusion and summary, and a thorough bibliography or reference list.
- -Additional material must be provided where appropriate (e.g. in appendices) and in sufficient detail to allow a clear and precise judgement to be made of the importance and originality of the research reported in the thesis.
- -In the case of manuscripts co-authored by the candidate and others, the candidate is required to make an explicit statement in the thesis as to who contributed to such work and to what extent. Supervisors must attest to the accuracy of such statements at the doctoral oral defense. Since the task of the examiners is made more difficult in these cases, it is in the candidate's interest to make perfectly clear the responsabilities of all the authors of the co-authored papers."

This thesis consists of six chapters. Chapter 1 describes the field of research pertaining to the present work. Chapters 2, 3, 4, 5 present the principle results of the research conducted, written in publication format. Chapter 6 contains general conclusions, contributions to knowledge and suggestions for future work.

The following are manuscripts written by the author and were used in the preparation of this thesis. Manuscripts #1, #2, #3 and #4 are included in Chapters 2, 3, 4 and 5, respectively. Following normal procedure, the papers have been either submitted or will be submitted for publication in scientific journals. A list of the papers is given below:

- 1. Jean A. Baldwin, Blanka Vickova, Ian S. Butler and Mark P. Andrews. "Surface Enhanced Raman Scattering of Mercaptopyridines and Pyrazinamide from Glass-Deposited Silver Metal Liquid-like Films." Submitted for publication in Langmuir.
- 2. Jean A. Baldwin, Mark P. Andrews, Wenbo Xu and Ian S. Butler. "Integrated Optics, Evanescent Wave, Surface-Enhanced Raman Spectra of 4,4'-Bipyridine". To be submitted for publication in *Journal of Physical Chemistry*.
- 3. Jean A. Baldwin, Norbert Schühler, Mark P. Andrews and Ian S. Butler. "Surface Enhanced Raman Scattering of Mercaptopyridines and the Fabrication of a Metal-Ion Chemical Sensor based on Integrated Optics, Evanescent Wave, Surface Enhanced Raman Scattering (IOEW-SERS)". Accepted for publication in Langmuir, July 1996.
- 4. Jean A. Baldwin, Alexander Brolo, Ian S. Butler and Mark P. Andrews. "Surface Enhanced Raman Scattering of 4-Mercaptopyridine on Silver Electrodes and the Interaction with Copper (II) ions. Submitted for publication in *Langmuir*

All of the above papers include the research co-directors, Dr. Ian. S. Butler and Dr. Mark P. Andrews as co-authors. Chapter 2 includes Dr. Blanka Vlckova as co-author, (Dept. of Physical and Macromolecular Chemistry, Charles University, Prague, Czech Republic) who co-wrote this paper, recognizing her expertise in MELLFs and for collecting some of the SPA and optical micrographs included in this Chapter. Chapter 3 includes Wenbo Xu as co-author, (McGill University, Montreal, Canada) who initially developed the IOEW-SERS technique and waveguide fabrication. Chapter 4 includes Dr. Norburt Schühler as co-author, (McGill University, Montreal, Canada) recognizing his advice on the preparation of samples for XPS and for collecting the XPS data used in this study. Chapter 5 includes Alexander Brolo as co-author, (Guelph-Waterloo Center for Graduate

Work in Chemistry, University of Waterloo, Waterloo, Canada) who assisted in the spectroelectrochemical experiments used in this Chapter. Other than the supervisors who gave advice and direction and the aforementioned contribution to the chapters, all of the work presented in this dissertation was performed by the author.

æ

ACKNOWLEDGEMENTS

I would like to thank my supervisors, Dr. Ian S. Butler and Mark P. Andrews for their guidance and support throughout the course of this work.

I would like to express my deepest gratitude to Dr. Stephane Brienne for proofreading this thesis. His time and interest in my work were indispensable.

I would also like to thank:

Dr. Tanya Kanigan for assisting me with the Raman instrumentation and for showing me the wonders of waveguiding;

Laura Deakin for proofreading this thesis and the great chats;

Antonella Badia and Shanti Singh for their assistance in collecting TEM data;

Dr. Ross Markwell and Andrew Vreugdenhil for keeping the computers alive and undoing all the wrong doing;

Messrs. Micheal Boulay, Rick Rossi and A. Kluck for their technical expertise;

Drs. Hongqi Li and Steven Barnett for their friendship and assistance in the early years of my work;

Réenee Sharon for her kindness and tireless support;

Henry Lin Soo from the PSE Library for providing a great service;

James for his wonderful nerve tonic;

Mark Wall for his love and support;

All my friends, Jason, Louise, Shaune, Nuna, Fred, Tara, Emmanuel, Louie, Karen, Michelle, Daphne, James, Phillip, Dan, Mary Jane, Dave, Claudine, SPAM and everybody else in the Otto Maass Chemistry and Pulp and Paper buildings who have supported me through the ups and downs and made my graduate years very memorable.

TABLE OF CONTENTS

R É S U M É			
ACI	KNOWLE	DGEMENTS	vi
LIS	T OF SY	ONTENTSMBOLS AND ABBREVIATIONS	vıı
LIST	Γ OF TAI	BLES	xiii
LIS	r of fig	URES	VIXXIV
~~~		·	
	APTER	<del>-</del>	_
	the second second second	ION	
1.1		RAMAN SCATTERING	
1.2		NCE RAMAN SCATTERING	
1.3	SURFACE	E ENHANCED RAMAN SCATTERING (SERS)	5
•	1.3.1	Surface Electromagnetic Field Enhancement (EM) Effect	6
•	1.3.2	Chemical or Charge-Transfer (CT) Enhancement Effect	8
1.4	ADSORB	ATE ORIENTATION AT METAL SURFACES	10
1.5	SURFACE	E ENHANCED RAMAN SCATTERING SYSTEMS	13
	1.5.1	Colloidal Silver Sols	13
	1.5.2	Roughened Electrodes	14
. •	1.5.2.1	Spectroelectrochemical Cell Instrumentation	16
٠.	1.5.2.2	Electrode Surface Preparation	16
ž.	1.5.3	Metal Liquid-Like Films (MELLFs)	18
	1.5.4	Integrated Optics Evanescent Waveguide	
		Surface Enhanced Raman Scattering (IOEW-SERS)	24
	1.5.4.1	Waveguide Raman Spectroscopy	24
	1.5.4.2	Coupling Mechanism	25
	1.5.4.3	Field Distribution	29
	1.5.4.4	Combining WRS and SERS	31
1.6	SELF ASS	SEMBLING MONOLAYERS (SAM)	35
		Mercaptopyridine	
1.7	AIMS AN	D STRUCTURE OF THE THESIS	37
REF			1.

CH.	APTER 2	
SUR	FACE ENHANCED RAMAN SCATTERING OF	
MEI	RCAPTOPYRIDINES AND PYRAZINAMIDE IN METAL	
LIQ	UID-LIKE FILMS (MELLFs)	44
2.1	SUMMARY	45
2.2	INTRODUCTION	46
2.3	EXPERIMENTAL	47
2.4	RESULTS AND DISCUSSION	51
	2.4.1 Ag Colloid-pza Films	51
	2.4.2 Ag Colloid-4-MPy Films	60
	2.4.3 Ag Colloid-2-MPy Films	69
2.5	CONCLUSIONS	76
	ERENCES	
CH	APTER 3	· · · · · · · · · · · · · · · · · · ·
INT	EGRATED OPTICS, EVANESCENT WAVE, SURFACE	
ENI	HANCED RAMAN SCATTERING OF 4, 4'-BIPYRIDINE	80
3.1	SUMMARY	81
3.2	INTRODUCTION	82
3.3	EXPERIMENTAL	85
3.4		91
	3.4.1 IOEW-SERS of Ag Colloid-Derivatized Waveguide	91
	3.4.2 IOEW-SERS of 4, 4'-Bipyridine Derivatized Waveguide	
3.5	CONCLUSIONS	100
REF	TERENCES	101
		}  }
CH	APTER 4	· []
SUI	RFACE ENHANCED RAMAN SCATTERING OF	
ME	RCAPTOPYRIDINES AND THE FABRICATION OF A METAL-	1
ION	N CHEMICAL SENSOR BASED ON INTEGRATED OPTICS,	;} ;}
EV.	ANESCENT WAVE, SURFACE ENHANCED RAMAN 🛒 💎 📑	ii !!
SC.	ATTERING (IOEW-SERS)	103
	SUMMARY	
	INTRODUCTION	105
12	FXPERIMENTAL	110

PAR	T 1. SERS	S STUDY of 2- and 4-MERCAPTOPYRIDINE	113
4.4	RESULT	S AND DISCUSSION	113
	4.4.1	SERS of 4-Mercaptopyridine	113
	4.4.2	SERS of 2-Mercaptopyridine	117
	4.4.3	Orientation	121
	4.4.4	Mode of Adsorption of 2- and 4-MPy on the SERS Substrate	
		Surface	125
PAR	T 2. IOEV	V-SERS STUDY OF THE SENSOR APPLICATION	129
4.5.	RESULTS	S AND DISCUSSION	129
	4.5.1	IOEW-SERS of Cu ²⁺ ion Binding	129
٠	4.5.2	IOEW-SERS of Proton Binding	133
	4.5.4	XPS ANALYSIS: RESULTS AND DISCUSSION	136
4.7	CONCLU	JSIONS	150
REF	ERENCES		152
CH	APTER	5	
SUR	RFACE E	NHANCED RAMAN SCATTERING OF 4-	
ME	RCAPTO	PYRIDINE ON SILVER ELECTRODES AND THE	
SUR	RFACE IN	NTERACTION WITH COPPER (II) IONS	155
5.1	SUMMAI	RY	156
5.2		UCTION	
5.3	EXPERIN	MENTAL	159
5.4	RESULT	S AND DISCUSSION	162
	5.4.1		162
	5.4.2	Electrochemical SERS of 4-MPy	
ر	5.4.3	Wavelength and Potential Dependence of 4-MPy	176
	5.4.4.	Immersion of a 4-MPy-Modified Ag Electrode in Aqueous	
	č	Cu(NO ₃ ) ₂ Solution	179
5.5.	CONCLU	JSIONS	
	Ĭ.	· · · · · · · · · · · · · · · · · · ·	
CH	APTER	6	
SUN	MARY.		188
		JSIONS	

6.3	SUGGESTIONS FOR FUTURE WORK	195
REF	ERENCES	19°

## LIST OF SYMBOLS AND ABBREVIATIONS

2-Mercaptopyridine 2-MPy 4-Mercaptopyridine 4-MPy pza pyrazinamide 3-MPT 3-mercaptopropyltrimethoxysilane HS(CH₂)₃Si(OCH₃)₃ **TPyP** Porphyrin RR Resonance Raman FT-Raman Fourier Transform Raman **SERS** Surface Enhanced Raman Scattering **IOEW-SERS** Integrated Optics, Evanescent Wave, Surface Enhanced Raman Scattering **MELLFs** Metal Liquid-Like Films **XPS** X-ray Photoelectron Spectroscopy TEM Transmission Electron Microscopy Scanning Electron Microscopy SEM **Electron Energy Loss Spectroscopy EELS SPA** Surface Plasmon Absorption

II.

TE

TM

UV

Transverse electric

Transverse magnetic

Ultraviolet

CT Charge Transfer

EM Electromagnetic

ORC Oxidation Reduction Cyclic

CV Cyclic Voltammetry

SCE Standard Calomel Electrode

UPD Under Potential Deposition

E_f Fermi Level

ITO Indium Tin Oxide

UHV Ultra High Vacuum

D Fractal dimensionality (D = log N/log (l), where N is the number of

generations and l is dilation factor)

## LIST OF TABLES

TABLE 2.1 Assignments and wavenumber positions (cm ⁻¹ ) for SERS and normal Raman spectra of pyrazinamide
TABLE 2.2 Assignments and wavenumber positions (cm ⁻¹ ) for SERS and normal Raman spectra of 4-mercaptopyridine65
TABLE 2.3 Assignments and wavenumber positions (cm ⁻¹ ) for SERS and normal Raman spectra of 2-mercaptopyridine71
TABLE 4.1 Assignments and wavenumber positions (cm ⁻¹ ) of normal Raman and SERS spectra for 4-mercaptopyridine
TABLE 4.2 Assignments and wavenumber positions (cm ⁻¹ ) of normal Raman and SERS spectra for 2-mercaptopyridine
TABLE 4.3 XPS binding energy shifts and FWHM (in brackets) for samples (A) - (E).
TABLE 4.4 Data from S 2p curve-fit (Figure 4.14) for samples (B) to (E)141
TABLE 5.1 Assignments and wavenumber positions (cm ⁻¹ ) of normal Raman and SERS spectra for 4-mercaptopyridine

## LIST OF FIGURES

FIGURE 1.1 Schematic representation of a room temperature Raman spectrum of CCl ₄ excited with 514.5-nm line of an argon ion laser. (Adapted from Butler, I. S. and Harrod, J. F. <i>Inorganic Chemistry: Principles and Applications</i> : Benjamin/Cummings Publ., Menlo Park, California, 1989)
FIGURE 1.2 The symmetry classes, Raman tensor components and relative enhancements of the vibrational modes of pyridine
FIGURE 1.3 Spectroelectrochemical cell used for SERS experiments
FIGURE 1.4 Cyclic voltammogram of an Ag electrode in 0.1 M KCl. A single oxidation reduction cycle (ORC) process consisting of a double potential sequence of -700 mV to +100 mV and back to -700 mV (vs.SCE) at 5 mV/s.
FIGURE 1.5 Schematic views of an interfacial MELLF (a), and interphase transfer of colloidal particles with adsorbate molecules in an organic phase (b)19
FIGURE 1.6 Photograph of a freshly prepared interfacial MELLF of 2-mercaptopyridine
FIGURE 1.7 Structural model of an interfacial MELLF. Loosely held aggregates in flooculated state
FIGURE 1.8 Schematic diagram showing the prism coupling assembly. The relation between the internal angle $\theta$ , and the external angle $\gamma$ , is $\sin \varphi = n_p \sin (\theta^* - \gamma)$ . Refractive index (n) conditions are met, i.e., n (prism) > n (film) > n (substrate) > n (air) such that the optical field is concentrated within the thin film.
FIGURE 1.9 A glass slab waveguide with prism and waveguide assembly. A Kr ⁺ laser beam is directed onto the prism at an angle by way of a beam steerer. The propagating light enters the waveguide and is seen as a streak through the length of the waveguide.interfaces for light to propagate along the waveguide
FIGURE 1.10 Optical field intensity distribution (TE wave) for a 2 $\mu$ m waveguide for m = 0 and m = 1 modes. Evanescent tails are shown in the air superstrate and the substrate dielectric. (Adapted from Rabolt, J. F. and Swalen, D. in <i>Spectroscopy of Surfaces</i> ; Clark, R. J. H.; Hester, R. E. Wiley: New York, 1988; Vol. 16, Ch.1.)30
FIGURE 1.11 A schematic diagram of the heterostructure assembly, glass/3-MPT/Ag
colloid, of the IOEW-SER substrate with an adsorbate layer, . The propagating evanescent wave, TE mode () leaks into the 3-MPT/Ag colloid overlayers increasing the Raman scattering cross section and enhancing the surface adsorbate vibrations. The adsorbate is immobilized on the Ag colloid surface
FIGURE 2.1 Optical micrographs of Ag colloid I-pza (Ag-pza I) (A), and Ag colloid II-pza (Ag-pza II) (B) films deposited from the water-dichloromethane interface

FIGURE 2.2 Surface plasmon absorption curves (SPA) of Ag colloid I-pza (Ag-pza I) (a), and Ag colloid II-pza (Ag-pza II) (b), films deposited from the water-dichloromethane interface.
FIGURE 2.3 SERS spectra of Ag-pza I (aqueous layer) (a), Ag-pza I (organic layer) (b), and Ag-pza II (c), glass deposited films
FIGURE 2.4 SERS spectrum of Ag colloid / pza system (a), and normal FT-Raman spectrum of neat pza (b)
FIGURE 2.5 TEM micrograph of Ag-4-MPy film II deposited onto a carbon covered grid.
FIGURE 2.6 SERS spectra of Ag-4-MPy I (a); and Ag-4-MPy II films (b); and Ag colloid / 4-MPy system (c), glass deposited films
FIGURE 2.7 Normal FT-Raman spectra of 4-MPy powder (a), and silver-4-MPy complex powder (b), (band labeled * is assigned to the $v_{sym}(NO_3^-)$ band of AgNO ₃ ). $\lambda_{ex} = 1064.1$ nm at 150 mW.
FIGURE 2.8 Thiol-thione tautomers of 4-MPy66
FIGURE 2.9 SERS spectra of Ag-2-MPy I from different 2-MPy concentrations. Ag-2-MPy I (2 x 10 ⁻⁵ M 2-MPy) (a); Ag-2-MPy I (1 x 10 ⁻³ M 2-MPy) (b); glass deposited films and Ag colloid/2-MPy system (c).
FIGURE 2.10 TEM micrograph of Ag-2-MPy film II deposited onto carbon covered grid. The film shows a 2D monolayer of Ag colloidal particles
FIGURE 3.1 Photograph of the assembly apparatus used for 3-MPT derivitization of glass cover slides. A Teflon block with lateral ridges holds glass cover slides separately. A Teflon coated stirbar is inserted into the bottom of the block. The block is inserted in a glass barrel, each half of the barrel is separated by a Teflon O-ring and Teflon sleeves are employed to eliminate the use of vacuum grease. Facilities for N ₂ flushing and entry/exit ports for liquid are attached at the top of the barrel.
FIGURE 3.2 A schematic of the waveguide assembly heterostructure. A glass cover slide reacts with molecular adhesive, 3-MPT (a); the hydrolysis and condensation reaction of 3-MPT is completed (b); and the derivatized glass is immersed in an Ag colloid hydrosol (c).
FIGURE 3.3 IOEW-SERS spectrum of an Ag derivatized waveguide (a), and normal FT-Raman spectrum of bulk liquid 3-MPT, (b). $\lambda_{ex} = 1064.1$ nm at 150 mW92
FIGURE 3.4 IOEW-SERS spectrum of C-H stretching region of an Ag derivatized waveguide (a), and unenhanced FT-Raman spectrum of bulk liquid 3-MPT (b).
$\lambda_{\text{ex}} = 1064.1 \text{ nm at } 150 \text{ mW}.$ 93
FIGURE 3.5 SERS of the waveguide surface. The spectrum was collected using the classical 900 backscatttering geometry

FIGURE 3.6 UV-extinction maxima of parent Ag colloid (A); $\lambda_{max} = 392$ nm,
waveguide derivatized with Ag colloid (B); $\lambda_{max} = 402$ nm, and Ag colloid derivatized
waveguide immersed in 2 mM 4,4'-bipyridine (C) $\lambda_{max} = 422$ nm96
FIGURE 3.7 SFRS of Ag colloid sol / 4,4 '-bipyridine system (20 $\mu$ l, 2 mM) to 2 ml of Ag colloid (a); IOEW-SERS of derivatized waveguide after immersion in 2 mM acetonitrile solution of 4, 4'-bipyridine (b); and unenhanced FT-Raman spectrum of bulk solid 4, 4'-bipyridine. $\lambda_{ex} = 1064.1$ nm at 150 mW (c).
FIGURE 4.1 A schematic diagram of the heterostructure assembly, glass / 3-MPT / Ag colloid, of IOEW-SERS substrate with an adsorbed layer of sensor coating, 4-MPy. The propagating evanescent wave, TE mode () leaks into the 3-MPT / Ag colloid overlayers increasing the Raman scattering cross section and enhancing the surface 4-MPy adsorbate vibrations. The selective sensor function of 4-MPy is depicted by the H+ ions of 4-MPyH+, ( $\square$ ) which are replaced by Cu ²⁺ ions ( $\blacksquare$ ).
FIGURE 4.2 SERS spectra of 4-mercaptopyridine (4-MPy) adsorbed on: MELLFs (2ml of 2 x $10^{-3}$ M 4-MPy in 2 ml of colloid) (a); IOEW-SERS (2 x $10^{-3}$ M of 4-MPy in acetonitrile) (b); and silver hydrosol (10 $\mu$ l of 2 x $10^{-4}$ M 4-MPy in 2 ml of colloid) (c)
FIGURE 4.3 Unenhanced normal FT-Raman spectra of silver-4-MPy complex (a), and 4-MPy in the solid state (b). $\lambda_{ex} = 1064.1 \text{ nm at } 150 \text{ mW}$ .  (*) Band assigned to $v_{sym}(NO_3^-)$ from AgNO3
FIGURE 4.4 SERS spectra of 2-mercaptopyridine (2-MPy): MELLFs (2 ml. 2 x 10 ⁻³ M 2-MPy in 2 ml colloid) (a); IOEW-SERS (2 x 10 ⁻³ M of 2-MPy in acetonitrile) (b); and silver colloid hydrosol (60 μl, 1 x 10 ⁻² M 2-MPy in 2 ml of colloid) (c)
FIGURE 4.5 Unenhanced FT-Raman spectra of silver-2-MPy complex (a), and 2-MPy in the solid state (b). $\lambda_{ex} = 1064.1 \text{ nm at } 150 \text{ mW}$ .  (*) Band assigned to $v_{sym}(NO_3^-)$ from AgNO ₃
FIGURE 4.6 IOEW-SERS spectra of v(C-H) stretching region of adsorbed 2-MPy (a), and 4-MPy (b).
FIGURE 4.7 Thiol-thione tautomers of 4-MPy127
FIGURE 4.8 IOEW-SERS spectra of 4-MPy after immersion in 2 x 10 ⁻³ M aqueous solution of Cu(NO ₃ ) ₂ : after 30 min immersion (a); after 10 min immersion (b); and before exposure to the Cu ²⁺ solution (c).
FIGURE 4.9 IOEW-SERS spectra of $v_1$ ring breathing mode of 4-MPy before exposure to $Cu^{2+}$ (a), and after exposure to $Cu^{2+}$ ion solution (b)
FIGURE 4.10 Unenhanced FT-Raman spectra of 4-MPy in different aqueous pH solutions at different pH; pH 14 (a); pH 8.3 (b); and pH 1 (c)

FIGURE 4.11 IOEW-SERS spectra of 4-MPy immersed in different aqueous solutions at different pH: pH 14 (a); pH 6.4 (b); and pH 1 (c)
FIGURE 4.12 XPS of sulfur 2p region with surface bulk Si plasmon for sample (A): Si wafer; sample (B): Si wafer modified with 3-MPT, (Si/3-MPT); sample (C): Si/3-MPT with adsorbed Ag colloid, (Si/3-MPT/Ag); sample (D): Si/3-MPT/Ag with adsorbed 4-MPy, (Si/3-MPT/Ag/4-MPy); and sample (E): Si/3-MPT/Ag/4-MPy immersed in aqueous Cu(NO ₃ ) ₂ solution, (Si/3-MPT/Ag/4-MPy/Cu)
FIGURE 4.13 XPS of sulfur 2p region without surface bulk Si plasmon140
FIGURE 4.14 Curve fitted S 2p peaks for samples (B): Si wafer modified with 3-MPT, (Si/3-MPT); sample (C): Si/3-MPT with adsorbed Ag colloid, (Si/3-MPT/Ag); sample (D): Si/3-MPT/Ag with adsorbed 4-MPy, (Si/3-MPT/Ag/4-MPy); and sample (E): Si/3-MPT/Ag/4-MPy immersed in aqueous Cu(NO3)2 solution, (Si/3-MPT/Ag/4-MPy/Cu).
FIGURE 4.15 XPS of Nitrogen 1s region for sample (C): Si/3-MPT with adsorbed Ag colloid, (Si/3-MPT/Ag); sample (D): Si/3-MPT/Ag with adsorbed 4-MPy, (Si/3-MPT/Ag/4-MPy); and sample (E): Si/3-MPT/Ag/4-MPy immersed in aqueous Cu(NO ₃ ) ₂ solution, (Si/3-MPT/Ag/4-MPy/Cu)
FIGURE 4.16 Curve fitted N 1s peaks for samples (D): Si/3-MPT/Ag with adsorbed 4-MPy, (Si/3-MPT/Ag/4-MPy); and sample (E): Si/3-MPT/Ag/4-MPy immersed in aqueous Cu(NO ₃ ) ₂ solution, (Si/3-MPT/Ag/4-MPy/Cu)
FIGURE 4.17 XPS of Copper 2p region for sample (A): Si wafer; sample (B): Si wafer modified with 3-MPT, (Si/3-MPT); sample (C): Si/3-MPT with adsorbed Ag colloid, (Si/3-MPT/Ag); sample (D): Si/3-MPT/Ag with adsorbed 4-MPy, (Si/3-MPT/Ag/4-MPy); and sample (E): Si/3-MPT/Ag/4-MPy immersed in aqueous Cu(NO ₃ ) ₂ solution, (Si/3-MPT/Ag/4-MPy/Cu)
FIGURE 4.18 Curvefitted Copper 2p peaks for sample (E): Si/3-MPT/Ag/4-MPy/Cu.
FIGURE 4.19 XPS of Silver 3d region for sample (A): Si wafer; sample (B): Si wafer modified with 3-MPT, (Si/3-MPT); sample (C): Si/3-MPT with adsorbed Ag colloid, (Si/3-MPT/Ag); sample (D): Si/3-MPT/Ag with adsorbed 4-MPy, (Si/3-MPT/Ag/4-MPy); and sample (E): Si/3-MPT/Ag/4-MPy immersed in aqueous Cu(NO3)2 solution, (Si/3-MPT/Ag/4-MPy/Cu)
FIGURE 5.1 Unenhanced FT-Raman spectra of bulk powder 4-MPy (a); bulk powder silver-4-MPy complex ( $\lambda_{ex} = 1064.1$ nm at 150 m) (b); Ag colloidal SERS spectrum of 4-MPy (10 $\mu$ l of 2 x 10-4 M in 2 ml of colloid) (c); and SERS spectrum of 4-MPy adsorbed
on Ag electrode at 0 V acquired with 514.5 nm excitation (d)
FIGURE 5.2 Thione-thiol tautomerism of 4-MPy
FIGURE 5.3 Cyclic voltammogram of 4-MPy (1 mM) adsorbed on an Ag electrode in 0.1 M KCl. The potential range is from 0 to -1.0 V (vs. SCE) with scan rate of

FIGURE 5.4 SERS spectra of 4-MPy adsorbed on an Ag electrode using 514.5 nm excitation at the potentials listed (vs. SCE)
FIGURE 5.5 SERS spectra of 4-MPy adsorbed on an Ag electrode using 633.47 nm excitation at the potentials listed (vs. SCE)
FIGURE 5.6 SERS spectra of 4-MPy, v ₁ ring breathing modes at 998 and 1019 cm ⁻¹ , at -1000 mV (vs. SCE) at excitation wavelengths: 488 (a); 514.5 (b); 633.47 (c); 651.5 n2 (d).
FIGURE 5.7 SERS spectra of C-S band region of adsorbed 4-MPy on Ag electrode at 0 mV (a), and -1000 mV (vs. SCE) using 514.5 nm excitation (b)
FIGURE 5.8 Normalised SERS intensities of the $v_1$ ring breathing mode of 4-MPy for; 633.47 nm (a), 514.5 nm (b), and 488 nm excitations (c), plotted as a function of applied electrode potential (vs. SCE).
FIGURE 5.9 SERS spectrum of adsorbed 4-MPy on Ag electrode at open potential after the addition of 10 ml (2 mM) Cu(NO ₃ ) ₂ solution to the electrolyte solution

# CHAPTER 1

# INTRODUCTION

## 1.1 NORMAL RAMAN SCATTERING

Raman scattering was predicted theoretically as early as 1923¹ but was only demonstrated experimentally in 1928.² This type of spectroscopy makes use of the optical frequency of monochromatic visible light to excite molecules to induce changes in vibrational energy states. The vibrational data obtained can provide a molecular fingerprint from which information such as structure, symmetry, and orientation can be extracted.

From classical theory,³ the Raman scattering effect results from the modulation of the induced dipole moment, **P**. The induced dipole is proportional to the electromagnetic field strength, E. The scaling factor,  $\alpha$ , is described as the polarizability of the molecule.

$$\mathbf{P} = \alpha \mathbf{E} \tag{1.1}$$

Using this simple model, a classical description of the Raman process can be derived. The electric field of incident radiation (wavelength  $\lambda$ ) is defined as:

$$E = E_0 \cos 2\pi v_0 t$$
 (1.2)

where  $E_0$  is the incident field maximum,  $v_0$  is the frequency, and t is the time. The induced dipole of a molecule in this oscillating field is obtained from combining equations (1.1) and (1.2):

$$\mathbf{P} = \alpha \, \mathbf{E}_0 \cos 2\pi \, \mathbf{v}_0 \, \mathbf{t} \tag{1.3}$$

The vibrational frequency of a bond in the absence of incident radiation is given as:

$$\alpha = \alpha_0 + (\Delta \alpha) \cos 2\pi \upsilon t \tag{1.4}$$

where  $\alpha_0$  is the equilibrium polarizability,  $\Delta \alpha$  is its maximum variation and v is the natural vibrational frequency of the bond. Combining equations (1.3) and (1.4) the induced dipole oscillation is given by:

Equation (1.5) predicts that the oscillating electric dipole radiates electromagnetic waves of frequency  $v_0$  (Rayleigh scattering),  $v_0 + v$  (anti-Stokes radiation) and  $v_0 - v$  (Stokes radiation). The elastic or Rayleigh scattering is merely the incident radiation scattered with frequency  $v_0$  and constitutes the major part of scattered light. A small fraction of the scattered radiation (1/1000) is scattered inelastically. One component results from molecules elevated to an excited vibrational "virtual" state which upon relaxation to an excited state (e.g., v=1) produces Raman scattered light called Stokes scattering. This scattering frequency is red-shifted,  $(v_0 - v)$ , from the wavelength of incident radiation. Another component results from molecules, elevated from an excited state (e.g., v=1) to an excited "virtual" state, returning to a ground state (v=0) and the scattered light is blue-shifted, ( $v_0 + v$ ), from the wavelength of incident radiation. A schematic representation is shown in Figure 1.1. The Stokes-shifted scattering is more intense than is the anti-Stokes scattering (at ambient conditions) and Raman spectra are usually displayed as Stokes-shifted spectra. Characteristic frequencies of scattered light can be associated with distinct vibrations of the molecule.

The weakness of the Raman effect ( $I_{Raman} \approx 10^{-8}$  to  $10^{-12} I_0$ ) and interference from sample fluorescence has hampered the use of normal Raman spectroscopy for routine sample analysis, whereas infrared spectroscopy has been more extensively used and has led to a substantial IR reference library. However, together with recent instrumental improvements (e.g., CCD detector, the Raman microscope etc.), applications such as resonance Raman (RR) and Surface Enhanced Raman Scattering (SERS) have advanced this technique to a point where it is now recognized as an effective and sensitive analytical tool.

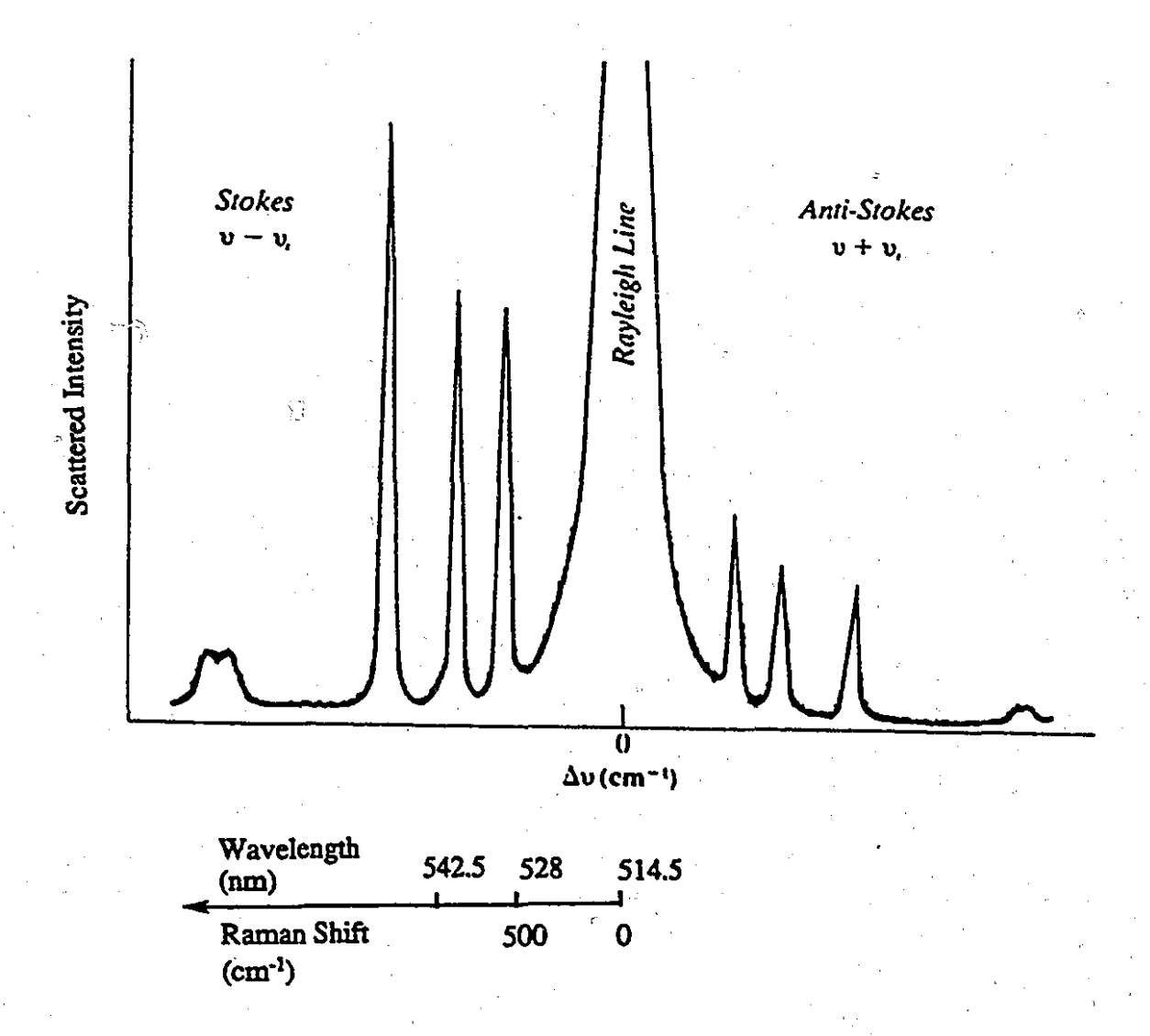


FIGURE 1.1 Schematic representation of a room temperature Raman spectrum of CCl₄ excited with 514.5-nm line of an argon-ion laser.

(Adapted from Butler, I. S. and Harrod, J. F. Inorganic Chemistry: Principles and Applications, Benjamin/Cummings Publ., Menlo Park, California, 1989)

#### 1.2 RESONANCE-RAMAN SCATTERING

If the exciting frequency is coincident, or almost coincident with an electronic transition of the molecule, the intensity of certain Raman bands will be greatly enhanced, often by factors of 10² to 10⁴. This is known as the resonance Raman effect. The most common enhancement mechanism is the Frank-Condon enhancement.⁵ Since the resonance Raman experiment involves absorption of the incident light, the intensity band profile roughly follows the shape of the absorption spectrum of the molecule. Resonance Raman spectroscopy has found extensive use in studying specific chromophoric regions of transition metal complexes and biological molecules.⁶

## 1.3 SURFACE ENHANCED RAMAN SCATTERING (SERS)

Surface Enhanced Raman Scattering (SERS) provides intense Raman signals from molecules adsorbed on specially roughened metal surfaces. The effect was originally discovered by Fleishmann *et al*. ⁷ in 1974 when an anomalously intense Raman signal was observed from pyridine adsorbed from aqueous solution onto an electrochemically roughened silver electrode surface. The high intensities were originally attributed to an increase in electrode surface area and a concomitant increase in the number of molecules. However, Jeanmaire and Van Duyne⁸ and Albrecht and Creighton⁹ were the first to recognize that an intrinsic surface enhancement effect was responsible for enhancement factors of up to 10⁶. Since this discovery, there has been a considerable volume of work published on SERS, both experimental and theoretical, aimed at understanding the enhancement effect. A number of reviews on SERS have been published. ¹⁰⁻¹³

As described above, the intensity of any Raman scattering is proportional to the change in molecular polarizability and incident electromagnetic field strength. Therefore, profound alterations in one or both of these components can provide a possible mechanism for the enhancement. Although some controversy still exists regarding the theoretical interpretation of SERS, two rationalizations are generally agreed upon. A purely physical

mechanism has been proposed in which metal surfaces are able to concentrate the electromagnetic radiation due to the incident light into a region of the surface. ^{12,14-16} The metal surfaces do this principally as a result of a resonant response of conduction electrons in the roughened or particulate surface to the electromagnetic field. There is also a chemical mechanism in which contributions to the resonance enhancement require an interaction between the adsorbate and substrate. ^{12,14-16} This interaction can take place in the form of a charge transfer between the metal and adsorbate or else formation of a molecule-metal atom complex with consequent molecular resonances. Contributions from these two kinds of mechanisms, electromagnetic and chemical, are not mutually exclusive - the current view is that the major contribution is electromagnetic. ¹⁷ These mechanisms are described in more detail below.

## 1.3.1 Surface Electromagnetic Field Enhancement (EM) Effect

Experimentally, it has been found that the most intense SERS spectra are obtained from molecules adsorbed on silver surfaces, although comparable intensities are also observed from copper and gold surfaces. Other metals including sodium, ¹⁸ aluminum¹⁹ and indium¹⁵ have been reported to show surface enhanced Raman scattering of similar intensity in some cases. The most successful theory which has been able to account for a large number of features of SERS is based on the response of small metal particles to electromagnetic fields. Known as the EM theory, enhancements up to 10⁶ have been estimated due to the presence of these microscopic surface structures combined with the optical properties of the metal substrate. ¹⁷ Metal particles of the substrate have an electromagnetic resonance, known as dipolar surface plasmons. These oscillating plasmons may be resonately excited by an electromagnetic wave of the same frequency. As a result of this "tuned" response, the metal surface then becomes highly polarizable leading to large field induced polarizations and thus large fields local to the surface are produced.

The surface field has been calculated for a spherical particle smaller than the

wavelength of the light since the electromagnetic field is uniform over the sphere and there is only a dipole response from which the polarizability can be estimated. 15,20,21 Considering only the dielectric components of the electromagnetic field, the maximum value of the local field is approximately equal to,

Re 
$$\varepsilon (\omega_p) / \operatorname{Im} \varepsilon (\omega_p)$$
 (1.6)

where  $\varepsilon$  is the complex dielectric constant of the metal inside the sphere at the plasmon resonance frequency  $\omega_p$ . The field inside the sphere is  $3E_0/(\varepsilon + 2)$  where  $E_0$  is the incident field ( $\varepsilon$  is relative to the surrounding medium) and outside the sphere the field is equal to  $E_0 + \alpha_s E_0$ , where  $\alpha_s$  is the polarizability at the center of the sphere,

$$\alpha_{S} = a^{3} \left( \varepsilon - 1 \right) / \left( \varepsilon + 2 \right) \tag{1.7}$$

in which a is the radius of the sphere. The resonance condition is observed when,

Re 
$$\varepsilon (\omega_{\rm p}) + 2\varepsilon_2 = 0$$
 (1.8)

Thus, a wavelength for which the real part of the dielectric constant of the metal sphere is equal to -2, such that Re  $[(\varepsilon, (\omega_p)] = -2(\varepsilon_2)]$  (where  $\varepsilon_2 = 1$ , relative to the surrounding medium), constitutes a dipole resonance response of the sphere.  $^{10(a-c)}$  Also, since at the resonance frequency the enhancement factor is proportional to Im  $\varepsilon$  ( $\omega_p$ )-4 of the metal, a small  $\varepsilon$  value increases the magnitude of the field enhancing response of the metal particle. Hence, the requirement of a metal for a large field enhancing response by the sphere is not only that the metal has Re ( $\varepsilon$ ) = -2 at the excitation wavelength, but also that Im ( $\varepsilon$ ) is small at that wavelength. The metals which satisfy these conditions are the alkali metals and coinage metals, i.e., copper, silver and gold. The resonance condition for these metals lies in or near the visible region of the spectrum. For silver in water, the enhancement maximum is at 380 nm where  $\varepsilon = i\sqrt{2}$  (for spheres of average diameter  $\le 10$  nm).  13 

The dependence of the enhancement upon excitation frequency is also greatly effected by particle size, the smallest showing a sharp resonance due almost exclusively to the excitation of the dipolar surface plasmons, while the larger particles show broader excitation spectra from higher multipole plasmons. In all of the surfaces, it is important for high SERS activity that the particles sizes which make up the solid substrate are not only small but are close together on a 10-100 nm scale. Particle shape also shifts the enhancement maximum, e.g., the calculated reponse of prolate (football-shaped) silver spheroids of various axial ratios shows the peak enhancement shifts to longer wavelengths as the axial ratio is increased. For sols, the peak for the enhancement maximum is redshifted to the  $\lambda_{max}$  of the sol. This behaviour is apparently associated with large aggregates of smaller individual metal particles.

The electromagnetic enhancement mechanism is largely molecule independent and has a long-range effect. For a small sphere of radius a, the enhanced fields die away as  $(a/d)^3$ , where d is the distance from the center of the sphere.²⁶ Overall, the enhancement depends on substrate roughness and electronic structure since the frequency of the surface plasmon resonances depends on these parameters.

## 1.3.2 Chemical or Charge-Transfer (CT) Enhancement Effect

There are several features in the SERS spectra that suggest chemical interactions between the adsorbate and substrate are important. SERS spectra of adsorbed pyridine on different metal substrates showed different intensity patterns for different vibrational modes. 12,27-29 In electrochemical experiments, the electrode potential had a marked effect on the SERS intensity. The potential at which the SERS intensity reaches a maximum, I_{max}, for a given adsorbate, is dependent on the particular adsorbate and also varies with wavelength excitation. Furthermore, the I_{max} shift is not always in the same direction but depends on the particular adsorbate. A resonance Raman-like process associated with electronic transitions (metal-adsorbate or adsorbate-metal) has been described which

accounts for the above observations. 12,14-16 This mechanism can explain the differing enhancements for different molecules, and for any specificity of the enhancement to molecules in the first monolayer, since only certain molecules will have the donor or acceptor levels of the correct energy to allow a charge transfer to or from the surface. 30 SERS spectra that show resonance-shaped intensity profiles as a function of applied potential display a potential range for which I_{max} varies linearly with excitation wavelength. This approach is based on tuning the CT excitation into and out of resonance by changing either the filled metal band Fermi level, Ef (by changing the applied potential, mV) or the energy of excitation, ho.^{28,29,31-33} The molecules can be divided into two classes: those for which I_{max} has a positive slope with hω and those for which the slope is negative. Molecule-to-metal CT, in which an electron is transferred from the highest occupied molecular orbital to an empty metal orbital, is associated with a negative slope in the Imax vs. hw plot. Conversely, when an electron is transferred from Ef to an empty molecular orbital (metal-to-molecule CT), a positive slope is observed. Electrochemical observations from pyridine adsorbed on silver electrodes have been studied extensively to support the theory related to the CT mechanism, ^{28-30,33,34}

Estimates of the contribution of charge transfer to the SERS effect have been in the  $10\text{-}10^3$  range. Another aspect of the chemical interaction is that the interactions between the analyte molecules and the substrate surface can effect the Raman emission by causing spectral shifts in certain bands or inducing changes in the intensity distribution of the spectrum. The process of molecules adsorbed on a metal surface is analogous to spectroscopic changes that are observed when ligands are complexed with metal ions in solution to form metal coordination complexes. As a result, in some SERS spectra, many features can be explained by the formation of a complex with the metal surface. All chemical (or CT) enhancement theories are related to changes in the polarizability  $\alpha$  of the metal-molecule system due to the formation of chemisorptive bonds.

Despite many efforts since the discovery of SERS, the CT mechanism is still poorly understood compared to the EM mechanism. Consequently, it has often been easier to explain experimental results or to test enhancement theories within the framework of the EM theory than to predict the outcome of an experiment using CT theory.

## 1.4 ADSORBATE ORIENTATION AT METAL SURFACES

The use of selection rules in the interpretation of vibrational spectra has historically proven to be a valuable approach for obtaining structural information on molecules. In the case of molecules at surfaces, the selection rules differ from those of free molecules because of the effect of the surface in modifying the EM field at the surface and in orienting the molecules relative to this field. Adsorbate orientation has generally been investigated with SERS under the premise that the electromagnetic (EM) effect is the predominant enhancement mechanism. SERS selection rules for orientation determination have been established and applied to several C_{2v} molecules, notably, pyridine, N-methylpyridine and substituted benzenes on silver substrates. 15,38-40 All the adsorbates chosen for the SERS studies in this thesis are pyridine derivatives; therefore, a review of the selection rules will be presented for the SERS prototype, pyridine. Pyridine ring vibrations are distributed between four symmetry species under C_{2v} symmetry, a₁, a₂, b₁ and b₂, all of which are Raman-active. The symmetry convention, polarizability tensor components and relative mode enhancements of pyridine are illustrated in Figure 1.2. The a₁ and b₂ modes involve in-plane motions while those of a2 and b1 symmetry are associated with out-of-plane vibrational motions. Using a generally accepted symmetry convention, where z is taken as the direction perpendicular to the surface and the molecular plane of the pyridine ring lies in the yz plane, the  $b_2$  modes contribute to the polarizability tensor component,  $\alpha_{VZ}$ , whereas the  $b_1$  and  $a_2$  modes contribute to the  $\alpha_{ZX}$  and  $\alpha_{XY}$  components, respectively. For a perpendicular orientation (yz plane), the b₁ and b₂ modes are expected to be enhanced relative to the a2 modes. For a flat orientation of the ring relative to the surface (xy plane), the relative intensities of the  $b_1$  and  $a_2$  modes are anticipated to be greater than those of the  $b_2$  modes. The  $a_1$  totally symmetric vibrational modes contain all three diagonal polarizability tensor elements  $\alpha_{XX}, \alpha_{YY}, \alpha_{ZZ}$ . The relative magnitude of each component is unknown and this can preclude the use of  $a_1$  modes for the purposes of orientation analysis. As observed for pyridine, bands due to  $a_1$  modes vary greatly with a change in surface potential. It has been established that some of the  $a_1$  modes undergo additional enhancement from a resonance Raman process, involving a CT mechanism, as discussed above. Clearly, therefore, if the  $a_1$  band intensities are to be interpreted from an EM point of view, it is necessary to show that there is not a large effect on the relative intensities from surface potential changes and resonance Raman effects.

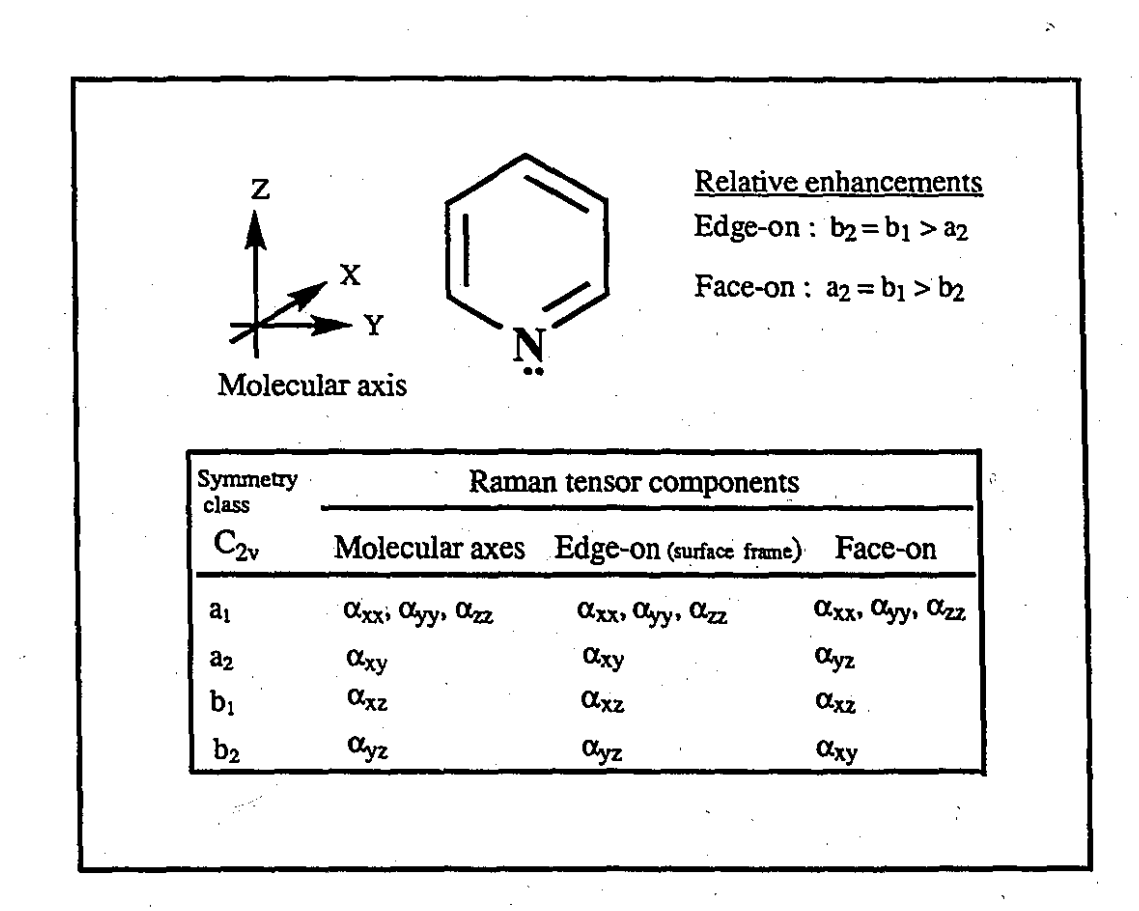


FIGURE 1.2 The symmetry classes, Raman tensor components and relative enhancements of the vibrational modes of pyridine.

## 1.5 SURFACE ENHANCED RAMAN SCATTERING SYSTEMS

Since the discovery of SERS, numerous SERS-active substrates have been explored for both theoretical and experimental applications of the effect. These include colloidal sols, roughened metal electrodes and Metal Liquid-Like Films (MELLFs), which utilize silver colloid aggregation between two immiscible phases. A new technique which involves grafting a self-assembly of silver colloid particles onto a planar waveguide combines both Waveguide Raman Spectroscopy (WRS) and SERS activity. The latter is introduced in this thesis as Integrated Optics, Evanescent Wave, Surface Enhanced Raman Scattering (IOEW-SERS).

## 1.5.1 Colloidal Silver Sols

Metal colloid hydrosols are frequently employed in producing SERS in liquid/liquid interfaces because of the apparent ease of colloid formation. Colloidal dispersions of Ag (and Au) in aqueous solutions were first used as a method for enhancing Raman scattering by Creighton et al.⁴¹ Silver sols produced from sodium borohydride give clear yellow sols with an extinction maximum (or surface plasmon absorption) near 400 nm⁴² and an average size particle diameter estimated between 8-13 nm depending on the method of preparation.^{20,43} Following addition of an analyte/adsorbate to the colloidal sol, aggregation occurs. Stable aggregates present in sols are predominantly chains of individual particles rather than compact clusters.⁴⁴ The effect of the close proximity of spheres within particle aggregates is to shift the plasma resonance to longer wavelengths, resulting in a change in the extinction spectrum.^{25,45} In earlier reports, it was shown that there is a similarity between the extinction profile and SERS scattering.^{41,44} The SERS excitation profile peaks at a wavelength close to the long wavelength extinction maximum of the sol.

Despite the simplicity of published procedures for preparing colloids, the routine is deceptive since there are a number of experimental parameters associated with the sol preparation.¹³ In particular, the maximum Raman signal obtained as the concentration of analyte is increased reflects saturation of available interaction sites at the silver surface. The concentration at which the maximum Raman signal is reached is characteristic of the particular analyte. As the concentration is increased, the extent of coagulation increases and the particulates can be precipitated. Particle coagulation is also dependent on the ionic strength and pH. Colloid hydrosols may be unstable over long periods of time. Thus, these interdependent parameters have resulted in poor reproducibility of SERS signals and a decrease in signal intensity over time.

## 1.5.2 Roughened Electrodes

Electrochemistry is an *in-situ* technique that can provide information concerning reactions at the metal-liquid interface.⁴⁶ The use of electrochemistry has the advantage that the surface potential of the conductor is in contact with the solution and hence the net surface charge may be varied in such a way as to control the processes of adsorption, oxidation and/or reduction. Many of the processes that occur at the electrode surface proceed without exhibiting current flow through the cell circuit and are therefore undetectable by electrochemical means alone. Consequently, spectroelectrochemical studies can offer a high degree of chemical specificity in characterizing reactions at the electrode surface. Electrochemical methods can measure and control factors such as the amount of analyte species at the surface of the electrode and, since SERS is localized to the vicinity of a metal surface, it means that this technique is a highly sensitive surface probe which can be used to study both the static and dynamic molecular processes at activated metal surfaces. A number of reviews and texts concerned with SERS and electrochemistry is available. ^{12,26,47,48}

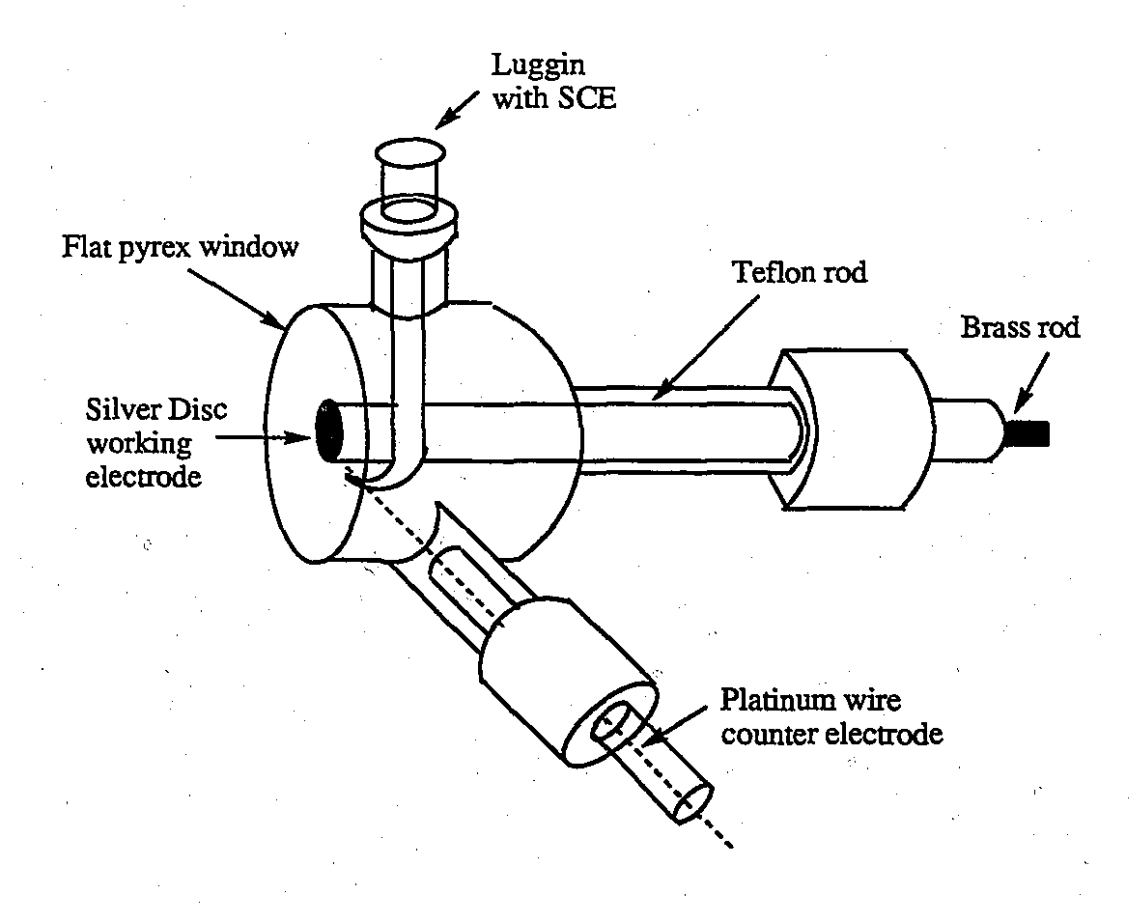


Figure 1.3 Spectroelectrochemical cell used for SERS experiments.

# 1.5.2.1 Spectroelectrochemical Cell Instrumentation

The electrochemical set-up generally consists of a three-electrode cell comprised of a SERS-active working electrode, an inert counter electrode and a reference electrode. The cell design used in our work employed a 90° collection geometry, as shown in Figure 1.3. The cell was made of glass with an optically flat Pyrex window. The reference electrode was kept in a separate compartment from the working and counter electrodes and was connected by a Luggin capillary. The reference potential was monitored at the tip of the Luggin capillary which was placed in the potential gradient induced by the current flow between the working and counter electrodes. A facility for solution degassing was available. A more detailed description of the electrodes used is given in Chapter 5.

# 1.5.2.2 Electrode Surface Preparation

To generate an electrode that is capable of enhancing the Raman signal of molecules at the electrode surface the metal is roughened by an oxidation-reduction cycle (ORC).⁴⁸ Electrochemical etching of the surface by oxidizing the silver in the presence of halide ions followed by reduction of the silver halide forms a layer of silver crystals on top of the electrode. In this work, prior to immersing the working electrode in the analyte solution, the electrode was roughened *in-situ* (0.1M KCl) by an anodic sweep, followed by a cathodic sweep at the same rate (-700 mV to +100 mV vs. SCE at 5mV/s). The initial potential was set negative to the onset of Ag oxidation and then swept to a potential where Ag oxidation occurred. Figure 1.4 shows the cyclic voltammogram for roughening pretreatment. The cathodic limit is imposed by the reduction of water, namely,

$$2H_2O + 2e^- \rightarrow H_2 + 2OH^-$$

SERS spectra are irreversibly lost at more negative potentials not only because of the reduction process but it has also been argued that SERS active sites are destroyed beyond this potential range.⁴⁸

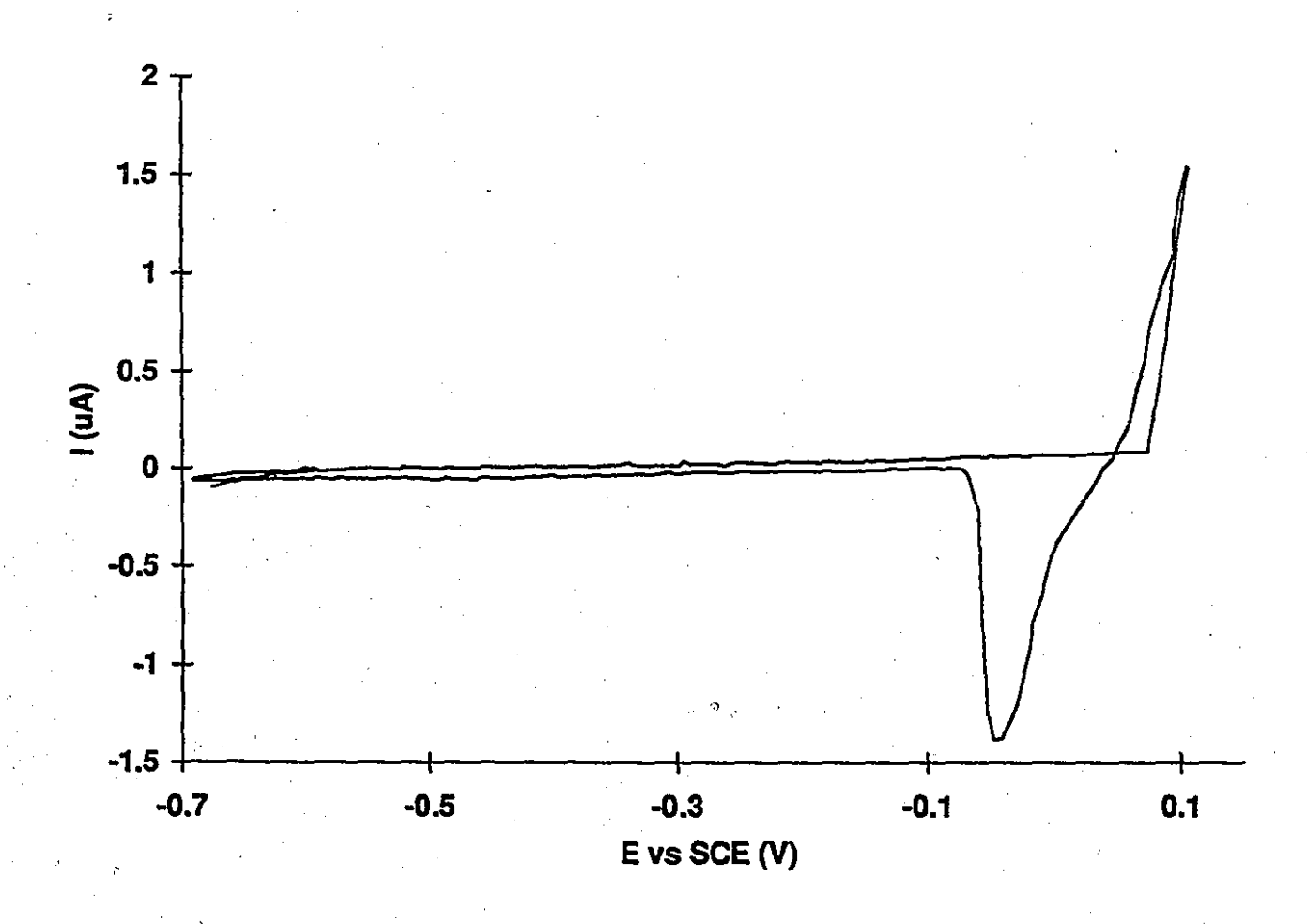


Figure 1.4 Cyclic voltammogram of an Ag electrode in 0.1 M KCl. One ORC process consisting of a double potential sequence of -700 mV to +100 mV and back to -700 mV (vs. SCE) at 5 mV/s.

The anodic limit is restricted by the oxidation of the Ag electrode surface in halide solution

$$Ag + Cl^- \rightarrow AgCl + e^-$$

The AgCl layer at the electrode surface is sparingly soluble and is removed reversibly (when the layer is limited to 100 monolayers) when the potential is reversed. The pretreatment process roughens the electrode surface, producing sites of large-scale roughness (nodules 25-500 nm in diameter) and molecular-scale roughness (adatoms or adatom clusters). It is widely agreed that the active sites produced by an ORC pretreatment are crucial in fixing the molecule to the surface, thereby permitting SERS to be observed. The SERS activity of an electrode has been shown to depend on the presence of laser illumination during the ORC.⁴⁹ Larger enhancements are achieved with illumination during an ORC.

# 1.5.3 Metal Liquid-Like Films (MELLFs)

Silver metal liquid-like films are thin films of a highly concentrated suspension of silver colloid confined to the interface between two mutually immiscible liquids, generally water and dichloromethane. Although most studies are of silver MELLFs, copper and gold colloids have also been reported to produce MELLFs. 50,51 MELLFs show a unique combination of characteristics: metallic luster characterized by specular reflectivity in the near UV, visible and IR ranges, practically zero conductivity, and liquid-like mechanical behaviour (described as "mercury-like" appearance) with the chemical properties of colloids. 52

MELLFs can be produced in a number of different ways.⁵³⁻⁵⁶ In our work, the adsorbate was dissolved in dichloromethane and vigorously shaken with an equal volume of silver sol in a tall stoppered glass vial (5 mL). The colloid was extracted into the organic phase containing the adsorbate and formed an adsorbate-silver particle layer at the interface. Figure 1.5 shows a schematic for a MELLF preparation. Figure 1.6 shows two photograph of a freshly prepared interfacial MELLF of 2-mercaptopyridine.

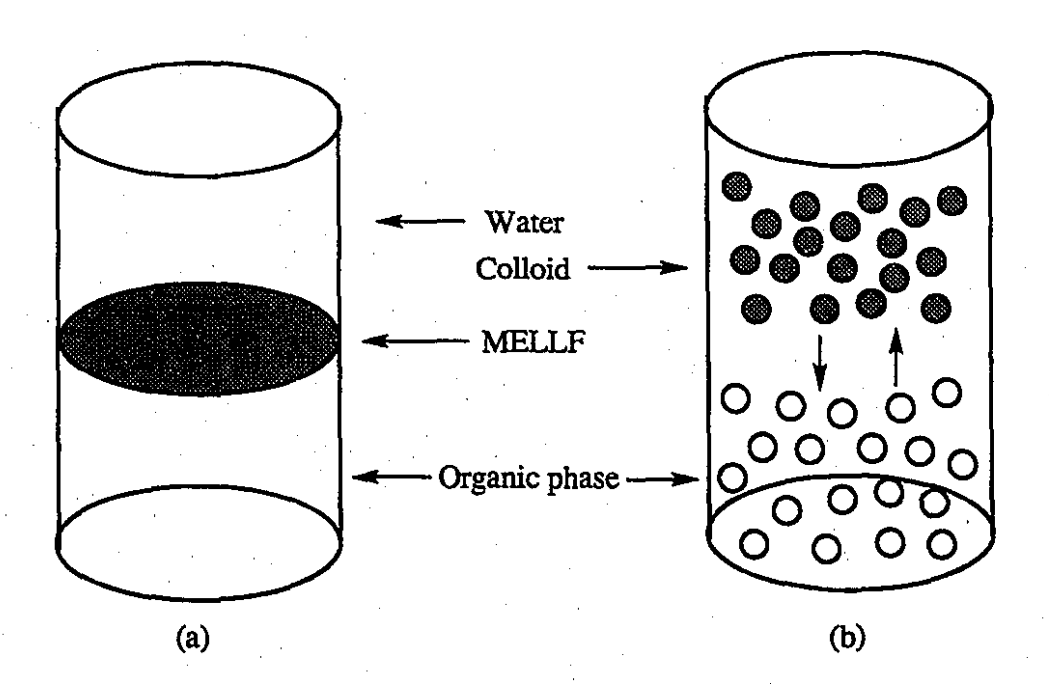
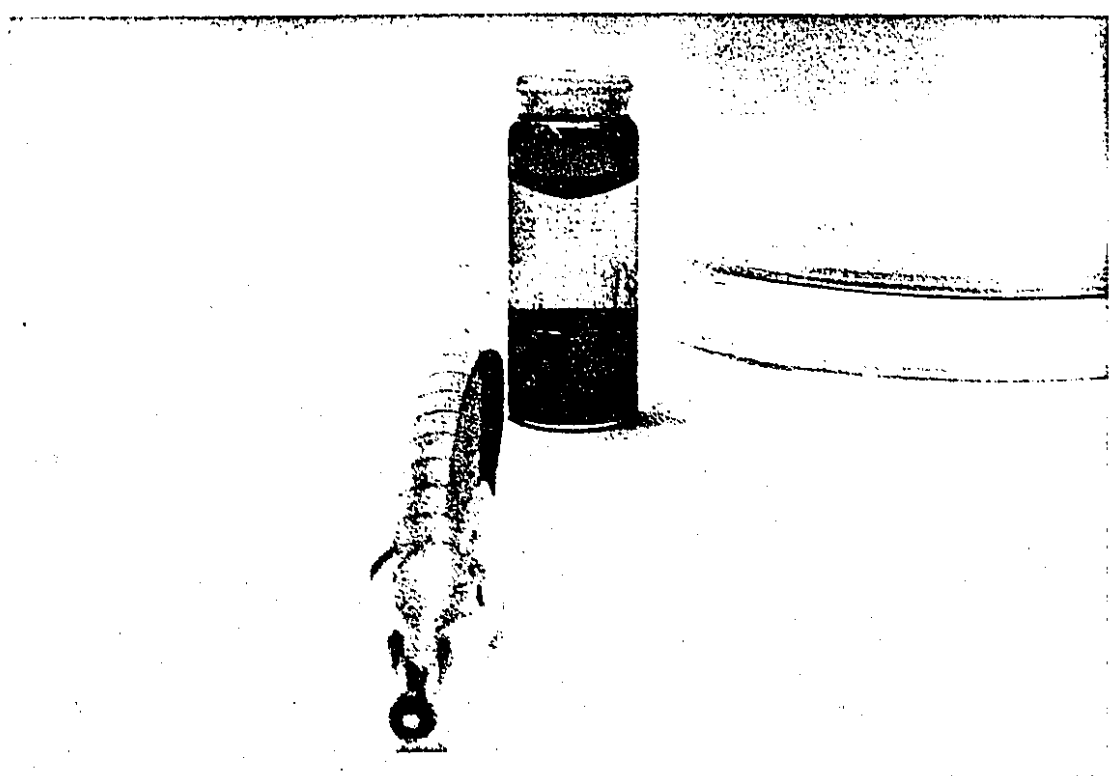
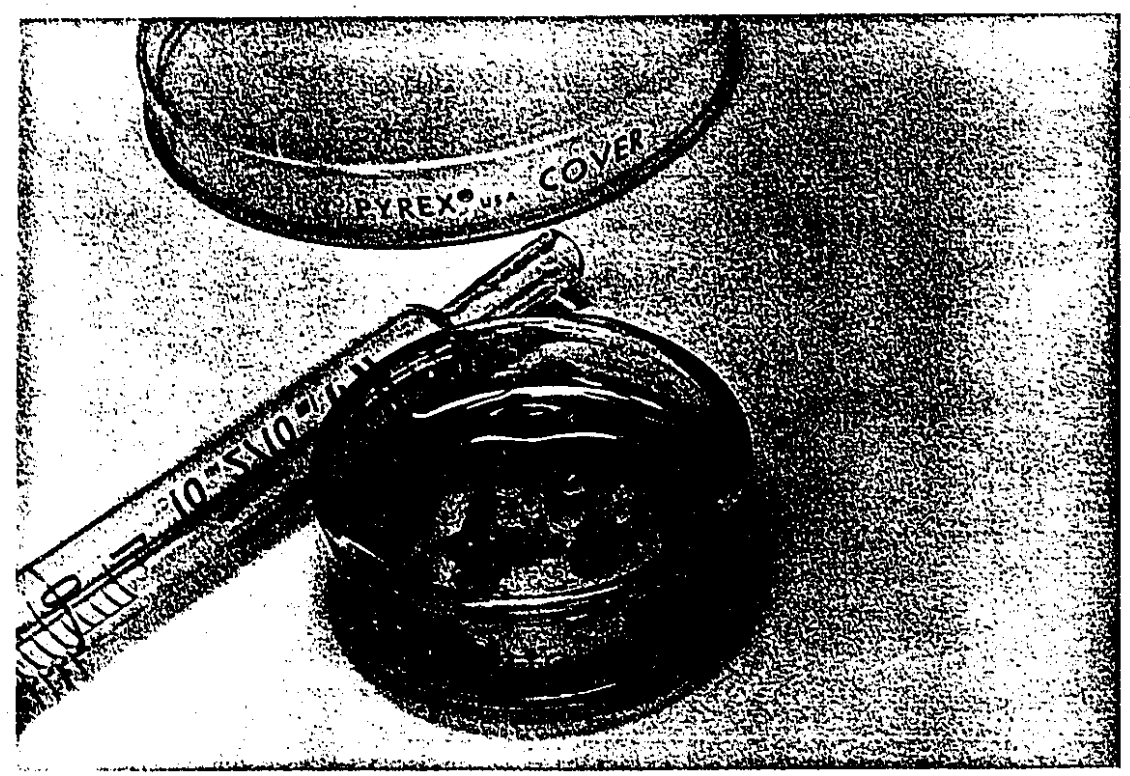
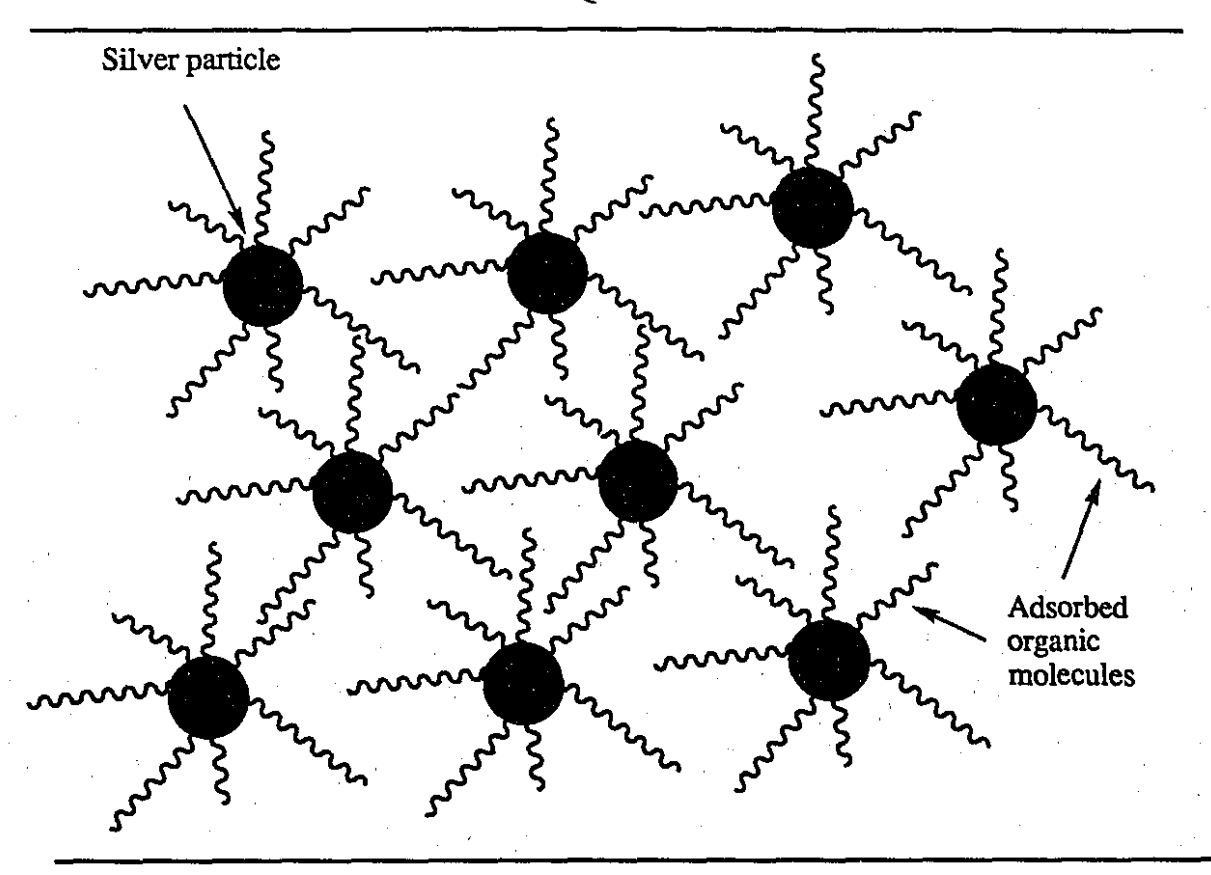


FIGURE 1.5 Schematic views of an interfacial MELLF (a), and interphase transfer of colloidal particles with adsorbate molecules in an organic phase (b).

FIGURE 1.6 Photographs of a freshly prepared interfacial MELLF of 2-mercaptopyridine.







ORGANIC PHASE

FIGURE 1.7 Structural model of an interfacial MELLF. Loosely held aggregates in a flocculated state.

The factors that constitute the delicate balance which keeps the colloidal particles confined to a small region but yet, keeps them apart, without coagulating and imparts liquid-like properties to the film are undoubtedly quite complex. The adsorbates stabilize colloid particles against aggregation, probably by steric replusions and some electrical charging. They also reduce the average density of the particles and thus decreases the tendency to precipitate. The adsorbed layer apparently shows its hydrophobic side to the aqueous solution side and therefore the particles tend to flocculate at the interface. A structural diagram of a continuous interfacial MELLF is shown in Figure 1.7.

Several experimental findings suggest that in the MELLF the colloid is in a flocculated state, i.e., loosely held reversible aggregates of basic colloidal particles. The overall structure is a rather open one, allowing easy motion of molecules between and among the silver cores. This composition is in accord with the lack of conductivity. UV-visible spectra (reflectance mode) of MELLFs *in-situ* ⁵⁷ and of dried glass-deposited films⁵³ [transmittance mode (SPA)] showed band shifts (red-shifted relative to the parent colloid) which indicate the presence of silver colloidal particles with various degrees of aggregation depending upon the conditions employed.

It is well known that the conditions for the generation of surface plasmon resonances which are necessary for the enhancement of optical processes experienced by adsorbed molecules are strongly dependent on the internal structure of the SERS-active system. Scanning electron microscopy (SEM) and transmission electron microscopy (TEM) have confirmed the findings of UV-visible spectroscopy and showed various levels of clustering in MELLFs. 50,54,58,59 In some cases, TEM photographs resemble self-similar fractal structures. 54

There are a number of experimental factors which control the formation and structure of interfacial MELLFs. Shaking the two-phase mixture is one of the conditions necessary to allow rapid interphase transfer of adsorbate from the organic to the aqueous phase and formation of a MELLF at the interface. In some cases, the adsorbate can transfer

from the organic to aqueous phase without shaking and form colloidal aggregates at the interface, e.g., 2,2'-bipyridine. No metallic films develop, however, with this slow "passive" interphase transfer.⁵³ The surface potential of borohydride-reduced Ag colloid can also influence aggregate-adsorbate infrastructure. The Ag colloid potential can be adjusted by aging or by adjusting the amount of excess BH₄⁻ ions in the electric bilayer enveloping the Ag colloidal particles. The latter method adjusts the AgNO₃ to NaBH₄ ratio and thus the amount of silver particles in the sol. The surface coverage of adsorbate on a silver particle can then be adjusted by either the silver or adsorbate concentration.

# 1.5.4 Integrated Optics, Evanescent Wave, Surface Enhanced Raman Scattering (IOEW-SERS)

# 1.5.4.1 Waveguide Raman Spectroscopy

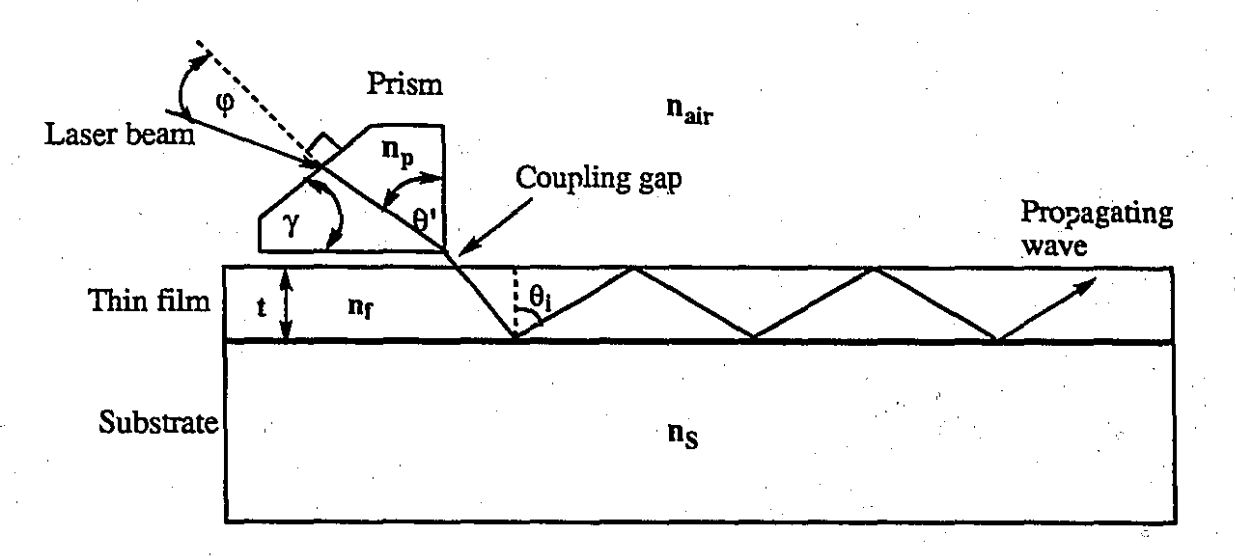
Combining two techniques, integrated optics and Raman spectroscopy, produces a versatile method capable of probing thin films. This method has been described as waveguide Raman spectroscopy (WRS). Initially, this technique was introduced by Levy et al.⁶⁰ in 1974 to perform spectroscopic measurements on polymer thin films. Optical waveguides seemed an ideal solution because the detection, identification, and observation of thin films on a substrate or at an interface with sufficient signal-to-noise required both a reasonable optical field at the surface and a long pathlength to increase the scattering volume. In an asymmetric slab waveguide, the optical field is contained in a narrow region near the surface. High irradiances are obtained interior to the thin film and one of two unique polarizations - s polarization (transverse electric, TE) or p polarization (transverse magnetic, TM) can be chosen. Slab waveguide substrates can be made from a variety of optically transparent materials that behave as a lens-like medium, such as glass, quartz and fused silica onto which the thin film is deposited. With recent detection capabilities down to monolayer levels, new thin film growth technologies have been embraced for optical

waveguide fabrication. These include sol-gel technology⁶¹ and Langmuir-Blodgett monolayers.⁶² A general review on waveguide devices is given by Tien.⁶³

In order to guide optical radiation efficiently in a thin film waveguide, certain conditions must be met. An optical waveguide is comprised of a high dielectric constant thin film normally coated on a non-optically absorbing substrate. A focused laser beam is coupled into the film at an angle by means of a high index prism. Providing that certain refractive index (n) conditions are met, i.e., n (prism) > n (film) > n (substrate) > n (superstrate, normally air), the optical field is concentrated within the thin film and has a particular distribution according to the waveguide mode excited. In addition, the film must be sufficiently thick, approximately 1  $\mu$ m for refractive index differences between the film and substrate of 0.05 to support a guided mode.

# 1.5.4.2 Coupling Mechanism

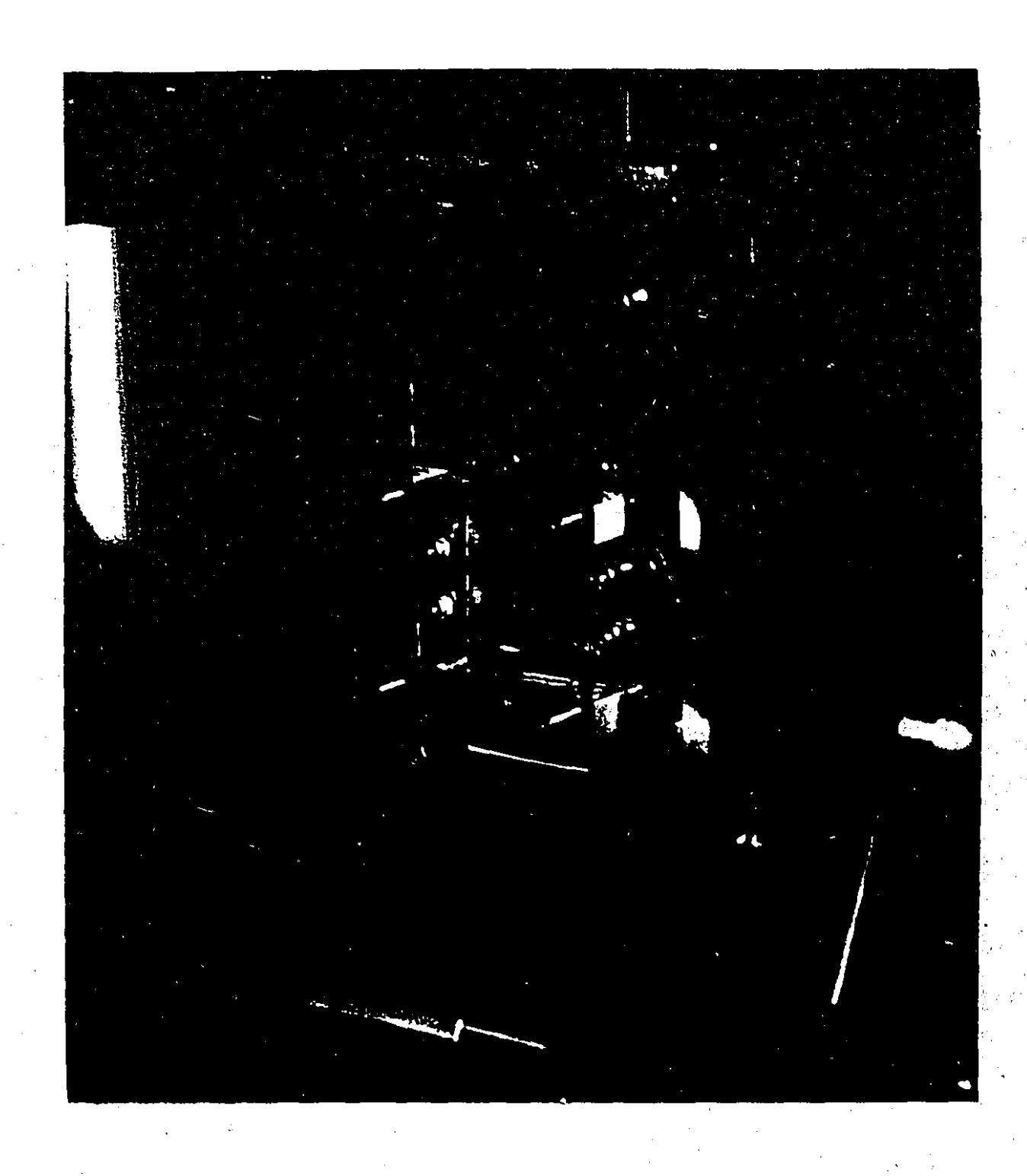
Since the integrated optics method requires trapping the incident radiation into a µm sized-waveguide, different mechanisms have been used for coupling the light to the waveguide. Details of these methods can be found in a review by Tien. ⁶³ Prism coupling is the method of choice used in our work and the principle procedures are discussed. A ray optics idealization of prism coupling is detailed in Figure 1.8. The prism is pressed down onto the waveguide by a prism coupling assembly and held in place by a pressure bar. With moderate pressure, a small air gap exists between the prism and film surface (because of surface roughness and some dust particles). This gap is required in the coupling mechanism to couple light from the prism into the waveguide. Light impinges on a corner of the prism at an angle such that total internal reflection can take place at the prism-air-interface. This reflection process causes an evanescent field, i.e., a propagating wave that decays exponentially, to be set up in the air gap. Coupling is obtained when the propagation vector of light in the evanescent field matches the propagation vector of a resonant eigenmode of the waveguide. When these two vector components are equal, the



 $n_p > n_f > n_s > n_{air}$ 

FIGURE 1.8 Schematic diagram showing the prism coupling assembly. The relation between the internal angle  $\theta$ , and the external angle  $\gamma$ , is  $\sin \phi = n_p \sin (\theta' - \gamma)$ . Refractive index (n) conditions are met, i.e., n (prism) > n (film) > n (substrate) > n (air) such that the optical field is concentrated within the thin film.

FIGURE 1.9 A glass slab waveguide with prism and waveguide assembly. A Kr⁺ laser beam is directed onto the prism at an angle by way of a beam steerer. The propagating light enters the waveguide and is seen as a streak through the length of the waveguide.



light wave in the prism will have the same velocity as that in the waveguide. Light penetrates the waveguide and the propagating wave can be approximated as traveling in a zigzag manner through the guiding film being reflected along the top and bottom surfaces. A photograph of a thin glass slide waveguide assembly with light wave propagation is shown in Figure 1.9. A description of the integrated optics spectrometer, including collection optics, Raman detection system and beam steering assembly used in this work are detailed in a previous thesis.⁶⁴ A brief outline of these features are given in Chapters 3 and 4.

#### 1.5.4.3 Field Distribution

Analysis of the optical waveguide propagation is achieved by using Maxwell's equations for matching electric and magnetic fields at each interface. There are a number of reviews and textbooks which discuss the theoretical background of optical waveguide transmission.  $^{65-67}$  Briefly, there are two fundamental requirements in order for a guided mode to propagate as illustrated in Figure 1.8. Firstly, the angle  $\theta_{i}$ , which the propagating beam makes between the top and bottom surfaces must be above the critical angle for total internal reflection. Secondly, rays traveling along the same phase front must have a total phase shift by an integral multiple of  $2\pi$ . To summarize, propagation of waves in a three-layer thin film, labeled: air (1) - film (2) - substrate (3) (for s or TE mode polarization) can be described by

$$\tan^{-1} \beta^{S}_{12} + \tan^{-1} \beta^{S}_{32} + m\pi = k_{z2}t_2$$
 (1.9)

where  $\beta^{S}_{ij} = k_{zj} / k_{zi}$ ,  $k_{zi}$  is the s polarized wave propagating coefficient (=  $k_0$   $n_i$  cos  $\theta_i$  for a non-absorbing film i, where  $k_0$  = vacuum wavevector,  $\theta_i$  = propagation angle, and  $n_i$  the refractive index) in a direction perpendicular to the substrate surface (z),  $t_2$  is the film thickness and m is the waveguide mode number (m = 0, 1, 2, ..., the number of antinodes in the field distribution). The Fresnel phase shift terms  $tan^{-1}$   $\beta^{S}_{ij}$  (which arise through

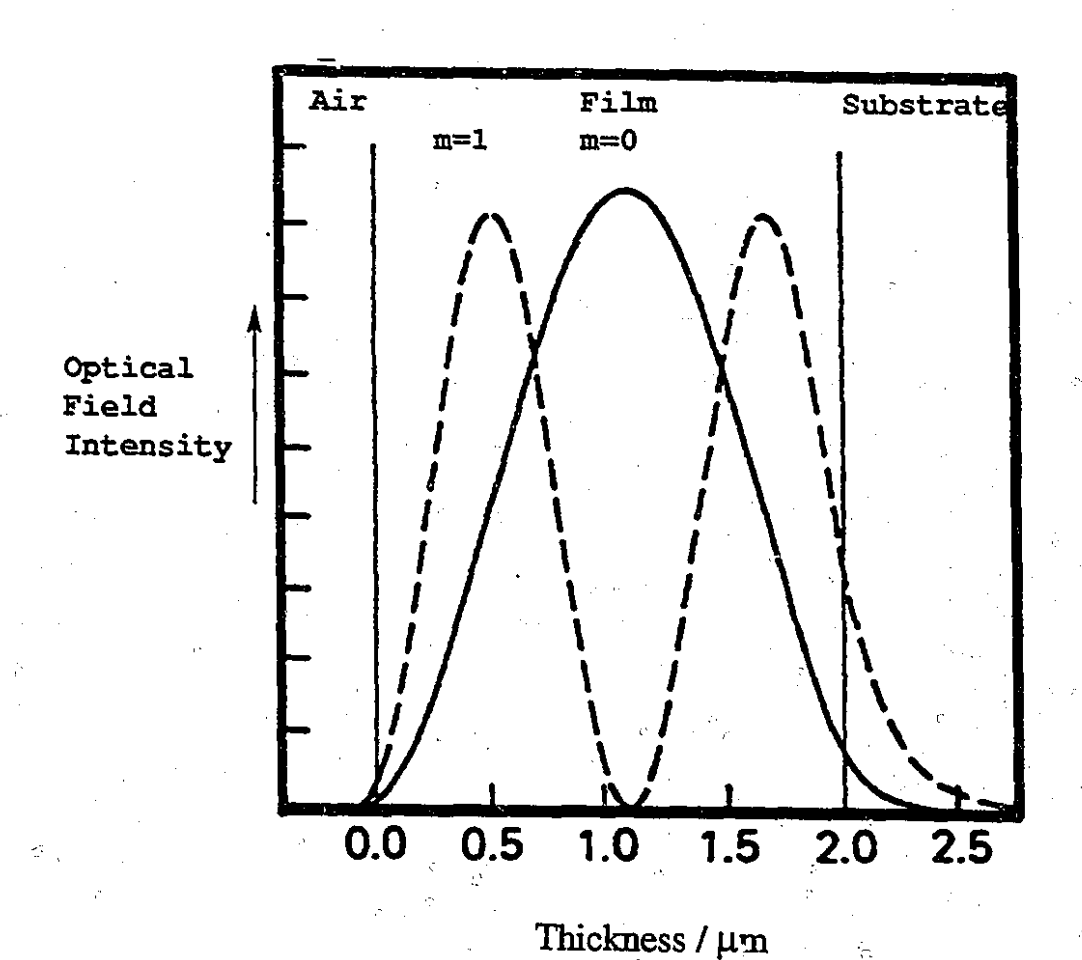


FIGURE 1.10 Optical field intensity distribution (TE wave) for a 2 μm waveguide for m = 0 and m = 1 modes. Evanescent tails are shown in the air superstrate and the substrate dielectric. (Adapted from Rabolt, J. F.and Swalen, D. in Spectroscopy of Surfaces; Clark, R. J. H.; Hester, R. E.Wiley: New York, 1988; Vol. 16, Ch.1.)

plane wave reflections between the film/superstrate (air) and film/substrate interfaces) are complex. The imaginary component arises from absorption losses in the waveguide. Small adsorption losses are necessary to allow for a calculated minimum. Thus, equation (1.9) can provide a means of calculating the waveguide modes, their characteristic angles and their optical fields in terms of reflection and transmission coefficients of each layer. A typical optical field intensity distribution is shown in Figure 1.10 for two different modes. This shows that the optical field near the substrate/film interface may be enhanced by changing the mode number (m = 0 to m = 1). This change can be made by altering the phase-matching coefficients in equation (1.9). For a given film and refractive index, the condition may be changed by altering the propagation angle. This is achieved by rotating the input beam. Alternatively, the film thickness to or refractive index n may be changed.

# 1.5.4.4 Combining WRS and SERS

The combination of WRS with SERS employing typical SERS-active bulk metal substrates cannot support the requirements of an integrated optical waveguide because of the extremely high absorptivity of bulk metals at visible wavelengths.⁶⁸ Since the unique optical properties of metal colloids are controlled by the degree of aggregation and cluster size, ⁶⁸ immobilization of SERS-active metal colloids on surfaces in nanoscale dimensions can lend itself to waveguide fabrication. Such a thin film structure was recently fabricated which is capable of SERS activity while retaining optical and geometric requirements for waveguiding. This complete waveguide-SERS substrate has been introduced as an integrated optics, evanescent wave, surface-enhanced Raman scattering (IOEW-SERS) technique.⁶⁹ This thin film assembly uses the sulfur termini of 3-mercaptopropyl-trimethoxysilane (3-MPT) grafted onto a glass film (glass microscope coverslip) to bind colloidal silver particles from an aqueous sol. The 3-MPT is chemically grafted onto a glass substrate, i.e., microscope coverglass slide, after subsequent hydrolysis and condensation reactions of the alkoxide termini to form siloxane bonds. The unreacted thiol

بيزغ

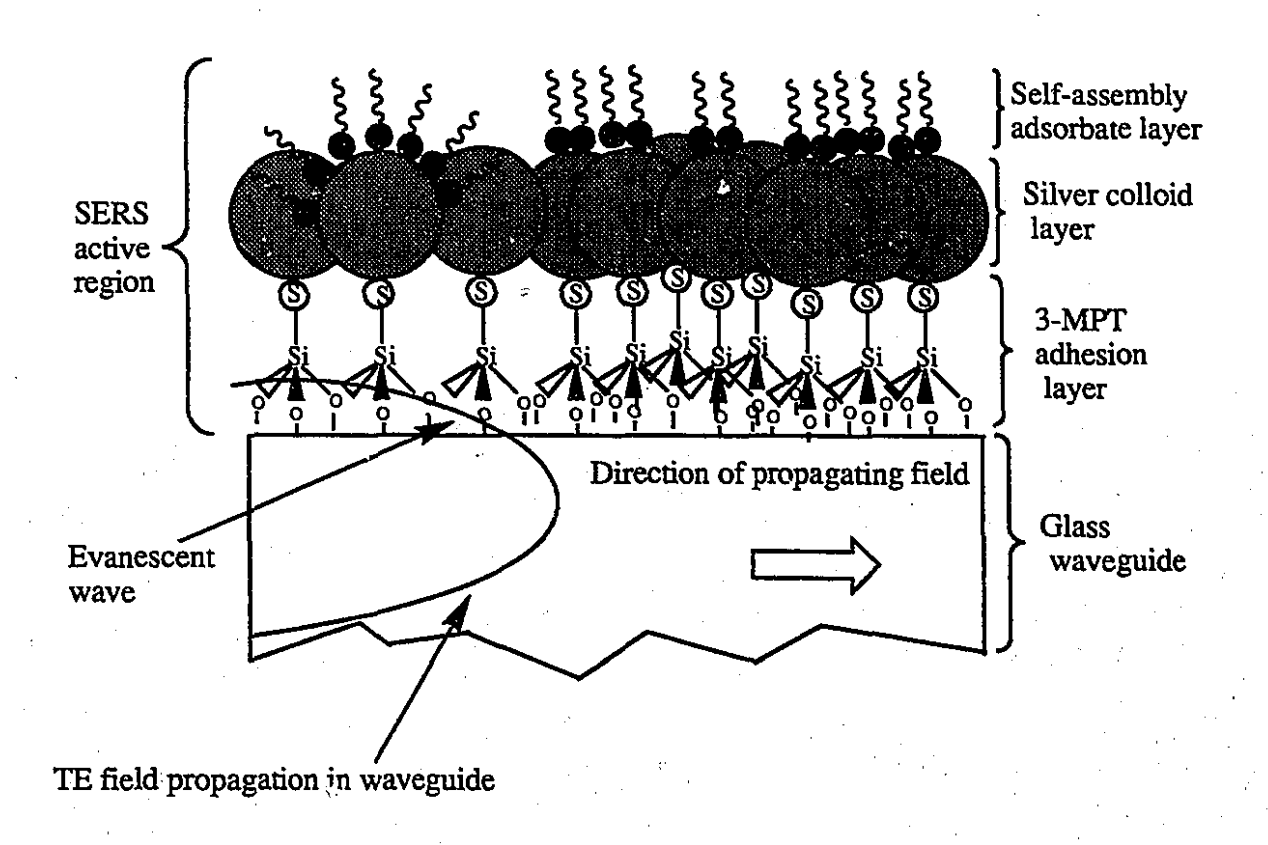


FIGURE 1.11 A schematic diagram of the heterostructure assembly, glass/3-MPT/Ag colloid, of the IOEW-SER substrate with an adsorbate layer, . The propagating evanescent wave, TE mode (----) leaks into the 3-MPT/Ag colloid overlayers increasing the Raman scattering cross section and enhancing the surface adsorbate vibrations. The adsorbate is immobilized on the Ag colloid surface.

termini can then bond covalently to a metal through the sulfur atoms. Immersion of the 3-MPT-derivatized glass in a dilute hydrosol of silver produces a 2-D colloidal silver array bonded to the surface. The IOEW-SERS assembly is illustrated in Figure 1.11. Using this approach, the deposition is thin enough to allow the evanescent wave to penetrate the colloidal silver layer and, in doing so, acts to intensify the effective cross-section for SERS. Thus a 2-D array of silver colloidal particles grafted onto a planar glass waveguide can support a propagating optical field while enhancing the evanescent optical field. Typical SERS analytes (e.g., pyridine and its derivatives) are able to adsorb passively on to the waveguide colloidal surface from solution. The propagating evanescent wave, TE mode (----) leaks into the 3-MPT/Ag colloid overlayers increasing the Raman scattering cross section and enhancing the surface adsorbate vibrations.

There are a number of advantages realized by both the spectroscopic technique and substrate assembly process in IOEW-SERS.

- (1) The self-assembly of colloidal Ag particles allows for a macroscopic surface that has a well defined and uniform nano-scale architecture. This process is highly reproducible (as with all nano-scale technology preparation it is crucial that all glassware and reagents are clean and purified). Controlling nano-structure is currently a central focus throughout materials research.
- (2) The entire waveguide preparation is inexpensive, simple to prepare and can be scaled up. Derivatized waveguides are stable for about one week (stored under N₂).
- (3) This solution-based process is extremely general, encompassing a number of substrates besides glass coverslips, viz., quartz slides and silicon wafers and for uses other than waveguiding, i.e., indium tin oxide surfaces, ⁷⁰ the glass face of a spectroeletrochemical cell, unmodified  $SiO_x$  coated TEM grids and the inside of a capillary tube. ⁷¹

- (4) The nature of waveguiding allows both lateral and depth spectral profiling of the waveguide. The derivatized waveguide behaves as an interfacial vibrational probe, revealing information about the waveguide and metal/adsorbate interfaces.
- (5) The construction of these waveguides can be generalized to explore a range of surface chemistries in gas and liquid phase (flow cell) environments, variable temperatures and chemical sensors.

# 1.6 SELF-ASSEMBLING MONOLAYERS (SAM)

Alkylthiol self-assembling monolayers (SAM's) are probably the most intensively studied SA monolayers on gold and silver surfaces, mainly due to their stability, organization, and potential application as basic building blocks for novel microstructures. SAM's can also be extended to aromatic thiols, dialkylsulfides and dialkyldisulfides on gold, organosilicon on hydroxylated surfaces and fatty acids on oxidized aluminum and silver. 62,72,73 A self-assembling molecule structure, from an energetics point of view, consists of three basic parts, a head group, a central alkyl or aromatic group and a terminal group. The head group provides the most exothermic process - chemisorption on the substrate surface. This can be covalent Si-O, in the case of organosilanes on hydroxylated surfaces, or a covalent but highly polar Au-S bond, in the case of alkylthiols. Chemisorption is a spontaneous process which brings molecules close together for short range van der Waals forces to become important. The second molecular part is for example an alkyl chain which can form an ordered and closely packed array through intramolecular van der Waals and electrostatic interactions. The third molecular part is the terminal functionality, e.g., CH3, OH, COOH, NH2 and PO3H. These surface groups introduce a range of different chemical properties to the substrate surface on a macromolecular scale such as hydrophilic/hydrophobic, acid/base, charge transfer, ion-binding and hydrogen bonding interactions. Self-assembly and related techniques have thus provided a means to fabricate, at ambient temperature and in an ordinary laboratory environment, interfaces of well-defined structure. Such a capability brings to mind applications in thin film technology, including optics, coatings for lubrication, adhesion, wetting and protection, sensors and transducers and biomolecular films.

# 1.6.1 Mercaptopyridine

In contrast with the extensive research on SA monolayers of alkylthiols, little attention has been given to aromatic thiol monolayers. 74-77 There have been some reports

on the SERS of an ambidentate ligand, 4-mercaptopyridine (4-MPy).  $^{78-80}$  Spectral interpretation was limited, however, to pH dependence, electrode potential dependence and electron transfer of cytochrome c on 4-MPy-modified Au electrodes. Recently, a series of articles by Crooks et al.  81  has demonstrated that 4-MPy modified Au electrodes exhibit a pH-dependent electrostatic binding interaction with probe molecules, shown by voltammetric capacitance experiments. This ambidentate ligand has multiple binding sites available; pyridine nitrogen, thiol and the  $\pi$ -ring and therefore a number of possible modes of adsorption and concomitant orientation can occur on a metal surface. Being a derivative of pyridine, 4-MPy is an intense Raman scatterer and has a relatively simple vibrational profile. SERS is an ideal spectroscopic technique to probe the substrate/adsorbate interface and provide a vibrational fingerprint of the metal-adsorbate interaction and adsorbate orientation. Furthermore, apart from pH studies,  80  interactions between 4-MPy and liquid-phase probe molecules or ions have not been observed previously by a vibrational technique. SERS thus offers the capability of characterizing the chemical interactions with surface-confined 4-MPy molecules at a molecular level.

#### 1.7 AIMS AND STRUCTURE OF THE THESIS

The principle subject of this thesis is the surface enhanced Raman spectroscopic study of adsorbates: pyrazinamide, and 2- and 4-mercaptopyridine. The approach to this study is threefold. Firstly, a novel SERS technique, IOEW-SERS is introduced. Its use as a spectroscopic tool to study surface-confined adsorbates will be demonstrated using 4,4'bipyridine. Secondly, the SERS of 2- and 4-mercaptopyridine is investigated for a range of SERS-active Ag substrates, e.g., Ag colloids, MELLFs, IOEW-SERS and roughened Ag electrodes. A comparative study of IOEW-SERS is made with these more classic SERS-active metal substrates to establish the extent to which the SERS effect is coextensive from one system to another. The fundamental aspects of adsorbate orientation and mode of adsorption are addressed. An attempt is made to compare the molecule/substrate interaction at liquid/liquid (colloid), metal/liquid (Ag electrode) and metal/molecular layer (ex situ IOEW-SERS and MELLFs) interfaces by way of Raman, TEM and XPS measurements. An additional SERS study of pyrazinamide using MELLFs is also discussed. Thirdly, we take advantage of the previously-demonstrated ion-binding capability of surface-bound 4-mercaptopyridine and investigate intermolecular interactions of this adsorbate with probe ions, viz., Cu²⁺ and H⁺ using SERS techniques: IOEW-SERS and Ag electrodes and XPS. The potential use of derivatized planar waveguides as a chemical sensor is demonstrated.

The general outline of this thesis is as follows;

(1) Chapter 2. Surface Enhanced Raman Scattering of Mercaptopyridines and Pyrazinamide from Glass-Deposited Silver Metal Liquid-Like Films (MELLFs).

This chapter describes the preparation and SERS of MELLFs and organosol systems using pyrazinamide and 2- and 4-MPy compounds. The macro and microstructure of the Ag

colloid/adsorbate system vary with Ag content of the parent colloid and adsorbate concentration in the organic phase. The infrastructures of deposited films are characterized using TEM and SPA.

(2) Chapter 3. Integrated Optics, Evanescent Wave, Surface-Enhanced Raman Spectra (IOEW-SERS) of 4,4'-Bipyridine.

This chapter describes a new technique combining integrated optics, WRS and SERS. The preparation of SERS-active waveguides, derivitization with a classic SERS-active adsorbate and the similarity of IOEW-SERS with other SERS substrates are discussed.

(3) Chapter 4. Surface Enhanced Raman Scattering of Mercaptopyridines and the Fabrication of a Metal-ion Chemical Sensor Based on Integrateu Optics, Evanescent Wave, Surface Enhanced Raman Scattering (IOEW-SERS).

The orientation and mode of adsorption of 2- and 4-MPy molecules on a waveguide colloidal surface are characterized by IOEW-SERS technique. A comparison of IOEW-SERS is made with Ag colloid sols and MELLFs. The ambidentate functionality of 4-MPy is explored by exposing the surface-confined 4-MPy layer on the waveguide surface to probe ions such as Cu²⁺ and H⁺. Spectral changes associated with 4-MPy pyridine nitrogen-probe ion interaction are discussed. The layer-by-layer construction of the 4-MPy derivatized waveguide, including exposure to Cu²⁺, is followed by using XPS.

(4) Chapter S. Potential Dependence of Surface Enhanced Raman Scattering of 4-Mercaptopyridine on Silver Electrodes and the Interaction with Copper(II) ions.

The potential dependent behaviour of 4-MPy adsorbed on an Ag electrode is discussed. The ambidentate nature of 4-MPy is utilized by the potential change at the electrode surface,

where either the pyridine nitrogen or thiolate sulfur are adsorbed preferentially to the Ag electrode over different potential ranges. The contribution of a CT mechanism to the intensity enhancement profile is investigated by wavelength and potential dependence. Probe Cu²⁺ ions are added to the electrolyte solution and the spectral changes observed are discussed in terms of a Cu-4-MPy pyridine nitrogen interaction at the electrode surface.

# (5) Chapter 6. Summary.

This chapter contains conclusions, claims to original research, and suggestions for future work.

#### REFERENCES

- (1) Smekal, A. Naturwissenschaft 1923, 11, 973.
- (2) Raman, C.; Krishnan, F. Nature 1928, 121, 501.
- (3) Harris, D. C.; Bertolucci, M. D. Symmetry and Spectroscopy: An Introduction to Vibrational and Electronic Spectroscopy.; Dover: New York, 1978.
- (4) Lin-Vien, D.; Colthup, N. B.; Fateley, W. G.; Grasselli, J. G. Handbook of Characteristic Infrared and Raman Frequencies of Inorganic Compounds; Academic Press: San Diego, 1991.
- (5) Asher, S. A. Ann. Rev. Phys. Chem. 1988, 39, 537.
- (6) Spiro, T. G. Biological Applications of Raman Spectroscopy; Wiley: New York, 1987; Vol. 2.
- (7) Fleishmann, M.; Hendra, P.; McQuillan, A. J. Chem. Phys. Lett. 1974, 26, 163.
- (8) Jeanmaire, D.; Van Duyne, R. J. Electroanal, Chem. 1977, 84, 1.
- (9) Albrecht, M.; Creighton, J. J. Am. Chem. Soc. 1977, 99, 5215.
- (10) Creighton, J. A. in Spectroscopy of Surfaces; Clark, J. H.; Hester, R. E.; Eds., Wiley: New York, 1988; Vol. 16, Ch. 2, p37; (a), Metiu, H. Progress in Surface Sci. 1984, 17, 153; (b), Pettinger, B. in Adsorption of Molecules at Metal Electrodes, Lipokowski, J. and Ross, P. N. Eds., VCH: New York, 1992, Ch. 6, p 285, (c).
- (11) Cotton, T. M. in Spectroscopy of Surfaces; Clark, R. J. H.; Hester, R. E.; Eds., Wiley: New York, 1988; Vol. 16, Ch.3, p91
- (12) Chang, R. K.; Furtak, T. E. Surface Enhanced Raman Scattering; Plenum Press: New York, 1982.
- Brandt, E. S., and Cotton, T. M. in Investigations of Surfaces and Interfaces- Part
   B, Physical Methods of Chemistry Series; 2nd edition, Rossiter, B. W.; Baetzold,
   R. C. Eds., Wiley: New York, 1993; Vol. IXB, p633.
- (14) Otto, A.; Mrozek, I.; Grabhorn, H.; Akemann, W. J. Phys. Condens. Matter 1992, 4, 1143.
- (15) Moskovits, M. Rev. Mod. Phys. 1985, 57, 783.
- (16) Otto, A.; Billman, J.; Eickmans, J.; Erturk, U.; Pettenkoffer, C. Surf. Sci 1984, 138, 319.
- (17) Murray, C.; Allara, D. J. Chem. Phys. 1982, 76, 1290.
- (18) Lund, P. A.; Tevault, D. E.; Smardzewski, R. R. J. Phys. Chem. 1984, 88, 1731.

- (19) Lopez-Rios, T.; Pettenkofer, C.; Pockrand, I.; Otto, A. Surf. Sci. 1982, 121, 541.
- (20) Kerker, M. Acc. Chem. Res. 1984, 17, 271.
- (21) Wang, D.-S.; Chew, H.; Kerker, M. Appl. Opt. 1980, 19, 2256.
- (22) Kerker, M.; Wang, D.S.; Chew, H. Appl. Opt. 1980, 19, 4159.
- (23) Busby, C. C.; Creighton, J. A. J. Electroanal. Chem. 1982, 140, 379.
- (24) Wang, D.S.; Kerker, M. Phys. Rev. B 1981, 24, 1777.
- (25) Siiman, O.; Bumm, L. A.; Callagan, R.; Blatchford, C. G.; Kerker, M. J. Phys. Chem. 1983, 87, 1014.
- (26) Efrima, S. in *Modern Aspects of Electrochemistry*; Conway, B. E.; White, R. E.; Bokris, J. O., Eds., Plenum: New York, 1985; Vol. 16, p285.
- (27) Creighton, J. A. Surf. Sci. 1986, 173, 665.
- (28) Chase, B.; Parkinson, B. J. Phys. Chem. 1991, 95, 7810.
- (29) Ingram, J. C.; Pemberton, J. E. Langmuir 1992, 8, 2034.
- (30) Furtak, T. E.; Roy, D. Surf. Sci. 1985, 158, 126.
- (31) Guzonas, D. A.; Irish, D. E.; Atkinson, G. A. Langmuir 1990, 6, 1102.
- (32) Furtak, T. E.; Roy, D. Phys. Rev. Lett. 1983, 50, 1301.
- (33) Lombardi, J. R.; Birke, R. L.; Lu, T.; Xu, J. Chem. Phys. 1986, 84, 4174.
- (34) Macomber, S. H.; Furtak, T. E. Surf. Sci. 1982, 122, 556.
- (35) Gersten, J. I.; Birke, R. L.; Lombardi, J. R. Phys. Rev. Lett. 1979, 43, 147.
- (36) Adrian, F. J. J. Chem. Phys. 1982, 77, 5302.
- (37) Wetzel, H.; Gerisher, H.; Pettinger, B. Chem. Phys. Lett. 1981, 78, 392.
- (38) Moskovits, M. J. Chem. Phys. 1982, 77, 4408.
- (39) Creighton, J. A. Surf. Sci. 1983, 124, 209.
- (40) Creighton, J. A. Surf. Sci. 1985, 158, 211.
- (41) Creighton, J. A.; Blatchford, C. G.; Albrecht, J. J. Chem. Soc. Faraday Trans. 1979, 75, 790.
- (42) Kerker, M.; Wang, D. S.; Chew, H. Appl. Opt. 1980, 19, 2256.
- (43) Fornasiero, D.; Grieser, F. J. J. Colloid Interface Sci. 1991, 141, 168.
- (44) Blatchford, C. G.; Campbell, J. R.; Creighton, J. A. Surf. Sci. 1982, 120, 435.
- (45) Clippe, R.; Evrard, R.; Lucas, A. A. Phys. Rev. B 1976, 14, 1715.
- (46) Bard, A. J.; Faulkner, L. Electrochemical Methods, Fundementals and Applications; Wiley: New York, 1980.
- (47) Chang, R. K. and Laube, B. L. in *CRC Critical Reviews in Solid State and Materials Science*, CRC Press: Baton rouge, Florida, 1984, Vol.12, p1.

- (48) Gale, R. J. Spectroelectrochemistry: Theory and Practice; Plenum Press: New York, 1988.
- (49) Tuschel, D. D.; Pemberton, J. E. Langmuir 1988, 4, 58.
- (50) Al-Obaidi, A. H. R.; Rigby, S. J.; McGarvey, J. J.; Walmsley, D. G.; Smith, K. W.; Hellemans, L.; J., S. J. Phys. Chem. 1994, 98, 11163.
- (51) Bell, S. E. J.; McGarvey, J. F.; Rigby, S. J. J. Raman Spectrosc. 1991, 22, 763.
- (52) Yogev, D.; Efrima, S. J. Phys. Chem. 1988, 92, 5754.
- (53) Vlckova, B.; Barnett, S. M.; Kanigan, T.; Butler, I. S. Langmuir 1993, 9, 3238.
- (54) Yogev, D.; Deutsch, M.; Efrima, S. J. Phys. Chem. 1989, 93, 4174.
- (55) Yogev, D.; Efrima, S. J. Colloid and Interface Sci. 1991, 147, 88.
- (56) Yogev, D.; Edelstein, R.; Efrima, S. J. Colloid and Interface Sci. 1991, 147, 78.
- (57) Farbman, I.; Efrima, S. J. Phys. Chem. 1992, 96, 8469.
- (58) Krech, J.; Lorenc, C.; Bradley, M. J. Colloid and Interface Sci. 1992, 153, 437.
- (59) Cermakova, K.; Vlckova, B.; Foft, V.; Lednicky, F. J. Mol. Struct. 1995, 349, 129.
- (60) Levy, Y.; Imbert, C.; Ciprani, J.; Racine, S.; Dypeyrat, R. Opt. Commun. 1974, 11, 66.
- (61) Yoldas, B. E. Appl. Opt. 1982, 21, 2960.
- (62) Swalen, J. D.; Rieckhoff, K. E.; Tacke, M. Opt. Com. 1978, 24, 146.
- (63) Tien, P. K. Rev. Mod. Phys. 1977, 49, 361.
- (64) Kanigan, T. Ph.D. Thesis 1995, McGill University, Montreal, Canada,
- (65) Rabolt, J. F. and Swalen, J. D. in *Spectroscopy of Surfaces*; Clark, R. J. H.; Hester, R. E., Eds.; Wiley: New York, 1988; Vol. 16, Ch1, p1.
- (66) Born, M.; Wolf, E. Principles of Optics; Pergamon: Oxford, 1975.
- (67) Heavens, O. S. Optical Properties of Thin Solid Films; Dover: New York, 1965.
- (68) Kreibeig, U. Light Scattering by Small Particles; Wiley: New York, 1981.
- (69) Andrews, M. P.; Xu, W. Manuscript in preparation
- (70) Doron, A.; Katz, E.; Willner, I. Langmuir 1995, 11, 1313.
- (71) Freeman, G. R.; Grabar, K. C.; Allison, K. J.; Bright, R. M.; Davis, J. A.; Guthrie, A. P.; Hommer, M. B.; Jackson, M. A.; Smith, P. S.; Walter, D. G.; Natan, M. J. Science 1995, 267, 1629.
- (72) Sabatani, E.; Cohen-Boulakia, J.; Breuning, M.; Rubeinstein, I. Langmuir 1993, 9, 2981.
- (73) Ulman, A. Ultrathin Organic Films from Langmuir-Blodgett to Self Assembly; Academic: New York, 1991.
- (74) Joo, T. H.; Yim, Y. H.; Kim, K.; Kim, M. S. J. Phys. Chem. 1989, 93, 1422.

- (75) Garrell, R. L.; Szafranski, C.; Tanner, W. SPIE Proceedings: Raman and Luminescence Spectrosc. in Tech. 1990, 1336, 264.
- (76) Gui, J. Y.; Stern, D. A.; Frank, D. G.; Lu, F.; Zapien, D. C.; Hubbard, A. T. Langmuir 1991, 7, 955.
- (77) Carron, K.; Hurley, L. G. J. Phys. Chem. 1991, 95, 9979.
- (78) Bryant, M. A.; Joa, S. L.; Pemberton, J. E. Langmuir 1992, 8, 753.
- (79) Taniguichi, I.; Iseki, M.; Yamaguchi, H.; Yasukouchi, K. J. Electroanal. Chem 1985, 186, 299.
- (80) Mullen, K. I.; Wang, D.; Crane, G. L.; Carron, K. T. Anal. Chem. 1992, 64, 930.
- (81) Jones, T. A.; Perez, G. P.; Johnson, B. J.; Crooks, R. M. Langmuir 1995, 11, 1318.

# CHAPTER 2

SURFACE ENHANCED RAMAN SCATTERING OF MERCAPTOPYRIDINES AND PYRAZINAMIDE IN GLASS-DEPOSITED SILVER METAL LIQUID-LIKE FILMS

#### 2.1 SUMMARY

This Chapter describes the preparation procedure for MELLFs/organosols using pyrazinamide and 2- and 4- mercaptopyridine as the adsorbates. Pyrazinamide and 2- mercaptopyridine form Ag colloid-adsorbate films at the interface between an aqueous Ag colloid and a solution of an adsorbate in dichloromethane. In comparison, 4- mercaptopyridine is the only adsorbate for which an interphase transfer of adsorbate-covered particles occurs from aqueous to organic phase forming adsorbate-colloid aggregates, described as an organosol. All adsorbate films and organosol samples were investigated by SERS. We demonstrate that for a particular adsorbate, the process of film and/or organosol formation, as well as the microstructure of the film and ultimately the SERS spectrum are influenced substantially by the Ag content of the parent Ag colloid and by the adsorbate itself. Transmission electron microscopy, optical microscopy and surface plasmon absorption techniques are used to characterize the MELLFs and organosol structures. Furthermore, we show by using SERS, that for 2-MPy interfacial films, the adsorbate concentration in the dichloromethane solution influences the orientation of 2-MPy relative to the Ag surface.

#### 2.2 INTRODUCTION

Glass-deposited Ag colloid-adsorbate films containing a variety of adsorbates such as N-bases,  1,2  porphyrins  2,3  and 17-ethynylestradiol,  4  have been analyzed by TEM and comparisons with previously reported MELLFs discussed. Both fractal and non-fractal monolayer films were prepared independent of the chemical nature of the adsorbate. A hypothesis relating the chemical nature of the adsorbate, the mechanism of formation of interfacial Ag-colloid-adsorbate film and the resulting fractal and/or non fractal structure of the film has also been presented. Furthermore, a transition from a non-fractal to fractal structures has been observed upon perturbation of the Ag-TPyP film in its interfacial state. Three types of Ag-colloid-adsorbate structures were discussed: fractal clusters of Ag colloidal particles (where the fractal dimensionality, D = 1.2), non-fractal monolayers of Ag colloidal particles (D = 1.97) and fractal, close to monolayer structures consisting of Ag colloidal particle clusters (D = 1.85). According to the hypothesis presented, the different structural types of Ag colloid-adsorbate films originate from differences in the mechanisms of aggregation which, in turn, result from differences in the chemical nature of the adsorbate (in particular, its hydrophobic/hydrophilic character).

In this Chapter, we further explore the factors influencing the structure of Agcolloid-adsorbate films. Attention has focused on the possibility of influencing the
mechanism of formation of a particular Ag colloid-adsorbate film in such a way that more
than one structural form of the particular Ag colloid-adsorbate film could be obtained. In
this study, the range of adsorbates incorporated into Ag colloid-adsorbate films is extended
to include pyrazinamide (pza), 4-mercaptopyridine (4-MPy) and 2-mercaptopyridine (2MPy). A previously unobserved mechanism of Ag colloid-adsorbate film formation is
reported for 4-MPy. All structural forms of the newly prepared films are investigated by
SERS and the effects of the particular film structure on the frequencies of the adsorbate
bands are discussed.

#### 2.3 EXPERIMENTAL

Materials. 2- and 4-Mercaptopyridine (Aldrich) were sublimed in vacuo immediately prior to use. Pyrazinamide (Aldrich) and all other reagents were used as received. Sodium borohydride (99+%, Janssen Chimica) and silver nitrate (p.a. Aldrich) were used for the Ag colloid preparations. Interfacial films were prepared using dichloromethane (UV spectral grade, ACS chemicals). High-purity water was obtained from a Milli-Q Ultrapure Millipore water system and was used in all preparations.

**Preparation Procedures.** Ag colloids were prepared by reduction of AgNO₃ with NaBH₄ following a procedure described previously.⁹ For Ag colloid I, the procedure was followed exactly, the concentration of silver being 9 mL of 2.2 x 10⁻³ M AgNO₃. For Ag colloid II, the procedure was modified by using 15 mL of 2.2 x 10⁻³ M AgNO₃. The surface potential of each Ag colloid differs, as the ratio of AgNO₃:NaBH₄ is different. The difference, however, is not crucial, as NaBH₄ is present in large excess.

Preparation of Silver-4-MPy Salt. To prepare the silver-4-MPy salt, equimolar quantities of AgNO₃ and 4-MPy (0.05 mol) were dissolved in ethanol/water solution to yield a pale yellow precipitate of silver-4-MPy. The precipitate was filtered, rinsed with ethanol and water, and then dried under vacuum. The FT-Raman spectra of 4-MPy and the silver-4-MPy complex were measured on the solid samples.

Preparation of Interfacial Ag Colloid-Pyrazinamide (Ag-pza) Films. The Agadsorbate films were prepared in a two-phase system consisting of an aqueous Ag colloid and a solution of the adsorbate in dichloromethane. The preparation of interfacial films and deposition on microscope glass slides followed the procedure described previously. Both Ag colloid I and II were used in the preparation of Ag-pza I and II films, respectively. The optimum results were obtained by mixing equal volumes (2 mL) of an aqueous Ag colloid and a dichloromethane solution of pza (2 x 10⁻³ M) in a tall, cylindrical, stoppered vial (5 mL). The mixture was shaken vigorously. The Ag-pza I films were formed within 1-2 min and two interfaces covered by Ag-pza I films were observed in this system-an upper

film on the surface of the aqueous phase and a lower interfacial film between the aqueous-dichloromethane phases. The lower film at the interface was removed carefully by immersing a small piece of glass slide (0.7 cm²) through the aqueous phase and then the film, which cracks. The film was then transferred onto the glass by lifting the glass from underneath the film and slowly withdrawing the glass with the adhered film back through the aqueous phase. However, before the lower phase was removed, the upper film was deposited on a glass slide in the same manner. As the lower phase of the two phase system is the organic phase, the upper film was deposited on a glass slide "organic phase up" and the lower "aqueous phase up". The Ag-pza II films were formed rapidly within 20 s and only one interface (the lower) was produced. This film was thus deposited on a glass slide "aqueous phase up."

Preparation of Ag Colloid-Mercaptopyridine (Ag-4-MPy and Ag-2-MPy) Films. Both Ag colloid I and II were used in the preparation of Ag-4-MPy I and II films, respectively. The concentration of 4-MPy in the dichloromethane solution was 2 x 10⁻³ M. Even after vigorous shaking, formation of an interfacial film was not observed. Instead, the Ag colloidal particles were transferred from the aqueous to the dichloromethane phase producing a yellow-orange organosol in which macroscopic aggregates (which appear as a cloudy particulate suspension) were formed at the interface. In the case of Ag-4-MPy I, the aggregates were brown while for the Ag-4-MPy II sample they were of a bright orange color. When deposited on a glass slide, the aggregates formed by Ag colloid I remained brown, while the orange aggregates of Ag colloid II changed color upon deposition and after the residual dichloromethane was evaporated, formed a lustrous, blue-violet film.

Interfacial Ag-2-MPy I films were prepared with Ag colloid I by vigorously shaking equal volumes (2 mL) of an aqueous Ag colloid and a dichloromethane solution of 2-MPy. (1 x  $10^{-3}$  M and 2 x  $10^{-5}$  M). Interfacial films were formed after 1 min of shaking and after deposition onto a glass slide showed a metallic lustrous appearance. No such film formation was observed using Ag colloid II.

Preparation of Ag Colloid/Mercaptopyridine and Ag Colloid/Pyrazinamide Systems. The Ag colloid/2-MPy system was prepared by adding an aqueous solution of 2-MPy (60  $\mu$ L of 1 x 10⁻³ M) to 2mL of the Ag colloid I. The colloid aggregated immediately turning a purple color. Similarly, the Ag colloid / 4-MPy system was prepared by adding an aqueous solution of 4-MPy (10  $\mu$ L of 2 x 10⁻⁴ M) to 2 mL of Ag colloid I. In this case, aggregation forming a purple-brown color was slow and the optimal SERS spectrum could be collected only after 12 hrs of aging. The Ag colloid/pza system was prepared by adding an aqueous solution of pza (50  $\mu$ L of 2 x 10⁻³ M) to 2 mL of Ag colloid I. Aggregation to a purple color occurred immediately. For the SERS measurements, the Ag colloidal mixtures were transferred to a capillary sample cell.

Instrumentation. All SERS spectral data were obtained using 514.5 nm (50 mW) radiation from a Spectra Physics Model 164 Ar+-laser. The detector system consisted of a liquid N2-cooled charged coupled device (CCD) interfaced to an Instruments S.A. HR640 spectrograph equipped with a holographic grating (1800 grooves mm⁻¹). The exciting radiation was focused into the glass-deposited film at a small angle adjustable by rotation of the laser beam using a computer controlled precision rotation stage. The Rayleigh scattering was removed by a Raman holographic edge filter (Physical Optics Corp.). The acquisition time employed was typically 30 s, for each 500 cm⁻¹ window. The FT-Raman spectra of 4-MPy powder and the silver 4-MPy complex were recorded on a Bruker IFS-88 spectrometer equipped with an FRA-105 Raman module and a liquid N2-cooled proprietary detector. The spectra were excited with a Nd3+:YAG laser operating at 1064.1 nm (150 mW), with 250 scans being typically collected. Surface plasmon absorption (SPA) spectra were measured with a Hewlett Packard HP 8452 UV/vis diode array spectrometer. Optical microscopy images of the Ag-pza samples were obtained using a Zeiss microscope equipped with a 40 x objective. The images were collected with a Sanyo color CCTV camera and were displayed on a Panasonic Video monitor, from which the photographs

were taken by a Polaroid camera. Transmission electron microscopy photographs were obtained with a Philips 410LS (80 kV) TEM, (Eindoven, Holland).

/*

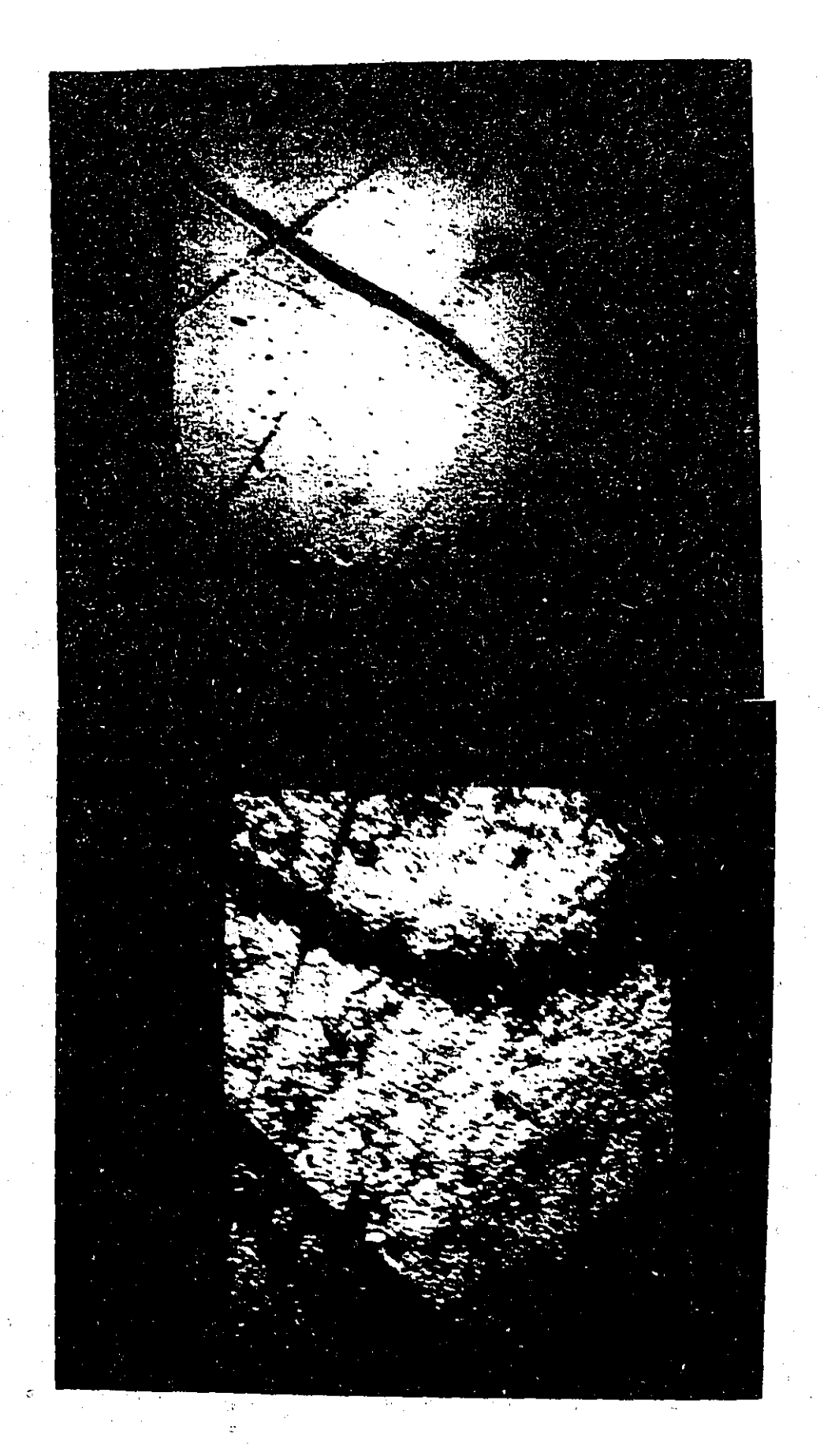
#### 2.4 RESULTS AND DISCUSSION

# 2.4.1 Ag Colloid-pza Films

The process of Ag colloid-pza film formation is influenced substantially by the Ag content of the parent Ag colloid. The factor of 1.7 increase of Ag content in Ag colloid II, by comparison with Ag colloid I, resulted in an increase in the rate of interfacial film formation from 1-2 min to 20 s and produced only one interfacial film (covering the water-dichloromethane interface) instead of two films (covering both the upper aqueous phase and lower dichloromethane-water interface). Optical micrographs of Ag colloid II-pza (Agpza II) and Ag colloid I-pza (Agpza I) films deposited from the water-dichloromethane interface are compared in Figure 2.1 [micrographs (A) and (B), respectively]. Structural differences can be observed between the two films. While Agpza I film is a continuous layer structure (probably a multilayer), the Agpza II film consists of aggregate Ag colloidal particles. Surface plasmon absorption (SPA) curves from both films are compared in Figure 2.2, [spectra (A) and (B)]. Both the optical micrographs and the SPA curves of Agpza II film resemble those of the deposited Ag colloidal aggregates 10,11 which have been shown to be composed of a fractal structure. 12-14 We did not undertake any electron microscopy studies to confirm whether or not the deposits were fractal.

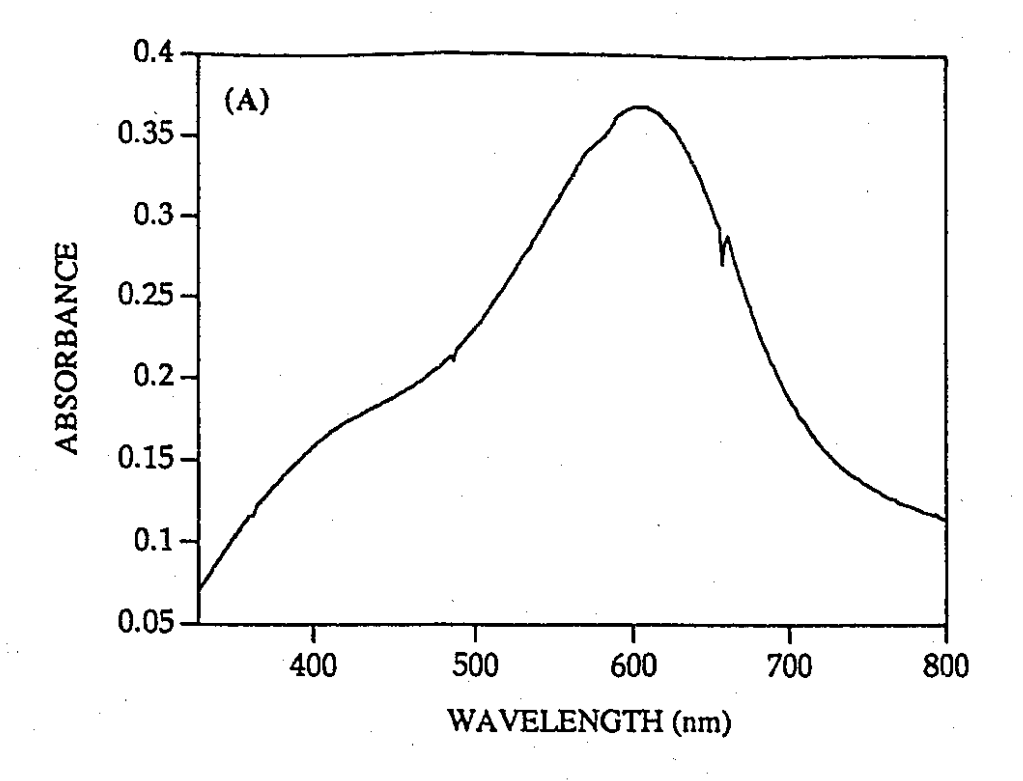
The SERS spectra of Ag-pza I (both aqueous and organic) and Ag-pza II films are compared in Figure 2.3. The SERS spectrum of the Ag colloid/pza system and the normal Raman spectrum of neat pza are compared in Figure 2.4. The vibrational assignments presented in Table 2.1 are based mainly on those reported previously,  15,16  as well as the assignments given for the normal Raman and SERS of pyrazine. The SERS spectra of all types of Ag-pza films show spectral bands of pza analogous to those of the Ag colloid/pza system, which, in turn, are in a good agreement with those previously reported. The band at 1630 cm⁻¹ in the Ag colloid/pza spectrum can be attributed to either a  $\delta(\text{H}_2\text{O})^{20}$  or an amide II [ $\delta(\text{NH}_2)$ ] band. Two weak and broad bands at ca. 620 and 930 cm⁻¹, observed in the SERS spectra of all types of Ag-pza films, are attributed to

FIGURE 2.1 Optical micrographs of Ag colloid II-pza (Ag-pza II) (A), and Ag colloid I-pza (Ag-pza I) (B) films deposited from the water-dichloromethane interface (magnification x40).



53

(B)



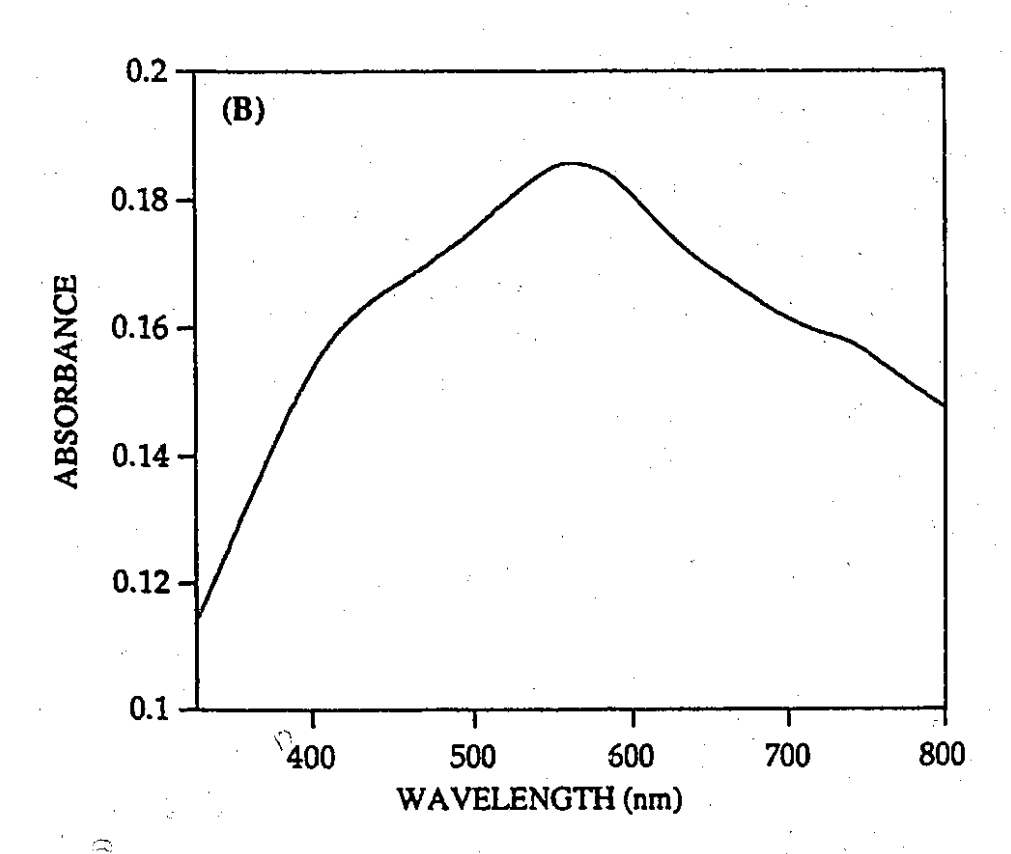


FIGURE 2.2 Surface plasmon absorption (SPA) curves of Ag colloid I-pza (Ag-pza I) (A), and Ag colloid II-pza (Ag-pza II) (B), films deposited from the water-dichloromethane interface. The small peak near 700 nm in the SPA curve (A) is artifact from a pixel.

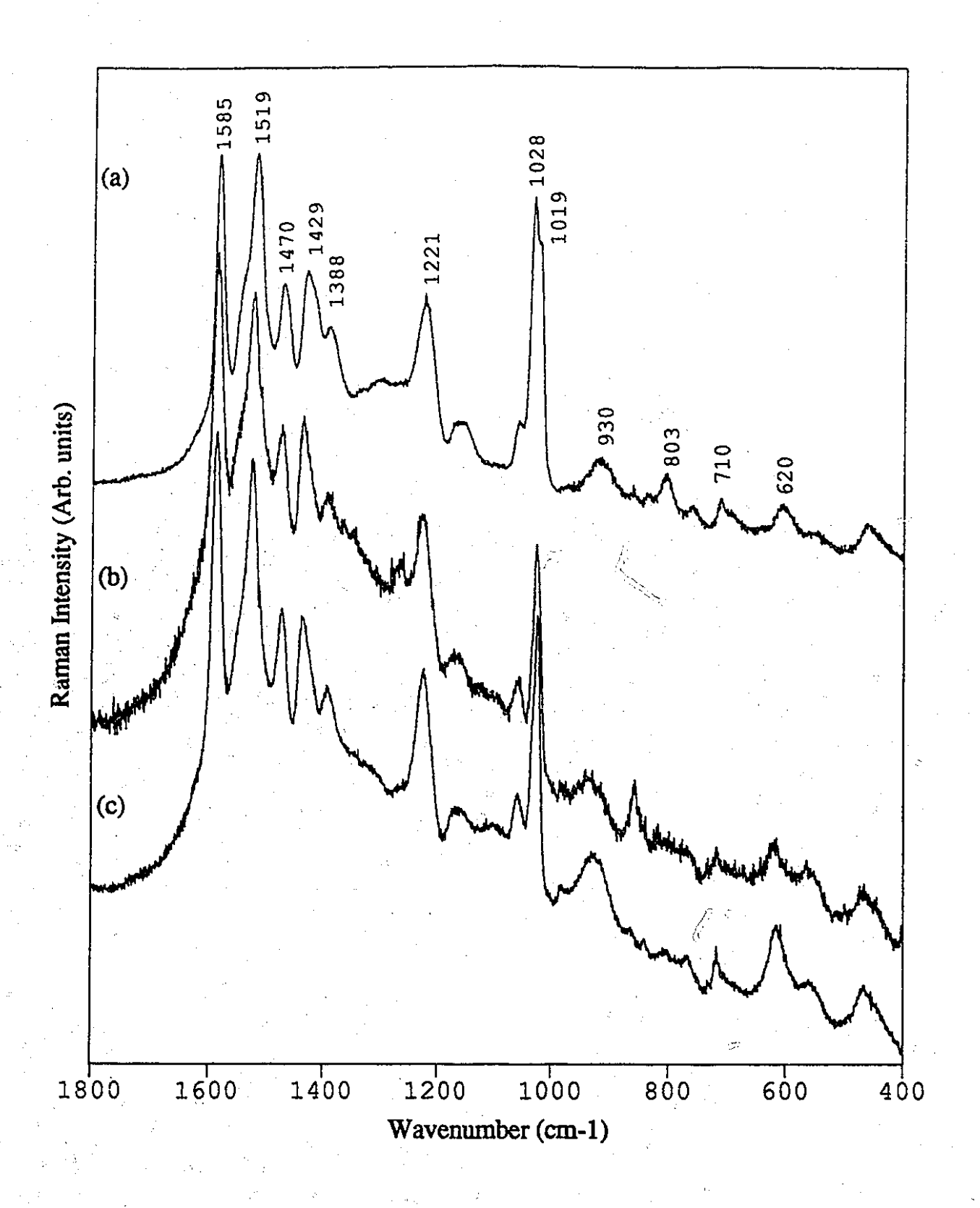


FIGURE 2.3 SERS spectra of Ag-pza II (a), Ag-pza I (aqueous layer) (b), and Ag-pza I (organic layer) (c), glass deposited films.

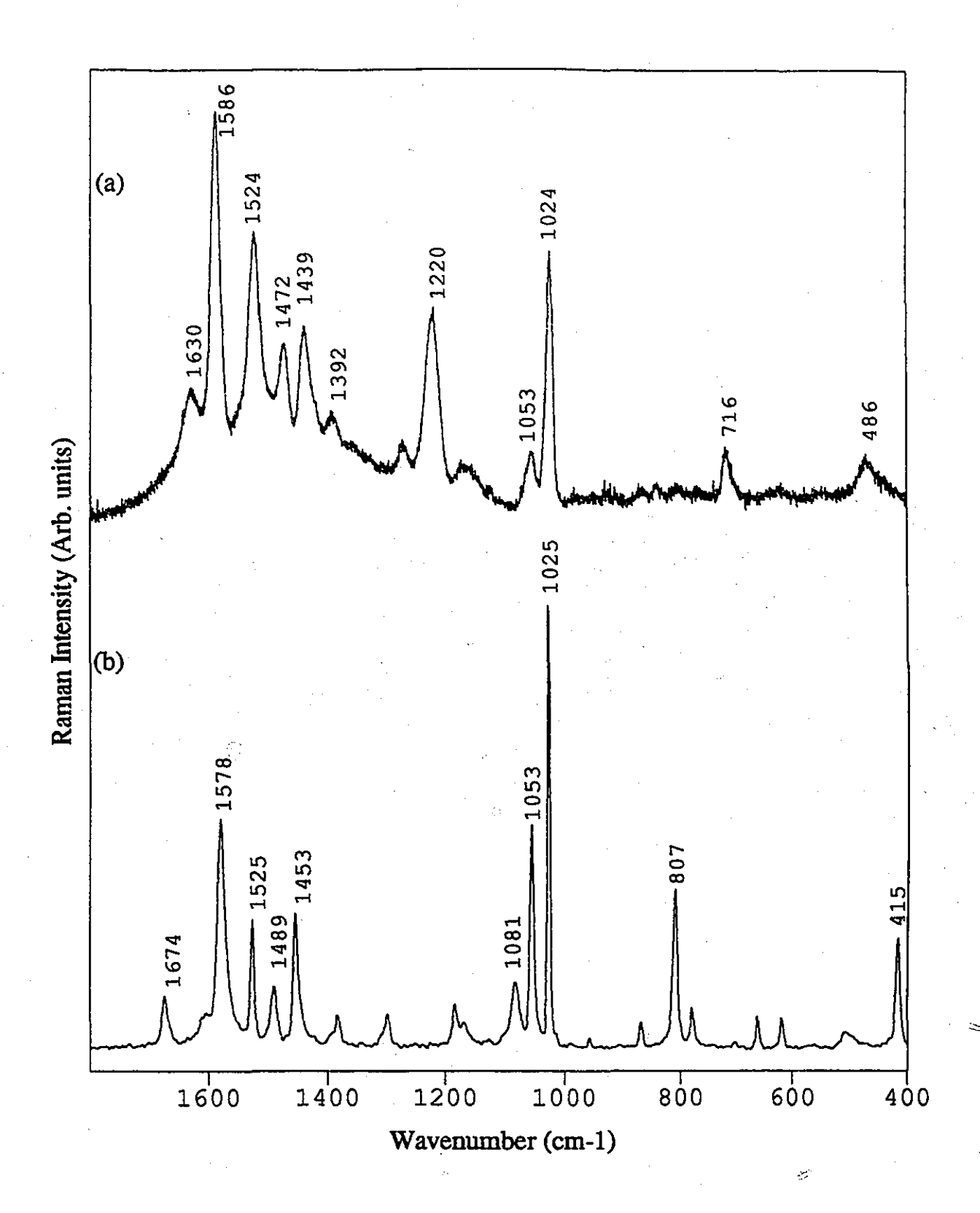


FIGURE 2.4 SERS spectrum of Ag colloid/pza system (a), and normal FT-Raman spectrum of neat pza (b).

**TABLE 2.1** Assignments and wavenumber positions (cm⁻¹) for SERS and normal Raman spectra of pyrazinamide.

			Ag-pza I	Ag-pza I	Ag-pza	Ag
Assignment (a)	Solid	Solution	(Organic-	(Aqueous-	$\operatorname{film} \Pi$	colloid/pza
			phase)	phase)		
16b	415	422				
	š.	•	466	466	461	486
6a	506	560				
6b	618	602				ε,
(NH ₂ ) _t	662	656				
			717	717	710	716
δ(CH)	778	778	et .	766	759	
Amide IV	807	800		•	803	
•	868	900	859			
ĺa	1025	1014	1025	1023	1019/	1024
					1028	
12a	1053	1044	1058	1059	1059	1053
$(NH_2)_t$	1081	1081		4	1 <del>7 1</del> 277 -	
14a	1182	1172	1165	1166	1163	1165
9a	÷	•	1225	1224	1221.	1220
δ(CH)	1297	1292	1269		*\	1270
Amide III	1382	1364	1386	1393	1388	1392
19b	1453	1434	1435	1437	1429	1439
19a #	1489	1472	1473	1472	1470	1472
8b	1525	1522	1523	1526	1519	1524
8a	1578	1578	1588	1589	1585	1586
Amide I /	1674	1628			*	÷ .
δ(H ₂ O)*		•				

⁽a) Assignments for normal Raman spectra of pyrazinamide from refs. 15-19.

^(*) See text.

borates.⁹ The in-plane ring stretching modes (8a, 8b, 19a and 19b) as well as the 1a ring breathing mode, retain similar relative intensities and frequency positions to those in the normal Raman of bulk pza. In view of the surface selection rules, 16,19 the frequencies and selective band intensities of pza ring modes observed in the SERS spectra of all Ag-pza systems are characteristic of a ring plane orientation perpendicular to the surface, in agreement with the previously reported SERS analysis of pza. 16 Adsorption of pza on the metal surface has been proposed to occur via the carboxamide moiety with prior dissociation of one of the amidic hydrogen atoms, since the ring modes, in particular the 1a mode, remain relatively unshifted from their spectral counterparts in the normal Raman spectrum of bulk pza. 16 Pyrazine proved unreactive to forming interfacial films or aggregates using the preparation protocol for Ag-pza films. Given the low affinity of pyrazine for metallic surfaces, 19 and the rapid formation observed for Ag-pza films, it is feasible to assume that pza adsorbs via the carboxamide substituent group. Only one SERS band attributed to the carboxamide group is observed, namely, the amide III [in-plane v(C-N)] band near 1390 cm⁻¹. This band is enhanced relative to the normal Raman spectrum of bulk pza which lends further support for the proposed mode of adsorption.

Some spectral differences are observed for Ag-pza II when compared with the spectra of Ag-pza I and Ag colloid/pza. The SERS spectrum of Ag-pza II displays some additional bands, notably, a shoulder at  $1019 \text{ cm}^{-1}$  on the lower frequency side of the 1a ring breathing mode ( $1028 \text{ cm}^{-1}$ ) and a weak band at  $803 \text{ cm}^{-1}$ . Furthermore, most of the bands assigned to the pza ring modes are shifted to slightly lower frequencies compared with the SERS spectra of both Ag-pza I films. These spectral variations suggest that there are two different pza environments observed for the Ag-pza II system. The additional 1a band, shifted to lower wavenumbers relative to the original 1a mode, is consistent with a molecular reorientation where the pza ring is tilted towards the surface, binding through the ring  $\pi$ -electrons. An aromatic ring breathing mode associated with a flat orientation is expected to decrease slightly from its value in the free or uncoordinated molecule since

utilizing  $\pi$ -electrons weakens the ring C=C bonds.¹⁹ A weak band at 803 cm⁻¹ observed in Ag-pza II spectrum has a similar spectral counterpart in the normal Raman spectrum of the bulk pza, assigned to an amide IV band [in-plane  $\delta$ (CO) bend].¹⁵ In addition, the amide III band for all Ag-pza I and II film spectra remains unshifted and of similar intensity which suggests that the substituent group remains bonded to the Ag particle surface for both perpendicular and tilted orientations in all Ag-pza films.

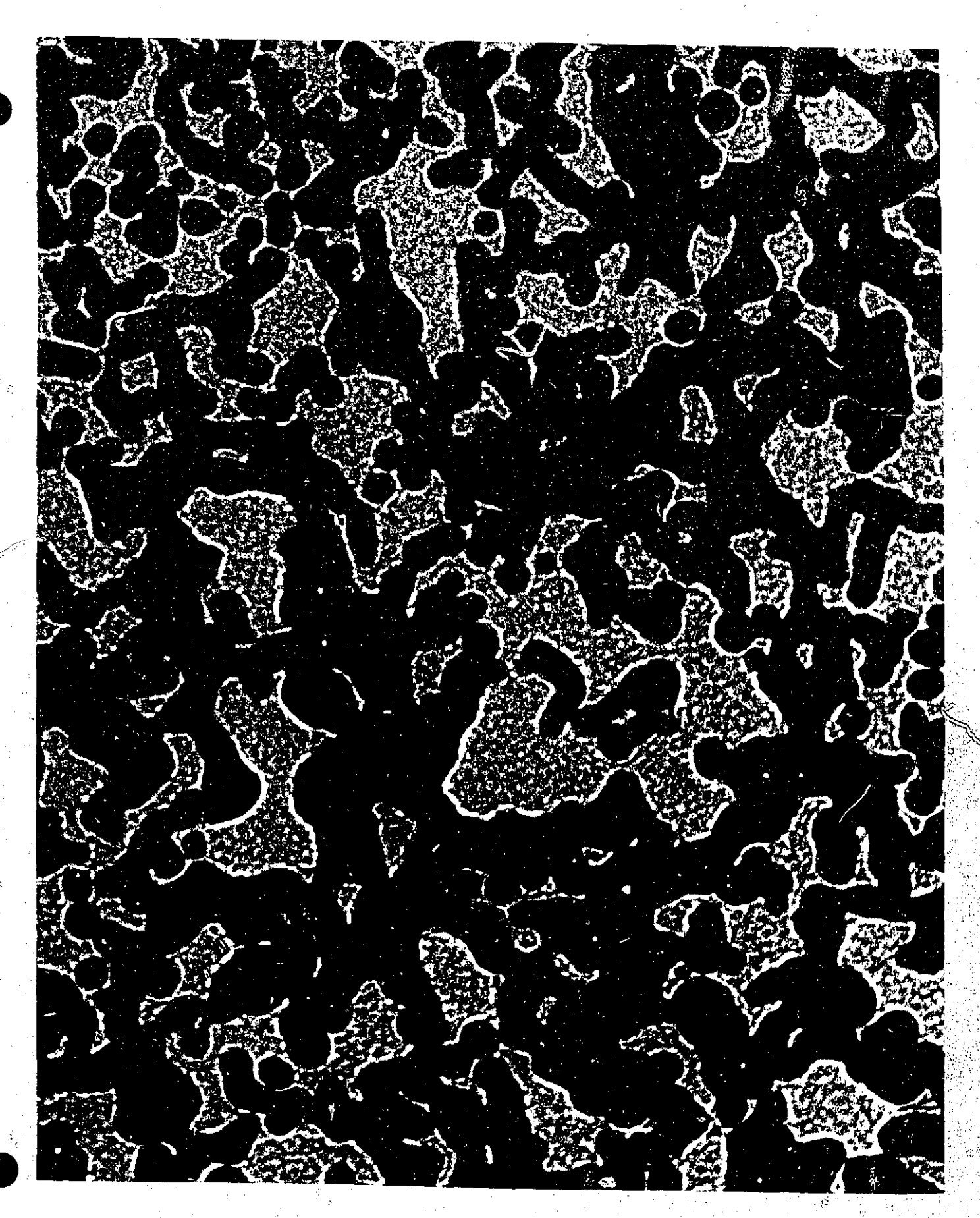
Changes in band intensities are also expected to accompany pza orientation differences in Ag-pza I and II films. In particular, the 8a and 8b v(C=C/C=N) modes which involve vibrational motion oriented largely in the direction along the N-N axis would be most enhanced when the ring is oriented normal to the surface. The intensity ratio for the  $v_{1a}$ :  $v_{8a}$  modes increases from 0.8 for Ag-pza I to 1.2 for Ag-pza II films and is consistent with molecular reorientation from a perpendicular to a flat orientation, respectively. The spectral changes observed for the Ag-pza II spectrum follow similar changes reported for the SERS of pyrazine at submonolayer and high (multilayer) surface coverage where pyrazine assumes flat and perpendicular orientations, respectively.²¹ Although the pza concentrations in Ag-pza I and II systems were the same, an excess of Ag particles was used for the latter colloid preparation. The SPA curves are similar for both Ag-pza I and II films, thus we can assume that there is an increase in the number of Ag particles rather than in the particle size. An increase in the number of Ag sites permits a small fraction of pza molecules to tilt towards a flat orientation in regions of low pza coverage. Since the SERS spectral changes observed for Ag-pza II film are minor (compared to Ag-pza I films), the majority of molecules are assumed to retain a perpendicular orientation similar to that observed for Ag-pza I films. It has been reported previously that colloid surfaces are heterogeneous, consisting of both positive and neutral charged Ag sites. 13 Variable amounts of Ag particles in the Ag colloid I and II preparation (as well as aging) may contribute to a disparity in the amount and distribution of these kinds of Ag sites and thus influence the mode of adsorption and orientation of adsorbates on the surface and, ultimately, the macro-structure of the adsorbate-colloid interaction, i.e., continuous or fractal films or aggregated particles.

## 2.4.2 Ag Colloid-4-MPy Films

No interfacial Ag-4-MPy films were formed under the conditions routinely used for preparation of Ag colloid-adsorbate films, i.e., upon vigorous shaking of a two-phase system consisting of the aqueous Ag colloid and a dichloromethane solution of 4-MPy. Instead, the 4-MPy-covered Ag particles were transferred into the organic phase where they formed cloudy aggregates of 4-MPy-covered organosol. The argument that the transferred Ag colloidal particles are covered by 4-MPy follows from a previous observation where, in the absence of any adsorbate, the Ag colloidal particles were not transferred into the dichloromethane phase. The character of the 4-MPy covered aggregates and their behavior upon deposition is different for Ag-4-MPy film I and II (originating from Ag colloids I and II, respectively) and is, thus, apparently affected by the Ag content in the parent Ag colloid. While the glass-deposited "film" I consists of irregularly spaced areas of brown organosol aggregates, the orange organosol from "film" II readily assembles upon deposition into a lustrous film, analogous in appearance to deposited interfacial films. A TEM photograph of the Ag 4-MPy film II, deposited on a carbon covered grid, is shown in Figure 2.5. The film consists of a 3-D aggregation of Ag particles.

The SERS spectra obtained for Ag-4-MPy I and II films and the Ag colloid/4-MPy system are compared in Figure 2.6 (a)-(c), respectively. The normal FT-Raman spectra of bulk 4-MPy and the silver-4-MPy complex are shown in Figure 2.7. The band positions in the SERS spectra, as well as in the normal Raman spectrum of bulk 4-MPy (solid and aqueous solution), are listed in Table 2.2. The assignments are based on those for *para*-substituted pyridine and thiophenol. 17,22,23 The spectral differences observed between the solid and solution normal Raman spectra of 4-MPy, in particular the bands at 1004 and 1626 cm⁻¹ which are shifted to higher wavenumber positions in the solution spectrum, are

FIGURE 2.5 TEM micrograph of Ag-4-MPy film II deposited onto a carbon covered grid (magnification x32000). The film shows 3-D silver colloid aggregates.



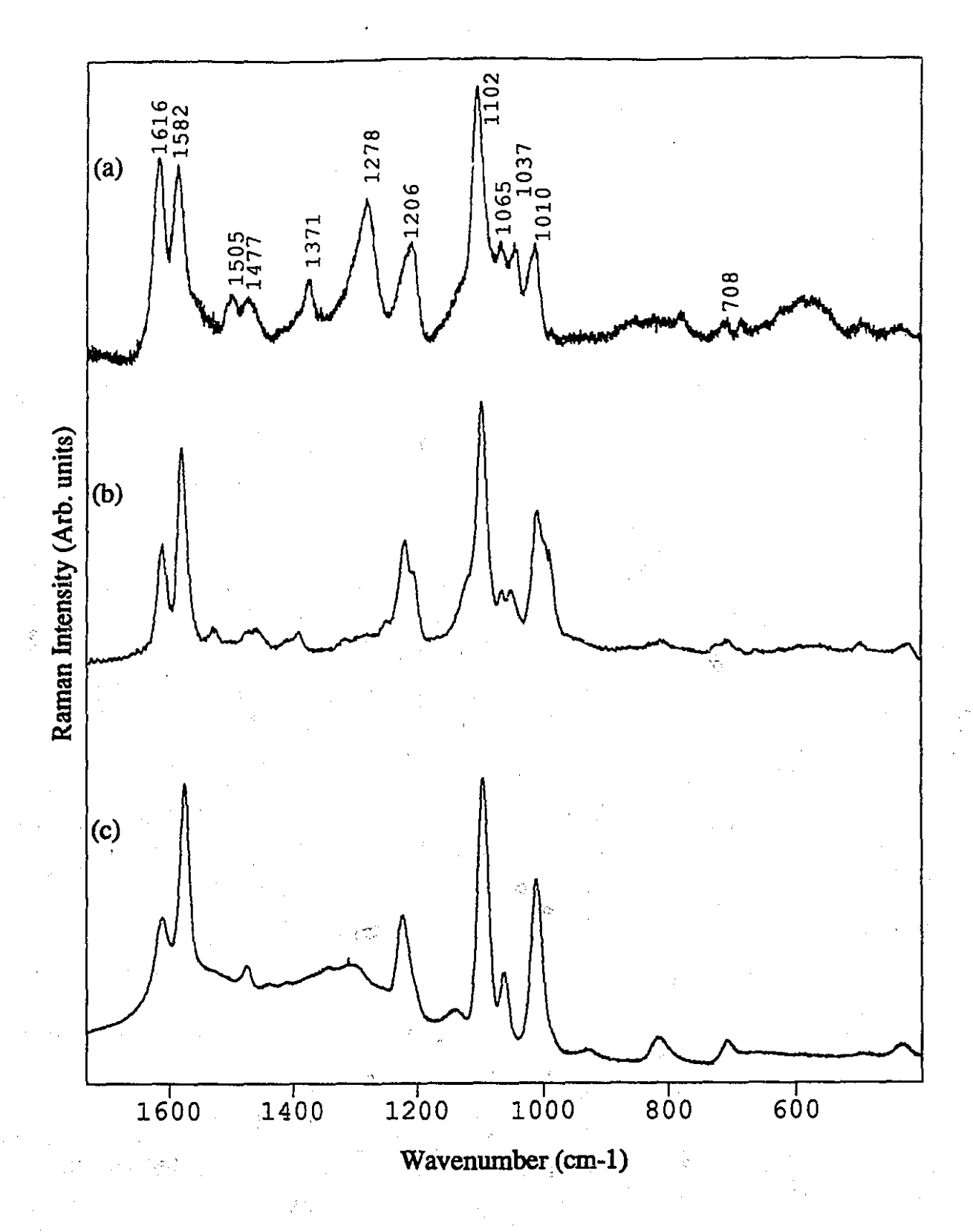


FIGURE 2.6 SERS spectra of Ag-4-MPy I (a); and Ag-4-MPy II (b); glass deposited films and the Ag colloid/4-MPy system (c).

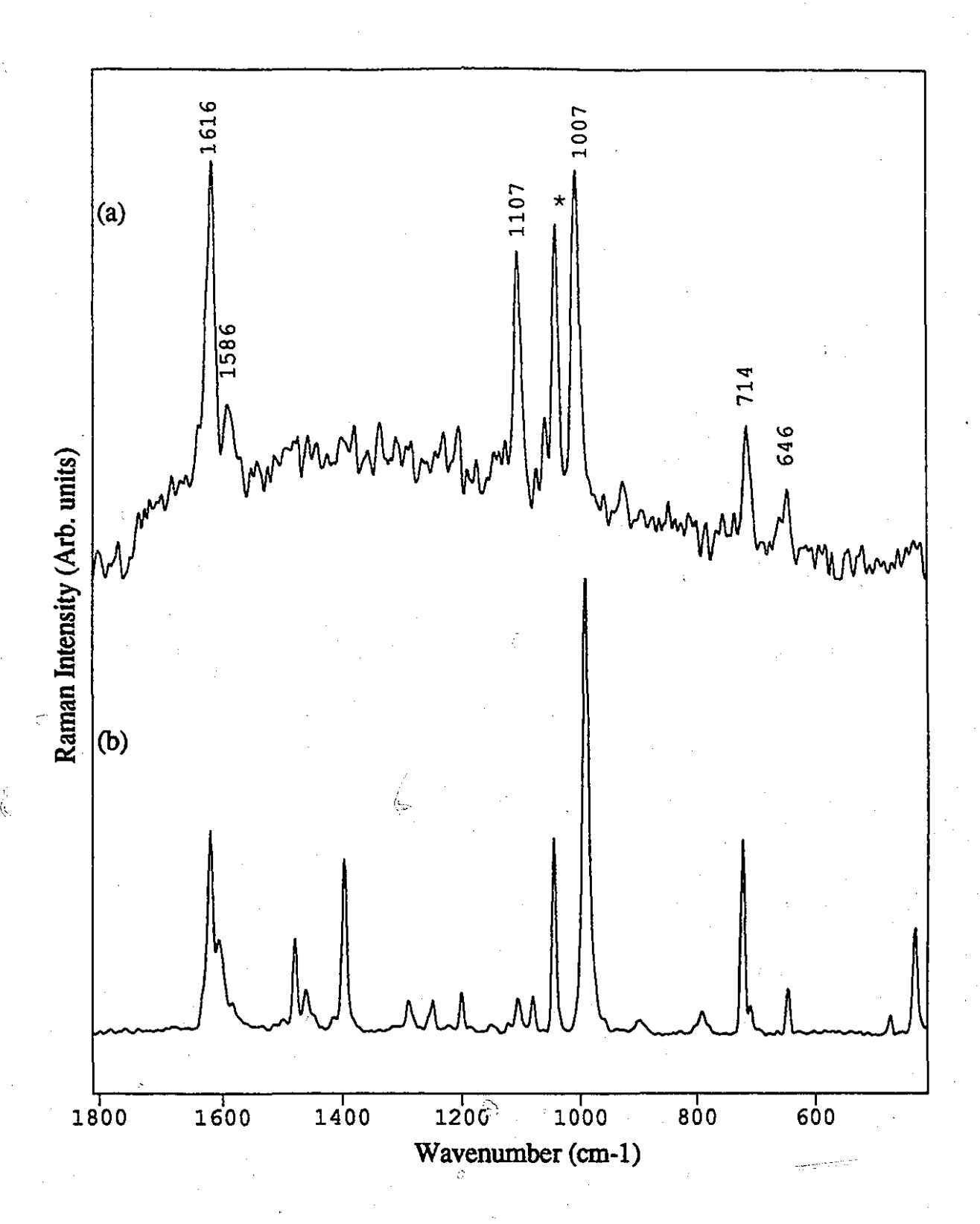


FIGURE 2.7 Normal FT-Raman spectra of silver-4-MPy complex powder (a), and 4-MPy powder (b).  $\lambda_{ex} = 1064.1$  nm at 150 mW.

(*) Band assigned to the  $v_{sym}(NO_3$ -) band of AgNO₃.

TABLE 2.2 Assignments and wavenumber positions (cm⁻¹) for SERS and normal Raman spectra of 4-mercaptopyridine.

Assignment (a)	Solution	Solid	Silver- 4-MPy complex	Ag-4-MPy film I	Ag-4-MPy film II	Ag colloid/ 4-MPy
7a ₁ , δ(C-S)/γ(CCC)	430	431	430		415	430
16b ₁ , γ(CCC)	ļ	471			497	•
6b ₂ , β(CCC)	655	647	646	682	•	
6a ₁ , (β(CC) / υ(C-S))	722	721	714	708	707	705
10b ₁ , γ(CH)		790		780	<b>811</b>	813
		901				
1a ₁ , v(Ring breathing)	1004	990	1007	1010	1001 (sh) / 1008	1007
18a ₁ , β(CH)	1053	1045	1014*	1037	1049	
18b ₂ , β(CH)		1080		1065	1064	1065
12a ₁ , v(Ring breathing) / (C-S)	1119	1106	1107	1102	1097	1098
9a ₁ , β(CH)		1200		1206	1204 (sh) / 1218	1222
	1255	1250	94			
3b ₂ , β(CH)		₀ 1290				
14b ₂ , υ(CC)		1394			1390	,
19b ₂ , υ(C=C/C=N)		1459			1458	
19a ₁ , υ(C=c/C=N)	1487	1478		1477	·	1470
				1505	1525	
8b ₂ ,υ(CC)		1604	1586	1582	1583	1573
8a ₁ , υ(CC)	1626	1617	1616	1616	1611	1615

⁽a) Assignments for the normal Raman spectra of 4-mercaptopyridine from refs. 17, 22 and 23.

^(*) Band assigned to the  $v_{sym}(NO_3^-)$  of AgNO3.

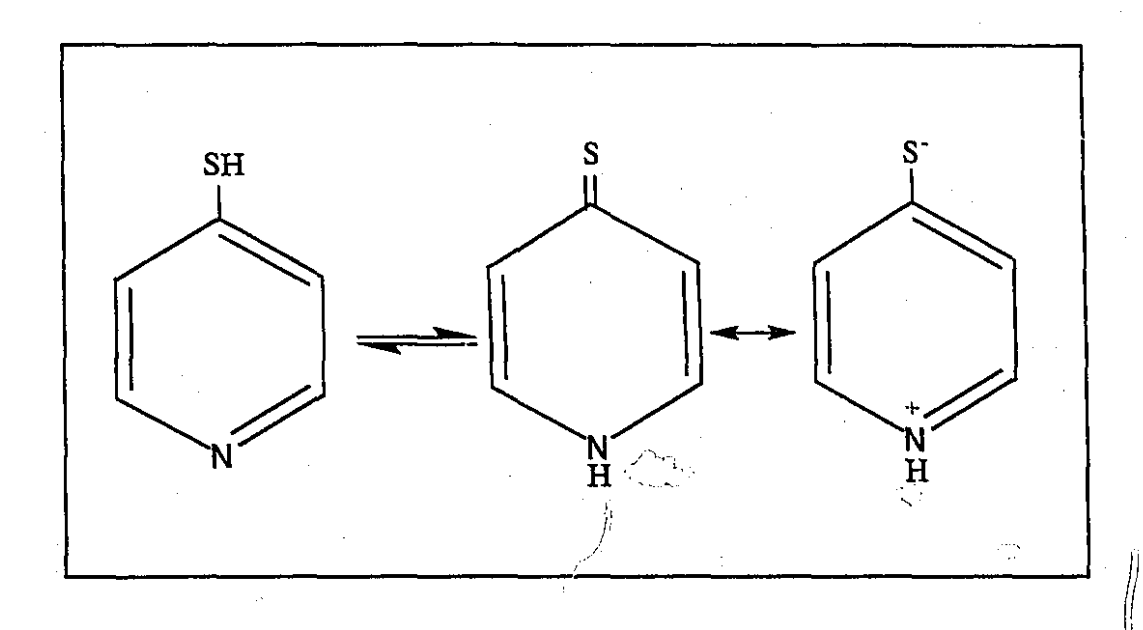


FIGURE 2.8 Thiol - thione tautomers of 4-MPy.

associated with the loss of intramolecular hydrogen bonding between the molecules in solution.

The SERS spectra of Ag colloid/4-MPy and Ag-MPy film II systems are comparable to previously reported SERS studies of 4-MPy adsorbed on Au, Pt and Ag surfaces²⁴⁻²⁶ and to the normal Raman spectrum of the silver-4-MPy complex. It has been concluded that 4-MPy adsorbs on the metal surface through the sulfur atom, the plane of the pyridine ring being perpendicular to the surface.²⁴⁻²⁶ For all SERS spectra, the relative enhancement of in-plane  $a_1$  and  $b_2$  modes namely,  $v_1$  and  $v_{12}$ , and the  $v_{8b}$  modes, which are perpendicular modes for a normal orientation, by analogy with the surface selection rules,^{29,30} indicate that the ring plane orientation of adsorbed 4-MPy is perpendicular to the surface. Out-of-plane modes, although inherently very weak in the normal Raman of bulk 4-MPy, remain unenhanced in the SERS spectra.

Adsorption of 4-MPy through the thiolate sulfur follows cleavage of the S-H bond. This adsorption mechanism, observed for alkylthiols and thiophenol assemblies on Au surfaces, is characterized by the absence of an intense v(SH) band at 2573 cm⁻¹.²³ However, 4-MPy exists as a thiol-thione tautomer in which the thione form predominates, ^{27,28} (Figure 2.8). As a result, a broad v(NH/SH) band appears in the 2900-2500 cm⁻¹ region. Thus, confirmation for adsorption *via* the thiolate sulfur is complicated by the absence of the v(SH) marker band. Other marker bands, such as the v(C-S) mode at 721 cm⁻¹ display characteristic spectral shifts to lower wavenumbers near 706 cm⁻¹ for all SERS spectra (see Table 2.2). In addition to this shift, the X-sensitive  $v_{12}[(\text{ring breathing}/v(C-S)]]$  mode at 1106 cm⁻¹ experiences a dramatic increase in intensity. Similar v(C-S) peak shifts and  $v_{12}$  enhancement have been observed for thiophenol adsorbed via the sulfur atom on SERS-active metal substrates. ^{23,25}

The SERS spectra of both Ag-4-MPy I and II films [Figures 2.6 (a) and (b)] show some differences with respect to the Ag colloid/4-MPy system [Figure 2.6 (c)], which are more pronounced for film I than for film II. Spectral features observed in the spectrum of

film II, namely, shoulders on the lower wavenumber side of 9a and v₁ bands and an additional band at 1049 cm⁻¹, have spectral counterparts in the normal Raman spectrum of bulk 4-MPy and are attributed to uncoordinated 4-MPy molecules, probably from a multilayer. The multilayer 4-MPy component makes only a minor contribution to the SERS spectrum of film II, while the major spectral features correspond with those in the SERS spectrum of Ag colloid/4-MPy. The SERS spectrum of film II thus indicates that most of the 4-MPy molecules are chemisorbed on the Ag particles. On the other hand, film I shows bands at 1010 and 1616 cm⁻¹, which are shifted to higher wavenumbers relative to the film II. Similar band shifts observed in other SERS studies of 4-MPy have been associated with a nitrogen coordinated pyridine and 4-MPy species. 31,32,33 The origin of bands at 1278 and 1371 cm⁻¹ is unknown but may result from a decomposition product. Both the Ag particle arrangement and their coverage by 4-MPy molecules are influenced by the Ag content in the parent Ag colloid, which in turn influences the Ag particle-toadsorbate ratio. Film I contains more adsorbate per particle and there is a higher probability of adsorbate multilayer formation. Moreover, the higher concentration of adsorbate in Ag-4-MPy I could tend to form aggregates (clusters of Ag particles linked by 4-MPy molecules forming a polymeric-like aggregates) instead of individual particles covered by a monolayer of 4-MPy, which is probably the case for the Ag colloid/4-MPy system. The additional spectral shifts observed for film I suggest that the 4-MPy, molecules behave as bidentate ligands (using both N and S atoms for coordination) influencing the 4-MPy-colloid aggregate structure, as opposed to the thiolate-bonded 4-MPy species in film II. The 4-MPy-covered particles of film II are only loosely aggregated in the organic phase, in contrast to the more compact brown aggregates originating from Ag colloid I. This is probably the reason why, upon deposition on a glass slide, the adsorbate-covered particles of Ag colloid II assemble into a lustrous film (analogous in appearance to the deposited interfacial films as well as to MELLFs), while deposition of film I gives more compact brown aggregates.

## 2.4.3 Ag Colloid-2-MPy Films

Interfacial Ag 2-MPy films were prepared from Ag colloid I under the conditions employed for Ag colloid-adsorbate film preparation. Films were formed using two different 2-MPy concentrations, 1 x 10⁻³ M (a) and 2 x 10⁻⁵ M (b). By contrast, no film formation was observed for Ag colloid II. The SERS spectra of both Ag-2-MPy films are compared with Ag colloid/2-MPy system in Figure 2.9 (a)-(c). The vibrational assignments for normal Raman spectrum of bulk 2-MPy and SERS of adsorbed 2-MPy presented in Table 2.3 are based on a previous report. 34,35 It is assumed that the 2-MPy molecule retains C_s symmetry in the normal Raman spectrum. The spectral bands observed for the Ag colloid/2-MPy spectrum are in good agreement with those published for 2-MPy adsorbed on an Au electrode. 36,37 Similarly to 4-MPy, 2-MPy adsorbs on the metal surface through the sulfur atom, the plane of the pyridine ring being perpendicular to the surface. 36,37

A TEM photograph of the interfacial Ag 2-MPy film I (a), deposited on a carbon covered grid is shown in Figure 2.10. The film consists of a monolayer of Ag colloidal particles. The absence of any 3-D aggregates confirms that the native interfacial film was formed by a 2-D aggregation of colloidal particles.

The 2-MPy ligand in metal-2-MPy complexes assumes either monodentate coordination through the sulfur atom or bidentate coordination, generally forming dimeric or trimeric complexes.³⁸⁻⁴¹ Although, relatively few studies have been reported for metal-4-MPy complexes³⁸, it is assumed that the sterically unhindered *para*-position of pyridine nitrogen favors polymeric coordination complexes. Factors related to the steric limitations of mercaptopyridine binding sites are thus manifested in the macrostructure of Ag colloid-adsorbates, resulting in 3-D polymeric-like Ag 4-MPy films and in 2-D monolayers of Ag 2-MPy films.

In this study, we use a comparison of the 2-MPy relative intensities of the  $v_1$  (ring breathing),  $v_{12}$  (ring breathing/v(C-S)) and 8b v(CC) modes, near 1000, 1117 and

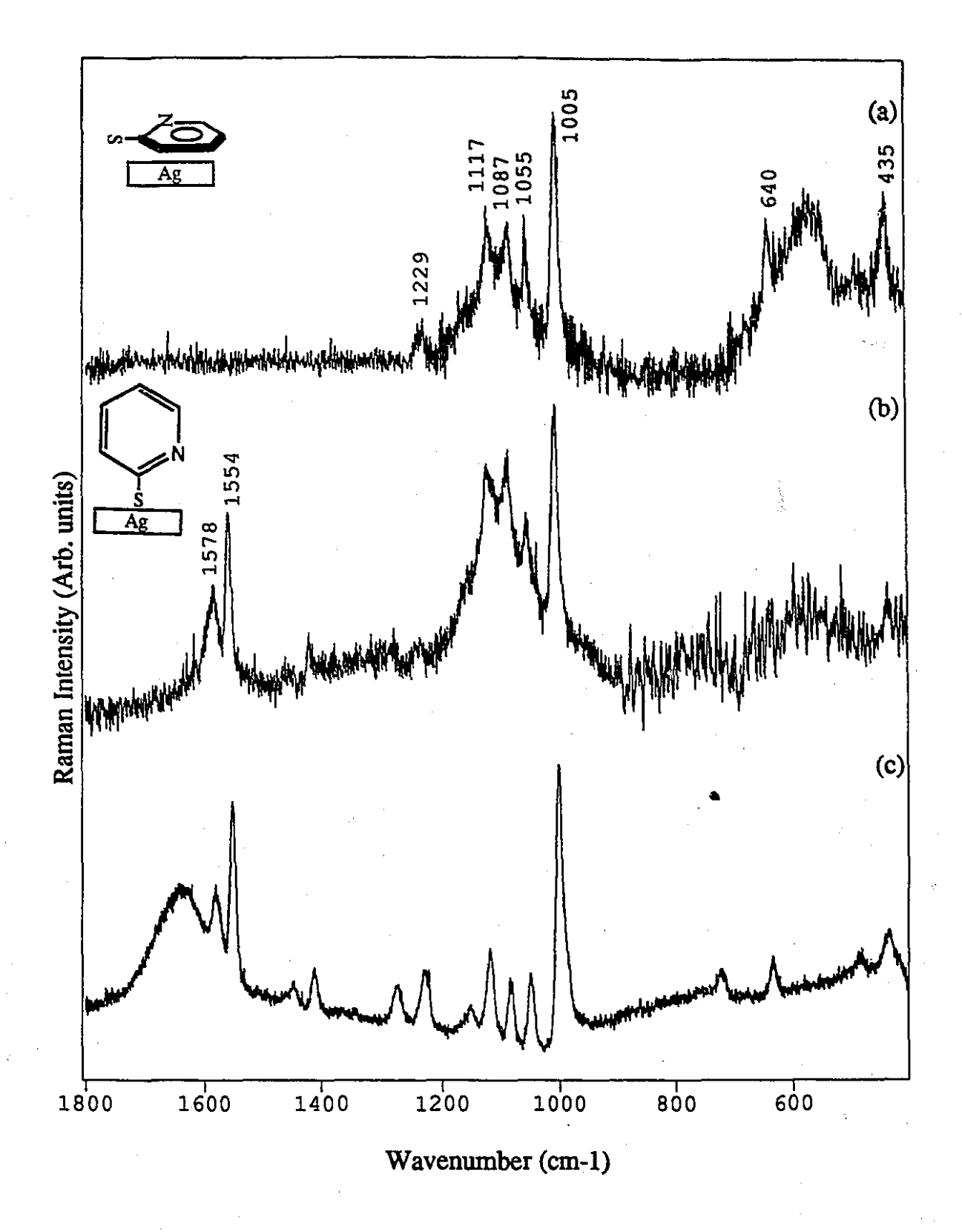


**FIGURE 2.9** SERS spectra of Ag-2-MPy I from different 2-MPy concentrations. Ag-2-MPy I (2 x  $10^{-5}$  M 2-MPy) (a); Ag-2-MPy I (1 x  $10^{-3}$  M 2-MPy) (b); glass deposited films and Ag colloid/2-MPy system (c).

 $\bigcirc$ 

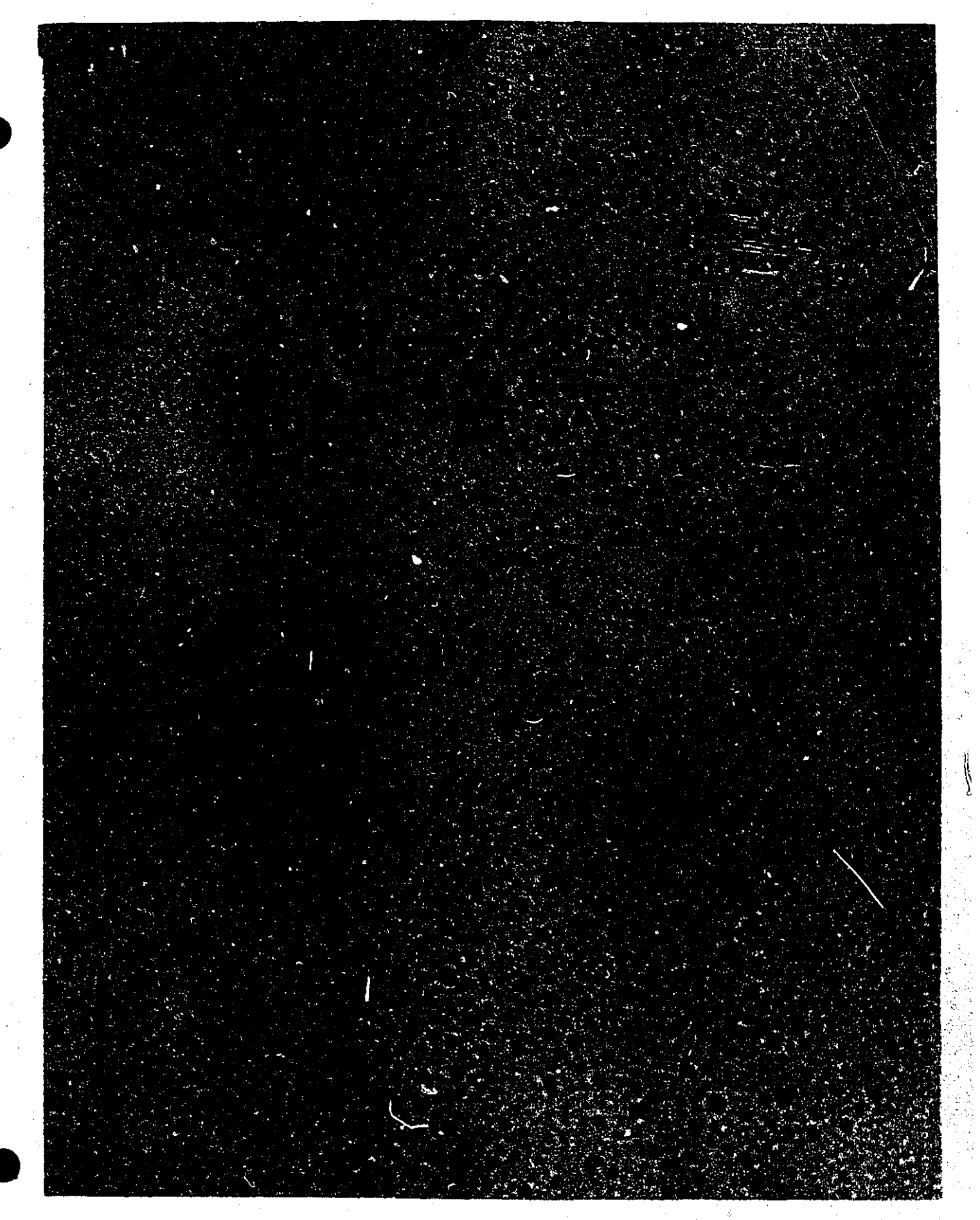
TABLE 2.3 Assignments and wavenumber positions (cm⁻¹) for SERS and normal Raman spectra of 2-mercaptopyridine.

Assignment (a)	Solid	Ag colloid/ 2-MPy	Ag-2-MPy film I (2 x 10 ⁻⁵ M)	Ag-2-MPy film I (1 x 10 ⁻³ M)
A" δ(C-S) / β(CCC)	445	435	435	
	•	485	491	
A" 6a, γ(CCC)	618	634	640	
A" β(CC)	711		i	
A' (C-S)	731	720	•	·
Α" γ(CH)	743			
Α" γ(NH)	893	-		'
Α" γ(CH)	949			
A" γ(CH)	980			
A' 1a, (Ring breathing)	988	998	1005	1004
A' 18a, β(CH)	1024	1048	1055	1054
A' 18b, β(CH)	1092	1084	1087	1082
A' 12a, (Ring breathing)	1133	1117	1117	1117
\n(C-S)				
e e	;	1150	٠	•
$\gamma(NH) / \delta(NH)$	1230	1228	1229	,
A' 14b, υ(C=C/C=N)	1261	1274		¥
Α" γ(CH)	1372			•
A' 19b, υ(C=C/C=N)	1444	1411		1417
A' 19a, υ(C=C/C=N)	1502	1448	,	
A' 8b, υ(C=C)	1569	1549	;	1554
A' 8a, υ(C=C)	1614	1579		1578

⁽a) Assignment for the normal Raman spectrum of 2-mercaptopyridine from refs. 35 and 36.

FIGURE 2.10 TEM micrograph of Ag-2-MPy film II deposited onto carbon covered grid (magnification x32000). The film shows a 2-D monolayer of Ag colloidal particles.

(>)



1550 cm⁻¹, respectively as a probe to indicate differences in the orientation of adsorbed 2-MPy with respect to the Ag surface in all SERS spectra. For the Ag-2-MPy film I (b) made with a higher 2-MPy concentration [Figure 2.9 (b)], the relative intensity of the ugh band is comparable to the v₁ and v₁₂ bands. Similarly, for the spectrum of Ag colloid/2-MPy [Figure 2.9 (c)], the vgb band is comparable in intensity to the v1 band however, the relative intensity of the v₁₂ band is lower. These spectral differences can be understood in terms of the surface selection rules. 19,30 Since the vgb mode involves symmetrical motion of the ring C=C bonds and the v₁₂ mode involves stretching motion of the C-S bond, they would be expected to be enhanced when 2-MPy is bonded via the sulfur atom to the metal surface with the C-S bond and ring plane normal to the surface. This is the case observed for the spectrum of Ag-2-MPy film I (b), at high surface adsorbate coverages. The lower v₁₂ band intensity in the Ag colloid/2-MPy spectrum implies that the Ag-S bond angle is less than normal relative to the Ag surface. The U8b band intensity remains strong relative to the v₁ mode because the plane of the pyridine ring still remains normal to the surface (as opposed to a flat "face-on" orientation), this reorientation is such that the ring 'tilts' on its side to allow the N atom to be in closer proximity to the surface. Furthermore, as a result of this tilt, the in-plane C=C/C=N modes in the region between 1230-1450 cm⁻¹ are enhanced. The spectrum of Ag 2-MPy film I (a) made with a lower 2-MPy concentration, Figure 2.9 (a), shows remarkable differences with respect to spectra in Figure 2.9 (b) and (c), indicating a reorientation of 2-MPy on the Ag surface. The v_{8a} and v_{8b} modes are absent and the v₁₂ mode intensity is decreased while the relative intensities of the out-ofplane  $\delta(C-S)/\beta(CCC)$  and 6a  $\gamma(CCC)$  modes at 435 and 640 cm⁻¹, respectively, are increased. This implies that the plane of the pyridine ring is parallel to the surface. The v₁ and v₁₂ bands remain unshifted compared to the band positions in the other Ag-2-MPy systems which confirms that 2-MPy remains bonded to the Ag surface via the sulfur atom in Ag-2-MPy film I (a). Similar spectral changes were observed in the SERS spectra of pyrazine and pyridine at high (multilayer) and low (submonolayer) coverage on Ag

surfaces.¹⁹ In this study, changes in surface orientation of 2-MPy were achieved by using different concentrations of adsorbate. In each case, both high and low concentrations produce a 2-D metallic interfacial film. This is in contrast to the 4-MPy adsorbate study, where varying the amount of Ag particles (using Ag colloid II and I) gave in each case a 3-D organosol aggregate in which the 4-MPy molecules coordinate with the colloidal Ag as monodentate and possibly bidentate ligands.

### 2.5 CONCLUSIONS

The results of this study confirm previous observations² that the process of formation of interfacial Ag colloid-adsorbate films at the interface between an aqueous Ag colloid and a solution of an adsorbate in dichloromethane, as well as the internal structure of the resulting films, are substantially influenced by the chemical nature of the adsorbate. The rate of the interphase transfer of the adsorbate from the organic to the aqueous phase and the rate of its adsorption on Ag colloidal surfaces are considered to be the most important adsorbate characteristics governing the film formation process. Our present observation of the formation of Ag-4-MPy aggregates under conditions routinely used for the preparation of Ag colloid-adsorbate interfacial films emphasizes the chemical specificity of the adsorbate even further. Unlike the wide range of adsorbates forming Ag colloidadsorbate films (several porphyrin species, N-bases such as 2,2'-bipyridine, 2,2',6,6'bipyrimidine as well as pyrazinamide and 2-mercaptopyridine discussed in this thesis), 4mercaptopyridine (4-MPy) is the only adsorbate for which an interphase transfer of adsorbate-covered particles from aqueous to organic phase (impossible for adsorbate free Ag colloidal particles) has been observed, instead of interfacial film formation. We attribute the particular chemical specificity of 4-MPy to the sterically unhindered position of the para-pyridine nitrogen which may influence the formation of a polymeric-like macrostructure and be responsible for the 3-D aggregation of 4-MPy-covered Ag particles in the organic phase. Whereas 2-MPy, which has a sterically restricted ortho-pyridine nitrogen and forms primarily sulfur bonded, dimeric or trimeric 2-MPy-metal complexes may influence the formation of the 2-D monolayer interfacial structure.

Furthermore, we have shown that for a particular adsorbate, the process of colloid aggregation, i.e., 3-D organosol vs. 2-D film monolayer, depends on the concentration of Ag in the parent Ag colloid. In the case of Ag-pza film, the difference between Ag colloid I and II leads to distinctly different structures of the resulting films. The Ag-pza I films form continuous layer(s) of pza covered particles, whereas the Ag-pza II film consists of a

aggregates, which appear fractal-like as observed from the SPA spectra. Further microscopy studies are required to confirm a fractal structure. Similarly upon deposition, the Ag-4-MPy II organosol aggregates can readily assemble into a film of contiguous particles, while the compact Ag-4-MPy I aggregates remain unchanged. In the case of pza and 4-MPy adsorbates, the ratio of adsorbate-to-metal was controlled by varying the concentration of Ag in the parent Ag colloid (Ag colloid I and II), while for the 2-MPy samples the adsorbate concentration in the organic phase was varied. High and low surface adsorbate coverages were shown to influence the orientation of 2-MPy in the interfacial film. The SERS spectra showed that for high adsorbate concentrations, the 2-MPy molecules are packed perpendicular to the surface and at low concentrations the molecules lie flat.

### REFERENCES

- (1) Vlckova, B.; Barnett, S. M.; Kanigan, T.; Butler, I. S. Langmuir 1993, 9, 3234.
- (2) Cermakova, K.; Vlckova, B.; Lednicky, F. Manuscript in preparation.
- (3) Cermakova, K.; Vlckova, B.; Fort, V.; Lednicky, F. J. Mol. Struct. 1995, 349, 129.
- (4) Barnett, S. M.; Vlckova, B.; Butler, I. S.; Kanigan, T. S. Anal. Chem. 1994, 66, 1762.
- (5) Yogev, D.; Deutsch, M.; Efrima, S. J. Phys. Chem. 1989, 93, 4174.
- (6) Yogev, D.; Efrima, S. J. Phys. Chem. 1988, 92, 5761.
- (7) Gordon, K. C.; McGarvey, J. J.; Taylor, K. P. J. Phys. Chem. 1989, 93, 6814.
- (8) Al-Obaidi, A. H. R.; Rigby, S. J.; McGarvey, J. J.; Walmsley, D. G.; Smith, K.
   W.; Hellemans, L.; J., S. J. Phys. Chem. 1994, 98, 11163.
- (9) Cermakova, K.; Sestak, O.; Matejka, P.; Baumruk, V.; Vlckova, B. Collect. Czech. Chem. Commun. 1993, 58, 2682.
- (10) Vlckova, B.; Gu, X.; Tsai, D.; Moskovits, M. Manuscript in press.
- (11) Vlckova, B.; Douketis, C.; Moskovits, M. Unpublished results.
- (12) Weitz, D. A.; Oliveria, M. Phys. Rev. Lett. 1984, 52, 1433.
- (13) Weitz, D. A.; Lin, M. Y.; Sandroff, C. J. Surf. Sci. 1985, 158, 147.
- (14) Meakin, P. J. J. Phys. Chem. 1985, 83, 3645.
- (15) Kalkar, A. K.; Bhossekar, N. M.; Kshirsagar, S. T. Spectrochim. Acta 1989, 45A, 635.
- (16) Arenas, A. F.; Castro, J. L.; Otero, J. C.; Marcos, J. L. J. Raman Spectrosc. 1992, 50, 249.
- (17) Dollish, F. R.; Fateley, W. G.; Bentley, F. F. Characteristic Raman Frequencies of Organic Compounds; Wiley: New York, 1974.
- (18) Miranda-Muniz, M.; Neto, N.; Sbrana, G. J. Phys. Chem. 1988, 92, 954.
- (19) Moskovits, M.; DiLella, D. P.; Maynard, K. J. Langmuir 1988, 4, 67.
- (20) Dornhaus, R.; Long, M. A.; Benner, R. E.; Chang, R. K. Surf. Sci. 1980, 93, 240.
- (21) Moskovits, M.; DiLella, D. P.; Maynard, K. J. Langmuir 1988, 4, 67.
- (22) Green, J. H. S.; Kynaston, W.; Paisley, H. M. Spectrochim. Acta 1963, 19, 549.
- (23) Joo, H. T.; Kim, M. S.; Kim, K. J. Raman Spect. 1987, 18, 57.
- (24) Taniguichi, I.; Iseki, M.; Yamaguchi, H.; Yasukouchi, K. J. Electroanal. Chem 1985, 186, 299.
- (25) Bryant, M. A.; Joa, S. L.; Pemberton, J. E. Langmuir 1992, 8, 753.

- (26) Xu, H.; Tseng, C. H.; Vickers, T. J.; Mann, C. K.; Schelenoff, J. B. Surf. Sci. 1994, 311, L707.
- (27) Stoyanov, S.; Petkov, I.; Antonov, L.; Stoyanova, T.; Karagiannidis, P.; Aslanidis, P. Can. J. Chem. 1989, 68, 1482.
- (28) Beak, P.; Fry, F. S.; Lee, J. J.; Steele, F. J. Am. Chem. Soc. 1976, 98, 171.
- (29) Creighton, J. A. Surf. Sci. 1983, 124, 209.
- (30) Moskovits, M.; Suh, J. S. J. Phys. Chem. 1984, 88, 5526.
- (31) Baldwin, J. A.; Schühler, N.; Andrews, M. A.; Butler, I. S. Manuscript in preparation.
- (32) Akyuz, S.; Dempster, B.; Morehouse, R. L.; Suzuchi, S. J. Mol. Struct. 1973, 17, 105.
- (33) Jeanmaire, D. L.; Van Duyne, J. J. Electronanal. Chem. 1977, 84, 1.
- (34) Lautie, A.; Hervieu, J.; Beloc, J. Spectrochim. Acta 1983, 39A, 367.
- (35) Shunmugam, R.; Sathyanarayana, D. N. Spectrochim. Acta 1984, 40A, 757.
- (36) Takahashi, M.; Fujita, M.; Ito, M. Surf. Sci. 1985, 158, 307.
- (37) Gui, J. Y.; Lu, F.; Stern, D. A.; Hubbard, A. T. J. Electroanal. Chem. 1990, 292, 245.
- (38) Kennedy, B. P.; Lever, A. B. P. Can. J. Chem. 1972, 50, 3489.
- (39) Evans, I. P.; Wilkinson, G. J. Chem. Soc. Dalton Trans. 1974, 946.
- (40) Kokkou, S. C.; Rentzeperis, P. J.; Fortier, S. Acta Crystallogr. 1983, C39, 178.
- (41) Masaki, M.; Matsunami, S. Bull. Chem. Soc. Japan 1976, 49, 3274.

# CHAPTER 3

INTEGRATED OPTICS, EVANESCENT WAVE, SURFACE-ENHANCED RAMAN SCATTERING (IOEW-SERS) OF 4,4'-BIPYRIDINE

#### 3.1 SUMMARY

This Chapter introduces a novel SERS technique that combines both waveguide Raman spectroscopy (WRS) and SERS. The method goes by the name of integrated optics, evanescent wave, surface enhanced Raman spectroscopy or IOEW-SERS. Waveguide fabrication involves a 2-D grafting of a silver colloid onto a 3-mercaptopropyltrimethoxysilane (3-MPT) derivatized planar glass waveguide. This nanoscale heterostructure satisfies the optical requirements for integrated optics waveguide Raman spectroscopy in allowing optically guided incident radiation to propagate into the thin film. The thin film of Ag adparticles can support surface plasmon excitation and yield SERS excitation by evanescent wave coupling. The vibrational structure of the waveguide interface is interrogated by IOEW-SERS and shows that the molecular adhesive, 3-MPT, is chemically bonded to both glass and colloid adlayers. To illustrate the benefit of optically guiding the light into the waveguide, a spectrum collected at a 90° scattering angle shows only carbonization of the waveguide. The waveguide Ag colloid surface is derivatized with 4,4°-bipyridine and a comparative study of IOEW-SERS and Ag hydrosol systems using 4,4°-bipyridine reveals similar vibrational spectra.

The optical properties of the parent aqueous phase colloid and surface attached Ag colloid at the waveguide are investigated by UV transmission. The extinction maxima,  $\lambda_{max}$ , show that adhesion of the colloid to 3-MPT prevents aggregation and immersion of the grafted colloid in a solution of 4,4'-bipyridine is accompanied by only a small shift in the  $\lambda_{max}$ .

### 3.2 INTRODUCTION

Investigation of the macroscopic, microscopic and surface interaction properties of thin films and monolayers requires efficient, highly sensitive, non-destructive spectroscopic probes. Moreover, information on the molecular specificity, spatial resolution in both lateral and depth dimensions and interfacial details for the complete characterization of these systems is required. A Raman technique recently developed for the study of substrate-supported thin films, waveguide Raman spectroscopy (WRS), satisfies these requirements.^{1,2} This technique is a non-classical spectroscopic approach involving the use of integrated optical structures to interrogate the vibrational structure of thin films. An optical waveguide consists of a thin film which is either coated or adsorbed onto a non-absorbing substrate (e.g., glass) with a real refractive index in the optical region of interest. The experiment is conducted in which a significant portion of the incident radiation is coupled into the thin film via a prism.³ The active portion of the thin film structure must be composed of a medium which has a higher refractive index than does the surrounding medium to allow the radiation to guide in the thin film. The effective scattering beam volume is defined by the focused laser beam cross-section and the film thickness; this introduces an increase in the scattering volume and also a large optical field at the surface. Under these conditions, high irradiances are obtained in the thin film. Using this approach, Raman scattering can be detected from very thin films to even monolayer coverages.^{3,4} These developments have established WRS as a versatile nondestructive and sensitive spectroscopic tool for applications in thin film analysis.

The observation of radiation-enhanced vibrational spectra of molecules adsorbed on some metal surfaces at monolayer coverages has become commonplace through the exploitation of surface enhanced Raman scattering (SERS).^{5,6} Enhancement factors of up to 10⁶ have been attained for adsorbates present on roughened metal surfaces, generally Cu, Ag and Au. A variety of different metal surfaces facilitate SERS, e.g., electrochemically roughened electrodes, metal sols and metal sputtered onto substrates.

Considerable interest has been generated in the properties of the surface-molecule interactions present in SERS. These include adsorbate orientation ^{7,8} and packing order. ⁹ Although the exact mechanism of SERS is still a matter of some controversy, it is clear that much of the enhancement results from a plasmon resonance which greatly amplifies the local electric field at the metal surface. ¹⁰⁻¹²

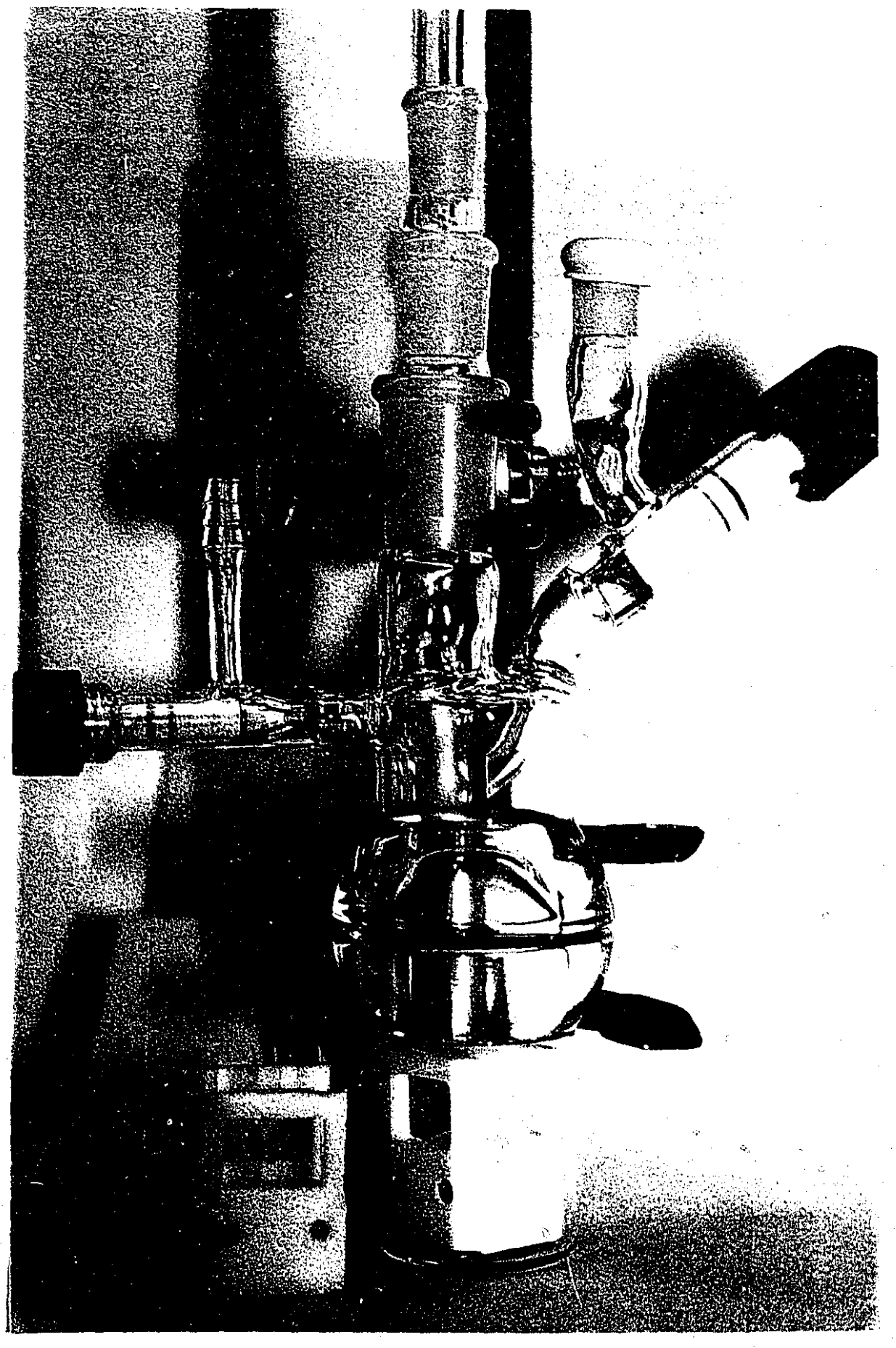
The unification of both WRS and SERS systems in a single structure can result in many advantages for the analysis of thin films, including the capability to probe the substrate-adsorbate interface in both lateral and depth dimensions. The combination of WRS with SERS employing typical SERS-active metal substrates cannot support the requirements of an integrated optical waveguide because of the extremely high absorptivity of metals at visible wavelengths. Recently, a multilayer structure has been designed which consists of three components - a silver colloid/coupling-molecular adhesive/glass arrangement capable of supporting an evanescent optical field. 13 The optical refractive index conditions are met whereby the optical field can penetrate the adhesive/metal superstrate film and this complete macroscopic array behaves as an optically responsive structure. The interfacial adhesive, 3-mercaptopropyltrimethoxy-silane (3-MPT), contains two terminal functional groups which permit its use as a molecular adhesive between two materials 14-18 - in our particular case, between a metal superstrate and glass substrate. The 3-MPT is grafted onto a glass substrate following hydrolysis and condensation reactions of the alkoxide termini to form siloxane bonds. The unreacted thiol termini are available to bond covalently to a metal through the sulfur atom. Immersion of the 3-MPT-derivatized glass in a dilute hydrosol of silver produces a 2-D colloidal silver array bonded to the surface. Using this approach, the deposition is thin enough to allow the evanescent wave to penetrate the colloidal silver layer without significant attenuation and, in doing so, acts to intensify the effective cross-section for SERS. Propagation of transverse electric (TE) waves can occur over the length of the waveguide (several cm). A schematic of the IOEW-SERS substrate and incident field intensity distribution is shown in Chapter 1 (Figure 1.11). Typical SERS analytes (e.g., pyridine and its derivatives) are able to adsorb passively on to the waveguide colloid surface from solution. This complete waveguide-SERS substrate is introduced as integrated optics, evanescent wave, surface-enhanced Raman scattering (IOEW-SERS). This technique is capable of discriminating between the waveguide interfacial features as well as the adsorbed monolayer on the colloid surface, providing information on vibrational and structural properties.

To demonstrate the utility of IOEW-SERS, the colloidal surface was exposed to a solution of 4,4'- bipyridine. A comparative SERS study is made of 4,4'- bipyridine using IOEW-SERS, a silver colloidal sol system, and previously published SERS studies. 19-23 We show that the waveguide substrate can support SERS of an adsorbate layer and the IOEW-SERS spectrum obtained is comparable to the SERS spectrum from a colloid sol system and previously reported spectra collected by more classic SERS substrates.

### 3.3 EXPERIMENTAL

Materials. 3-MPT (Petrarch) was used without further purification. 4,4'-bipyridine (Aldrich) was sublimed *in vacuo* immediately prior to use. High purity water was obtained from a Milli-Q Ultrapure Millipore water system. Acetonitrile was spectroscopic grade (Aldrich). The Ag colloids were prepared by reduction of AgNO₃ with NaBH₄, following an established procedure.²⁴ Glass cover microscope slides (24 x 30 mm x 150 μm) were purchased from Fisher Scientific, while quartz slides were obtained from Chem Glass Inc.

Methodology. Glass cover slides were first sonicated in a detergent solution for 30 min, rinsed continuously with Millipore water and sonicated for a further 30 min. The slides were next immersed in hot piranha solution [1:4 H₂O₂ (30%)/H₂SO₄] for 30 min. CAUTION: Piranha solution is extremely corrosive, heat gently. The slides were removed with Teflon tweezers and rinsed continuously with Millipore water and sonicated again for 30 min. The slides were then mounted into a Teflon block equipped with lateral ridges to allow each slide to be secured separately. The Teflon block was placed in a Teflon-sealed glass apparatus, shown in Figure 3.1, and heated at 260°C for 10 min under vacuum until all residual water had been removed. The apparatus was then flushed with N2 and the slides were left for 1 h under a refluxing mixture of 3-MPT (1%) in dry distilled toluene, after which time the hydrolysis and condensation of the 3-MPT-modified surfaces was complete. The solution was removed by syringe and the slides were washed several times with dry toluene under  $N_2$ . The bulk of the solvent was removed and the residual solvent was evaporated under vacuum. The 3-MPT-derivatized glass cover slides were then removed from the glass apparatus and placed in an aqueous Ag colloid solution for 2 h at room temperature. The Ag colloid attaches to the pendant thiol group of the derivatized glass cover slides and the Ag monolayer surface appears as a yellow-golden color. A schematic of the waveguide preparation is shown in Figure 3.2. The adsorbate was introduced to freshly prepared colloidal-derivatized waveguides by immersion for 10 min in FIGURE 3.1 Photograph of the assembly apparatus used for 3-MPT derivitization of glass cover slides. A Teflon block with lateral ridges holds glass cover slides separately. A Teflon coated stirbar is inserted into the bottom of the block. The block is inserted in a glass barrel, each half of the barrel is separated by a Teflon O-ring and Teflon sleeves are employed to eliminate the use of vacuum grease. Facilities for N₂ flushing and entry/exit ports for liquid are attached at the top of the barrel.



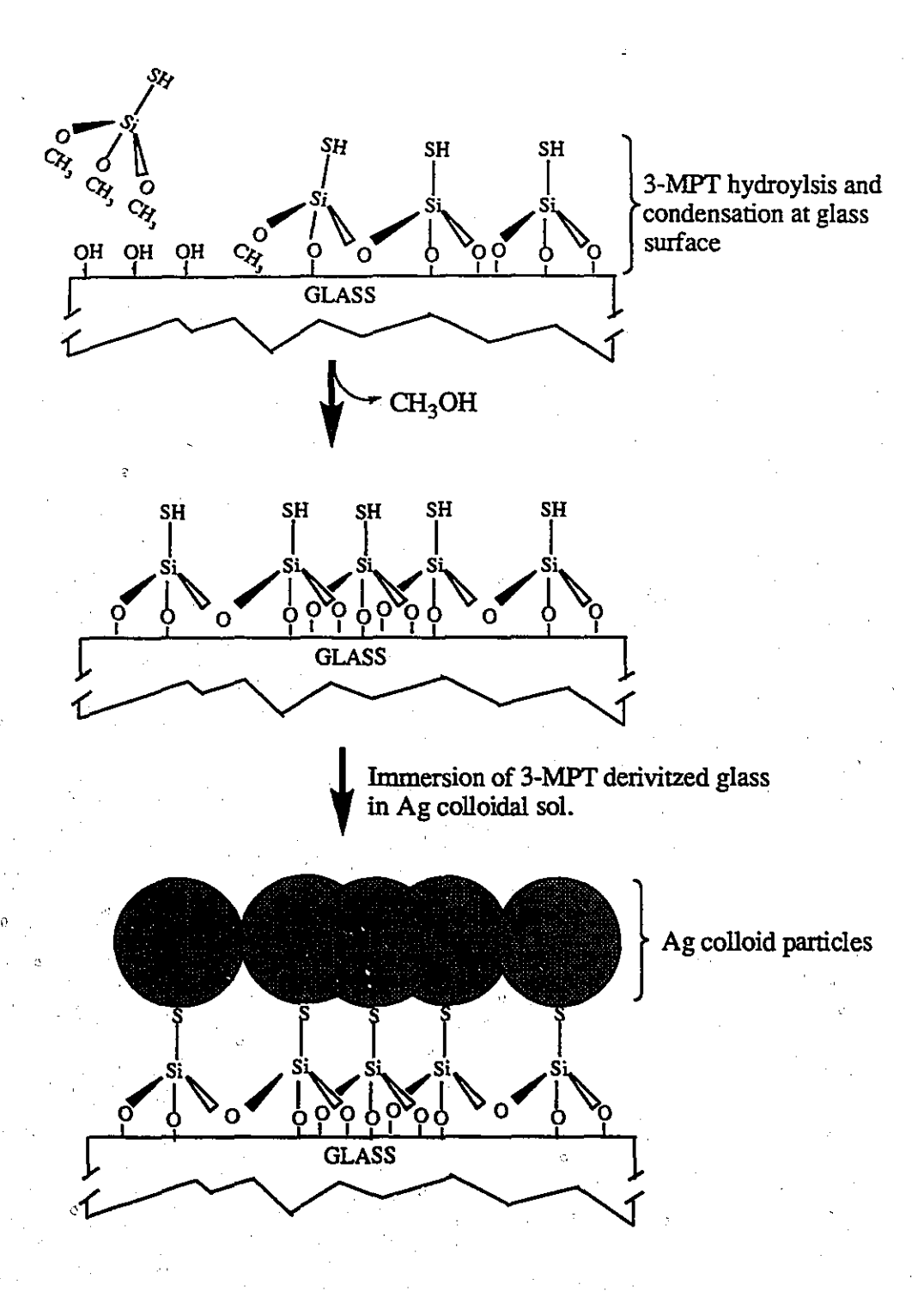


FIGURE 3.2 A schematic of the waveguide assembly heterostructure. A glass cover slide reacts with molecular adhesive, 3-MPT (a); the hydrolysis and condensation reaction of 3-MPT is completed (b); and the derivatized glass is immersed in an Ag colloid hydrosol (c).

a 2-mM acetonitrile solution containing 4,4'-bipyridine and subsequent washing with acetonitrile. The preparation of 3-MPT-derivatized quartz slides was identical to that described for the glass slides.

The Ag colloid (sol) of 4,4'-bipyridine was prepared by adding an aqueous solution of 4,4'-bipyridine (20  $\mu$ l, 2 mM) to 2 mL of Ag colloid. Aggregation of the colloid to a blue/grey color was slow and optimal SERS signals were obtained 24 h after initial sample preparation.

Instrumentation. All SERS spectral data were obtained using 514.5-nm (50 mW) radiation from a Spectra Physics Model 164 Ar⁺ laser on an integrated optics spectrometer bench constructed in-house. The detector system consisted of a liquid N₂-cooled charged coupled device (CCD) interfaced to an Instruments S.A. HR 640 spectrograph equipped with a holographic grating (1800 grooves mm⁻¹). The acquisition time employed was typically 30 s for each 500 cm⁻¹ window. The FT-Raman spectra of bulk 3-MPT and 4,4'-bipyridine were recorded on a Bruker IFS-88 spectrometer equipped with an FRA-105 Raman module and a liquid N₂-cooled proprietary detector. The spectrum was excited with a Nd³⁺:YAG laser operating at 1064.1 nm (150 mW), with 250 scans typically being collected. The electronic extinction spectra of the quartz waveguides were measured on a Hewlett Packard diode-array UV-visible absorption spectrometer - Model 8452A.

Optical Set-up. The focused laser beam is coupled into the waveguide at an angle by means of a high refractive index prism. The waveguide and prism are mounted into a rectangular holder. A horizontal bar provides uniform pressure to the prism to maintain weak coupling to the waveguide. This assembly is held vertically in place on the optical bench by a platform which is then strategically positioned with a combined x-y-z adjustment. The incident angle by which the beam penetrates the waveguide is controlled by an optical rotation stage. The optical system is aligned such that the incident laser beam is focused onto the back of a Newport 38 rectangular mounting platform. A precision rotation stage is centered on the opposite face of this plate. The stage is driven by a

microstepping motor with an interface to a Compumotor PC-21 indexer for rotation control. The beam is deflected through a series of mirrors assembled in Newport MFM-075 holders attached to an adjustable mounting bracket. The light is focused through a convex lens onto the prism which is centered on the axis of rotation. This arrangement allows the light to be rotated through an arbitrary angle onto the back edge of the coupling prism. The incident angle by which the beam penetrates the waveguide controls the optical field density distribution within the waveguide. The evanescent field can then be maximized by fine tuning the incident angle while optimizing the signal from the adsorbed bipyridine monolayer. The variation in the spectra on changing the incident angle occurs as an increasing proportion of the field interacts with the enhanced Raman scattering intensity of the adsorbate vibrational modes and selects against the interface and glass modes. The light scattered from the waveguide streak is imaged on the slit of the monochromator through an achromatic f/2 collimating lens. The Rayleigh line is removed by a supernotch holograpic Bragg filter (Kaiser) positioned in front of the slit. A detailed description of the optical set-up has been reported previously.²⁵

### 3.4 RESULTS AND DISCUSSION

# 3.4.1 IOEW-SERS of Ag Colloidal-Derivatized Waveguide.

IOEW-SERS of the 3-MPT-colloid-derivatized waveguide interphase and the normal FT-Raman spectrum of bulk liquid 3-MPT are compared in Figures 3.3 and 3.4. The vibrational assignments follow those for a similar surface reaction reported by Pemberton et al. 15 in which 3-MPT was first reacted with a polycrystalline Ag surface and then the alkoxide termini were subjected to hydrolysis and condensation. When 3-MPT undergoes hydrolysis and condensation on the glass, absence of the v_s(CH₃) band at 2844 cm⁻¹ in the IOEW-SERS spectrum (Figure 3.4) confirms that the methoxy groups of 3-MPT have reacted. The remaining bands are assigned to the v(CH) methylene stretching modes of the 3-MPT propyl chain. Absence of the v(SH) band at 2574 cm⁻¹ in the IOEW-SERS spectrum [Figure 3.4 (a)] is strong evidence for coupling of Ag with the thiol S-H linkage. Further confirmation regarding the thiolate bonding between the sulfur and Ag surface can be gained from the  $v(C-S)_G$  (G = gauche) and  $v(C-S)_T$  (T = trans) vibrations which are shifted to lower energies in the IOEW-SERS spectrum. In Figure 3.3, the v(C-S)_G and  $v(C-S)_T$  bands of the bulk sample at 742 and 649 cm⁻¹ are lowered in the waveguide spectrum to 698 and 625 cm⁻¹, respectively. This energy decrease has previously been reported as an indication of the thiolate bonding between Ag and the thiolate sulfur atom. ²⁶ Although the v(Si-C) and v(Si-O) vibrations are also present in this region, it appears that the v(C-S) vibrations are enhanced relative to the latter modes, probably as a result of the closer proximity of sulfur to the Ag surface.

The v(Si-O) vibrations, shown in Figure 3.3, also contain useful information about the assembly of 3-MPT on the glass surface. The formation of a Si-O-Si network after hydrolysis and condensation is indicated by the appearance of two intense bands attributable to siloxane v(Si-O-Si) vibrations. The v(Si-O-Si) and the  $v_a(Si-O)$  bands of 3-MPT are observed as broad shoulder bands centered at 1077 and 800 cm⁻¹, respectively. The intense band at 913 cm⁻¹, situated between both 3-MPT modes, is attributed to a

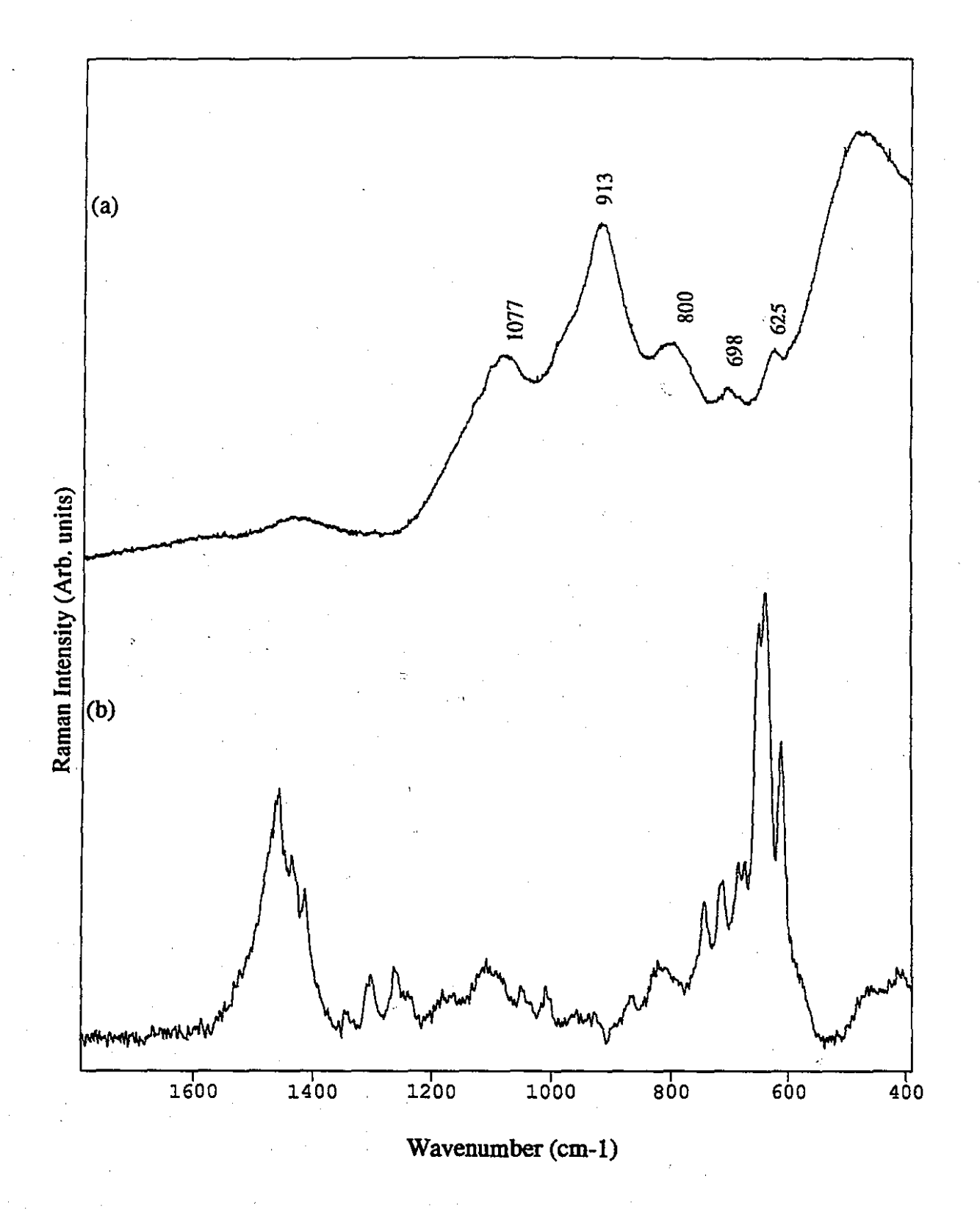


FIGURE 3.3 IOEW-SERS spectrum of an Ag derivatized waveguide (a), and normal FT-Raman spectrum of bulk liquid 3-MPT, (b).  $\lambda_{ex} = 1064.1$  nm at 150 mW.

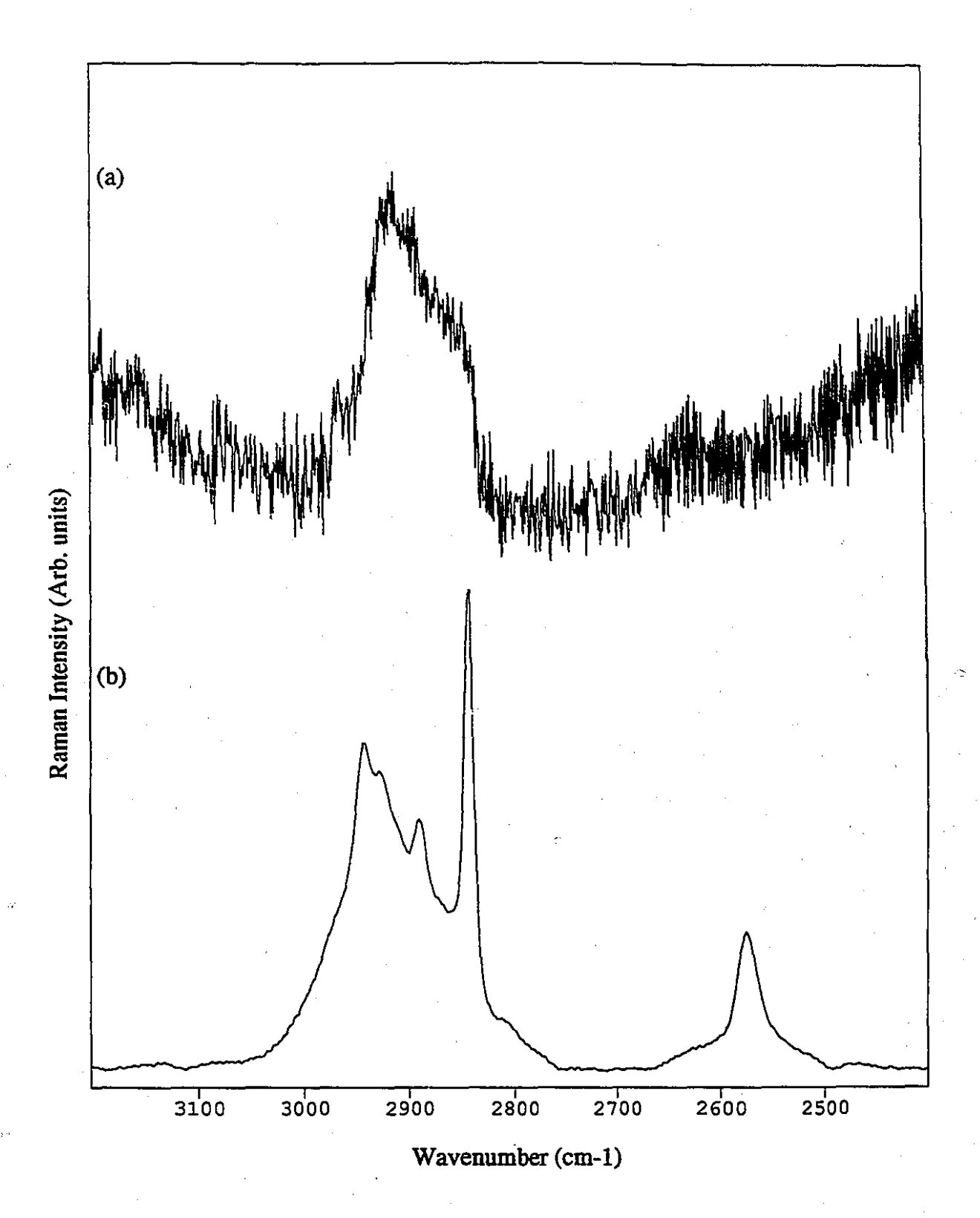


FIGURE 3.4 IOEW-SERS spectrum of C-H stretching region of an Ag derivatized waveguide (a), and unenhanced FT-Raman spectrum of bulk liquid 3-MPT (b).  $\lambda_{ex} = 1064.1 \text{ nm}$  at 150 mW.

 $\nu(Si-O)$  band from the glass substrate. The  $\nu(C-C)$  band of the propyl chain is observed as a weak shoulder on the higher energy side of the  $\nu(Si-O)$  band from the glass. The very intense band near 470 cm⁻¹ is also attributed to the glass substrate.

To illustrate the benefit of optically guiding the light into the waveguide, the spectrum in Figure 3.5 was obtained without introducing an evanescent wave into the waveguide. The spectrum was produced for the classical backscattering angle of 90° on the Ag-derivatized waveguide. A strong broad feature in the 1600-1300 cm⁻¹ region and a virtual loss of all vibrational information on the interface are observed. This broad band has been attributed to graphite formation resulting from decomposition of the organic material. Apparently, "photografitization", otherwise known as "laser carbonization", of the organic compounds located near the metal surface rather than the metal itself is responsible for this particular laser-induced SERS phenonenom.^{27,28} Given that the carbon film thickness was estimated to be 100-200 nm on a roughened Ag electrode surface, the SERS of a carbonized surface is considerably weaker than the scattering from the adsorbate layer.

# 3.4.2 IOEW-SERS of 4, 4'-Bipyridine Derivatized Waveguide

The optical properties of the waveguide were measured for a quartz-derivatized slide to eliminate spectral UV-absorption interference resulting from the glass. Figure 3.6 (A - C) shows the extinction maxima for the parent Ag colloid used to derivatize the waveguide surface, the Ag colloid derivatized waveguide and 4,4'-bipyridine derivatized waveguide, respectively. The reported spectra are not corrected for reflection losses and therefore the term extinction is used instead of absorbance. The extinction band observed is attributed to excitation of surface plasmons in the metal. The surface plasmon frequency is largely determined by the dielectric function of the metal but is also governed by the size and shape of the particles and the interparticle spacing. The extinction maximum of the Ag colloid-derivatized waveguide at ~402 nm is shifted slightly from the maximum of 392 nm

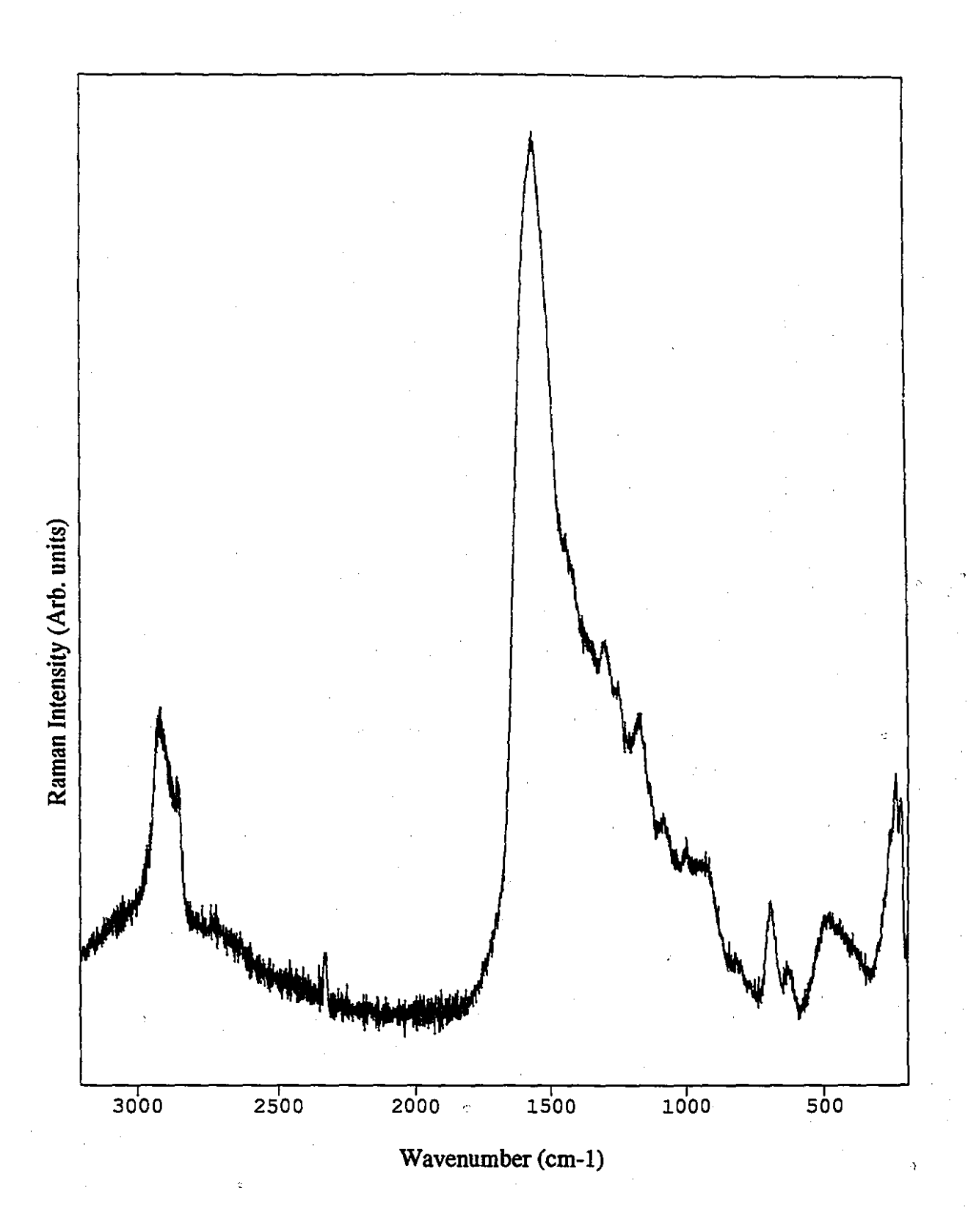


FIGURE 3.5 SERS of the waveguide surface. The spectrum was collected using the classical  $90^{\circ}$  backscattering geometry.

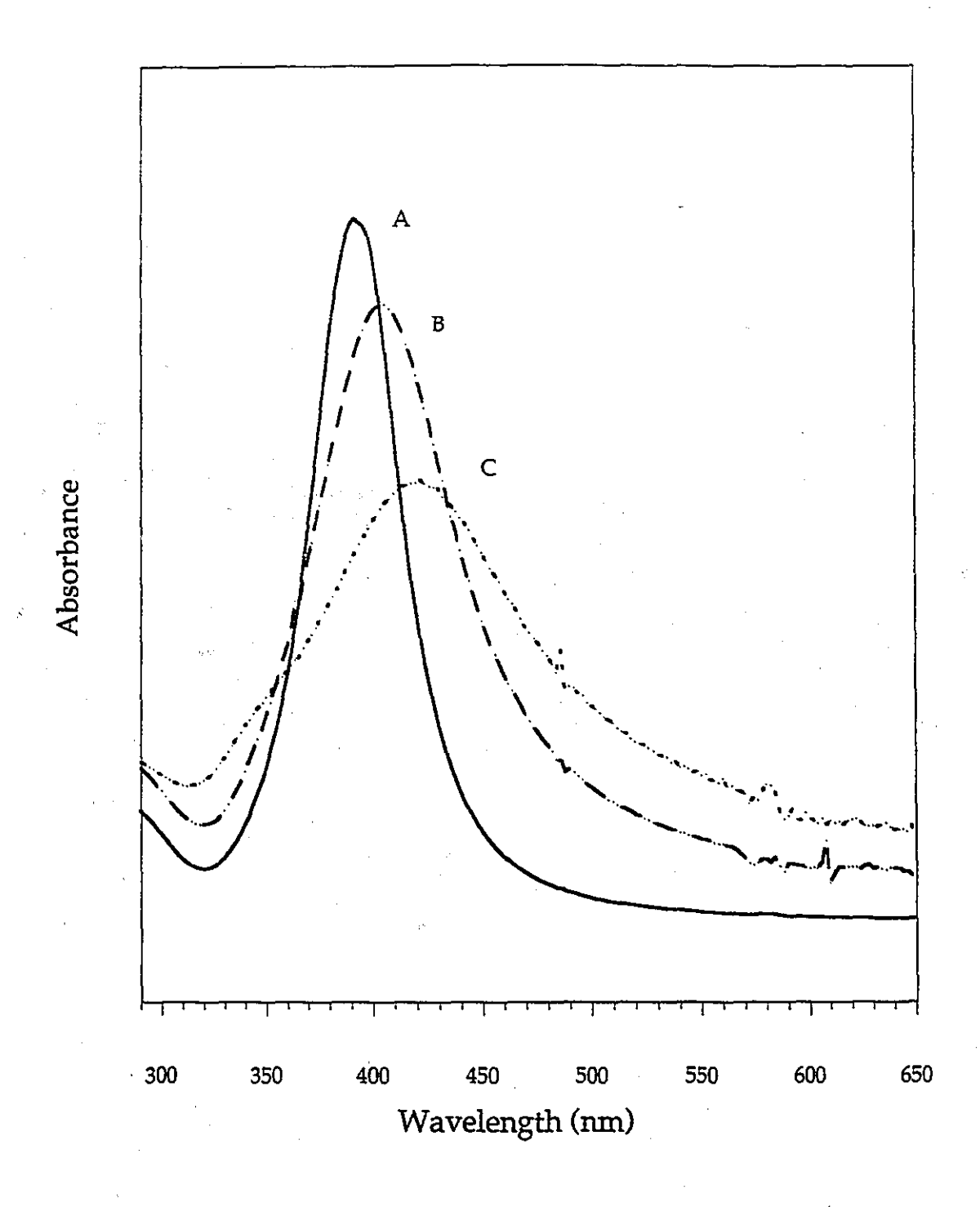


FIGURE 3.6 UV-Extinction maxima of parent Ag colloid (A);  $\lambda_{max} = 392$  nm, waveguide derivatized with Ag colloid (B);  $\lambda_{max} = 402$  nm, and Ag colloid derivatized waveguide immersed in 2 mM 4,4'-bipyridine (C);  $\lambda_{max} = 422$  nm.

observed for the parent Ag colloid used to coat the waveguide. This slight shift and broadening of the band indicate that the isolated Ag particles of the colloid are in closer contact on the waveguide surface but remain unaggregated. Although 4,4'-bipyridine does not have an electronic transition close to the extinction maximum of the colloid film on the waveguide (302 nm), adsorption of 4,4'-bipyridine does affect the optical properties of the colloid. The extinction maximum is shifted to 422 nm and the band is broadened [Figure. 3.6 (C)]. The dielectric properties of 4,4'-bipyridine, in addition to the structure, homogeneity, and distribution of Ag particles contribute to the change in the optical response of the colloid.³³ No spectral contribution from the acetonitrile solvent was

detected. Spectra obtained after immersion in acetonitrile are comparable to those shown in

Figure 3.6 (B) and (C).

IOEW-SERS, Ag colloidal sol SERS spectra and the normal FT-Raman spectrum of bulk 4,4'-bipyridine are compared in Figure 3.7. The IOEW-SERS spectrum is analogous to the SERS spectrum of the Ag colloid system, which, in turn, are in a good agreement with those previously reported. 19-23 The presence of broad background peaks between 1700 and 1000 cm⁻¹ in the IOEW-SERS spectrum has been observed in previous SERS studies and was attributed to carbon contamination^{22,28} The relative intensities of the bipyridine vibrational modes are, however, enhanced compared with bands from the glass and interface background. Raman scattering from the interface and glass substrate was not subtracted in order to emphasize the enhancement of spectral information from the bipyridine adsorbate on the Ag colloidal surface. This remarkable enhancement is achieved even though more than 98% of the electric field resides in the glass waveguide.³⁴ The most prominent Raman features are located in the 1700-700 cm⁻¹ region, which is essentially free from the substrate background vibrational modes. This region is associated with in-plane vibrational modes of the bipyridine molecule such as C-C and C-N stretching and C-H wagging. 35,36 The totally symmetric modes are subjected to a greater degree of enhancement, while the out-of-plane modes located below 1000 cm⁻¹ are not observed.

The generally accepted interpretation of these observations exploits the surface propensity rules for adsorbate vibrations^{32,37,38} and is consistent with 4,4'-bipyridine being adsorbed on the Ag surface *via* the nitrogen with the aromatic rings oriented perpendicular relative to the surface. Interaction with the Ag surface occurs through  $\sigma$  donation of the nitrogen lone pair assuming a *cis* conformation with both nitrogen atoms interacting with the Ag atoms in a chelating fashion.²³

The spectral similarities of both SERS spectra illustrate the fact that the IOEW-SERS substrate structure, with an immobilized Ag colloidal surface has the ability to promote similar SERS-active Ag sites like that of aggregated colloidal sols.

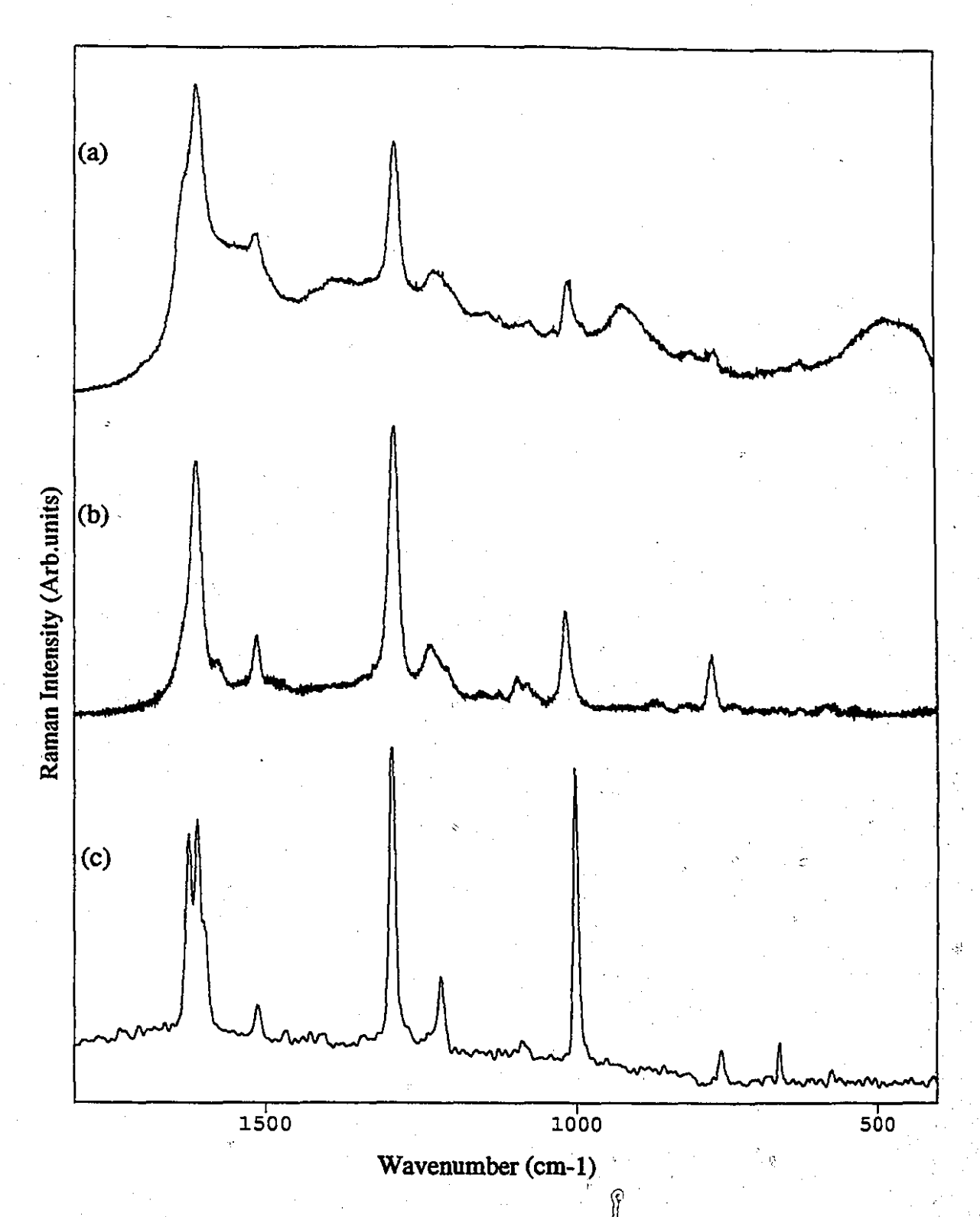


FIGURE 3.7 SERS of Ag colloid sol / 4,4 '-bipyridine system (20  $\mu$ l, 2 mM) to 2 ml of Ag colloid (a); IOEW-SERS of derivatized waveguide after immersion in 2 mM acetonitrile solution of 4, 4'-bipyridine (b); and unenhanced FT-Raman spectrum of bulk solid 4, 4'-bipyridine.  $\lambda_{ex} = 1064.1$  nm at 150 mW (c).

#### 3.5 CONCLUSIONS

In this study, we have described a technique for attaching Ag colloid via a bifunctional organic molecule, 3-MPT, to a glass substrate. This nanoscale Ag colloid/3-MPT/glass heterostructure simultaneously satisfies boundary conditions for integrated optics, evanescent wave propagation and the optical conditions for surface enhanced Raman scattering (IOEW-SERS). The colloid adlayer can couple with an evanescent wave propagating in an underlying waveguide through resonant interactions with the conduction electrons of the metal particles (surface plasmon excitations). The colloid overlayer therefore acts as a field intensifier, increasing cross sections for optical processes such as Raman scattering. Vibrational information from both the waveguide interface and adsorbates confined to the colloid surface are revealed. The interfacial structure of 3-MPT in the waveguide assembly can be probed by optically guided light, whereas a classical 900 scattering geometry results in carbonization of the waveguide surface. Optical properties of the Ag colloid before and after deposition on the waveguide are characterized by transmission UV. The  $\lambda_{max}$  (392 nm) of the parent colloid undergoes a small shift after Ag colloid deposition (402 nm) which indicates that there is little colloidal aggregation upon deposition on the 3-MPT underlayer. The Ag colloidal surface was derivatized with 4,4'bipyridine and the IOEW-SERS spectrum collected was analogous to an Ag colloidal sol system of 4,4'-bipyridine. The  $\lambda_{max}$  (422 nm) of the 4,4'-bipyridine derivatized waveguide is shifted relative to that of the underivatized waveguide which indicates some changes occur in the optical properties of the colloidal particles, however, the colloid surface remains predominantly unaggregated.

#### REFERENCES

- (1) Tien, P. K. Rev. Mod. Phys. 1977, 49, 361.
- (2) Bohn, P. W. Trends. Anal. Chem. 1987, 6, 223.
- (3) Rabolt, J. F.; Swalen, J. D. in *Spectroscopy of Surfaces*; Clark, R. J. H. and Hester, R. E., Eds.; Wiley: New York, 1988, Ch.16, p1.
- (4) Ellahi, S.; Hester, R. E. Analyst 1994, 119, 491.
- (5) Cotton, T. M. in *Spectroscopy of Surfaces*; Clark, R. J. H. and Hester, R. E., Eds.; Wiley: New York, **1988**, Ch.16, p91.
- (6) Chang, R. K.; Furtak, T. E. Surface Enhanced Raman Scattering; Plenum Press: New York, 1982.
- (7) Pemberton, J. E.; Bryant, M. A.; Sobocinski, R. L.; Joa, S. L. J. Phys. Chem 1992, 96, 3776.
- (8) Carron, K. T.; Hurley, L. G. J. Phys. Chem 1991, 95, 9979.
- (9) Bryant, M. A.; Pemberton, J. E. J. Am. Chem. Soc. 1991, 113, 3629.
- (10) Milton, K. Acc. Chem. Res. 1984, 17, 271.
- (11) Moskovits, M. Review. Mod. Phys. 1985, 57, 783.
- (12) Metiu, H.; Das, P. Ann. Rev. Phys. Chem. 1984, 35, 507.
- (13) Freeman, G. R.; Grabar, K. C.; Allison, K. J.; Bright, R. M.; Davis, J. A.; Guthrie, A. P.; Hommer, M. B.; Jackson, M. A.; Smith, P. S.; Walter, D. G.; Natan, M. J. Science 1995, 267, 1629.
- (14) Thompson, W. R.; Pemberton, J. E. Chem. Mater. 1995, 7, 130.
- (15) Thompson, W. R.; Pemberton, J. E. Chem. Mat. 1993, 5, 241.
- (16) Doron, A.; Katz, E.; Willner, I. Langmuir 1995, 111, 1313.
- (17) Goss, C. A.; Charych, D. H.; Majda, M. Anal. Chem 1991, 63, 85.
- (18) Schneider, T. W.; Buttry, D. A. J. Am. Chem. Soc. 1993, 115, 12391.
- (19) Cotton, T. M.; Dwarakannath, K.; Iorga, D. J. Am. Chem. Soc. 1983, 105, 7462.
- (20) Cotton, T. M.; Vavra, M. Chem. Phys. Lett. 1984, 106, 491.
- (21) Lu, T.; Cotton, T. M.; Birke, R. L.; Lombardi, J. R. Langmuir 1989, 5, 406.
- (22) Ni, F.; Cotton, T. M. Anal. Chem. 1986, 58, 3159-3163.
- (23) Stekas, T.; Diamandopoulos, P. J. Phys. Chem. 1990, 94, 1986-1991.
- (24) Vlckova, B.; Materjka, P.; Simonova, J.; Cermakova, K.; Pancoska, P.; Baumruk, V. J. J. Phys. Chem. 1993, 97, 9719.
- (25) Kanigan, T. Ph.D Thesis 1995, McGill University, Montreal. Canada.
- (26) Joo, T. H.; Kim, K.; Kim, M. S. J. Mol. Struct. 1987, 158, 265.

- (27) Lee, T. G.; Yeom, H. W.; Oh, S.; Kim, K.; Kim, M. S. Chem. Phys. Lett. 1989, 163, 98.
- (28) Cooney, R. P.; Mahoney, M. R.; Howard, M. W.; Spink, J. A. Langmuir 1985, 1, 273.
- (29) Kerker, M. Pure Appl. Chem. 1981, 53, 2083.
- (30) Schlegel, R. L.; Cotton, T. M. Anal. Chem. 1991, 63, 241.
- (31) Fornasiero, D.; Grieser, F. J. Chem. Phys. 1987, 87, 3213.
- (32) Creighton, J. A. in *Spectroscopy of Surfaces*; Clark, R. J. H. and Hester, R. E., Eds.; Wiley: New York, 1988, Ch.16, p37.
- (33) Kotler, Z.; Nitzan, A. J. Phys. Chem. 1982, 86, 2011.
- (34) Andrews, M. P. Unpublished results.
- (35) Dollish, F. R.; Fareley, W. G.; Bentley, F. F. Characteristic Raman Frequencies of Organic Compounds; Wiley: New York, 1974.
- (36) Strukl, J. S.; Walter, J. L. Spectrochim. Acta. 1971, 27A, 209.
- (37) Moskovits, M. J. Phys. Chem. 1982, 77, 4408.
- (38) Moskovits, M.; Suh, J. S. J. Phys. Chem. 1984, 88, 5526.

# **CHAPTER 4**

SURFACE ENHANCED RAMAN SCATTERING OF
MERCAPTOPYRIDINES AND THE FABRICATION OF A
METAL-ION CHEMICAL SENSOR BASED ON INTEGRATED
OPTICS, EVANESCENT WAVE, SURFACE ENHANCED
RAMAN SCATTERING (IOEW-SERS)

#### 4.1 SUMMARY

We have shown in Chapter 3 the construction and utilization of a planar glass waveguide decorated with 2-D aggregates of Rayleigh limit silver particles by covalent attachment through a propylthiolate moiety anchored at one end to the glass surface. The evanescent field of propagating TE waves was enhanced by coupling with surface plasmon modes of metal particles. In this Chapter, adsorption of 2- and 4-mercaptopyridine on Ag colloid attached to the surface of a waveguide is studied through a comparative analysis of their SERS spectra obtained from metal liquid-like films (MELLFs) and Ag hydrosols. Spectral analysis of adsorbate intensities and frequency band shifts reveals information about surface orientation as well as the mode of adsorption. Both molecules adopt roughly perpendicular orientations when bonded through the sulfur atom to the silver surface. The 4-MPy-modified waveguide was exposed to both proton and metal-ions to explore the possibility of adapting the waveguide as a thin film chemical sensor. Accordingly, a reversible acid-base titration of surface-bound 4-mercaptopyridine (4-MPy) was observed. In contrast, Cu²⁺ is coordinated irreversibly. Spectral changes to the vibrational fingerprint of surface-confined 4-MPy suggest a Cu-pyridine nitrogen interaction binds the Cu²⁺ ions to the surface. X-ray photoelectron spectroscopy (XPS) provides insight into the waveguide fabrication and sensing process as the multi-layer structure is evaluated step-bystep from a silica substrate to the copper ion at the outermost layer. The N 1s region of the XPS spectrum attributed to the pyridine nitrogen of surface-confined 4-MPy molecules and displays a characteristic shift to lower binding energies upon exposure to Cu²⁺ ions.

#### 4.2 INTRODUCTION

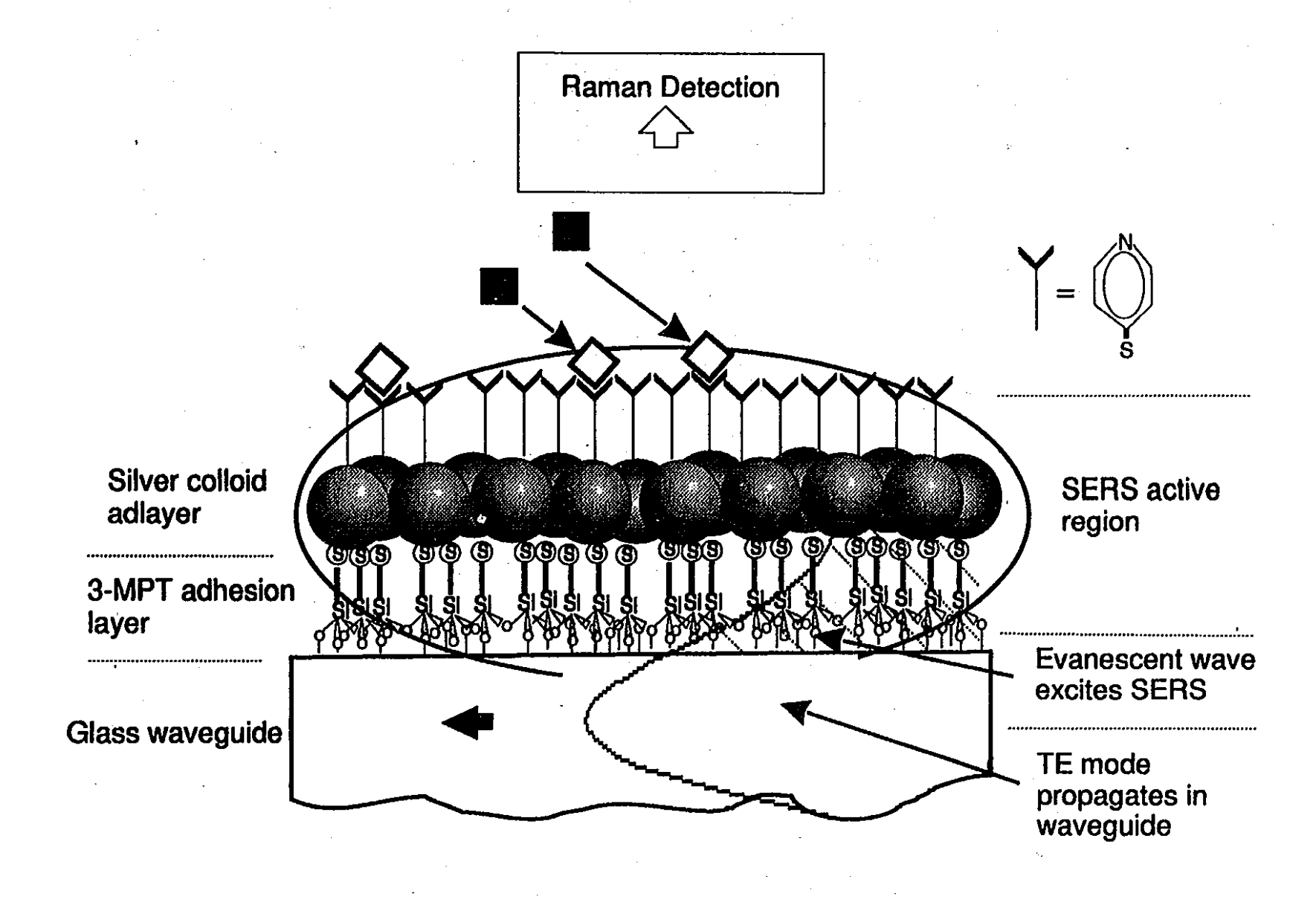
The development of the surface enhanced Raman scattering (SERS) technique has provided an important tool for characterizing organic adsorbates on a variety of metal surfaces, predominately Ag, Au and Cu.^{1,2} In many cases, the SERS effect appears to require the presence of a roughened surface where enhancements of up to a factor of 106 have been achieved. Roughened surfaces have been fabricated in a number of different ways, e.g., by electrochemical roughening of electrodes, through colloidal sols and metal liquid-like films (MELLFs).^{1,3} Recently, a SERS substrate has been constructed in which Ag and Au colloidal particles are anchored onto a supported organic thin film.⁴ This substrate consists of a multilayer structure of three components, viz., an immobilized silver colloidal sol, a coupling-molecular adhesive, and a glass substrate. A bifunctional interfacial adhesive, 3-mercaptopropyltrimethoxysilane (3-MPT), can be used as a molecular adhesive between the colloid and the glass substrate. The 3-MPT is grafted onto the glass substrate by hydrolysis and condensation reactions of the alkoxide termini to form siloxane bonds. Unreacted thiol termini can then bind covalently to a metal colloid. Immersion of the 3-MPT-derivatized glass in a dilute solution of silver hydrosol produces a 2-D colloidal silver array bonded to the surface.⁴ Optically guided light can propagate into the thin colloidal film as an evanescent wave and couple with surface plasmon modes so that the efficiency of waveguiding^{5,6} can be combined with the inherent advantages of SERS⁷. With this approach, the colloidal deposit is thin enough to allow the evanescent wave to propagate against a boundary having a complex refractive index and the refractive index conditions are met whereby the optical field can penetrate the adhesive/metal superstrate film. We describe this complete waveguide-SERS substrate configuration as integrated optics, evanescent wave, surface-enhanced Raman scattering (IOEW-SERS). Typical SERS analytes (e.g., pyridine and its derivatives) are able to adsorb passively on to the waveguide colloid surface from solution. This construction is capable of discriminating

between the waveguide interfaces, thereby providing information on vibrational and structural properties of the adsorbate. This has previously been demonstrated in Chapter 3.

This SERS active optical waveguide structure demonstrates the self-assembly of molecular films to produce precisely controlled surfaces. Thin film surfaces, which provide nanoscale ordered arrays, have far-reaching implications in advancing interface science and materials technologies. Potential uses for organized molecular assemblies, apart from optical waveguides, include surface modification for protective coatings, chemically active surfaces for electrodes, lubrication, sensors, and biologically active surfaces.⁸ In this present work, we further explore the use of this SERS-active optical waveguide as a thin film chemical sensor. Chemical sensors usually consist of a chemically sensitive coating which responds selectively to a particular analyte.9 Sensor fabrication relies upon rational design based on known bulk-phase interactions between the analyte and the functional group of the selective coating. Practical difficulties in the design and use of selective coatings can be limited by using thin films consisting of molecules, known to self-assemble and with simple ion-responsive terminal functional groups. 10 With this in mind, the waveguide surface is modified by a self-assembly process using functionalized organic thiols, 2- and 4-mercaptopyridines (2- and 4-MPy). We investigate the SERS and the application of 4-MPy as a metal-ion based chemical sensor coating using IOEW-SERS. The heterogenous assembly of the waveguide and sensor layer is illustrated in Figure 4.1.

In the first part of this chapter, we compare SERS of 2- and 4-MPy on different silver SERS substrates viz., MELLFs, IOEW-SERS and an Ag colloidal sol. The purpose of this comparison is to establish the extent to which the SERS effect is coextensive from one Ag system to another. Since 2- and 4-MPy are at least ambidentate, 11 they offer several possible modes of adsorption and orientation on a metal surface. The SERS of 2- and 4-MPy have been previously investigated on modified Au, Ag and Pt substrates 12-14 It has been concluded that both 2- and 4-MPy adsorb on the metal surface through the sulfur

FIGURE 4.1 A schematic diagram of the heterostructure assembly, glass/3-MPT/Ag colloid, of IOEW-SER substrate with an adsorbed layer of sensor coating, 4-MPy. The propagating evanescent wave, TE mode (----) leaks into the 3-MPT/Ag colloid overlayers increasing the Raman scattering cross section and enhancing the surface 4-MPy adsorbate vibrations. The selective sensor function of 4-MPy is depicted by the H⁺ ions of 4-MPyH⁺, (□) which are replaced by Cu²⁺ ions (■).



atom with the pyridine ring oriented approximately normal to the metal surface. This mode of adsorption is not surprising considering the strong affinity of thiols for Au surfaces. The surface chemistry of 2- and 4-MPy on Ag(111) electrodes studied by EELS, LEED and Auger spectroscopy also supports this mode of bonding. 16

In the second part of this paper, we examine the intermolecular interaction between the adsorbed 2- and 4-MPy layers with  $H^+$  and  $Cu^{2+}$  ions using IOEW-SERS. Interactions between modified 4-MPy metal substrates and probe ions have been studied by electrochemical methods and were shown to undergo specific analyte interactions involving the uncoordinated pyridine nitrogen. For example, cytochrome c is capable of binding to a 4-MPy-modified Au electrode allowing an electron-transfer reaction between the electrode and cytochrome c. At low pH, modified 4-MPy Au electrodes can electrostatically bind sulfonated anthroquinones. c

We demonstrate that the IOEW-SERS technique is sensitive to metal ion induced perturbations of 4-MPy at submonolayer coverage. SERS spectra of selected modes can be recorded in roughly 45 s of detector integration time, despite the fact that almost all of the power resides in the waveguide. With TE polarization, this is accomplished without optical damage. Finally, we use X-ray photoelectron spectroscopy (XPS) to construct a layer-by-layer interpretation of the 4-MPy derivatized waveguide from the waveguide substrate to the Cu²⁺ ion.

### 4.3 EXPERIMENTAL

Materials. 2- and 4-MPy (Aldrich) were sublimed *in vacuo* immediately prior to use. Other reagents were used as received. Sodium borohydride (99+%, Janssen Chimica) and silver nitrate (p.a. Aldrich) were used for Ag colloid preparation. 3-MPT (Patrarch) was used to functionalize waveguides. For the pH studies, HCl (99.99%, Aldrich) and NaOH (99.99%, Aldrich) were used. Dichloromethane and acetonitrile (Aldrich) were of spectroscopic grade. High-purity water was obtained from a Milli-Q Ultrapure Millipore water system. Glass cover slides (24 x 30 mm x 150 μm, Fisher Scientific) were used as waveguide substrates. Silicon (110) wafers (Vackers Chemitronics) were used for XPS.

**Preparation Procedures.** The Ag colloids used for the waveguide preparation, MELLFs and colloidal sols, were prepared by reduction of AgNO₃ with NaBH₄, following an established method.³

Waveguide Derivatization. Glass waveguide preparation, including derivatization with 3-MPT and the Ag colloid has been detailed in Chapter 3.⁷ The 4-MPy and 2-MPy compounds were adsorbed onto freshly prepared Ag colloidal-derivatized waveguides by immersion for 10 min in a 2 mM acetonitrile solution containing the adsorbate. For the IO-EWSERS experiments with metal-ion probe modification, 2- and 4-MPy derivatized waveguides were immersed in a 2 mM aqueous solution of Cu(NO₃)₂ for 10 min and repeatedly washed with Millipore water. Spectral changes were monitored as a function of the waveguide immersion time in the copper solution. The same waveguide was reimmersed in the copper ion solution after each IOEW-SERS spectrum was collected.

Metal-Liquid-Like Films. Preparation of MELLFs films followed the procedure described in Chapter 2. Optimal results were obtained by mixing equal volumes (2 mL) in a tall, cylindrical glass vial (5 mL), of an aqueous Ag colloid and a dichloromethane solution containing 2 x 10⁻³ M 4-MPy or 1 x 10⁻³ M 2-MPy. The 2-MPy formed a lusterous metallic film at the interface between the aqueous and dichloromethane layers. The 4-MPy adsorbate did not form an metallic film. Instead, the Ag colloidal particles were

transferred from the aqueous to the dichloromethane phase and formed a yellow-orange organosol in which macroscopic aggregates (which appear as a cloudy particulate suspension) were formed at the interface. The "films" were removed from the interface by carefully immersing a small piece of glass slide  $(0.7 \times 0.7 \text{ cm})$  through the solvent phase, transferring the film from the aqueous layer onto the glass and then withdrawing the glass slowly through the solvent phase.

Ag Colloid Sol Systems. The Ag colloid sol of 2-MPy was obtained by adding an aqueous solution of 2-MPy (60 µl, 10 mM) to 2 mL of the colloid. The colloid aggregated immediately, producing a purple color. The mixture was transferred to a capillary sample cell for the SERS measurement. Similarly, the 4-MPy Ag colloidal sol was obtained by adding an aqueous solution of 4-MPy (10 µl, 0.2 mM) to 2 mL of Ag colloid. In this case, aggregation occurred slowly, and gave a purple-brown color. The optimal SERS spectrum was collected after 12 h.

Silver-2- and 4-MPy salts. To prepare the silver-2-MPy and silver-4-MPy salts, equimolar quantities of AgNO3 and 4-MPy or 2-MPy (0.05 mol) were dissolved in ethanol/water solution to yield pale yellow and white precipitates of silver-4-MPy and silver-2-MPy, respectively. The precipitate was filtered, rinsed with ethanol and water, and then dried under vacuum. The FT-Raman spectra of the silver-2- and 4-MPy complexes were measured on the solid samples.

pH Studies. For the pH studies, aliquots of HCl or NaOH were added to an aqueous solution of 4-MPy until the desired pH was reached. Acidic pH studies were also repeated with HClO₄. The FT-Raman spectra of 4-MPy solutions were recorded immediately after preparing the solutions.

Instrumentation. All SERS spectral data were obtained using 514.5-nm (50 mW) radiation from a Spectra Physics Model 164 Ar⁺-laser with an integrated optics spectrometer bench constructed in-house.^{20,21} The detector system consisted of a liquid N₂-cooled charged coupled device (CCD) detector interfaced to an Instruments S.A.

HR640 spectrograph equipped with a holographic grating (1800 grooves mm⁻¹). An acquisition time of 30 s was typically employed for each 500 cm⁻¹ window.

FT-Raman spectra of the 2-and 4-MPy powders, pH solutions and silver-2- and 4-MPy complexes were recorded on a Bruker IFS-88 spectrometer equipped with an FRA-105 Raman module and a liquid N₂-cooled proprietary detector. The spectra were excited with a Nd³⁺:YAG laser operating at 1064.1 nm (150 mW), with 250 scans being typically collected.

X-ray Photoelectron Spectroscopy. For layer-by-layer analysis of the multilayer waveguide by XPS, samples were prepared on the silica overlayer of a conducting silicon wafer. Sample preparation followed the same recipe as that used to prepare the glass substrate waveguides in Chapter 3. We identify each sample with the following label: sample (A): Si wafer; sample (B): Si wafer modified with 3-MPT (Si/3-MPT); sample (C): Si/3-MPT with adsorbed Ag colloid; (Si/3-MPT/Ag); sample (D): Si/3-MPT/Ag with adsorbed 4-MPy, (Si/3-MPT/Ag/4-MPy); and sample (E): Si/3-MPT/Ag/4-MPy immersed in aqueous Cu(NO₃)₂ solution, (Si/3-MPT/Ag/4-MPy/Cu). XPS measurements were performed with a Fisons VG ESCALAB 220i-XL spectrometer. A monochromatized Al Kα radiation source equipped with a magnetic lens (XL) was used. Photoelectrons were collected in constant analyzer energy mode. The high-resolution spectra were collected at a constant pass energy of 20 eV. The base pressure of the turbo-molecularly pumped UHV chamber during XPS analysis was typically 4 x 10-10 torr. The instrument work function of 4.25 eV was referenced to a Au 4f binding energy at 84.0 eV. XPS data were analysed with Fisons Eclipse v1.7p, software provided with the XPS instrument.

#### PART 1. SERS STUDY of 2- and 4-MERCAPTOPYRIDINE

### 4.4 RESULTS AND DISCUSSION

## 4.4.1 SERS of 4-Mercaptopyridine

The SERS spectra obtained for 4-MPy adsorbed on MELLFs, IOEW-SERS and Ag colloid sol substrates are shown in Figure 4.2 (a), (b) and (c), respectively. Peak positions and proposed band assignments for 4-MPy are given in Table 4.1. The assignments are based on those for *para*-substituted pyridine and thiophenol.²²⁻²⁵ Bands assigned to the 3-MPT interface in the waveguide assembly are observed below 1000 cm⁻¹. The 3-MPT adhesive interposed between the silver adlayer and the waveguide glass is a poor Raman scatterer so its contributions to the 4-MPy derivatized IOEW-SERS spectrum are negligible. For comparison, the normal FT- Raman spectra of the bulk silver-4-MPy complex and pure solid 4-MPy are shown in Figure 4.3 (a) and (b), respectively.

SERS spectra of 4-MPy and the normal unenhanced Raman spectrum of silver-4-MPy complex show remarkable similarity in their vil ational profile. Bands at 1616, 1586 1107, 1007, 714, and 430 cm⁻¹ of the silver-4-MPy complex have similar counterparts, though with different intensities, in the SERS spectra of adsorbed 4-MPy on different substrates, e.g., bands at 1617, 1583, 1098, 1015, 709, and 435 cm⁻¹ in the IOEW-SERS spectrum, Figure 4.2 (c). The  $\upsilon_1$  all ring-breathing mode near 1000 cm⁻¹ remains intense for both the normal Raman spectrum of the silver-4-MPy complex and SERS spectra. In the silver complex the intense band at 1041 cm⁻¹ is assigned to a  $\upsilon_{\text{sym}}(\text{NO}_3^-)$  mode from AgNO3. The shoulder at 1051 cm⁻¹ on the higher wavenumber side of the nitrate band is assigned to the 18a₁  $\beta$ (CH) mode. This mode is absent in the IOEW-SERS and colloidal SERS spectra being replaced by a band at 1065 cm⁻¹which we tentatively assign to the 18b₂  $\beta$ (CH) mode. By way of comparison, both the 18a₁ and 18b₂ modes are observed as weak bands in the MELLFs spectrum. The greatest similarity between the SERS spectra and the normal unenhanced Raman spectrum of the silver complex is the dramatic increase

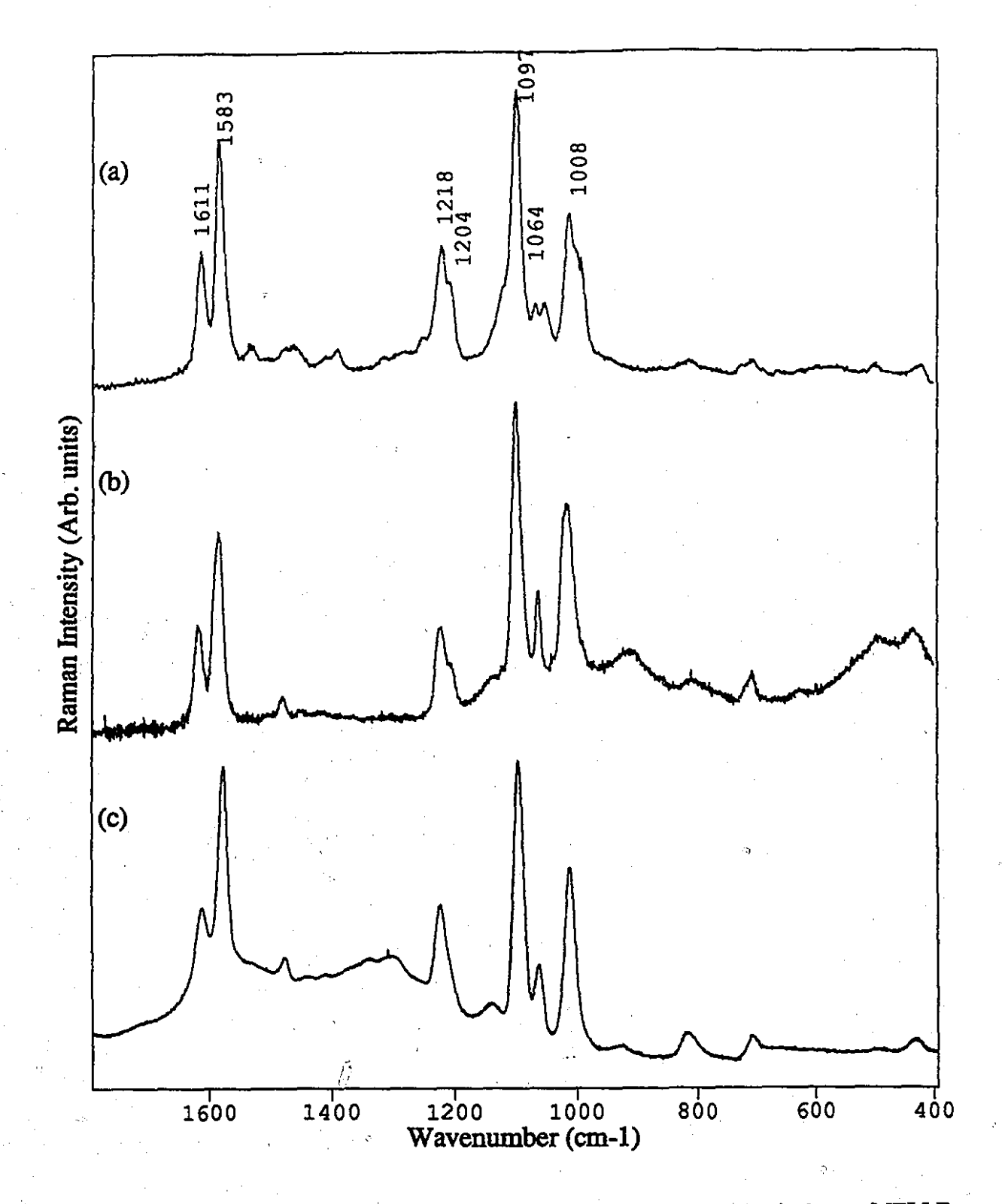


FIGURE 4.2 SERS spectra of 4-mercaptopyridine (4-MPy) adsorbed on: MELLFs (2mL of 2 x  $10^{-3}$  M 4-MPy in 2 mL of colloid) (a); IOEW-SERS (2 x  $10^{-3}$  M of 4-MPy in acetonitrile) (b); and silver hydrosol (10  $\mu$ l of 2 x  $10^{-4}$  M 4-MPy in 2 mL of colloid) (c).

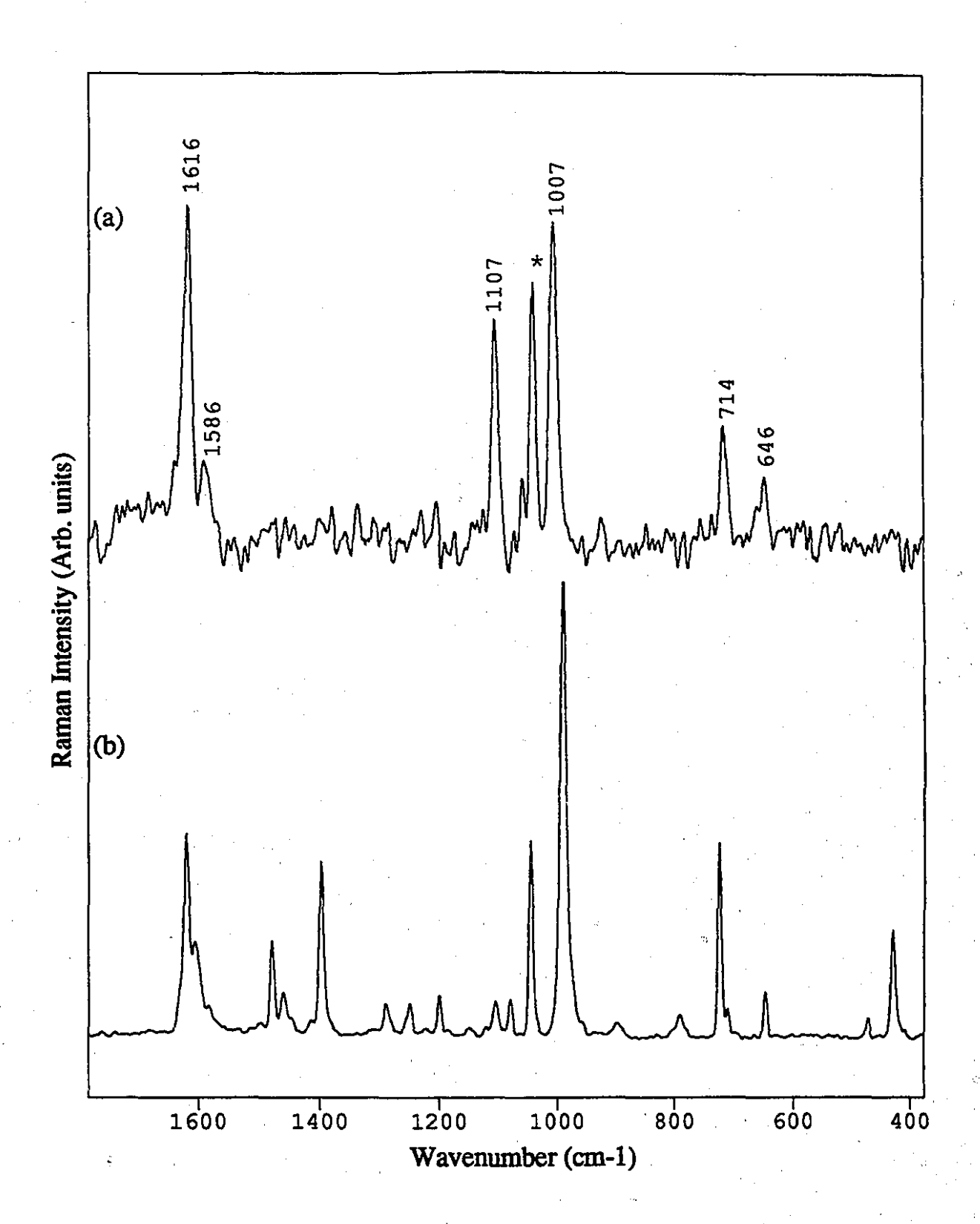


FIGURE 4.3 Unenhanced normal FT-Raman spectra of silver-4-MPy complex (a), and 4-MPy in the solid state (b).  $\lambda_{ex} = 1064.1 \text{ nm}$  at 150 mW.

(*) Band assigned to  $v_{sym}(NO_3^-)$  from AgNO3.

TABLE 4.1 Assignments and wavenumber positions (cm⁻¹) of normal Raman and SERS spectra for 4-mercaptopyridine.

Assignment (a)	Solid	Silver-4- MPy complex	MELLFs	Colloidal sol	IOEW- SERS
7a ₁ , δ(C-S)/γ(CCC)	431	430	415	430	435
16b ₁ , γ(CCC)	471		497		490
6b ₂ , β(CCC)	647	646			
6a ₁ , β(CC)/υ(C-S)	721	714	707	705	709
10b ₁ , γ(CH)	790		811	813	810
	901				
1a _{1,} (Ring breathing)	990	1007	1008	1007	1015
		1041*	•		
18a ₁ , β(CH)	1045		1049		,
18b ₂ , β(CH)	1080		1064	1065	1062
12a ₁ ,(Ring	1106	1107	1097	1098	1098
breathing) / υ(C-S)		•			
	•	•		1135	
$\beta(CH) / \delta(NH)$	1200		1204		1207
9a ₁ , β(CH)	1250	, <del>-</del>	1218	1222	1221
3b ₂ , β(CH)	1290			1305	
		•		1338	
14b ₂ , υ(CC)	1394		1390	1407	
19b ₂ , υ(C=C/C=N)	1459	1	1458	1433	
19a ₁ , ບ(C=C/C=N)	1478		r	1470	1478
			1525		
8b ₂ ,ນ(CC)	1604	1586	1583	1573	1583
8a ₁ , v(CC)	1617	<u>1</u> 616	1611	1615	1617

⁽a) Assignments for the normal Raman spectrum of 4-mercaptopyridine from refs. 22-25.

^(*) Band assigned to  $v_{sym}(NO_3$ -) from AgNO3.

in intensity of the  $v_{12}$  a₁ mode near 1098 cm⁻¹. This band is attributed to a so-called X-sensitive mode. X-sensitive modes are described as modes that are strongly coupled substituent and aromatic ring modes. Coupling is modulated by the local environment of the X substituent. A similar band intensity increase is observed for the SERS of thiophenol,  26  the electrochemical SERS of 4-MPy on Au electrodes  14  and to a lesser extent for the normal Raman of pyridine-metal complexes.  27  This 1098 cm⁻¹ band is assigned to a  $v_{12}a_1$  ring breathing mode coupled to a v(C-S) stretching mode.  $^{14,22-24}$ 

All SERS spectra display an enhanced band near 1220 cm⁻¹. There is no corresponding band observed in the normal Raman spectrum of the silver-4-MPy complex. A band, similar in intensity and frequency position, has been observed for the Ag colloid SERS of pyridine and pyrazine and is assigned to a 9a₁ β(CH) mode.²⁸ Where the normal spectrum of silver-4-MPy complex is featureless between 1580-1250 cm⁻¹, this region in the SERS spectra is populated by vibrational features from 4-MPy that depend on the method of fabricating the SER substrate. Colloidal sol SERS shows peaks at 1470, 1433, 1407, 1338, and 1305 cm⁻¹. Weak vibrational features are observed in the MELLFs spectrum at 1515, 1458, and 1390 cm⁻¹. Interestingly, only one band at 1478 cm⁻¹ dominates the IOEW-SERS spectrum in this region. It is not clear what causes these differences on changing from one SERS substrate to another. Arguments relating to differences in surface potential, adsorbate polarizability, and scale of roughness have been advanced to rationalize similar observations in the past. ^{1,29,30}

## 4.4.2 SERS of 2-Mercaptopyridine

The MELLFs, IOEW-SERS and Ag colloidal SERS spectra of 2-MPy are shown in Figure 4.4 (a), (b) and (c), respectively. The normal FT-Raman spectra of pure 2-MPy and the silver-2-MPy complex are compared in Figure 4.5 (a) and (b), respectively. The vibrational assignments given in Table 4.2 follow those of a previous report and assume that the 2-MPy molecule retains C_s symmetry.³¹ In the solid state, 2-MPy exists as a weak

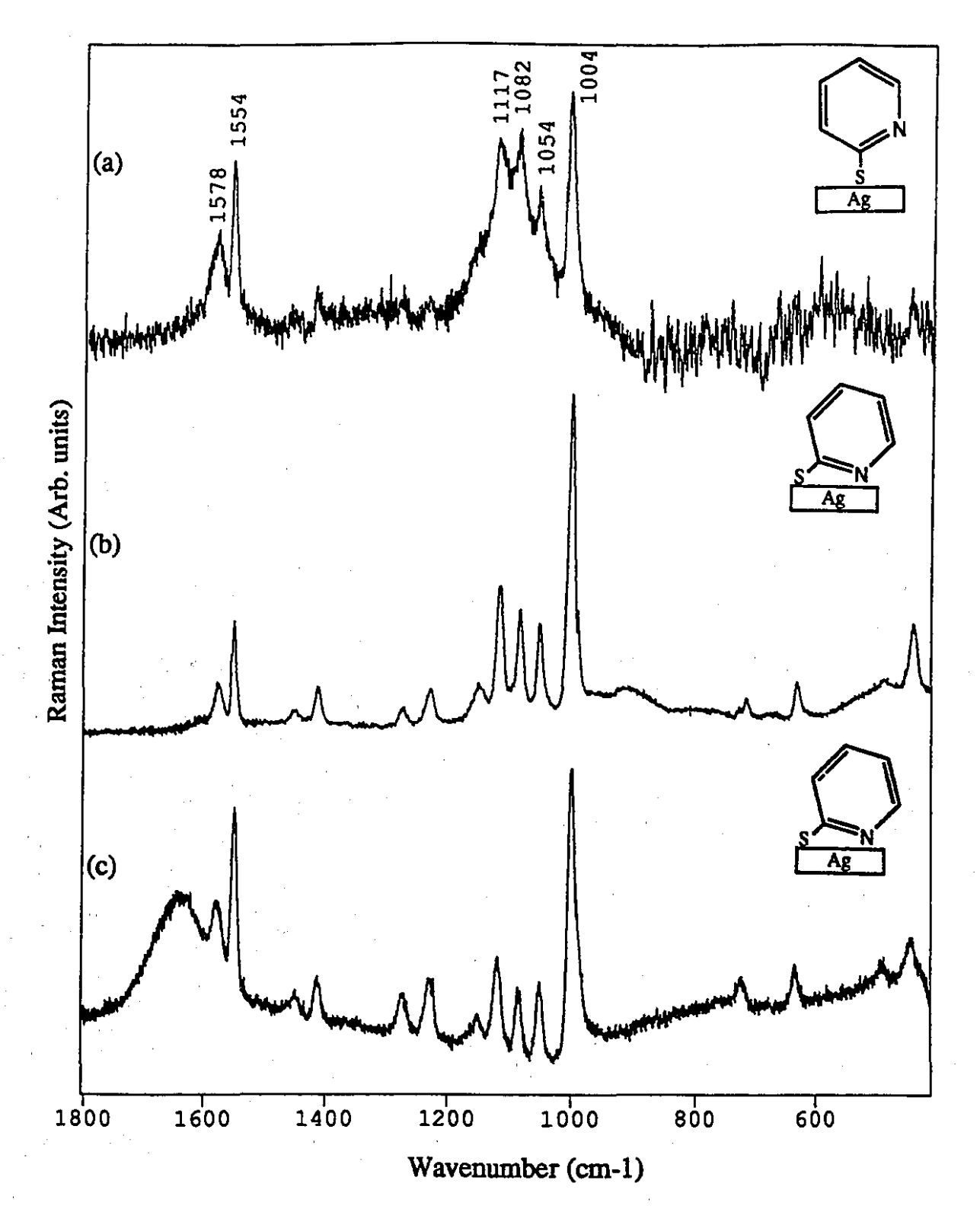


FIGURE 4.4 SERS spectra of 2-mercaptopyridine (2-MPy): MELLFs (2 mL, 2 x  $10^{-3}$  M 2-MPy in 2 mL colloid) (a); IOEW-SERS (2 x  $10^{-3}$  M of 2-MPy in acetonitrile) (b); and silver colloid hydrosol (60  $\mu$ l, 1 x  $10^{-2}$  M 2-MPy in 2 mL of colloid) (c).

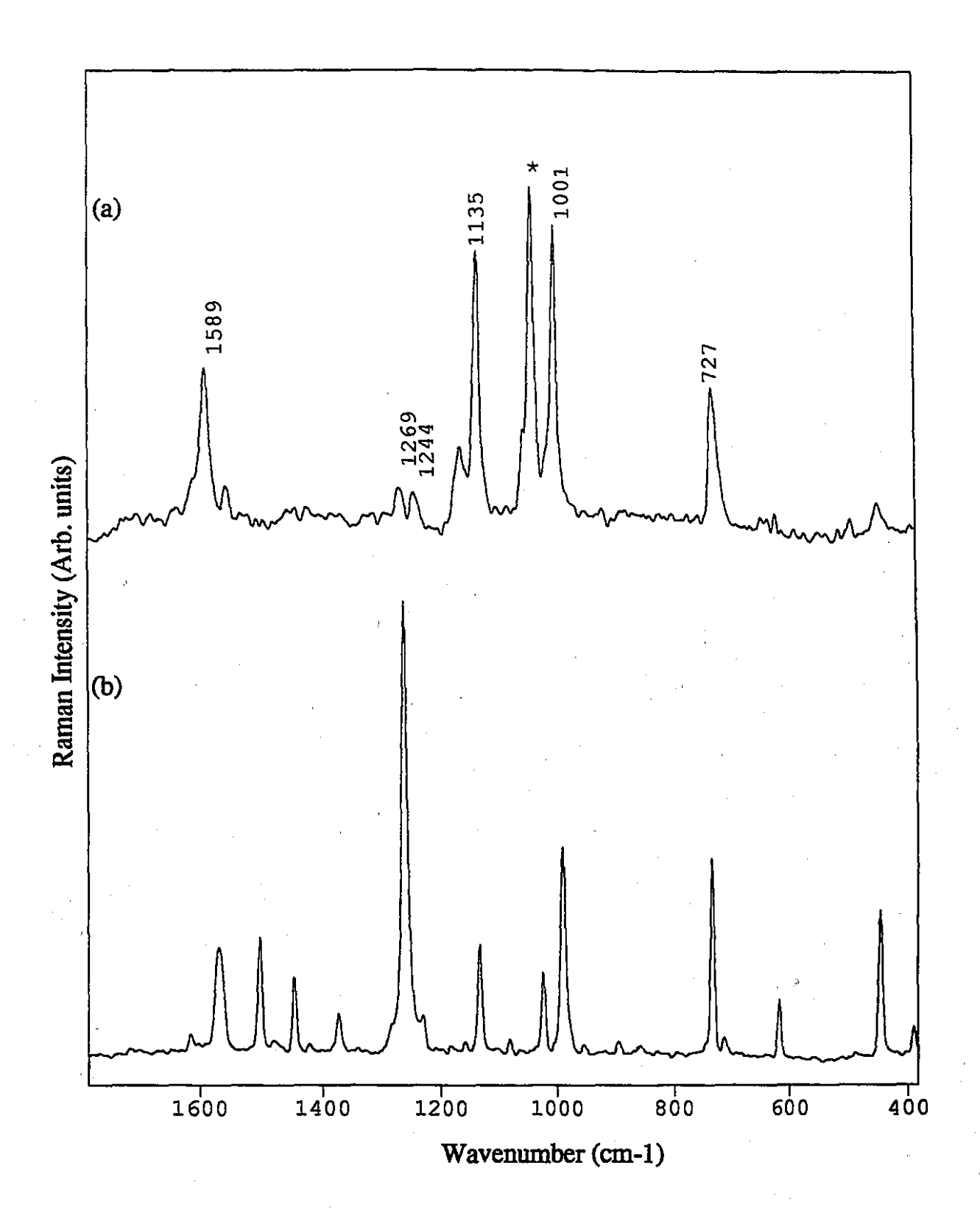


FIGURE 4.5 Unenhanced FT-Raman spectra of silver-2-MPy complex (a), and 2-MPy in the solid state (b).  $\lambda_{\rm ex}=1064.1$  nm at 150 mW.

(*) Band assigned to  $v_{sym}(NO_3^-)$  from AgNO3.

TABLE 4.2 Assignments and wavenumber positions (cm⁻¹) of normal Raman and SERS spectra for 2-mercaptopyridine.

Assignment (a)	Solid	Silver-2- MPy complex	MELLFs	Colloidal sol.	IOEW- SERS
A" 16a, γ(CCC)	389				
δ(C-S) / β(CCC)	445	446		435	432
				485	
A' 6a, γ(CCC)	618			634	630
A" β(CC)	711			2	
A' (C-S)	731	727		720	714
A" γ(CH)	743				
Α" γ(ΝΗ)	893				
Α" γ(CH)	949				
A" γ(CH)	980		•		
A' 1a, (Ring breathing)	988	1001	1004	998	1001
		1041*			
A' 18a, β(CH)	1024	•	1054	1048	1050
Α' 18b, β(CH)	1092		1082	1084	1081
A' 12a, (Ring	1133	1135	1117	1117	1114
breathing)\v(C-S)			*		
ļ		1164		1150	1150
β(CH) / δ(NH)	1230	1244		1228	1230
A' 14b, υ(C=C/C=N)	1261	1269		1274	1272
A' δ(CH)	1372		1417	1411	1413
A' 19b, υ(C=C/C=N)	1444		r.	1448	1451
A' 19a, υ(C=C/C=N)	1502				
A' 8b, υ(C=C)	1569	1589	1554	1549	1551
A' 8a, υ(C=C)	1614		1578	1579	1576

⁽a) Assignments for the normal Raman spectrum of 2-mercaptopyridine given in ref. 31.

^(*) Band assigned to  $v_{sym}(NO_3$ -) from AgNO3.

intramolecularly H-bonded dimer of  $C_{2h}$  symmetry. The normal unenhanced Raman spectrum of the silver-2-MPy complex is similar to that of the silver-4-MPy complex, i.e., the spectrum is dominated by the more intense bands assigned to the  $\upsilon(C\text{-}S)$  modes (1135 and 727 cm⁻¹) and the in-plane ring modes (1589 and 1001 cm⁻¹). The IOEW-SERS and colloidal SERS spectra of 2-MPy display similar band positions with some differences in relative intensities. The Ag colloid SERS spectrum exhibits an additional broad band at 1627 cm⁻¹, tentatively assigned to a  $\delta(H_2O)$  mode from the hydrosol system.³² The X-sensitive mode near 1114 cm⁻¹ remains unenhanced in both substrates relative to the normal Raman spectrum of 2-MPy. By contrast, this mode is enhanced considerably in the MELLFs spectrum. The relative band intensity variations among all SERS spectra may be attributed to orientation effects which are discussed in more detail below.

#### 4.4.3 Orientation

Clearly, it is important to know for the purpose of fabricating a chemical sensor that for a surface confined sensing molecule, the terminal functional group binding site is free to coordinate probe ions from solution. Therefore, an understanding of the orientation of both 2- and 4-MPy ligands on the colloid surface is crucial. Surface selection rules are often applied to molecules on SERS-active substrates to deduce orientations. For C₂v molecules, all four symmetry species are required to define orientation because each contributes information through the polarizability tensor components. Pyridine ring vibrations (under C₂v symmetry) are distributed between, a₁, a₂, b₁ and b₂ symmetry species, all of which are Raman-active. The a₁ and b₂ modes involve in-plane motions while those of a₂ and b₁ symmetry are associated with out-of-plane vibrational motions. The normal Raman spectrum of 4-MPy in the 1800-400 cm⁻¹ region is dominated by the more intense a₁ modes, with the exception of a strong band at 1394 cm⁻¹, assigned to a 14b₂ ring mode. The a₂ modes are inherently very weak in aromatic ring systems and bands assigned to these modes as well as the b₁ modes are weak in the normal Raman

spectrum of bulk 4-MPy. The a₂ modes are not observed and the b₁ modes remain very weak in the SERS spectra of 4-MPy obtained on any substrate. In general, the SERS spectra of 4-MPv are dominated by the more intense bands assigned to b₂ and a₁ modes. For perpendicular orientation, the relative enhancement of bands is in the order of species  $b_1 = b_2 > a_2$ . Molecules lying flat on the surface will experience enhancements such that  $a_2$  $= b_1 > b_2$ . In the SERS spectra of 4-MPy, the  $a_1$  modes remain mostly unenhanced while the relative intensities of the strong a₁ modes at 1617, 1045, 721, and 431 cm⁻¹ have decreased relative to the normal unenhanced Raman spectrum. The most dramatic vibrational enhancements belong to the in-plane modes,  $v_{12}a_1/v(C-S)$ ,  $v_8b_2$  (CC) and  $9a_1$ β(CH). The other b₂ modes that remain unenhanced in the SERS spectra are absent in the normal Raman spectrum of the silver-4-MPy complex. These b2 modes are weak bands in the normal Raman spectrum of pure 4-MPy with the exception of the  $v_{14}b_2$  mode at 1394 cm⁻¹, which appears as a weak band in the MELLFs spectrum. For all SERS spectra, the inherent weakness of the b₁ modes and absence of the a₂ modes makes a comparison of their relative intensites with the a₁ and b₂ modes difficult.²⁶ Moreover, this observation complicates the use of the SERS selection rules in terms of the polarizability tensor components to clearly define the orientation.

Some insight may be gained, however, by considering the directional plane of vibrational modes. Normal modes that involve the in-plane motion of the ring C=C and C=N bond stretches would be expected to be most enhanced for a perpendicular orientation (especially those assigned to  $a_1$  totally symmetric modes that derive significant intensity from the  $\alpha_{ZZ}$  tensor component). The out-of plane  $a_2$  and  $b_1$  modes should experience little enhancement. Alternatively, if the molecule were adsorbed *via* donation of the ring  $\pi$  system, the plane of the aromatic ring would lie parallel to the surface and the totally and nontotally symmetric  $a_1$  and  $b_2$  in-plane modes would be expected to have little or no enhancement, while certain out-of-plane modes would show some enhancement. In the SERS spectra of 4-MPy, the  $v_1a_1$  in-plane totally symmetric ring mode appears as an

intense band. Preferential enhancement of the in-plane  $v_{12a_1}$ ,  $9a_1$   $\beta$ (CH) and  $v_8b_2$  modes suggests that the pyridine plane adopts a perpendicular orientation to the surface.

In the IOEW-SERS and colloidal SERS spectra of 2-MPy, the most intense band is assigned to the  $v_{1}a_{1}$ , ring breathing mode. The in-plane  $v_{8}b_{2}$  and  $v_{1}a_{1}$  modes are also intense but remain unenhanced relative to their counterparts in the normal Raman spectrum of neat 2-MPy. The relative intensity differences observed between the v8b2 stretch mode near 1549 cm⁻¹ and the ring breathing modes,  $v_{1}a_{1}$  and  $v_{1}a_{1}$  at 1000 and 1117 cm⁻¹ respectively, suggest subtle differences in the orientation of 2-MPy on each SERS substrates. In the MELLFs spectrum, the relative intensity of the ugb2 mode is comparable to the  $v_1a_1$  and  $v_1a_1$  modes. Similarly, for the colloidal SERS spectrum, the  $v_2b_2$  mode is comparable in intensity to the  $v_{121}$  mode; however, the relative intensity of the  $v_{1221}$ mode is reduced. Since the v₈b₂ mode involves symmetrical motion of the ring C=C bonds and the  $v_{12a_1}$  mode involves motion of the C-S bond, they are expected to be enhanced when 2-MPy is adsorbed via the sulfur, placing the C-S bond and ring plane normal to the surface. This is the case observed for the MELLFs spectrum. By contrast, the smaller intensity of the v_{12a1} mode in the colloidal SERS spectrum implies that the C-S bond angle is less than normal relative to the colloid surface. The v8b2 mode remains intense relative to the v₁a₁ mode because the plane of the pyridine ring still remains normal to the surface. The ring 'tilts' such that the N atom is in closer proximity to the surface compared to the MELLFs spectrum. In the IOEW-SERS spectrum, the intensity of the  $v_8 b_2$  mode is decreased relative to the  $v_1 a_1$  and  $v_1 a_2$  modes. By analogy, this implies that the plane of the pyridine ring is not normal to the surface, but tilted. This tilted orientation is further supported by the observed out-of-plane  $\delta(C-S)$  band intensity increase at 435 cm⁻¹. A spectral analysis of the v(C-H) stretching region reveals that, overall, this tilt relative to the metal surface is very small.

The spectral region between 2900-3150 cm⁻¹, shown in Figure 4.6, covers the  $\nu$ (C-H) stretching bands of the IOEW-SERS spectra for adsorbed 2- and 4-MPy. The

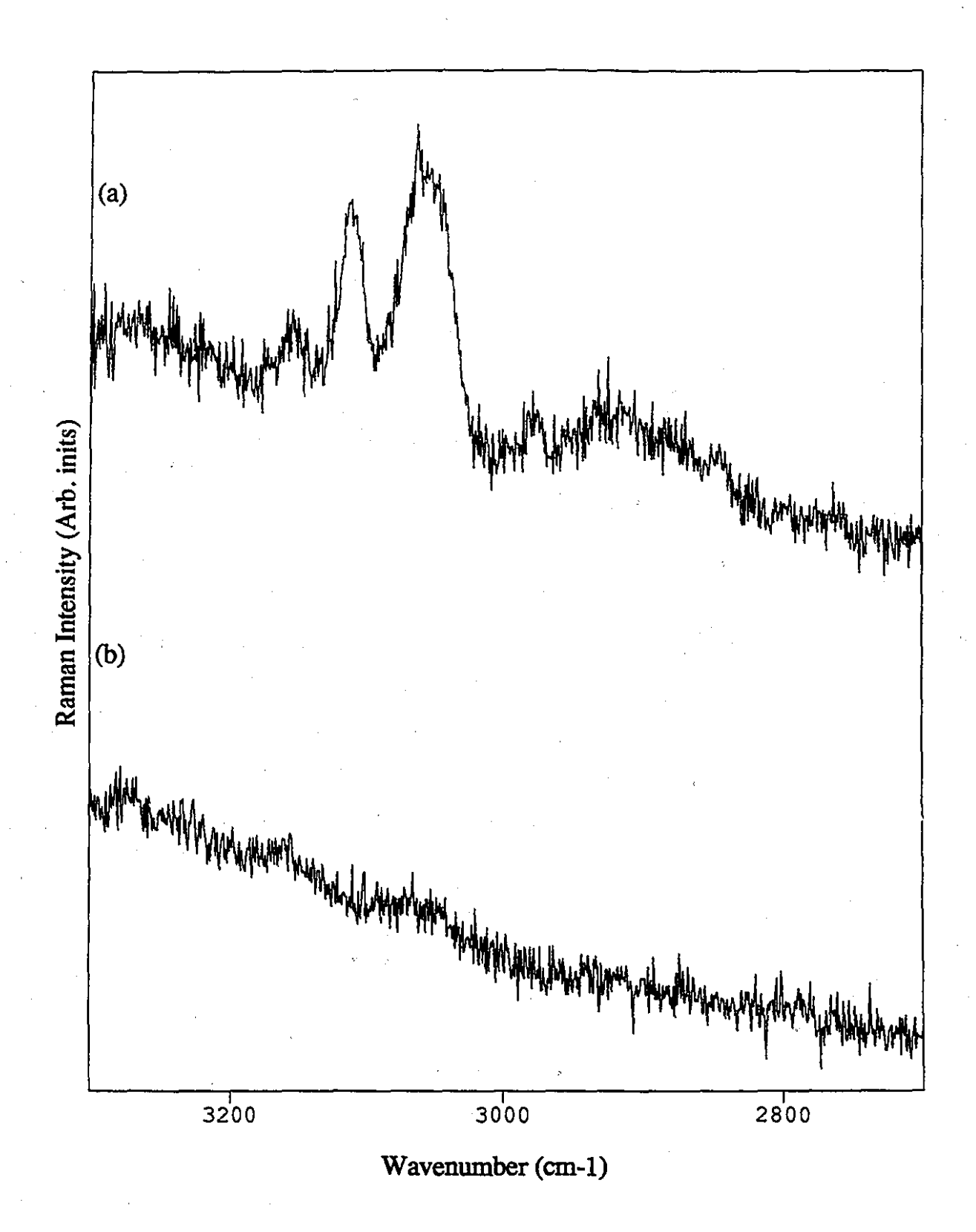


FIGURE 4.6 IOEW-SERS spectra of  $\upsilon(\text{C-H})$  stretching region of adsorbed 2-MPy (a), and 4-MPy (b).

IOEW-SERS spectrum of 2-MPy shows two bands at 3061 and 3109 cm⁻¹ assigned to the totally symmetric C-H stretches.³¹ In contrast, there is only marginal band intensity observed in the IOEW-SERS spectrum of 4-MPy. These observations further support the assigned perpendicular orientation for 2- and 4-MPy. These modes have been used in previous reports to clarify the orientation of aromatic adsorbates on roughened metal surfaces. 29,36 The SERS intensity associated with the v(C-H) mode depends upon the angle at which the C-H bond lies in relation to the silver surface. For a perpendicular orientation, the maximum intensity will be expected for the C-H stretching mode that vibrates normal to the surface. As the angle of the C-H bond relative to the surface decreases, the SERS intensity is expected to decline. Thus for 2-MPy adsorbed normal or near normal to the surface via σ donation through either the nitrogen and/or the thiolate, the C-H stretching modes, should contribute predominantly to the most enhanced band.³⁶ This is particularly true for a C-H bond para to the pyridine nitrogen and/or the sulfur atom. The other C-H bonds lie near 30° (in the molecular plane of the ring) relative to the surface and should exhibit relatively smaller enhancements. Alternatively, 4-MPy adsorbed via the thiolate or nitrogen moiety in a perpendicular orientation would have no C-H bonds normal to the surface. Furthermore, the ortho and meta C-H modes should experience little or no enhancement. The absence of v(C-H) modes in the IOEW-SERS spectrum of 4-MPy is consistent with this interpretation.

### 4.4.4 Mode of Adsorption of 2- and 4-MPy on the SERS Substrate Surface

As discussed previously, studies have indicated that the pyridine ring resides perpendicular to the metal surface for both 2- and 4-MPy. For this orientation, adsorption is expected to occur via  $\sigma$  donation through either the nitrogen and/or the sulfur atoms. Aromatic and aliphatic thiols, e.g., thiophenol, adsorb via the thiolate sulfur and form assembled monolayers on Ag, Au and Cu surfaces, adopting a near-perpendicular

orientation. This mode of adsorption is accompanied by the disappearence of the intense, polarized  $\upsilon(S-H)$  bond located between 2590-2560 cm⁻¹ following cleavage of the S-H bond. The presence of such a diagnostic band is complicated in the case of 2- and 4-MPy since both molecules exist in a thione/thiol tautomeric equilibrium, illustrated in Figure 4.7. The normal Raman spectrum of solid 4-MPy, where the thione tautomer predominates, a broad band is observed between 2500 and 2900 cm⁻¹ attributed to the  $\upsilon(SH)$  and  $\upsilon(NH)$  band contributions associated with the tautomeric structure. The observed band profile is similar to that found in intramolecular hydrogen bonded systems and no changes in the  $\upsilon(S-H)$  band region on either metal complexation or adsorption on a SERS substrate were detected. 39-41

The mode of adsorption on the surface may alternatively be identified by determining the behaviour of C-S bond related vibrations. Among such modes that involve the sulfur atom is the  $v_{6}a_{1}$ , v(C-S) stretching mode, assigned to an X-sensitive mode. 23,41,42 This band shifts to lower wavenumber upon S-methylation or metal ion complexation. In the normal Raman spectra of silver-2- and 4-MPy complexes, the v(C-S) band positions have decreased by 4 and 7 cm⁻¹ from 731 and 721 cm⁻¹, respectively. In the IOEW-SERS spectra of 4- and 2-MPy, the v(C-S) band positions decreased by 12 cm⁻¹ (from 721 cm⁻¹ to 709 cm⁻¹) and 17 cm⁻¹ (from 731 to 714 cm⁻¹), respectively. A similar peak shift has been observed for other aromatic thiols adsorbed via the thiolate such as thiophenol adsorbed on SERS-active metal substrates. 26,43,44 Studies using Auger spectroscopy and EELS conclude that 2- and 4-MPy and thiophenol attach to an Ag(111) electrode substrate primarily through the S atom and that the aromatic ring adopts a perpendicular orientation relative to the surface. 16,45 Preferential enhancement of the υ₁₂a₁/υ(C-S) band at 1098 cm⁻¹ observed in the IOEW-SERS spectrum of 4-MPy is also observed in the SERS of thiophenol. 24,26,44 The most intense SERS enhanced bands of 4-MPy, associated with ring modes (1015, 1098 and 1583 cm⁻¹), have similarly intense counterparts in the SERS spectrum of thiophenol (1000, 1073 and 1573 cm⁻¹). The

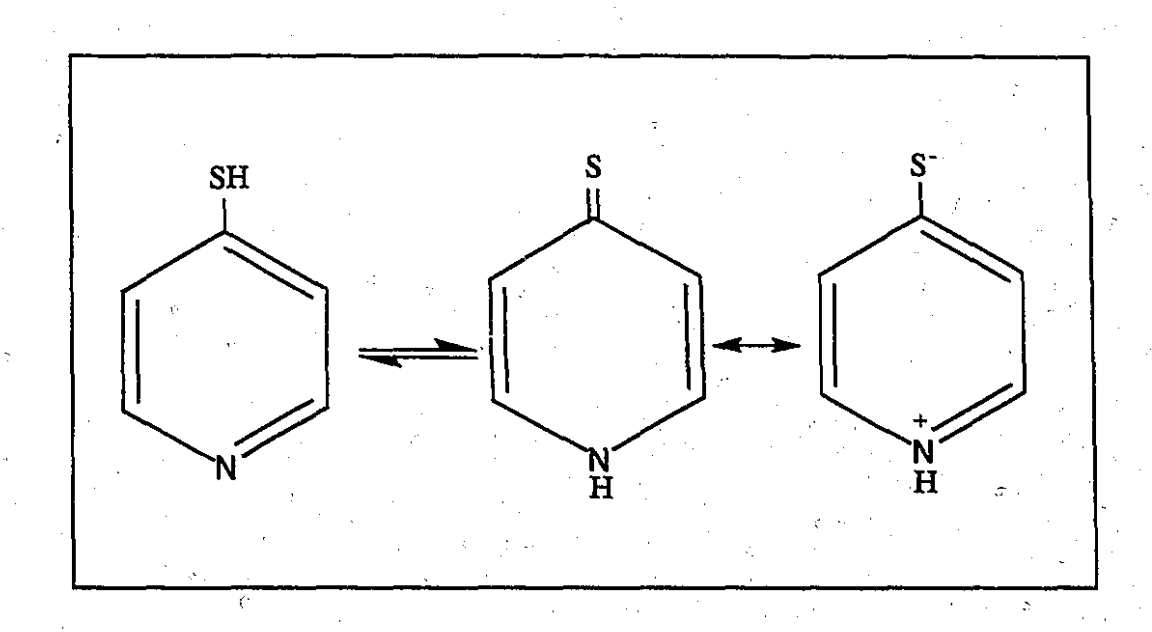


FIGURE 4.7 Thiol-thione tautomers of 4-MPy.

spectral similarities provide further confirmation that 4-MPy is adsorbed *via* the thiolate moiety.

# PART 2. IOEW-SERS STUDY OF THE SENSOR APPLICATION OF ADSORBED 4-MERCAPTOPYRIDINE

#### 4.5 RESULTS AND DISCUSSION

### 4.5.1 IOEW-SERS of Cu²⁺ Ion Binding

To demonstrate the principle of the IOEW-SERS substrate as a metal-ion sensor, the adsorbed 4-MPy layer was exposed to different aqueous metal nitrate solutions prepared from  $M(NO_3)_2$  where  $M = Mn^{2+}$ ,  $Co^{2+}$ ,  $Ni^{2+}$  and  $Cu^{2+}$ . Spectral changes were observed only in the case of  $Cu^{2+}$  ion. The IOEW-SERS spectra of 4-MPy collected as a function of time after immersion in the  $Cu^{2+}$  ion solution, are shown in Figure 4.8. Vibrational modes below  $1000 \text{ cm}^{-1}$  derived from the 3-MPT interface are more apparent in these spectra as the angle of the incident beam relative to the prism is decreased to obtain the optimal spectrum of 4-MPy. We observed that with increased immersion time the relative intensities of some of the 4-MPy modes show a concomitant enhancement relative to the  $v_1$  and  $v_{12}$  bands. A gradual decrease and eventual disappearence of the  $v_{8a_1}$  band at 1617 cm⁻¹ is observed. This is followed by a simultaneous increase in intensity of the  $v_{8b_2}$  band at 1585 cm⁻¹, as well as the appearance of a shoulder at 1015 cm⁻¹, on the higher wavenumber side the  $v_1$  band. This shoulder becomes clearly resolved into a weak band at 1034 cm⁻¹ (Figure 4.9).

Similar spectral changes have been reported for an electrochemical SERS experiment of 4-MPy adsorbed on a gold electrode. At positive potentials, the bands at 1010 and 1585 cm⁻¹ decrease in intensity and eventually disappear at potentials more positive than 0.5 V. This observation has been interpreted in terms of a loss of aromaticity of the pyridine ring. Some insight into the interaction of copper with surface-confined 4-MPy may be gained by comparison with pyridine coordination complexes. Changes observed in the internal vibrational frequencies of pyridine on metal-ion complexation are, however, minor. Generally, the metal-pyridine modes which appear below 400 cm⁻¹ are

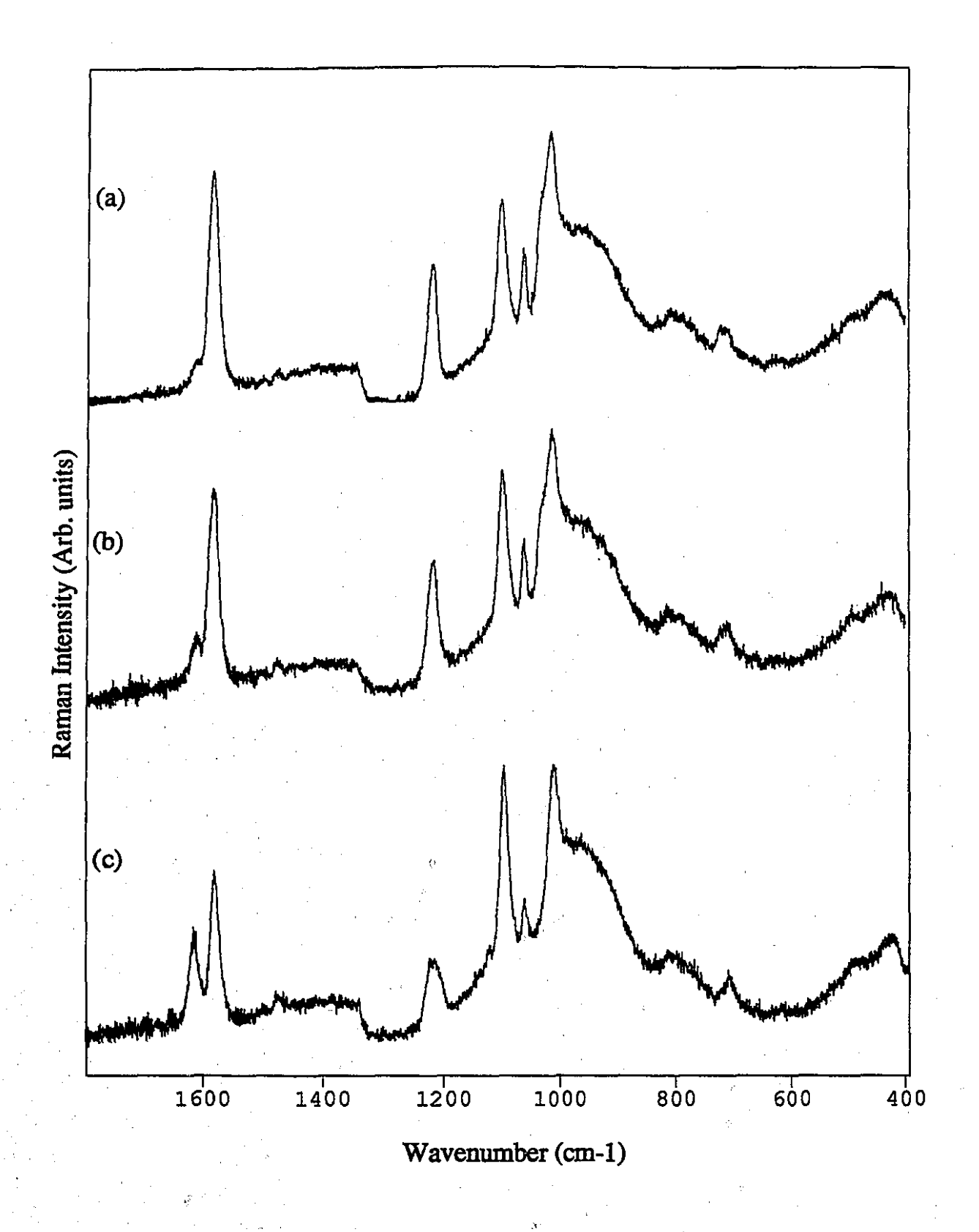


FIGURE 4.8 IOEW-SERS spectra of 4-MPy after immersion in 2 x  $10^{-3}$  M aqueous solution of Cu(NO₃)₂: after 30 min immersion (a); after 10 min immersion (b); and before exposure to the Cu²⁺ solution (c).

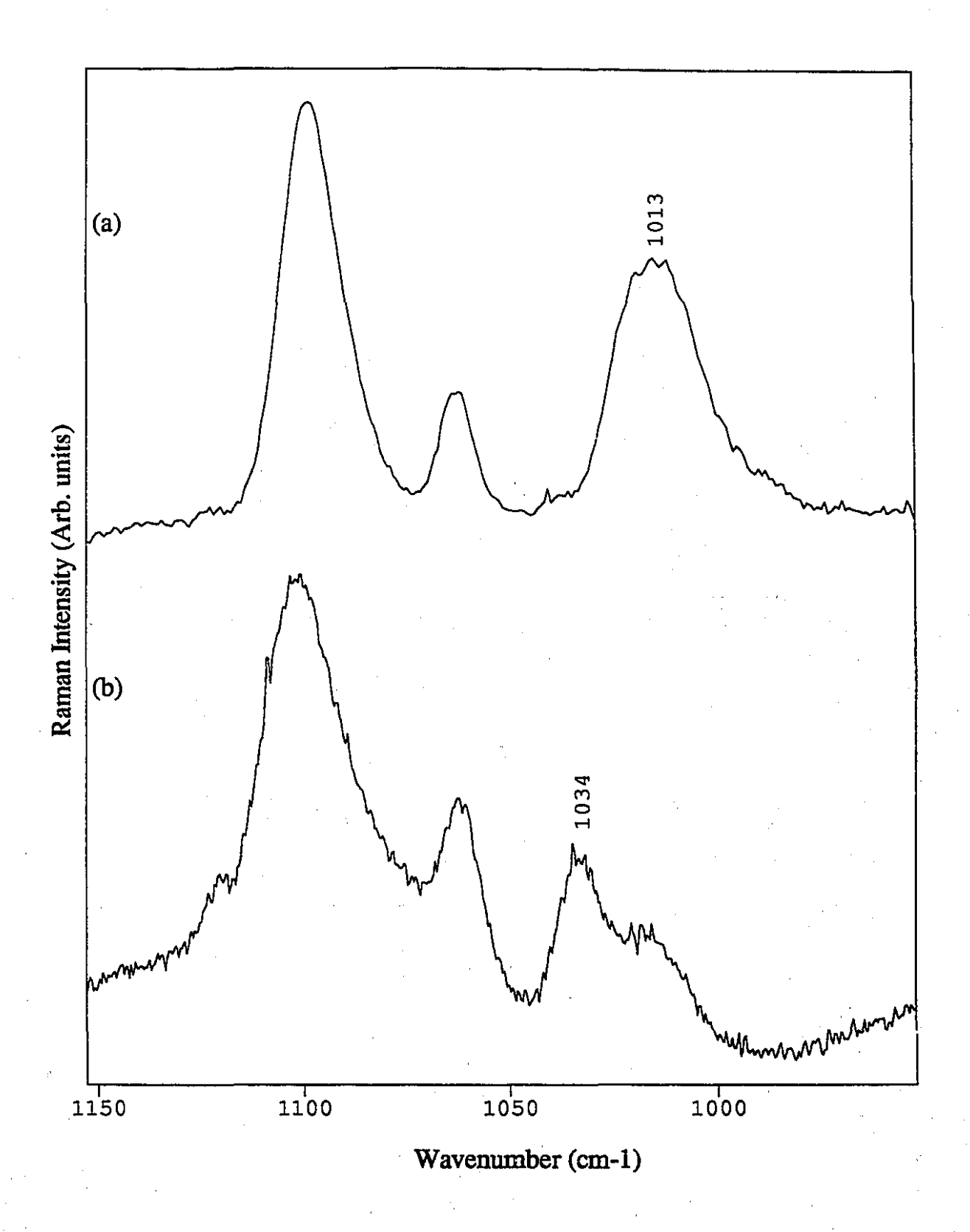


FIGURE 4.9 IOEW-SERS spectra of  $\upsilon_1$  ring breathing mode of 4-MPy before exposure to  $Cu^{2+}$  (a), and after exposure to  $Cu^{2+}$  ion solution (b).

reported since these are characteristic vibrational changes indicating complexation.⁴⁶ Minor perturbations are detected for the ring stretches and C-H deformations of pyridine and substituted pyridines.^{27,47} Among the changes observed is the shift of the  $v_1$  band to higher energies due to coordination to the pyridine nitrogen.⁴⁸ For example, the  $v_1$  mode in free 4-methylpyridine shifts from 996 to 1036 cm⁻¹ in CuCl₂(4-methylpyridine) and from 991 in free pyridine to 1020 cm⁻¹ in Cu(NO₃)₂(pyridine)_x, where x = 2, 4, and 6.⁴⁹

The IOEW-SERS spectrum of 4-MPy after exposure to  $Cu^{2+}$  shows a decrease in the relative intensity ratio for the  $\upsilon_1$ :  $\upsilon_{12}$  bands. The SERS of neutral pyridine adsorbed on Ag electrodes has also revealed similar changes. The  $\upsilon_{12}$  band at 1035 cm⁻¹ increases in intensity relative to the  $\upsilon_1$  mode at 1010 cm⁻¹ near zero potential charge (pzc). Intensity ratio differences were attributed to the presence of both chemisorbed (Lewis acid type coordination) and physisorbed, weakly bound species on different Ag sites. Accordingly, we assign the band at 1034 cm⁻¹ in the IOEW-SERS spectrum of 4-MPy to the  $\upsilon_1$ , ring breathing mode of a coordinated pyridine nitrogen. The  $\upsilon_1$  band at 1015 cm⁻¹ does not completely disappear, presumably since not all of the pyridine nitrogen of the surface confined 4-MPy molecules are accessible or are located in regions on the colloid where insufficient numbers of 4-MPy molecules are anchored to form stable coordination complexes.

By comparison, the IOEW-SERS spectrum of 2-MPy exhibited no significant differences after immersion in the copper nitrate solution. The interaction of Cu²⁺ with a para-substituted pyridine nitrogen is reasonable assuming the 4-MPy molecules are adsorbed in a perpendicular orientation exposing the pyridine nitrogen binding site. On the other hand, the unchanged spectrum observed for 2-MPy upon Cu²⁺ addition is consistent with a sterically hindered nitrogen position which is unable to interact with copper.

To shed further light on spectral changes associated with nitrogen coordination of surface-confined 4-MPy, pH studies were conducted. A simple test of the sensing ability of a surface-confined 4-MPy overlayer is to quarternize the pyridine nitrogen.

#### 4.5.2 IOEW-SERS of Proton Binding

Figures 4.10 and 4.11 show the unenhanced FT-Raman and IOEW-SERS spectra of the vga₁ and vgb₂ band region of 4-MPy under three different pH conditions. In acidic solution, the normal Raman spectrum of 4-MPy displays a band at 1626 cm⁻¹. This band position is similar to a band near 1630 cm⁻¹, assigned earlier to the free pyridinium species, pyH⁺, of pyridine hydrochloride and aqueous *para*-substituted pyridine hydrochloride²⁵. In basic conditions, only one band at 1585 cm⁻¹ is observed, which is attributed to the deprotonated tautomeric thiolate ion species of 4-MPy. At pH 8.4, two bands are present at 1626 and 1585 cm⁻¹, which can be attributed to the presence of both the protonated and non-protonated tautomeric forms. This pH value is comparable to the pKa' value of 8.65 for 4-MPy.⁵¹⁻⁵³

The sensitivity of adsorbed 4-MPy to pH was monitored by IOEW-SERS. The 4-MPy derivatized waveguide was immersed in the appropriate pH solution and removed after 10 min. The IOEW-SERS spectra collected from a waveguide immersed in solutions at pH 14 and pH 6.4 are shown in Figs. 4.11 (a) and (b), respectively. Relative intensity changes observed in the solution-phase normal Raman spectra under different pH conditions were similar to those observed in the IOEW-SERS spectra. The IOEW-SERS spectrum of 4-MPy from pH 14 solution shows an intensity increase of the 1585 cm⁻¹ band relative to the 1617 cm⁻¹ band. The former band is assigned to the deprotonated thiolate component by analogy with the normal Raman spectrum of 4-MPy in basic solution (see above). The weak band at 1617 cm⁻¹ band indicates some 4-MPy molecules remain protonated, as 4-MPyH⁺, on the colloid surface. The relative intensity of the 1617 cm⁻¹ band increases dramatically after immersion in a pH 1 solution, Figure 4.11 (c). This band remains unshifted from that observed in the normal unenhanced Raman spectrum of solid 4-MPy where the thione form predominates but occurs at a lower frequency than expected for free pyridinium ion (1630 cm⁻¹). The absence of the 1585 cm⁻¹ band in the IOEW-SERS spectrum at pH 1 reflects the predominance of a pyridinium cation species. As the

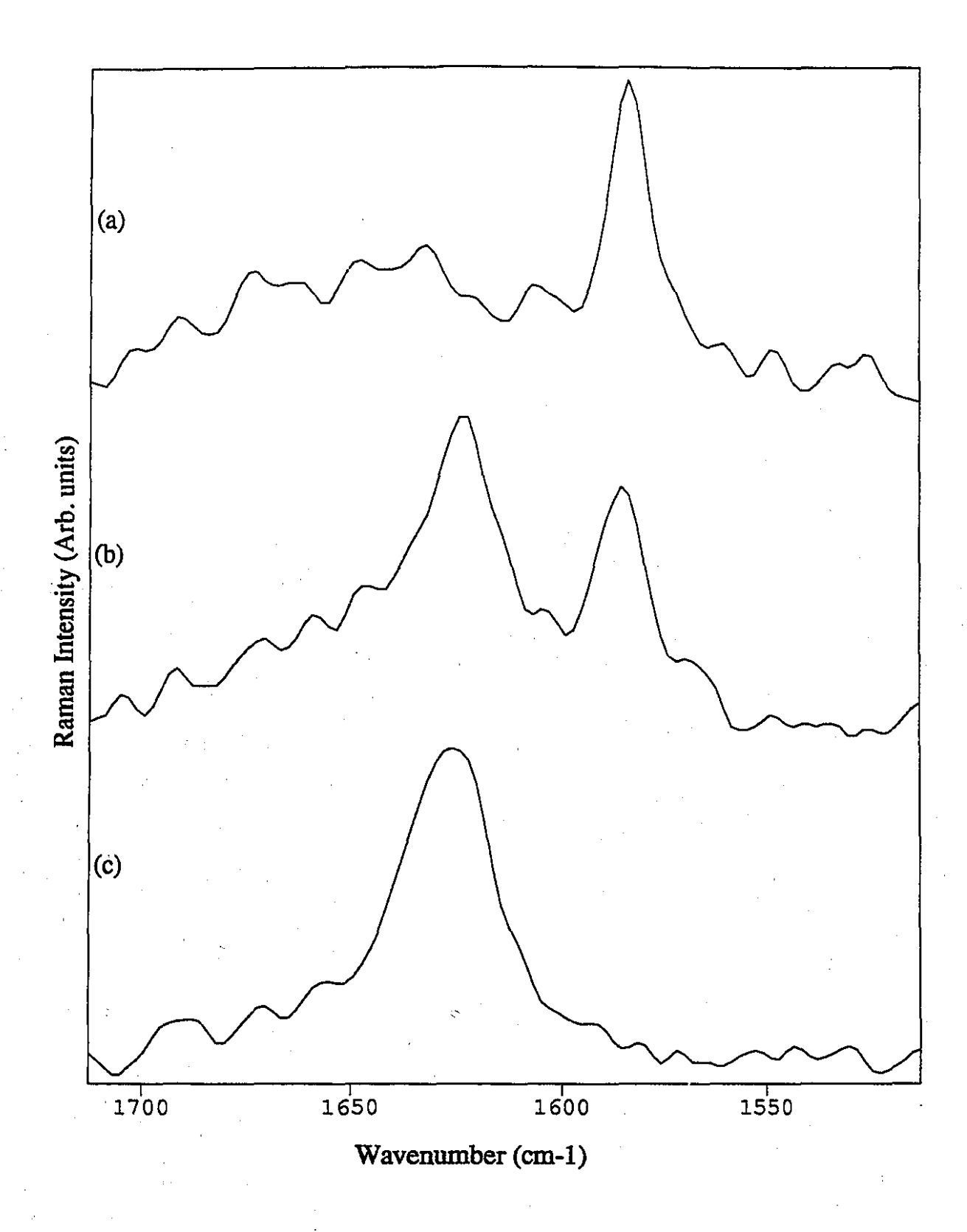


FIGURE 4.10 Unenhanced FT-Raman spectra of 4-MPy in different aqueous pH solutions at different pH: pH 14 (a); pH 8.3 (b); and pH 1 (c).

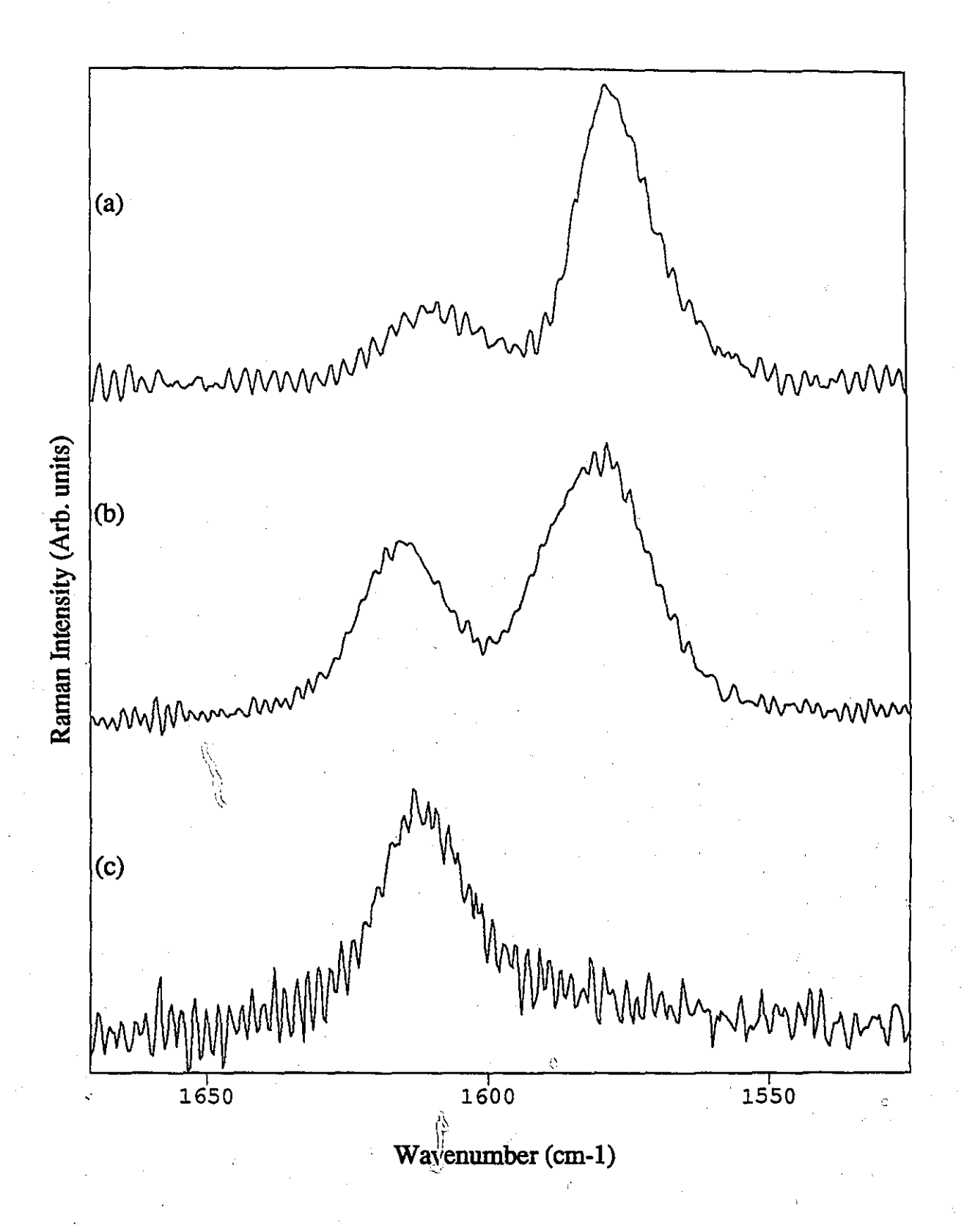


FIGURE 4.11 IOEW-SERS spectra of 4-MPy immersed in different aqueous solutions at different pH: pH 14 (a); pH 6.4 (b); and pH 1 (c).

pH is increased to pH 6.4, the presence of both 1617 and 1585 cm⁻¹ bands suggests that the adsorbed 4-MPy overlayer is an equilibrium between both protonated and non-protonated pyridine nitrogen forms. The spectral changes observed in the IOEW-SERS spectrum were reversible when the waveguide was reimmersed in either strongly acidic or basic solution. These findings are similar to those reported for the SERS study of 2-MPy adsorbed on a Au electrode at various pH conditions where a similar reversibility was noted.¹³

The IOEW-SERS spectra of 4-MPy, the pH of which had been adjusted with HClO₄, were similar to the spectra obtained with HCl. The HClO₄ anion, in contrast to HCl, is relatively non-adsorbed on Ag substrates. Spectral changes reported for pyridinium chloride adsorbed on an Ag electrode (Raman bands at 1024 and 1026 cm⁻¹) associated with an electrostatic bonded PyH+Cl⁻ species where not observed in the IOEW-SERS spectra.⁵⁴.

In comparison, a non-reversible spectral change was observed after the protonated/non-protonated waveguide was reimmersed in the Cu²⁺ solution. Spectral changes were observed associated with Cu²⁺-4-MPy coordination (see above) and after reimmersion in pH 1/pH 14 solutions, no spectral changes were observed.

# 4.5.4 X-Ray Photoelectron Spectroscopy (XPS) Analysis: Results and Discussion

XPS was used to examine each layer that makes up the heterogenous multilayer structure of the waveguide, from the glass substrate to the Cu²⁺ ions. Each sample was examined in the following regions: S 2p, Ag 3d, Cu 2p and N 1s. The binding energy shifts and the full width at half maximum (FWHM) of the peaks obtained from curve fitting for S 2p, N 1s and Cu 2p, are presented in Table 4.3, for samples (A)-(E). The curve fitting for each atom of each layer of the waveguide, in particular for the S 2p region, was performed based on a model (Fig. 4.1) derived from spectroscopic data obtained from the

previous IOEW-SERS experiment (including Chapter 3). The resulting XPS peak deconvolution can thus be used as a qualitative supplement to IOEW-SERS interpretation.

The first step in preparing the waveguide is to functionalize the glass with 3-MPT. We turn our attention first to the S 2p region, shown in Figure 4.12. The S 2p peak of 3-MPT is located near a bulk Si plasmon (167.9 eV) which is observed for the clean Si substrate, (sample A) and is included as a constant contribution in the curve fitting of S 2p peak maxima positions. An additional broad band is curve fitted (170.5 eV) in the Si plasmon region as a result of the background from the asymmetric Si plasmon peak. The S 2p envelope is clearly observed simply by subtracting the normalized bulk Si plasmon and the remaining S 2p contribution is given in Figure 4.13. The curve fit and parameters obtained for the S 2p region of each sample are shown in Figure 4.14 and Table 4.3, respectively. The S 2p spin-orbit splitting used (1.2 eV) and relative height ratio of 1:2 was taken from the literature.⁵⁵ Spectral line widths (FWHM) for some S 2p peaks were larger than reported literature values of 1.0 eV.55 These variable line widths may reflect the compositional heterogeneity of the sulfur environment. The spectrum obtained from sample B exhibits a peak assigned to the S 2p_{3/2} transition at 163.7 eV. This binding energy is within the range expected for an unreacted thiol.⁵⁵ This signal is attenuated substantially after the addition of Ag colloid in sample C, Figure 4.12 (C). In addition, a new S 2p_{3/2} peak at lower binding energy (162.4 eV) is observed. Studies of alkylthiols and thiophenol on various metal surfaces report similar lower binding energy shifts which have been attributed to the formation of a thiolate species (RS-M).55-59 Both the attenuation of the total S 2p intensity and the lower binding energy contribution indicate that a chemical interaction between the sulfur of the 3-MPT interface and the adsorbed Ag colloid has occurred. This interpretation complements the spectral analysis of the IOEW-SERS spectrum given in Chapter 3. Preferential enhancement and decrease in energy of the v(C-S) bands of the 3-MPT interface (relative to the normal unenhanced Raman spectrum of bulk 3-MPT) were attributed to the formation of an Ag-S bond in the Ag

TABLE 4.3 XPS binding energy shifts (eV) and FWHM (in parentheses) for samples (A) - (E).

		····			
Samples	(A)	(B)	(C)	(D)	(E)
	Si (plasmon)	Si/3-MPT	Si/3-MPT/Ag	Si/3-MPT/Ag/	Si/3-MPT/Ag/
Element	<u> </u>			4-MPy	4-MPy/Cu
	170.5 (7.0)*				
Si (plasmon)	167.9 (5.3)				. •
S 2p _{3/2}		163.7 (1.2)	163.7 (1.6)	163.6 (1.7)	163.6 (1.5)
	,		162.4 (1.6)	163.4 (1.2)	163.4 (1.2)
				162.4 (1.6)	162.3 (1.8)
S 2p _{1/2}		164.9 (1.2)	164.9 (1.6)	164.8 (1.7)	164.8 (1.5)
		$\frac{1}{ x_i } = \frac{1}{ x_i } = \frac{1}{ x_i }$	163.6 (1.6)	164.6 (1.2)	164.6 (1.2)
				163.6 (1.6)	163.5 (1.8)
N 1s	* · · · · · · · · · · · · · · · · · · ·			401.2 (1.8)	401.0 (2.5)
				399.5 (1.8)	399.0 (1.6)
				er en	
Cu 2p _{3/2}	:				934.9 (2.0)
			•		933.0 (1.6)
	•, •				•
Cu 2p _{1/2}					954.7 (2.2)
					952.7 (1.9)

^{*} See text.

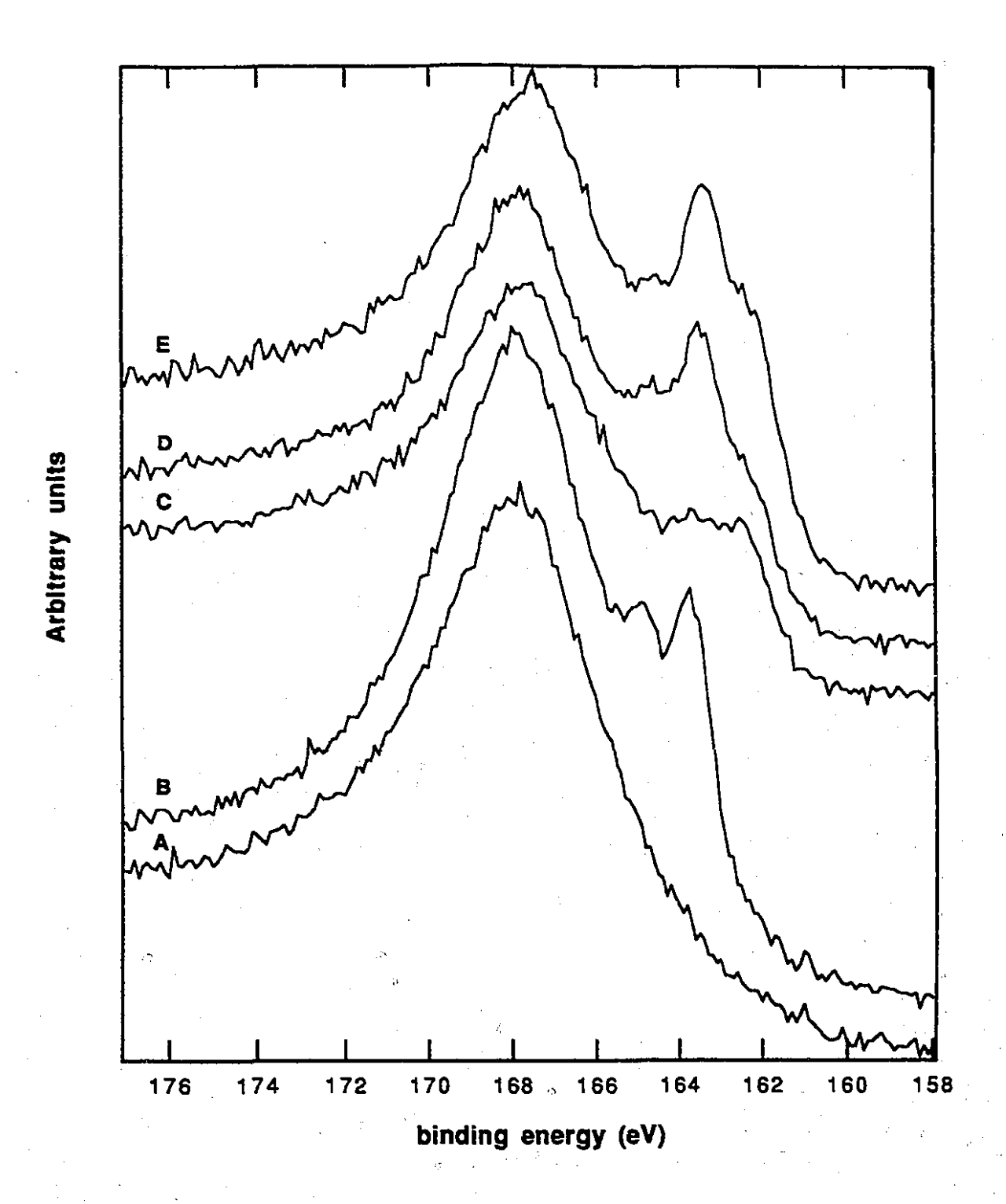
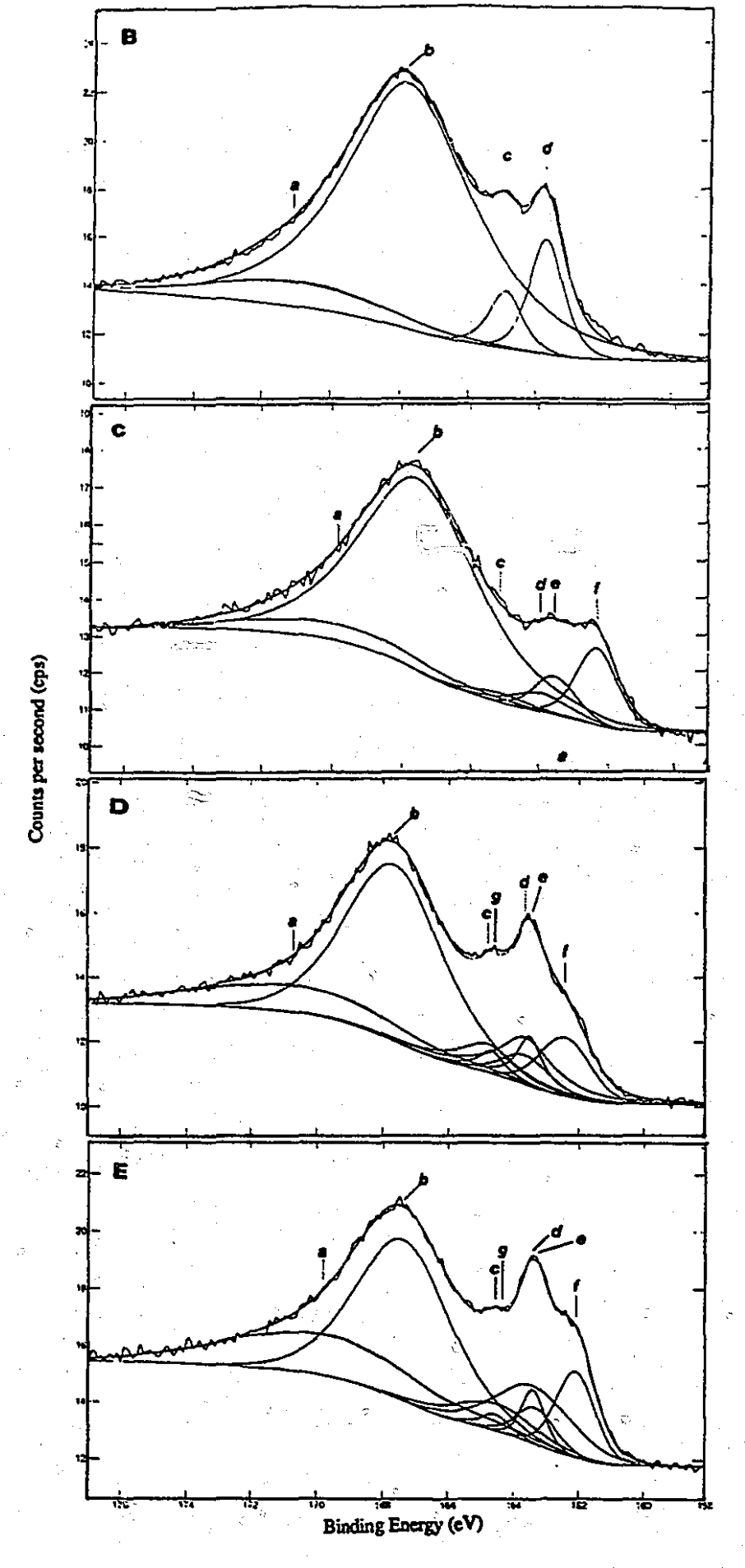


FIGURE 4.12 XPS of Sulfur 2p region with surface bulk Si plasmon for sample (A): Si wafer; sample (B): Si wafer modified with 3-MPT, (Si/3-MPT); sample (C): Si/3-MPT with adsorbed Ag colloid, (Si/3-MPT/Ag); sample (D): Si/3-MPT/Ag with adsorbed 4-MPy, (Si/3-MPT/Ag/4-MPy); and sample (E): Si/3-MPT/Ag/4-MPy immersed in aqueous Cu(NO₃)₂ solution, (Si/3-MPT/Ag/4-MPy/Cu).

FIGURE 4.13 XPS of Sulfur 2p region without surface bulk Si plasmon.

FIGURE 4.14 Curve fitted S 2p peaks for samples (B): Si wafer modified with 3-MPT, (Si/3-MPT); sample (C): Si/3-MPT with adsorbed Ag colloid, (Si/3-MPT/Ag); sample (D): Si/3-MPT/Ag with adsorbed 4-MPy, (Si/3-MPT/Ag/4-MPy); and sample (E): Si/3-MPT/Ag/4-MPy immersed in aqueous Cu(NO₃)₂ solution, (Si/3-MPT/Ag/4-MPy/Cu).



colloid derivatized waveguide. The S 2p signal becomes more complex after the adsorption of 4-MPy in sample D, Figure 4.14 (D). The S 2p region now consists of an additional peak centered at 163.4 eV and a number of overlapping peaks. The thiolate S 2p_{3/2} peak from the Ag/3-MPT interface remains unshifted at 162.4 eV and retains the same FWHM (1.6 eV). Although curve fitting does not provide an unambiguous result because of the relatively featureless band envelope, it clearly shows an additional S 2p peak contribution from the sulfur atom of 4-MPy after the adsorption of 4-MPy to the colloidal silver surface. After immersion of sample D in an aqueous solution of Cu(NO₃)₂, there is a further increase in the peak complexity of the S 2p envelope. Several sets of components represented the S 2p envelope equally well. However, there is clearly an increase in the intensity of a shoulder to the lower binding energy side of the S 2p envelope.

The interaction of Cu(NO₃)₂ with 4-MPy molecular adsorbate is more evident in the N 1s peak region since it is at nitrogen where coordination of  $Cu^{2+}$  is most likely to occur. The pyridine nitrogen N 1s peaks for samples C, D and E and the fits obtained are shown in Figures 4.15 and 4.16, respectively. Sample C (without 4-MPy) shows no N 1s intensity and after derivatization with 4-MPy (sample D), the N 1s region consists of two peaks. These bands are located at 401.2 and 399.5 eV with intensity ratios of 2:1, respectively. The observation of two N 1s binding energy peaks in sample D suggests that there are two different nitrogen environments. Whereas previous reports have indicated at least two binding energies for N-bonded and physisorbed "pyridine" on crystalline metal surfaces⁶⁰⁻⁶⁵, coordination to a silver surface ion our case, seems unlikely, in view of our spectroscopic analyses thus far. Accordingly, we have observed from the IOEW-SERS study of the 4-MPy derivatized waveguide that a band at 1617 cm⁻¹ is associated with a pyridinium 4-MPyH⁺ species. This band is present even after immersion in pH 14 solution. Therefore we tentatively assign the two N 1s binding energies in sample (D) to thiolate bound 4-MPy (399.5 eV) and 4-MPyH+ (401.2 eV) species on the colloid surface. After addition of Cu²⁺ in sample E, two new N 1s peaks appear at 400.0 and 399.0 eV,

respectively. These shifts to lower binding energy are consistent with trends reported for pyridine nitrogen chemisorption interactions on metal surfaces.⁶³ In this case, the N 1s binding energy changes may result from uncoordinated and copper nitrogen or from nitrogen in different coordination environments with copper ion.. Copper coordinates to 4-MPy without nitrate counterion since no nitrate N 1s peak (406.0 eV) was observed for this anion.

The Cu 2p peaks obtained from sample E are shown in Figure 4.17. The curve fit for Cu 2p, shown in Figure 4.18, displays two intense bands for both the Cu 2p_{3/2} and 2p_{1/2} regions at 933.0 eV and 952.7 eV, respectively. Shoulders on the higher binding energy side of each peak are resolved at 934.9 eV and 954.7 eV, respectively. The oxidation state(s) of copper is, however, not distinguishable solely on the basis of their 2p_{3/2} binding energies.^{67,68} In addition to a Cu-N interaction, the Cu 2p_{3/2} peak at 933 eV could also arise from either a copper oxide species^{68,69} or from photoreduction process initiated by XPS irradiation.^{70,71} In addition, thiols are known to be oxidized to a disulfide while Cu(II) is reduced to a stable Cu(I) species.⁷² The IOEW-SERS spectrum is complicated by a broad background from the waveguide interface and an indication of a possible Cu-sulfur interaction, either by the appearance of a v(S-S) band¹⁴ or by v(C-S) frequency shifts cannot be confirmed.

The Ag 3d spectra, shown in Figure 4.19, corroborates the formation of an Ag-S bond at the 3-MPT/Ag interface already observed in the S 2p spectra. After immersing the Si/3-MPT substrate (sample B) in silver colloid, an Ag 3d doublet was observed, shown in sample C. The doublet feature reflects a spin-orbit coupling of 6 eV. The peak maximum of the Ag 3d_{5/2} peak is located at 368.3 eV, a similar value has been reported for thiophenol adsorbed on silver. 66 However, the attenuation of the Ag 3d peak in sample D after the addition of 4-MPy, shown in Figure 4.19 (D), is consistent with a coverage of 4-MPy molecules on top of the colloidal surface.

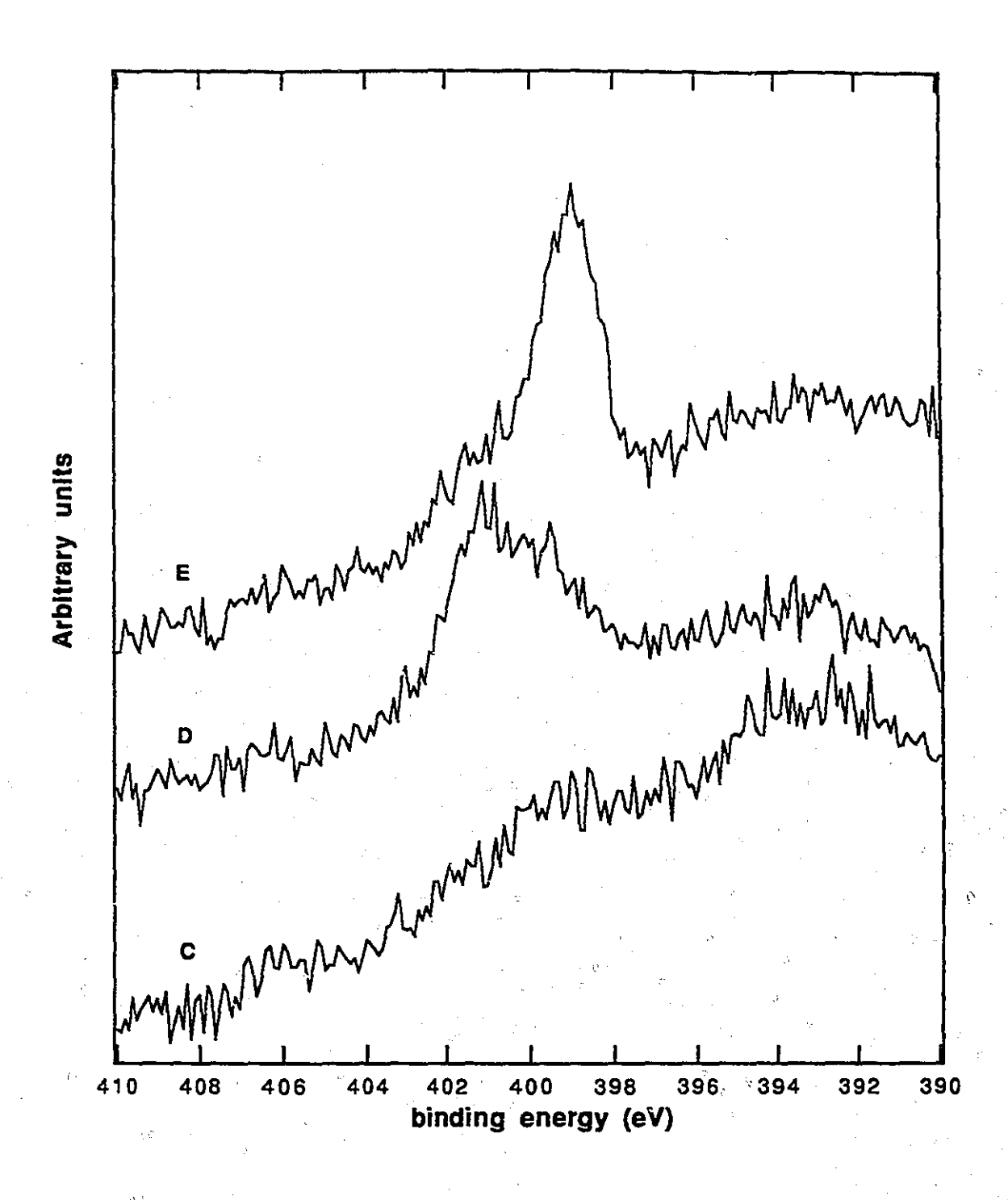


FIGURE 4.15 XPS of Nitrogen 1s region for sample (C): Si/3-MPT with adsorbed Ag colloid, (Si/3-MPT/Ag); sample (D): Si/3-MPT/Ag with adsorbed 4-MPy, (Si/3-MPT/Ag/4-MPy); and sample (E): Si/3-MPT/Ag/4-MPy immersed in aqueous Cu(NO₃)₂ solution, (Si/3-MPT/Ag/4-MPy/Cu).

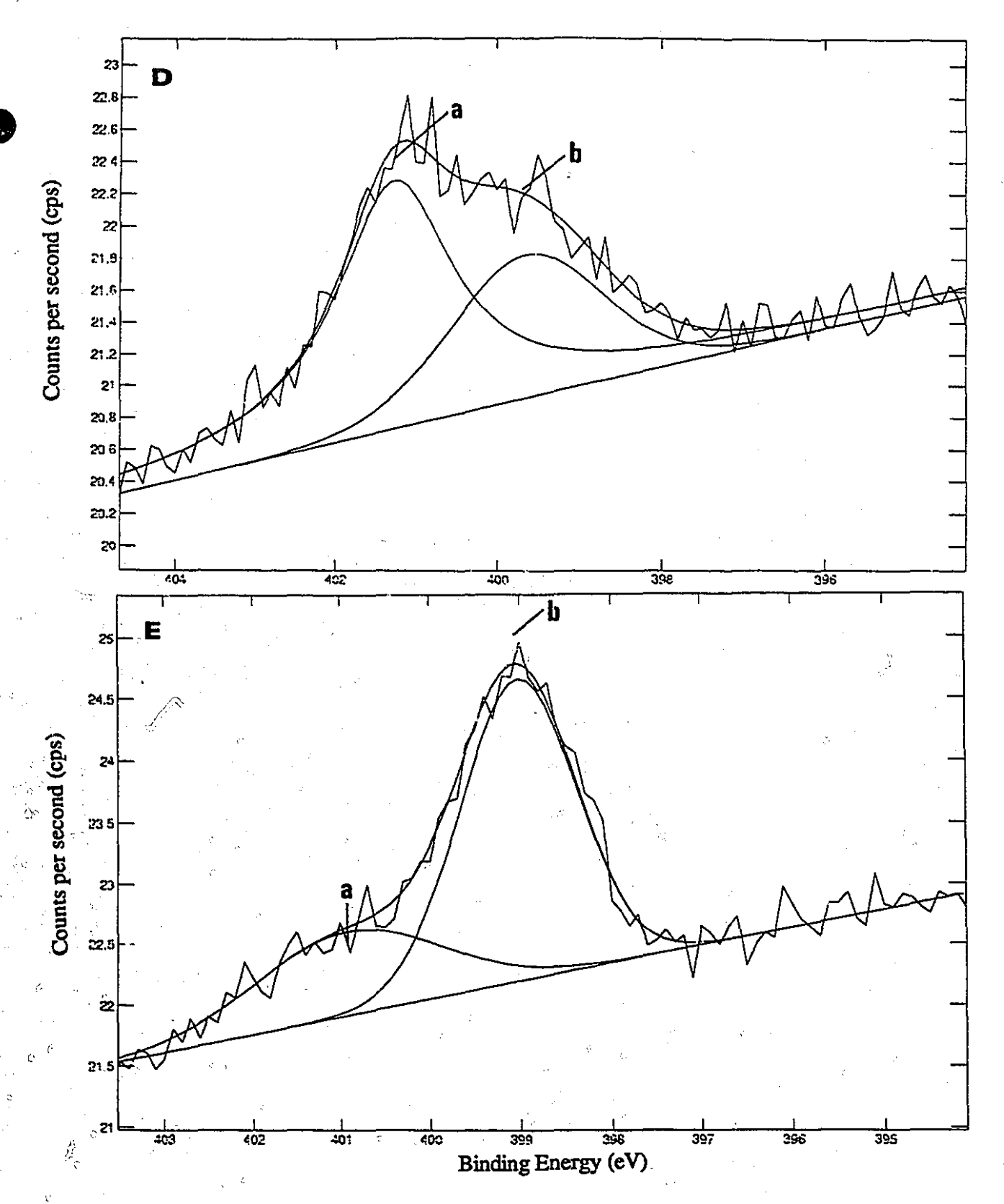


FIGURE 4.16 Curve fitted N 1s peaks for samples (D): Si/3-MPT/Ag with adsorbed 4-MPy, (Si/3-MPT/Ag/4-MPy); and sample (E): Si/3-MPT/Ag/4-MPy immersed in aqueous Cu(NO₃)₂ solution, (Si/3-MPT/Ag/4-MPy/Cu).

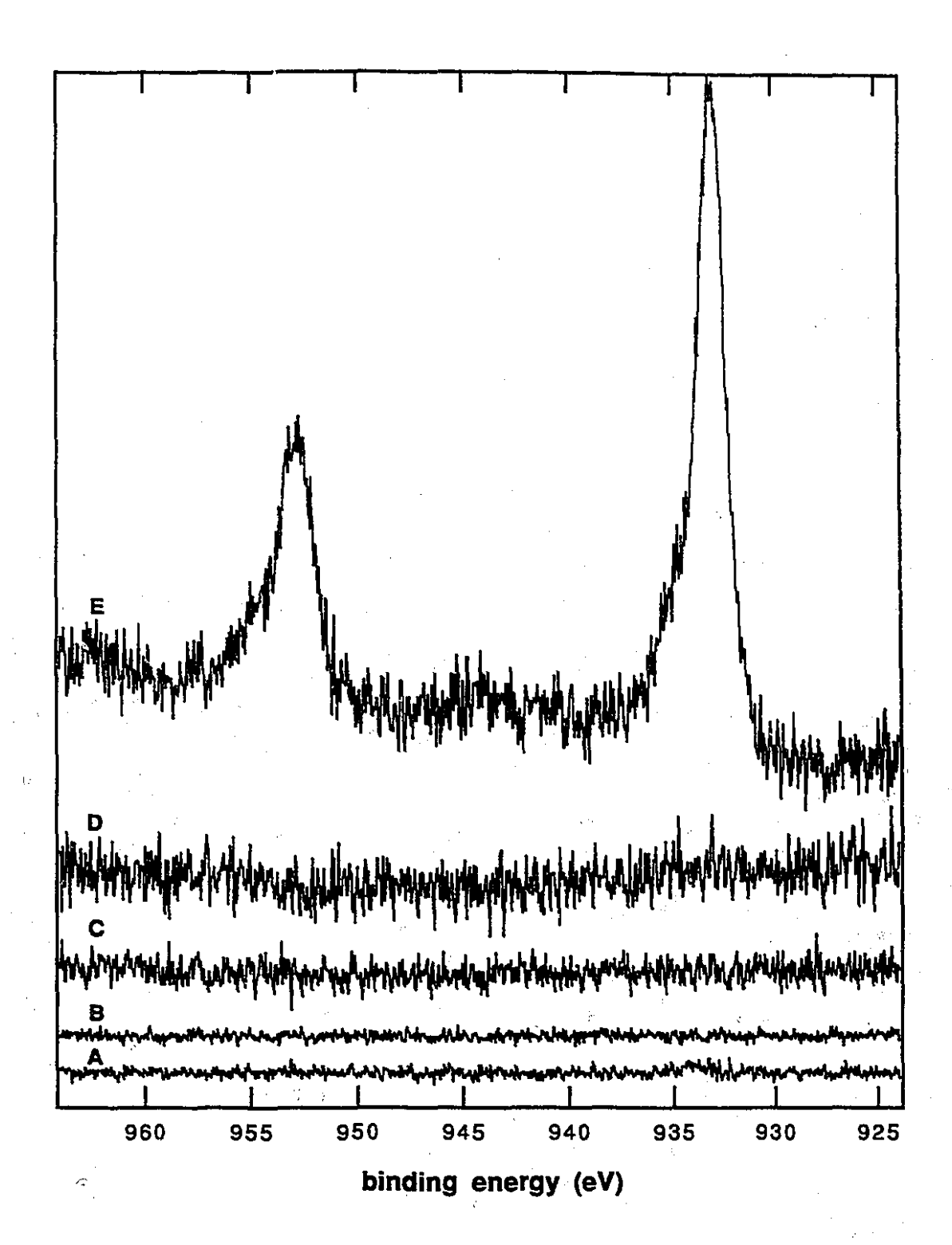


FIGURE 4.17 XPS of Copper 2p region for sample (A): Si wafer; sample (B): Si wafer modified with 3-MPT, (Si/3-MPT); sample (C): Si/3-MPT with adsorbed Ag coiloid, (Si/3-MPT/Ag); sample (D): Si/3-MPT/Ag with adsorbed 4-MPy, (Si/3-MPT/Ag/4-MPy); and sample (E): Si/3-MPT/Ag/4-MPy immersed in aqueous Cu(NO₃)₂ solution, (Si/3-MPT/Ag/4-MPy/Cu).

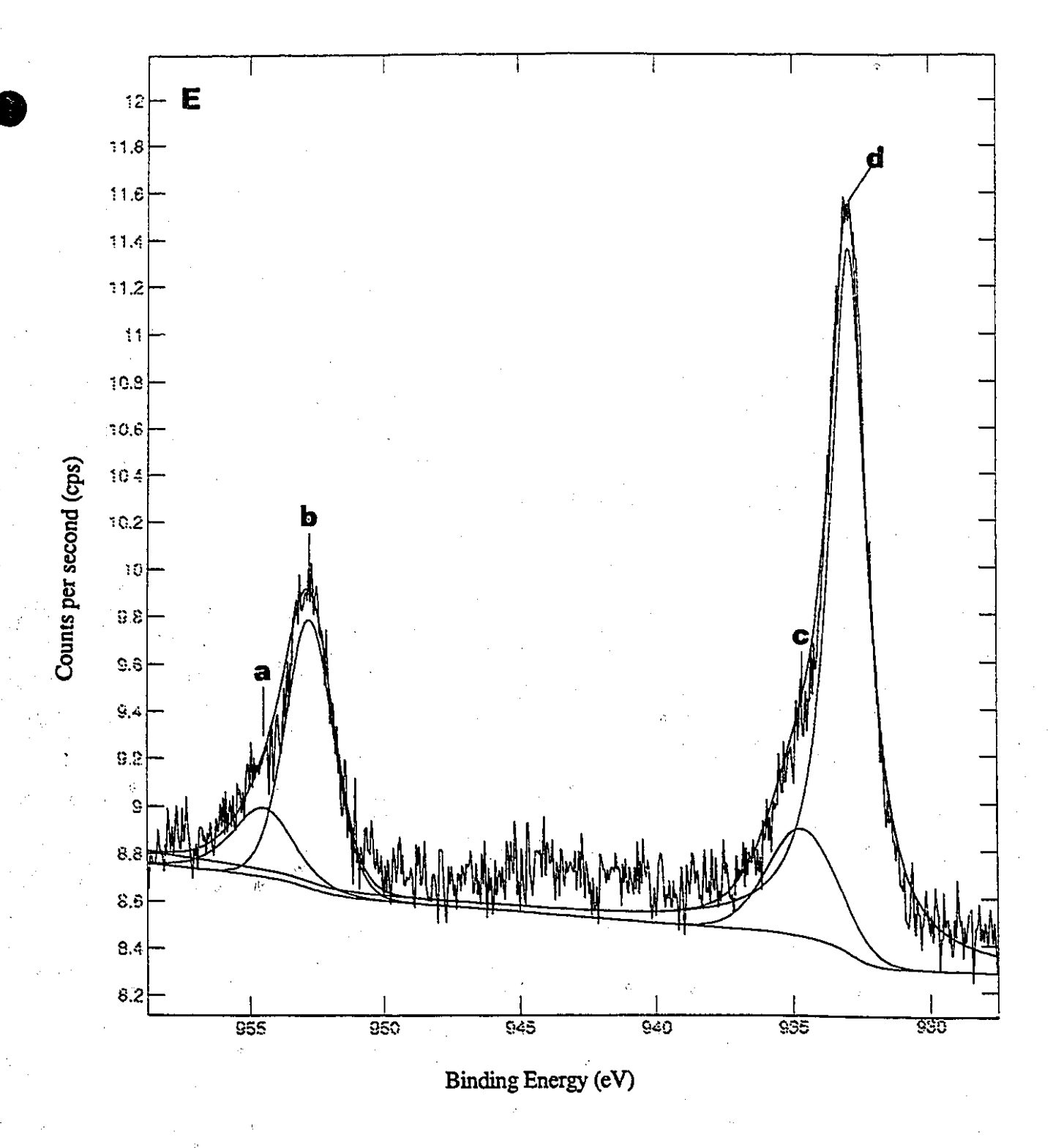


FIGURE 4.18 Curve fitted Copper 2p peaks for sample (E): Si/3-MPT/Ag/4-MPy/Cu.

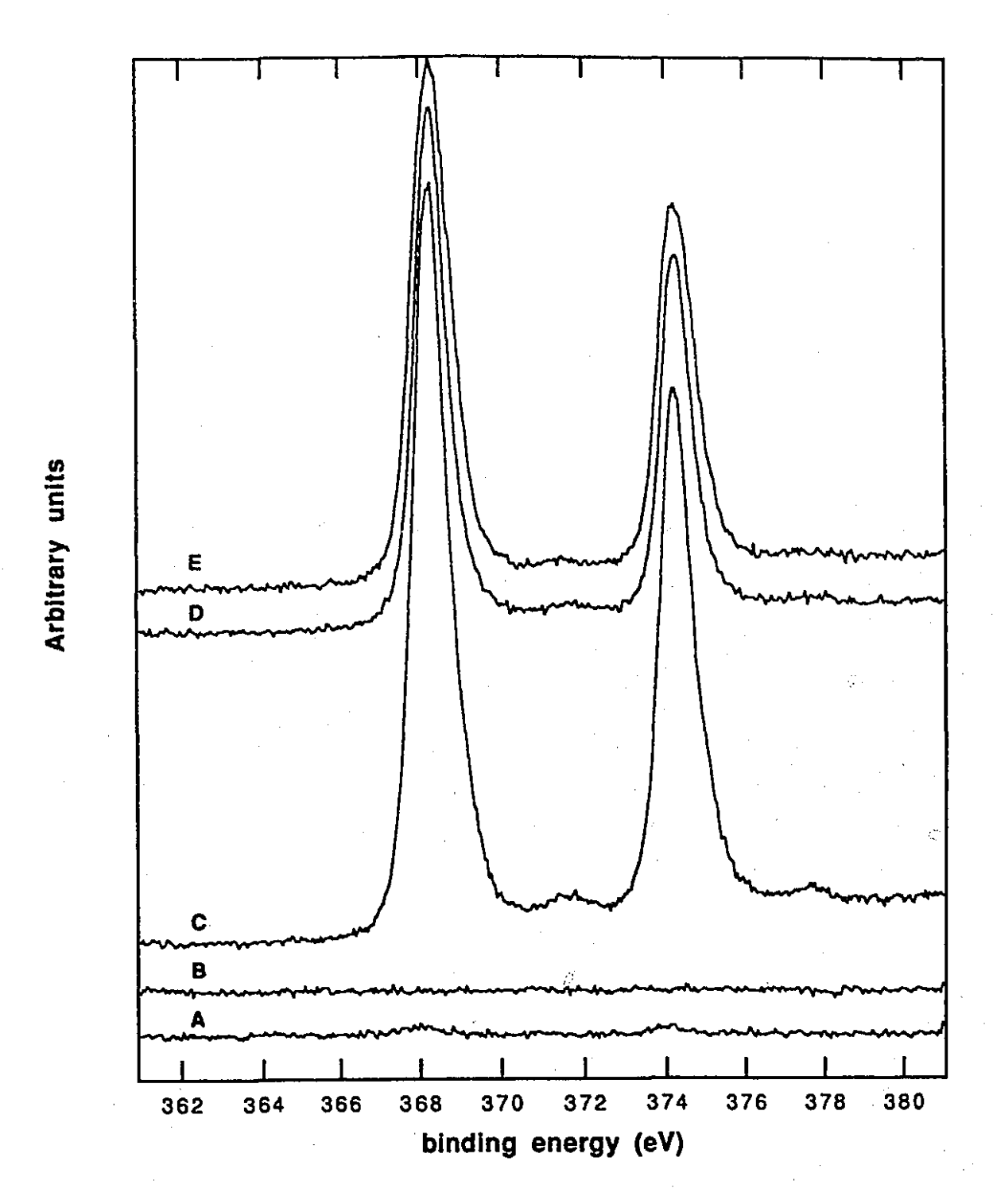


FIGURE 4.19 XPS of Silver 3d region for sample (A): Si wafer, sample (B): Si wafer modified with 3-MPT, (Si/3-MPT); sample (C): Si/3-MPT with adsorbed Ag colloid, (Si/3-MPT/Ag); sample (D): Si/3-MPT/Ag with adsorbed 4-MPy, (Si/3-MPT/Ag/4-MPy); and sample (E): Si/3-MPT/Ag/4-MPy immersed in aqueous Cu(NO₃)₂ solution, (Si/3-MPT/Ag/4-MPy/Cu).

#### 4.7 CONCLUSIONS

The IOEW-SERS study shows that the para-position of the pyridine nitrogen on the surface-confined 4-MPy molecular layer proves to be essential in providing a binding site which is capable of interacting with probe  $Cu^{2+}$  ions. In contrast, the IOEW-SERS spectrum of sterically hindered 2-MPy shows no observable change in the presence of  $Cu^{2+}$  ions.

The IOEW-SERS of 2- and 4-MPy have been compared with other SERS substrates such as MELLFs and Ag colloidal sols. It was concluded from the analysis of relative intensity changes and frequency shifts that 2- and 4-MPy adsorb to the colloidal surface through the thiolate sulfur in which the pyridine ring plane has an orientation perpendicular to the surface. The free uncoordinated pyridine nitrogen of the surfaceconfined 4-MPy is thus available to interact with probe ions. The principal focus of this study has been to demonstrate the ability of a 4-MPy adsorbed layer to behave as a metalion sensor using IOEW-SERS. Spectral changes were observed in the IOEW-SERS spectrum of 4-MPy after immersion in an aqueous solution of Cu(NO₃)₂. A combination of intensity changes including, the appearance of a band at 1034 cm⁻¹, assigned to a  $v_1$  ring breathing mode were attributed to a Cu-4-MPy interaction. In comparison, no spectral changes were observed in the IOEW-SERS spectrum of 2-MPy upon exposure to Cu²⁺ ions. The para-nitrogen position of 4-MPy proved to be crucial in providing a binding site for Cu²⁺ ions since the sterically hindered ortho-nitrogen of 2-MPy was unavailable for coordination. The sensing 4-MPy layer was also quarternized reversibly with H⁺. A v_{8a} band intensity increase similar to that of a pyridinium ion was observed after exposure to a solution of pH 1. Subsequent exposure to Cu²⁺ ions resulted in irreversible spectral changes associated with Cu-4-MPy interaction. A layer-by-layer analysis of the derivatized waveguide was conducted by XPS, beginning with silica and finishing with Cu²⁺ exposure. The N 1s region of 4-MPy consisted of two peaks attributed to two pyridine nitrogen environments of 4-MPy, a chemisorbed and a physisorbed species on the Ag colloid surface. Interaction with Cu²⁺ gave a characteristic shift to lower binding energies, thereby providing further evidence of a Cu-4-MPy interaction.

#### REFERENCES

- (1) Brandt, E. S. and Cotton, T. M. in *Physical Methods of Chemistry Series*; Rossiter, B. W.; Baetzold, R. C., Eds.; Wiley: New York, 1993; Vol. IXB; Ch. 8, p 633.
- (2) Chang, R. K.; Furtak, T. E. Surface-Enhanced Raman Scattering; Plenum Press: New York, 1982.
- (3) Vlcková, B.; Barnett, S. M.; Kanigan, T.; Butler, I. S. Langmuir 1993, 9, 3234.
- (4) Freeman, G. R.; Grabar, K. C.; Allison, K. J.; Bright, R. M.; Davis, J. A.; Guthrie, A. P.; Hommer, M. B.; Jackson, M. A.; Smith, P. S.; Walter, D. G.; Natan, M. J. Science 1995, 267, 1629.
- (5) Bohn, P. W. Trends Anal. Chem. 1987, 6, 223.
- (6) Tien, P. K. Rev. Mod. Phys. 1977, 49, 361.
- (7) Baldwin, J.; Wenbo, X.; Andrews, M. P.; Butler, I. S. Manuscript in preparation.
- (8) Swalen, J. D.; Allara, D. L.; Andrade, J. D.; Chandross, E. A.; Garoff, S.; Israelachvilli, I.; McCarty, T. J.; Murray, R.; Pease, R. F.; Rabolt, J. F.; Wynne, K. L.; Yu, H. Langmuir 1987, 3, 932.
- (9) Bard, A. J.; Abruna, H. D.; Chidsey, C. E.; Faulkner, L. R.; Feldberg, S. W.; Itaya, K.; Majda, M.; Melroy, O.; Murray, R. W.; Porter, M. R.; Soriaga, M. P.; White, H. S. J. Phys. Chem. 1993, 97, 7147.
- (10) Keplay, L. J.; Crooks, R. M.; Ricco, A. J. Anal. Chem. 1992, 64, 3191.
- (11) Kennedy, B. P.; Lever, A. B. P. Can. J. Chem. 1972, 50, 3489.
- (12) Bryant, M. A.; Joa, S. L.; Pemberton, J. E. Langmuir 1992, 8, 753.
- (13) Takahashi, M.; Fujita, M.; Ito, M. Surf, Sci. 1985, 158, 307.
- (14) Taniguichi, I.; Iseki, M.; Yamaguchi, H.; Yasukouchi, K. J. Electroanal. Chem 1985, 186, 299.
- (15) Bain, C. D.; Troughton, E. B.; Tao, Y. T.; Evall, J.; Whitesides, G. M.; Nuzzo,
   G. M. J. Am. Chem. Soc. 1989, 111, 321.
- (16) Gui, J. Y.; Lu, F.; Stern, D. A.; Hubbard, A. T. J. Electroanal. Chem. 1990, 292, 245.
- (17) Xie, Y.; Dong, S. Electroanal. 1994, 6, 567.
- (18) Sagara, T.; Niwa, K.; Hinnrn, C.; Niki, K. Langmuir 1990, 6, 254.
- (19) Jones, T. A.; Perez, G. P.; Johnson, B. J.; Crooks, R. M. Langmuir 1995, 11, 1318.
- (20) Andrews, M. P.; Kanigan, T.; Xu, W.; Kuzyk, M. SPIE Proceedings:

  Photopolymers and Applications in Holography, Optical Data storage, Optical

  Sensors and Interconnects. 1994, 2042, p366.

- (21) Kanigan, T. Ph.D. Thesis 1995, McGill University, Montreal, Canada.
- (22) Green, J. H. S.; Kynaston, W.; Paisley, H. M. Spectrochim. Acta 1963, 19, 549.
- (23) Spinner, E. J. Chem. Soc. 1963, 3860.
- (24) Joo, H. T.; Kim, M. S.; Kim, K. J. Raman Spectrosc. 1987, 18, 57.
- (25) Dollish, F. R.; Fateley, W. G.; Bentley, F. F. Characteristic Raman Frequencies of Organic Compounds; Wiley: New York, 1974.
- (26) Carron, K.; Hurley, L. G. J. Phys. Chem. 1991, 95, 9979.
- (27) Akyuz, S.; Dempster, B.; Morehouse, R. L.; Suzuchi, S. J. Mol. Struct. 1973, 17, 105.
- (28) Moskovits, M.; DiLella, D. P.; Maynard, K. J. Langmuir 1988, 4, 67.
- (29) Cotton, T. M. in *Spectroscopy of Surfaces*; Clark, R. J. H.; Hester, R. E., Eds.; Wiley; New York, 1988; Vol. 16, Ch. 3, p91.
- (30) Creighton, J. A. Surf. Sci. 1986, 173, 665.
- (31) Lautie, A.; Hervieu, J.; Beloc, J. Spectrochim. Acta 1983, 39A, 367.
- (32) Dornhaus, R.; Long, M. A.; Benner, R. E.; Chang, R. K. Surf. Sci. 1980, 93, 240.
- (33) Moskovits, M.; Suh, J. S. Rev. Mod. Phys. 1985, 57, 7893.
- (34) Creighton, J. A. Surf. Sci. 1985, 158, 211.
- (35) Creighton, J. A. Surf. Sci. 1983, 124, 209.
- (36) Stekas, T.; Diamandopoulos, P. J. Phys. Chem. 1990, 94, 1986.
- (37) Beak, P.; Fry, F. S.; Lee, J. J., Steele, F. J. Am. Chem. Soc. 1976, 98, 171.
- (38) Stoyanov, S.; Petkov, I.; Antonov, L.; Stoyanova, T.; Karagiannidis, P.; Aslanidis, P. Can. J. Chem. 1989, 68, 1482.
- (39) Nowak, M. J.; Leszek, L.; Hanna, R.; Les, A.; Adamowicz, L. J. Phys Chem. 1990, 94, 7406.
- (40) Lautie, A.; Novak, A. Chem. Phys. Lett. 1979, 71, 290.
- (41) Lin-Vien, D.; Colthup, N. B.; Fateley, W. G.; Grasselli, J. G. Handbook of Characteristic Infrared and Raman Frequencies of Inorganic Compounds; Academic Press: San Diego, 1991.
- (42) Shunmugam, R.; Sathyanarayana, D. N. Spectrochim. Acta 1984, 40A, 757.
- (43) Joo, T. H.; Yim, Y. H.; Kim, K.; Kim, M. S. J. Phys. Chem. 1989, 93, 1422.
- (44) Garrell, R. L.; Szafranski, C.; Tanner, W. SPIE Proceedings: Raman and Luminescence Spectrosc. in Tech. 1990, 1336, 264.
- (45) Gui, J. Y.; Stern, D. A.; Frank, D. G.; Lu, F.; Zapien, D. C.; Hubbard, A. T. Langmuir 1991, 7, 955.
- (46) Thornton, D. A. Coord. Chem. Rev. 1990, 104, 251.

- (47) Akyuz, S. J. Mol. Struct. 1977, 42, 59.
- (48) Jeanmaire, D. L.; Van Duyne, J. J. Electronanal. Chem. 1977, 84, 1.
- (49) Baldwin, J. Unpublished results
- (50) Chang, R. K.; Furtak, T. E. Surface-Enhanced Raman Scattering; Plenum Press: New York, 1982, Ch. 2, p281.
- (51) Jones, R. A.; Katritzky, A. R. J. Chem. Soc. 1958, 3610.
- (52) Albert, A.; Barlin, B. Current Trends in Heterocyclic Chemistry; Butterworths: London, 1958.
- (53) Albert, A.; Barlin, G. B. J. Chem. Soc. 1959, 2384.
- (54) Chang, C. H.; Hwang, K. C. J. Am. Chem. Soc. 1984, 106, 6586.
- (55) Laibinis, P. E.; Whitesides, G. M.; Allara, D. L.; Tao, Y.; Parikh, A. N.; Nuzzo,R. G. J. Am. Chem. Soc. 1991, 113, 7152.
- (56) Nuzzo, R. G.; Zegarski, B. R.; Dubois, L. H. J. Am. Chem. Soc. 1987, 109, 733.
- (57) Uvdal, K.; Bodo, P.; Liedberg, B. J. Colloid. Interface. Sci. 1992, 149, 163.
- (58) Rufael, T. S.; Huntley, D. R.; Gland, J. L. J. Phys. Chem. 1994, 98, 13022.
- (59) Golzhauser, A.; Panov, S.; Woll, C. Surf. Sci. 1994, 314, L849.
- (60) Serafin, J. G.; Friend, c. M. J. Phys. Chem. 1989, 93, 1998.
- (61) Cohen, M. R.; Merrill, R. P. Surf. Sci. 1991, 245, 1.
- (62) Cohen, M. R.; Merrill, R. P. Langmuir 1990, 6, 1282.
- (63) Eesley, G. L.; Burkstrand, J. M. Phys. Rev. B. 1981, 24, 582.
- (64) Henry, R. M.; Walker, B. W.; Stair, P. C. Surf. Sci. 1985, 155, 732.
- (65) Pan, F. M.; Stair, P. C.; Fleisch, T. H. Surf. Sci. 1986, 177, 1.
- (66) Xue, G.; Zhang, J.; Ma, M.; Lu, Y.; Carron, K. T. J. Colloid. Interface. Sci. 1992, 150, 1.
- (67) Briggs, D.; Seah, M. P. Practical Surface Analysis; Wiley: New York, 1990.
- (68) Czandema, A. W.; King, D. E.; Spaulding, D. J. Vac. Sci. Tech. A 1991, 9, 2607.
- (69) Schon, G. Surf. Sci. 1973, 35, 96.
- (70) Walton, R. A. Inorg. Chem. 1980, 21, 1100.
- (71) Lyons, A. M.; Vasile, M. J.; Pearce, E. M.; Wsacrzak, J. V. Macromol. 1988, 21, 3125.
- (72) Karlin, K. D.; Zubieta, J. Copper Coordination Chemistry: Biochemical and Inoganic Perspectives; Adenine Press: 1986.

## CHAPTER 5

SURFACE ENHANCED RAMAN SCATTERING OF 4-MERCAPTOPYRIDINE ON SILVER ELECTRODES AND THE SURFACE INTERACTION WITH COPPER(II) IONS

#### 5.1 SUMMARY

The potential dependent SERS is reported for 4-mercaptopyridine (4-MPy) adsorbed on a polycrystalline Ag electrode. The SERS spectra at low negative potentials (E > -0.6V) are comparable to previously reported SERS studies of 4-MPy adsorbed on a metal surface via the thiolate moiety. With increasing negative potentials (E < -0.6V), spectral band changes occur in a direction which resembles more the normal Raman spectrum of bulk 4-MPy. In addition, bands associated with 4-MPy adsorbed through the thiolate sulfur are observed. The appearance of additional bands, in particular, an additional v₁ ring breathing mode, suggests that a new 4-MPy species is adsorbed on the electrode surface. This species is adsorbed through the pyridine nitrogen, which is stabilized on the electrode surface in the potential range -0.6 to -1.0V. To investigate further the spectral changes associated with metal-nitrogen coordination of surface bound 4-MPy, the electrochemical cell was exposed to a solution of Cu²⁺ ions at open potential. At this potential, 4-MPy is adsorbed on the electrode surface via the sulfur atom leaving the "free" uncoordinated nitrogen available to interact with Cu²⁺ ions on the solution side of the electrode interface. Spectral changes are observed similar to those which occur at more negative potentials (E < -0.6V) in the absence of Cu²⁺ ion and, by analogy, these changes are associated with a Cu-pyridine nitrogen interaction on the electrode surface. Essentially, we have demonstrated that a 4-MPy-modified Ag electrode can behave as a metal ion sensor similar to the IOEW-SERS study.

A possible contribution from a charge transfer (CT) process to the potential dependent band enhancement profile of adsorbed 4-MPy was identified by plotting the relative band intensities as a function of applied potential and excitation wavelength (488.0, 514.5, 633.47 and 651.5 nm).

#### 5.2 INTRODUCTION

Considerable research has been directed towards the SERS investigations of pyridine adsorbed on electrode surfaces. There now appears to be general agreement that both electromagnetic (EM) and charge transfer (CT) mechanisms are involved in the overall enhancement of Raman signals. 1-3 The EM mechanism predicts enhancement based on the interaction of incident photons with roughened features of the metal which produce large EM fields through coupling with surface plasmons. The CT mechanism, a resonance Raman-like process, requires direct proximity between the molecules and the surface. The degree that each mechanism contributes, in particular the CT process has been studied extensively for pyridine adsorbed on Ag electrodes. 1,4-8 Relatively few electrochemical SERS studies have been conducted on substituted pyridines^{7,9-11} and only a few electrochemical SERS studies of 4-mercaptopyridine (4-MPy) on Au electrodes have been reported. 12,13 Furthermore, while alkylthiol self-assembling monolayers (SAMs) are the most intensively studied SA monolayers on gold surfaces, 14 little attention has been given to aromatic thiols. 14-18 Monomolecular films formed from organosulfur surfactant molecules possess a head group that binds to a particular metal and a tail group that has a specific chemical functionality. Alkylthiols have demonstrated their utility as a means of controlling the interfacial reactivity of a metal in adhesion, lubrication, chemical sensors and electroanalysis. 19 Aromatic thiols have also shown similar properties, in particular, surface-confined 4-MPy can electrostatically bind probe ions from solution.²⁰

Recent reports have shown that the aromatic thiol SAM of benzenethiol is stable to applied potentials, ²¹ at least over a cathodic potential range while enhanced oxidation currents observed by cyclic voltammetry (CV) on Au electrodes suggest oxidation of the monolayer itself. ¹⁴ Similar to benzenethiol, 4-MPy is reported to adsorb on Ag, Au and Pt metal surfaces through the sulfur atom with the pyridine ring oriented approximately normal to the metal surface. ^{12,14,22-24} Electronic energy loss spectra (EELS) of 4-MPy adsorbed on an Ag(111) single crystal electrode at negative potentials (E < -0.4 V) were

shown to resemble the IR spectrum of bulk 4-MPy. A similar interpretation was given for the spectral changes observed at negative potentials (E < -0.5V) for the SERS of 4-MPy modified Au electrodes.¹² It was also suggested that apart from a potential dependent adsorption/desorption, adsorbed 4-MPy remains inert towards electrochemical oxidation and reduction.²³

We focus on the potential dependent SERS study of adsorbed 4-MPy for three reasons: firstly, since 4-MPy is an ambidentate ligand, a number of different modes of surface adsorption are possible. These include adsorption via the thiol, pyridine nitrogen or the  $\pi$ -ring system. An important consideration is the effect of surface potential on the stability of the metal-adsorbate interaction. Secondly, a wavelength-potential dependence study on the SERS band intensity profile can be used to clarify if the potential-dependent intensity changes are attributable to a CT mechanism, as is observed for pyridine. Thirdly, the ion-binding capability of surface-confined 4-MPy has been previously demonstrated by cyclic voltammetry methods.¹⁴ We have previously observed metal-ion binding of 4-MPy, using a novel SERS technique, integrated optics, evanescent wave, surface enhanced Raman scattering (IOEW-SERS) and demonstrated the potential use of this method as a chemical sensor.²⁵ The IOEW-SERS study showed that the para-position of the pyridine nitrogen on the surface confined molecular layer is essential in providing a binding site which is capable of interacting with probe ions such as Cu²⁺. In this present work, a 4-MPv derivatized Ag electrode is exposed to a solution of Cu²⁺ ions at open potential and the Cu-4-MPy interaction at the electrode surface can be monitored on a molecular level.

#### 5.3 EXPERIMENTAL

Materials. 4-Mercaptopyridine (Aldrich) was sublimed *in vacuo* immediately prior to use. All other reagents were used as received. Analytical grade KCl (Analar BDH) was used to prepare the electrolyte in Milli-Q water. Silver nitrate (p.a. Aldrich) was used to prepare the silver-4-MPy complex. Cu(NO₃)₂ (p.a. Aldrich) was introduced into the electrochemical cell as a probe ion.

Ag Colloid Sols. Silver colloid was prepared by reduction of AgNO₃ with NaBH₄ following a procedure described previously.²⁷ The Ag colloid sol of 4-MPy was obtained by adding an aqueous solution of 4-MPy (0.2 mM, 10 mL) to Ag colloid (2 mL). Aggregation occurred slowly to give a purple-brown color. The colloid was transferred to a capillary sample cell for SERS measurements.

Silver-4-MPy Complex. To prepare the silver-4-MPy salt, equimolar quantities of AgNO₃ and 4-MPy (0.05 mol) were dissolved in an ethanol/water solution to yield a pale yellow precipitate of silver-4-MPy. The precipitate was filtered, rinsed with ethanol and water, and then dried under vacuum. The normal FT-Raman spectra of 4-MPy and the silver-4-MPy complex were measured on solid samples.

Electrochemical SERS Measurements. Raman experiments were performed on a Dilor OMARS-89 spectrometer, equipped with an optical multichannel analyzer. The spectrometer was fitted with a 1800 grooves mm⁻¹ grating operating in the subtractive mode. A third dispersing grating was employed to image the output radiation onto a 512 channel thermoelectrically cooled diode-array detector. For data acquisition, the spectrometer was interfaced to an IBM AT computer. The 514.5-nm laser line from a Coherent Innova 70 argon-ion laser was used to excite the samples together with other lines from a Coherent CR-599 dye laser. The dye DCM (Lambda Physik) could provide excitation in the wavelength 610-710 nm region. Unwanted laser lines were removed by an Anaspec 300-S tunable laser filter. The mechanical slit width employed in the measurements was 300 μm and the laser power at the sample was typically 80 mW. All

spectra were acquired over a 2 s integration period. The electrode was positioned so that the incident beam was at an angle of ca. 55° with respect to the surface normal and the scattered light was collected at an angle of ca. 60° with respect to the surface normal.

The three-electrode electrochemical cell design used in these experiments was reported previously. 26 A polycrystalline Ag disk working electrode (99.9% Aldrich) was polished to a mirror finish with progressively finer grades of alumina slurries, down to 0.06 mm on (Metron) polishing cloths, rinsed with copious amounts of triply distilled Milli-O water, and sonicated in triply distilled water for ca. 15 min to remove any trapped alumina before use. A Pt wire (99.9% Aldrich) was used as a counter electrode. All potentials are reported versus a saturated calomel electrode (SCE). The electrolyte consisted of 0.1M KCl which was degassed with Ar for 1 hr and the electrode was held at -1.2V to reduce any organic or inorganic matter prior to spectral acquisition. Potentials were controlled by a Princeton Applied Research Model 273 potentiostat. Cyclic voltammograms were recorded on a Kipp & Zonen X-Y recorder. Roughening of the electrode was accomplished by transferring the electrode to the spectroelectrochemical cell and applying three oxidation-reduction cycles (ORC) with laser illumination. The electrode was roughened by an anodic sweep, followed by a cathodic sweep at the same rate (-700 to +100 mV at 5mV/s). The electrode was then removed from the electrochemical cell and immersed in a 2 x 10⁻³ M aqueous solution of 4-MPy for 5 min. The electrode was removed from this solution, washed with Milli-Q water, transferred to the spectroelectrochemical cell and a single ORC was applied with potential being stepped back to -100 mV. A single ORC was applied before the SERS spectra were collected for each wavelength.

An electrochemical investigation of adsorbed 4-MPy with Cu²⁺ ion deposition was carried out after the potential-wavelength dependence studies. Prior to Cu²⁺ exposure a single ORC was applied after which the cell was left at open potential. A solution of

Cu(NO₃)₂ (2 mM, 10 mL) was introduced into the electrolyte solution in the electrochemical cell.

Normal Raman Measurements. FT-Raman spectra of 4-MPy powder and the silver 4-MPy complex were recorded on a Bruker IFS-88 spectrometer equipped with an FRA-105 Raman module and a liquid N₂-cooled proprietary detector. The spectra were excited with a Nd³⁺:YAG laser operating at 1064.1 nm (150 mW), with 250 scans being typically collected at 2 cm⁻¹ resolution.

#### 5.4 RESULTS AND DISCUSSION

### 5.4.1 SERS Spectra of 4-MPy

Figure 5.1 shows the SERS spectra of 4-MPy adsorbed on a roughened Ag electrode at 0 V, 4-MPy adsorbed on colloidal sol, and the unenhanced FT-Raman spectra of the silver-4-MPy complex and bulk 4-MPy powders. The SERS spectra collected at 0 V and at open potential for all excitation wavelengths display spectral profiles similar to previously reported SERS spectra of 4-MPy. 12,22,25 These in turn correspond to the unenhanced spectral profile of the bulk silver-4-MPy complex [(Figure 5.1(a)]. Note that the intense band at 1041 cm⁻¹ observed in the spectrum of the silver-4-MPy complex is assigned to the  $v_{\text{sym}}(NO_3^-)$  mode of the nitrate anion in AgNO3. Proposed band assignments for neat 4-MPy and the SERS spectra are given in Table 5.1. The assignments are based on those for para-substituted pyridine and thiophenol. 15,28-31 The similarities between the SERS spectrum of adsorbed 4-MPy from the Ag electrode and that of the normal Raman spectrum of bulk silver-4-MPy complex suggest the formation of an silver-4-MPy complex on the electrode surface. The overlap of these bands makes the identification of an adcluster-molecule complex formed from the redox process difficult. Such complexes have been observed for other compounds on electrode surfaces, e.g., 4,4'-bipyridine.32,33

By comparison with the bulk Raman spectrum, the SERS spectrum is dominated by bands attributed to a₁ modes and two b₂ in-plane ring modes (see Table 5.1). Application of the surface selection rules, ^{17,34,35} reveals that the a₁ and b₂ modes (for C_{2v} molecules with the molecular z axis normal to the surface) with polarizability components perpendicular to the surface are enhanced preferentially relative to the out-of-plane, a₂ and b₁ modes when the plane of the ring lies normal to the surface. Previous studies of 4-MPy adsorbed on a variety of metal surfaces including Ag, Au and Pt using SERS, ^{12,22,24} EELS and Auger²³ techniques have also led to the conclusion that the ring lies normal to the surface. Adsorption to the metal surface has been proposed to occur through the

FIGURE 5.1 Unenhanced FT-Raman spectra of bulk powder 4-MPy (a); bulk powder silver-4-MPy complex ( $\lambda_{ex}=1064.1$  nm at 150 m) (b); Ag colloidal SERS spectrum of 4-MPy (10  $\mu$ L, 2 x 10⁻⁴ M in 2 mL of colloid) (c); and SERS spectrum of 4-MPy adsorbed on Ag electrode at 0 V acquired with 514.5 nm excitation (d).

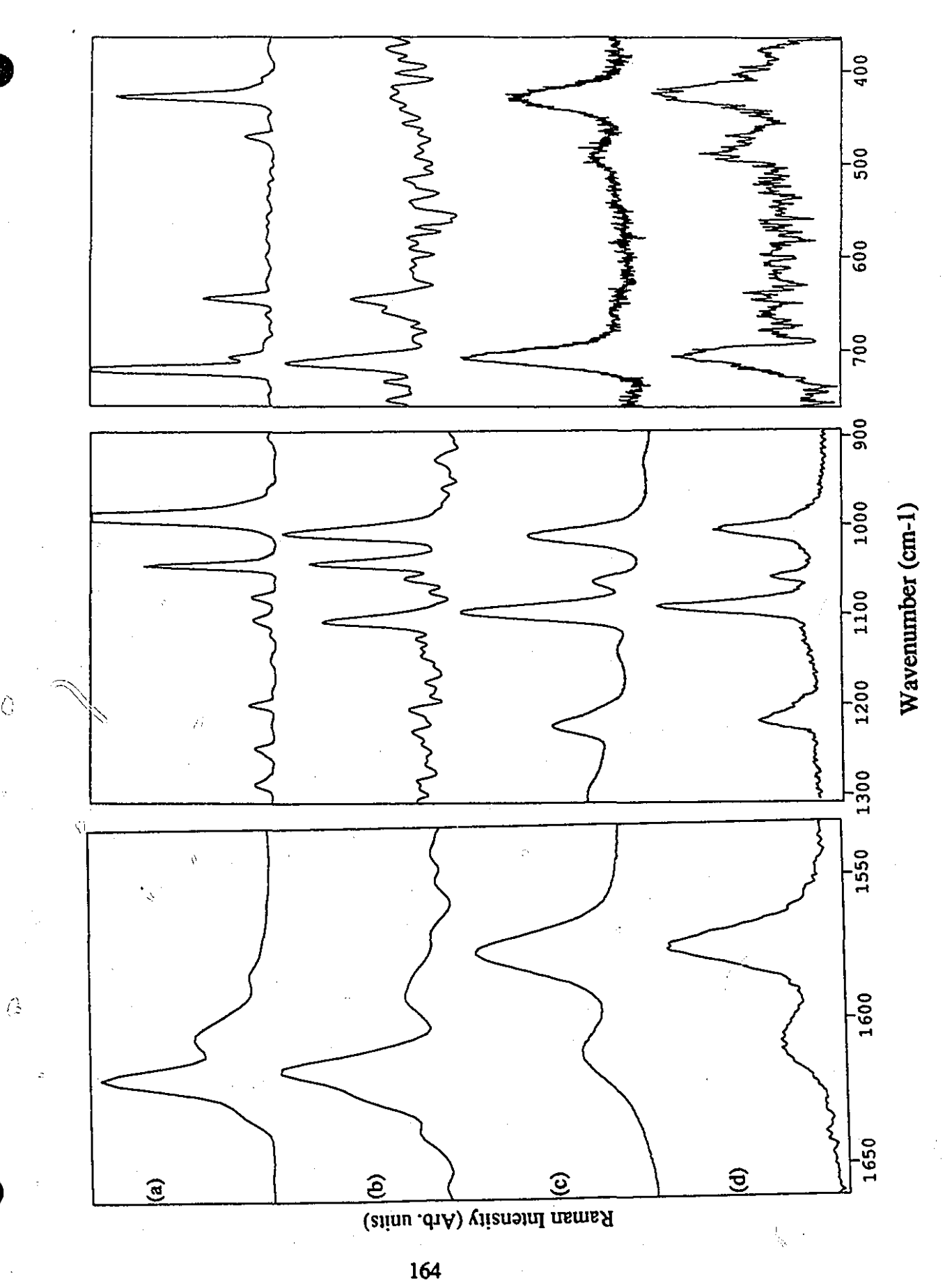


TABLE 5.1 Assignments and wavenumber positions (cm⁻¹) of normal Raman and SERS

spectra for 4-mercaptopyridine.

spectra for 4-mercaptopyridine.						
Assignment (a)	Solid	Silver-4-	Colloidal			
		MPy	sol.	0 mV	-1000 mV	open
		complex		(mV vs SCE)	(mV vs SCE)	potential
				Type I	Type II	with Cu ²⁺
70. 8(0.5)/	421	420	430	405	A A 7	442
7a ₁ , δ(C-S) /	431	430	430	425	447	442
γ(CCC)	471			400	400	400
16b ₁ , γ(CCC)	471	646		489	490	498
6b ₂ , β(CCC)	647	646	-0-			
6a ₁ , (β(CC) /	721	714	705	706	702/718	711/723
υ(C-S))						
10b ₁ , γ(CH)	790		813			
	901					
1a _{1,} (Ring breathing)	990	1007	1007	1005	998/1019	1013
		1041*				
18a ₁ , β(CH)	1045			1057 <i>-</i>	1057	1057
18b ₂ , β(CH)	1080		1065	, Carr	1072	
12a ₁ , (Ring	1106	1107	1098	1091	1091	1098
breathing)/v(C-S)			•			
÷			1135	· 5		
β(CH) / δ(NH)	1200		1222	1218	1206	1213
9a ₁ , β(CH)	1250	!.	38			
3b ₂ , β(CH)	1290	(1 \\\\\\\\\\\\\\\\\\\\\\\\\\\\\\\\\\\\	1305			
		",	1338			
14b ₂ , υ(CC)	1394		1407			
19b ₂ , υ(C=C/C=N)	1459		1433		•	
19a ₁ , υ(C=C/C=N)	1478		1470	' <del>ل</del> اقِيَّ		**************************************
		•*			•	
8b _{2,} v(CC)	1604	1586	1573	1574	1572/1569	1578
8a ₁ , υ(CC)	1617	1616	1615	1608	1585	

⁽a) Assignment for normal Raman of 4-mercaptopyridine from refs. 15, 28-31.

^(*) Band assigned to  $v_{sym}(NO_3^-)$  from AgNO3.

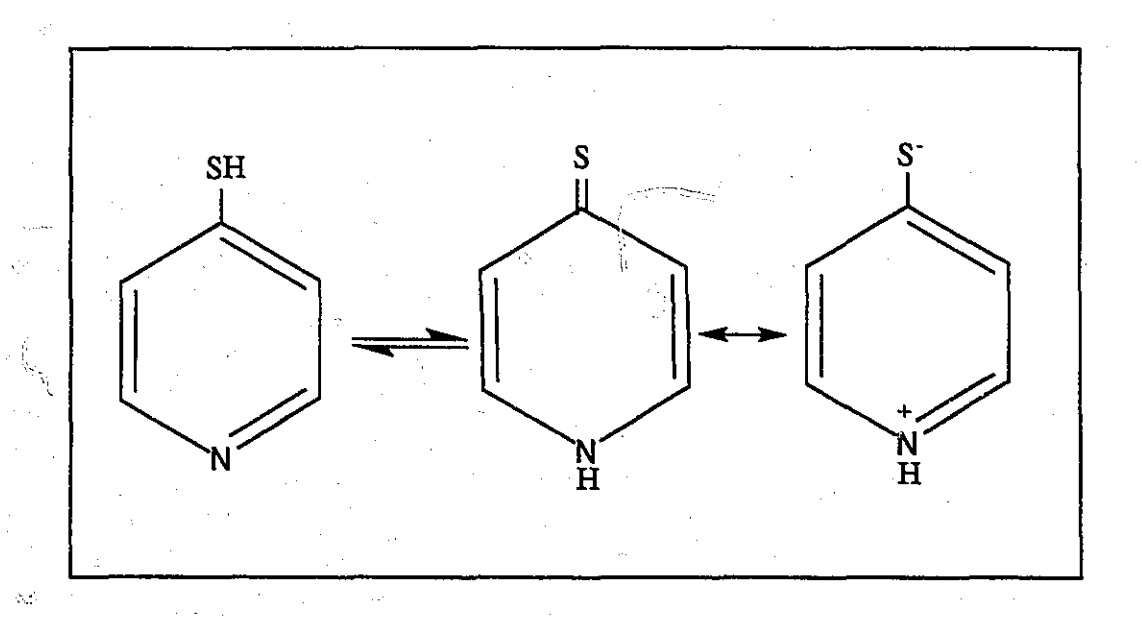


FIGURE 5.2 Thione-thiol tautomerism of 4-MPy.

thiolate sulfur, following cleavage of the S-H bond. This adsorption mechanism, observed for alkylthiols and thiophenol adsorbed on Au surfaces, is characterized by the absence of an intense v(SH) band at 2573 cm⁻¹. As discussed previously, 25 4-MPy exists as a thiol-thione tautomer for which the thione form predominates^{36,37} (Figure 5.2) and instead, a broad v(NH/SH) band appears in this region in the normal unenhanced Raman spectrum of bulk 4-MPy.²⁵ Thus, confirmation for this mode of adsorption (via a Ag-thiolate bond) is complicated by the absence of the v(SH) marker band. Other marker bands, such as the υ(C-S) mode at 720 cm⁻¹, display characteristic spectral shifts to lower wavenumbers near 706 cm⁻¹ on adsorption to the surface (see Table 5.1). A similar peak shift has been observed for other aromatic thiols, e.g., thiophenol adsorbed via the sulfur atom on SERSactive metal substrates. 15-17 Further evidence for Ag-thiolate interaction is given by spectral changes associated with the X-sensitive  $v_{12}$  [ring breathing/v(C-S)] mode at 1106 cm⁻¹. This band experiences a dramatic increase in intensity for all SERS spectra of 4-MPy. This enhancement is similar to that observed for both the SERS spectrum of thiophenol on Au electrodes 15,17 and the normal unenhanced Raman spectrum of the silver-4-MPy complex. Although relatively few studies have been reported for metal-4-MPy complexes, it is reasonable to assume that the Ag atom is bonded primarily through the sulfur atom in the silver-4-MPy complex similar to metal-2-MPy complexes. The possibility of a secondary interaction through the pyridine nitrogen cannot be excluded.³⁸

## 5.4.2 Electrochemical SERS of 4-MPy

Cyclic voltammograms (CV) of an Ag electrode prepared for SERS measurements with and without 4-MPy were measured in the potential region from 0 to -1000 mV vs. SCE in 0.1M KCl electrolyte (Figure 5.3). Both voltammograms are similar and may, therefore, be an indication that the 4-MPy layer remains electrochemically inert within the applied potential range on the electrode surface. A similar conclusion was made for electrochemical studies of thiophenol and 4-MPy modified electrode surfaces. ^{12,14,23}

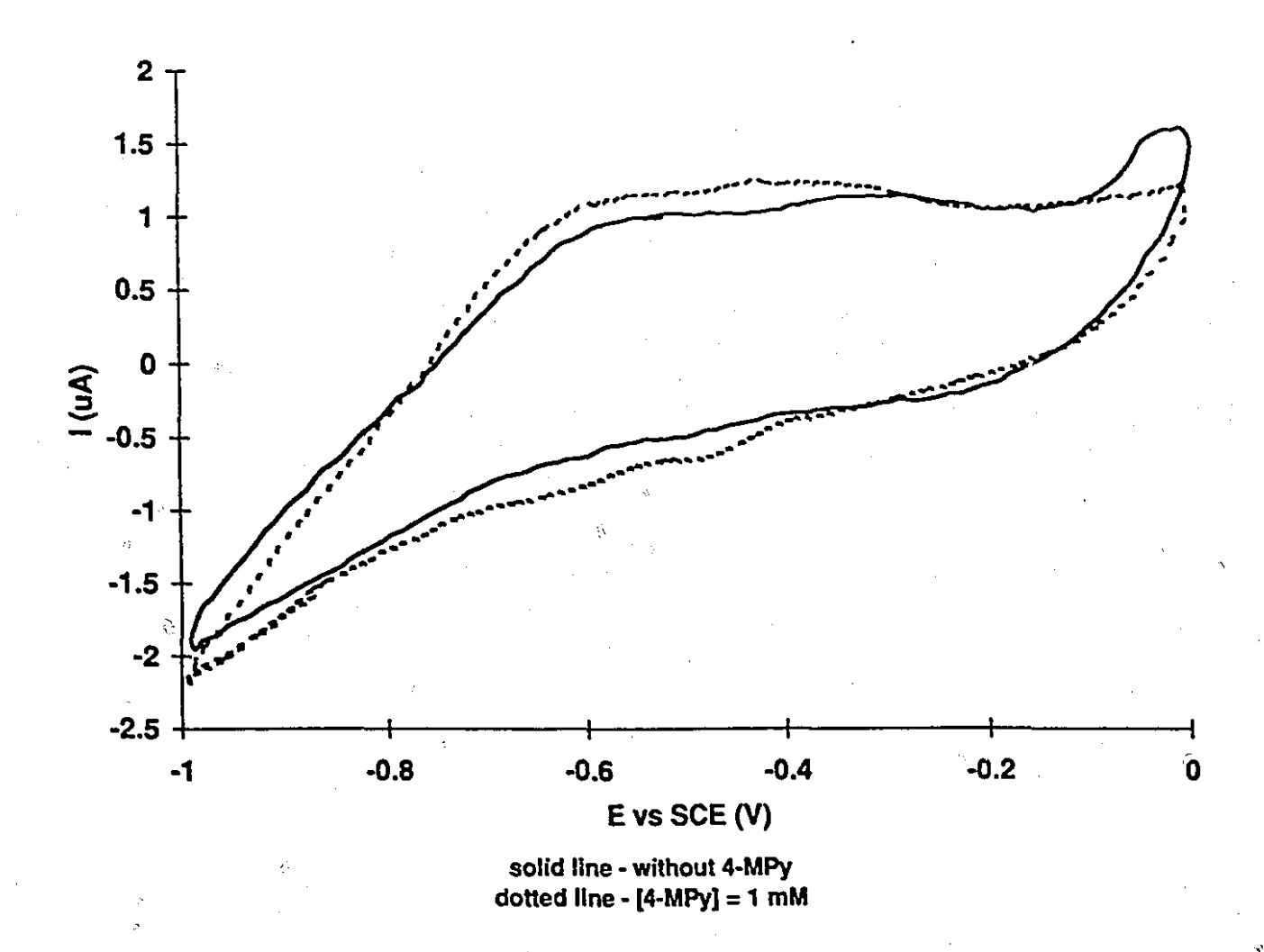


FIGURE 5.3 Cyclic voltammogram of 4-MPy (1 mM) adsorbed on an Ag electrode in 0.1 M KCl. The potential range is from 0 to -1.0 V (vs. SCE) with scan rate of 10 mV/s.

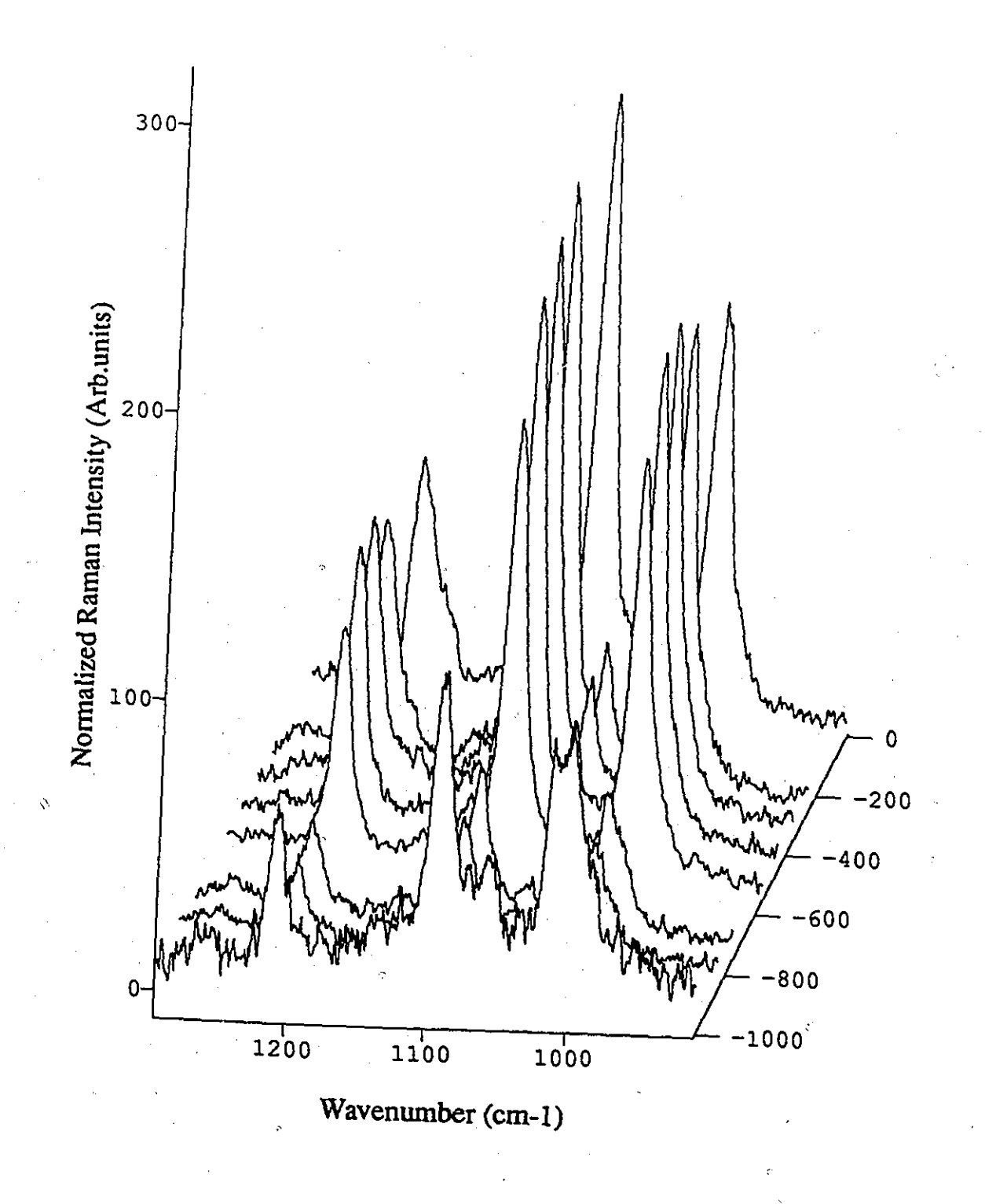


FIGURE 5.4 SERS spectra of 4-MPy adsorbed on an Ag electrode using 514.5 nm excitation at the potentials listed (vs. SCE).

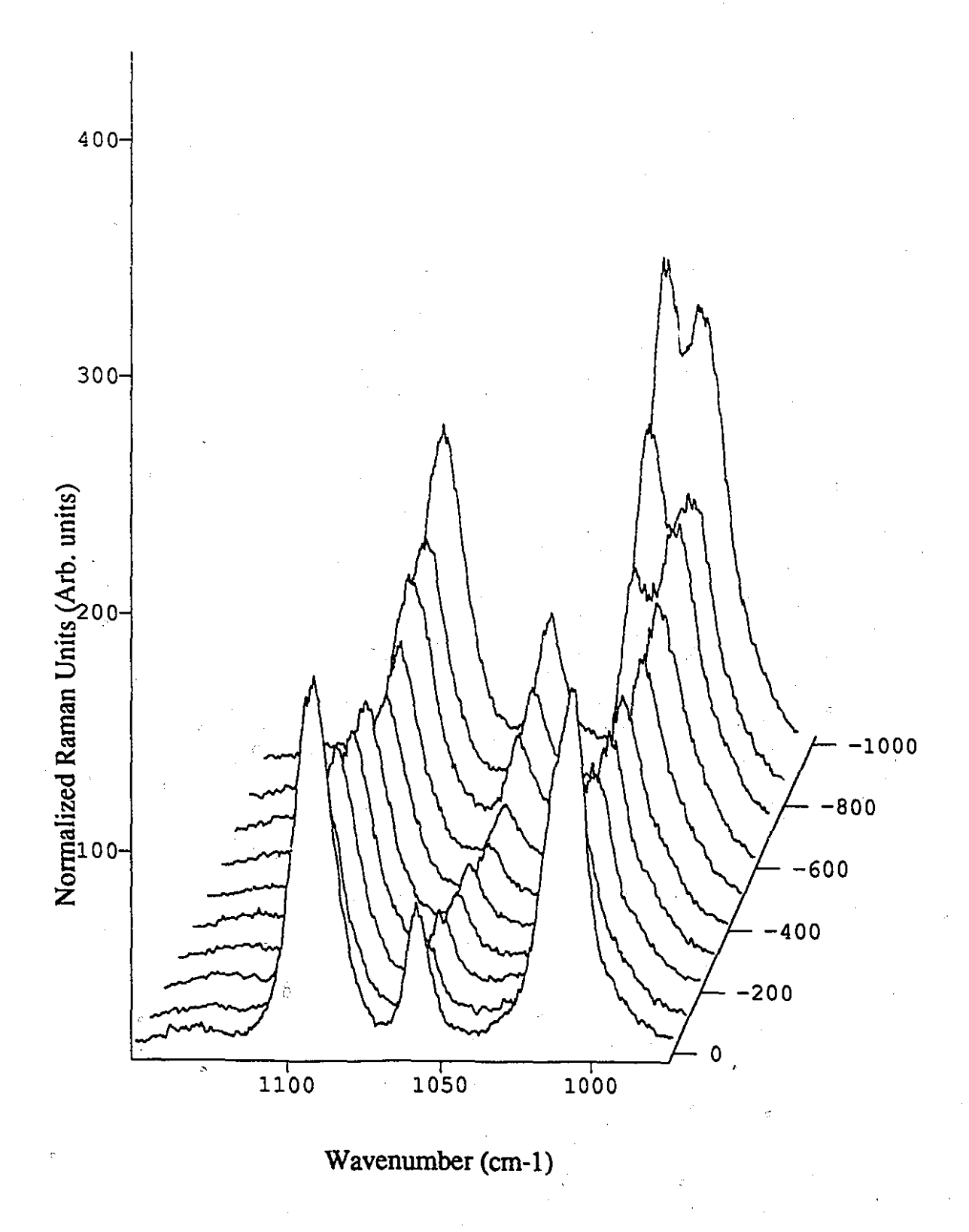


FIGURE 5.5 SERS spectra of 4-MPy adsorbed on an Ag electrode using 633.47 nm excitation at the potentials listed (vs. SCE).

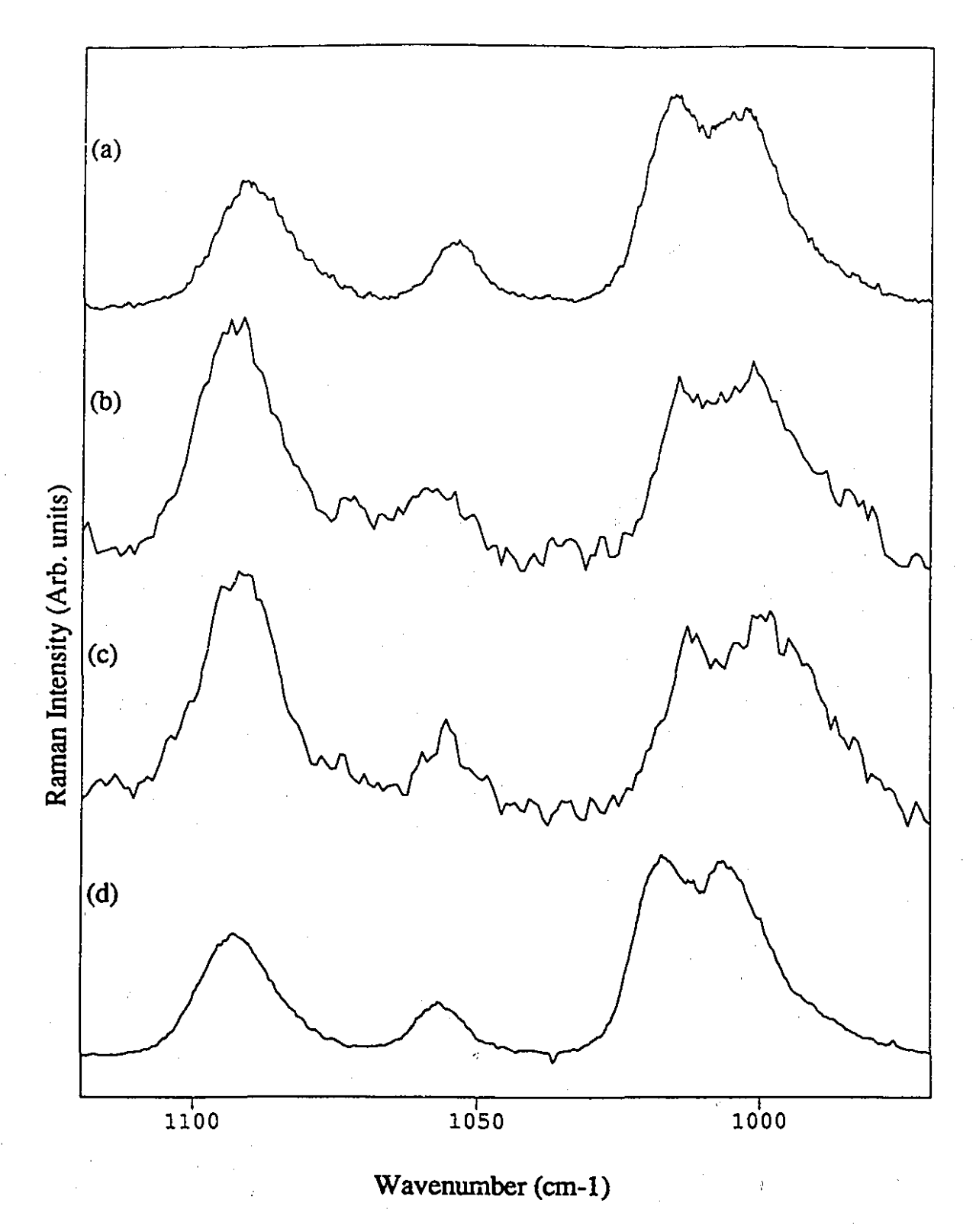


FIGURE 5.6 SERS spectra of 4-MPy,  $v_1$  ring breathing modes at 998 and 1019 cm⁻¹, at -1000 mV (vs. SCE) at excitation wavelengths: 488 (a); 514.5 (b); 633.47 (c); 651.5 nm (d).

The SERS spectra of adsorbed 4-MPy on the Ag electrode in the absence of an applied potential or at 0 V are significantly modified in terms of intensity, position and band profile compared to the spectra observed for applied potentials near -600 mV. Figures 5.4 and 5.5 show 3-D displays of the SERS spectra collected for the  $\upsilon_1$  ring breathing mode region using 514.5 and 633.47 nm excitation wavelengths. At potentials more negative than -600 mV, a new band appears at 1019 cm⁻¹ to the higher wavenumber side of the  $\upsilon_1$  mode and is fully resolved at -1000 mV. Similar spectral changes were observed within the potential range -600 to -1000 mV for all excitations, as shown in Figure 5.6. The appearance of additional bands at negative potentials for all excitation wavelengths suggests that an electrochemically induced change in the 4-MPy environment at the electrode surface has occurred. Spectral changes observed at potentials more negative than -600 mV are as follows:

- (1) The  $v_1$  ring breathing mode near 1005 cm⁻¹ develops a shoulder on the higher wavenumber side with increasing negative potential and, at -900 mV, this band becomes clearly resolved into an additional band at 1019 cm⁻¹, while the original  $v_1$  band is shifted from 1005 to 998 cm⁻¹. The band at 1019 cm⁻¹ gains intensity to become more intense than the original  $v_1$  mode when the potential is -1000 mV. The ring breathing mode,  $v_{12}$ , decreases progressively in intensity relative to the  $v_1$  mode and remains unshifted with increasing negative potential.
- (2) The  $9a_1$   $\beta$ (CH) mode at 1219 cm⁻¹ shifts to 1206 cm⁻¹ at potentials near -1000 mV.
- (3) The  $v_{8a_1}$  (C-C) ring stretching mode at 1608 cm⁻¹ decreases in intensity at more negative potentials and is barely observed beyond -600 mV. The  $v_8b_2$  mode shifts from 1575 to 1569 cm⁻¹ and a weak band develops at 1585 cm⁻¹ at around -800 mV, as the original  $v_{8a_1}$  band is simultaneously shifted to lower wavenumbers.
- (4) The lower frequency region between 800-200 cm⁻¹ covers bands assigned to the  $\delta$ (C-S) and  $\upsilon$ (C-S) modes at 425 and 706 cm⁻¹, respectively. With increasing negative potentials, the latter band develops a shoulder on the higher wavenumber side which is

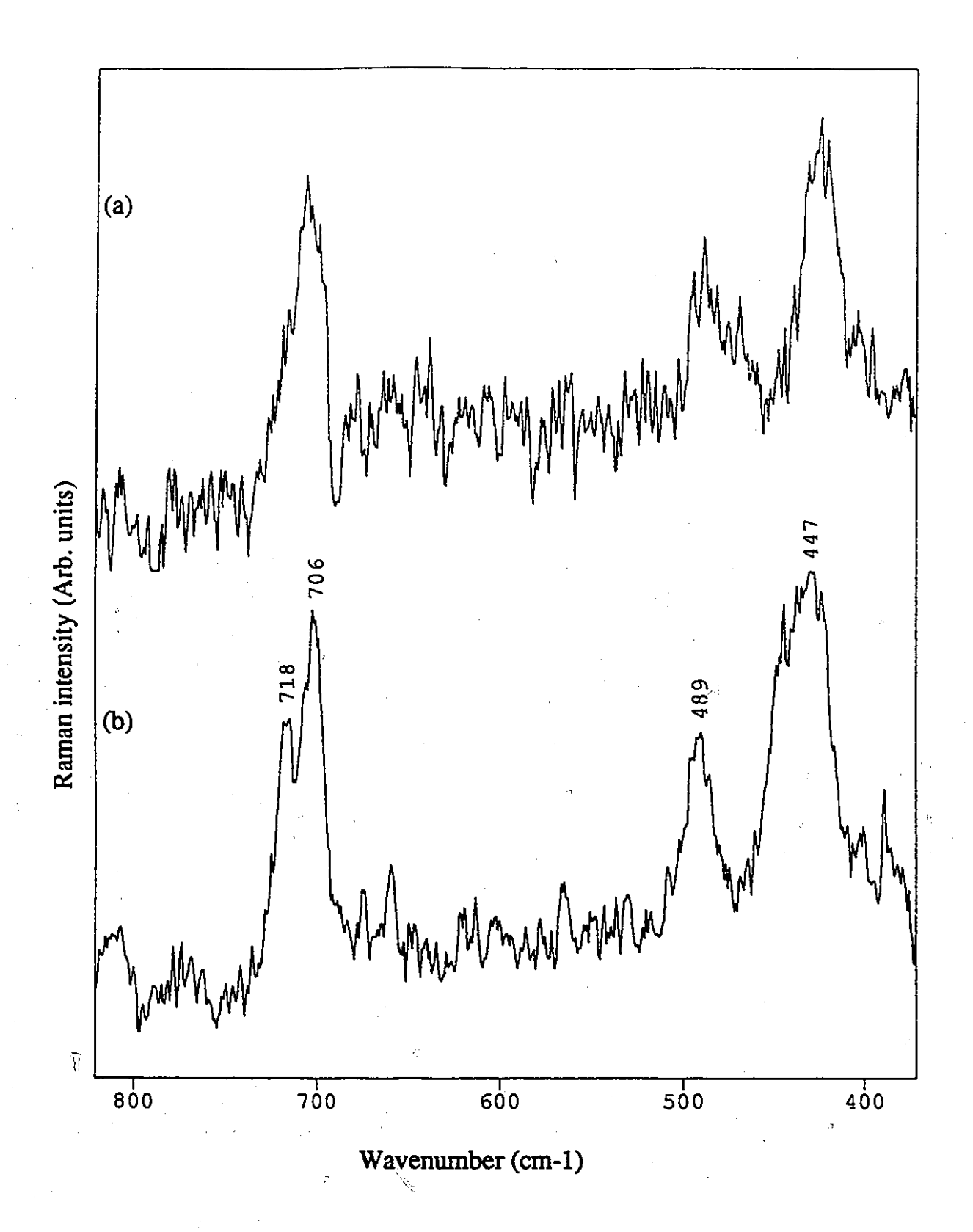


FIGURE 5.7 SERS spectra of C-S band region of adsorbed 4-MPy on Ag electrode at 0 mV (a), and -1000 mV (vs. SCE) using 514.5 nm excitation (b).

resolved at 718 cm⁻¹ and gains intensity compared to the original band at 706 cm⁻¹ near -1000 mV. The 428 cm⁻¹ band simultaneously broadens and is centered at 447 cm⁻¹ near -1000 mV. Figure 5.7 shows the spectral changes observed for both (C-S) bands at -1000 mV for 514.5 nm excitation.

No cathodic reaction was observed by CV (Figure 5.3.) in the potential range -600 to -1000 mV that could be attributed to an electrochemically reduced species produced on the Ag electrode in the SERS experiment. The spectral changes were reversible and responded quickly when the potential range was reversed from -1000 mV back to 0 V indicating that adsorbate desorption from the surface did not occur. Since the potential range was not scanned past -1000 mV, the differences attributable to changes resulting from loss of SERS active adatom sites is unlikely.³⁹ The appearance of additional 4-MPv bands, namely the  $v_1$ ,  $v_3 b_2$  and v(C-S) modes and two other bands which have shifted to 1206 and 1569 cm⁻¹, can be associated with a new surface 4-MPy species, referred to as Type II, whereas the thiolate bonded species (the only 4-MPy species observed with the potential range 0 to -600 mV) is referred to as Type I. The C-S bond modes give some insight as to the identity of this new species. The v(C-S) and  $\delta(C-S)$  modes of Type  $\mathcal{H}$  are at 718 and 447 cm⁻¹, respectively and are similar to the band positions, 721 and 431 cm⁻¹, observed for bulk 4-MPy. A possible reason for the appearance of such modes associated with Type II species lies in the stability of the Ag-thiolate bond (Type I) at higher negative potentials. As the potential is made more negative, a negatively charged thiolate sulfur maybe less stabilized on the Ag electrode surface while a thione (C=S) species (the species predominant in bulk 4 MPy), which has a weaker interaction with the electrode surface, is stabilized relative to the thiolate bonded species at these potentials. This change in adsorbate structure is manifested by the shift of C-S bands to higher energies. The spectral changes observed in this work are in contrast to those reported for 4-MPy on Au electrodes, 12 where the thiol tautomer is reported to be the preferential adsorbate at potentials more negative than -500 mV.

Other Type II bands with spectral counterparts associated with bulk 4-MPy are also observed. The  $1206 \, \mathrm{cm}^{-1}$  band, is similar in position to the  $1200 \, \mathrm{cm}^{-1}$  band assigned to the  $\delta(\mathrm{NH})/\delta(\mathrm{CH})$  mode of bulk 4-MPy. In addition, a weak band at  $1072 \, \mathrm{cm}^{-1}$  appears at  $-1000 \, \mathrm{mV}$  which has a spectral counterpart in bulk 4-MPy at  $1080 \, \mathrm{cm}^{-1}$  assigned to  $\beta(\mathrm{CH})$ . Since the potential profile is reversible within the established range it appears that the Type II species assembles on the electrode surface, in addition to the 4-MPy thiolate bonded species. Unlike self-assembly of alkylthiol monolayers on Au surfaces, aromatic thiols on polycrystalline Au form poorly defined, less compact surface coverages. Band changes such as these may arise, either from a multilayer formation (manifested by bands which have similar counterparts to bulk 4-MPy) or alternatively from a 4-MPy species which exhibits a different bonding conformation on the electrode surface, i.e., 4-MPy adsorbed via the pyridine N atom.

It appears unlikely, however, that the Type II species is associated with multilayer formation. Spectral features that support this assertion maybe associated with the Type II band at 1019 cm⁻¹ assigned to a  $\upsilon_1$  mode. This Type II  $\upsilon_1$  ring breathing band is shifted considerably to higher wavenumbers from the corresponding  $\upsilon_1$  band position in the normal unenhanced Raman spectra of bulk 4-MPy ( $\Delta\upsilon=29~{\rm cm}^{-1}$ ), silver-4-MPy complex ( $\Delta\upsilon=12~{\rm cm}^{-1}$ ) and the SERS spectra of 4-MPy adsorbed on the Ag electrode ( $\Delta\upsilon=21~{\rm cm}^{-1}$ ) within the potential range 0 to -600 mV. Pyridine vibrational modes, upon metal complexation, typically experience relatively small perturbations. However, among the changes observed on complexation is an increase of the  $\upsilon_1$  ring breathing mode frequency. Normal Raman studies of pyridine adsorbed on  $\gamma$ -alumina have identified Lewis acid-coordinated pyridine associated with a  $\upsilon_1$  mode at 1019 cm⁻¹. Similarly, pyridine chemisorbed on an Ag electrode is associated with a band at 1024 cm⁻¹. The presence of 4-MPy molecules (Type II) adsorbed on the electrode surface via the pyridine-nitrogen is thus confirmed by the appearance of a  $\upsilon_1$  mode at 1019 cm⁻¹ at higher negative potentials, whereas surface-bound 4-MPy (Type I) with an uncoordinated pyridine-

nitrogen atom has a characteristic band at 998 cm⁻¹. Previous SERS studies of pyridine reveal a preferential mode of adsorption which varies with potential, e.g., neutral pyridine adsorbs on a silver electrode surface *via* the nitrogen lone pair at potentials closer to the point of zero charge (pzc; estimated to be -700 mV vs. SCE in 0.1M KCl),⁴⁵ whereas the pyridinium chloride forms the more stable adsorbate at more positive potentials.⁴⁶ The preferential adsorption through the pyridine nitrogen atom occurs at potentials similar to those for which the appearance of 4-MPy Type *II* bands is observed. The preliminary indication from this v₁ band red-shift is that the surface N-adsorbed Type *II* species binds more strongly (Lewis acid) to the electrode surface at very negative potentials than do the thiolate-adsorbed 4-MPy molecules which are stabilized at more positive potentials. The effect is remimiscent of coordination of N by a Lewis acid.

## 5.4.3 Wavelength and Potential Dependence of 4-MPy

To evaluate the possible contribution of a CT process to the potential dependent band enhancement profile of adsorbed 4-MPy, the relative band intensities are plotted as a function of applied potential and excitation wavelength (488, 514.5, 633.47 and 651.5 nm). The relative intensity ratio of the ring breathing modes,  $Iv_1/Iv_{12}$ , increases with increasing negative potential for all wavelengths; however, the  $v_1$  band is more wavelength dependent. The intensity-potential profile for the  $v_1$  band at 488, 514.5 and 633 nm wavelengths is shown in Figure 5.8. The band intensities are normalized to the maximum value observed in the investigated potential range for each excitation wavelength. The plot displays a shift in the peak intensity maximum to more negative potentials as the excitation energy is decreased, in agreement with the trends reported for metal-to-adsorbate CT excitation for pyridine adsorbed on Ag electrodes.  $^{1.4.5}$  A similar CT mechanism (for  $v_2$  modes) has also been reported for  $v_2$ -aminothiophenol⁴⁷ adsorbed  $v_2$  the thiolate sulfur on Ag electrodes. This approach is based on tuning a CT excitation into and out of resonance by changing the applied potential or the excitation energy.  $^{1.4.5}$  In electrochemical

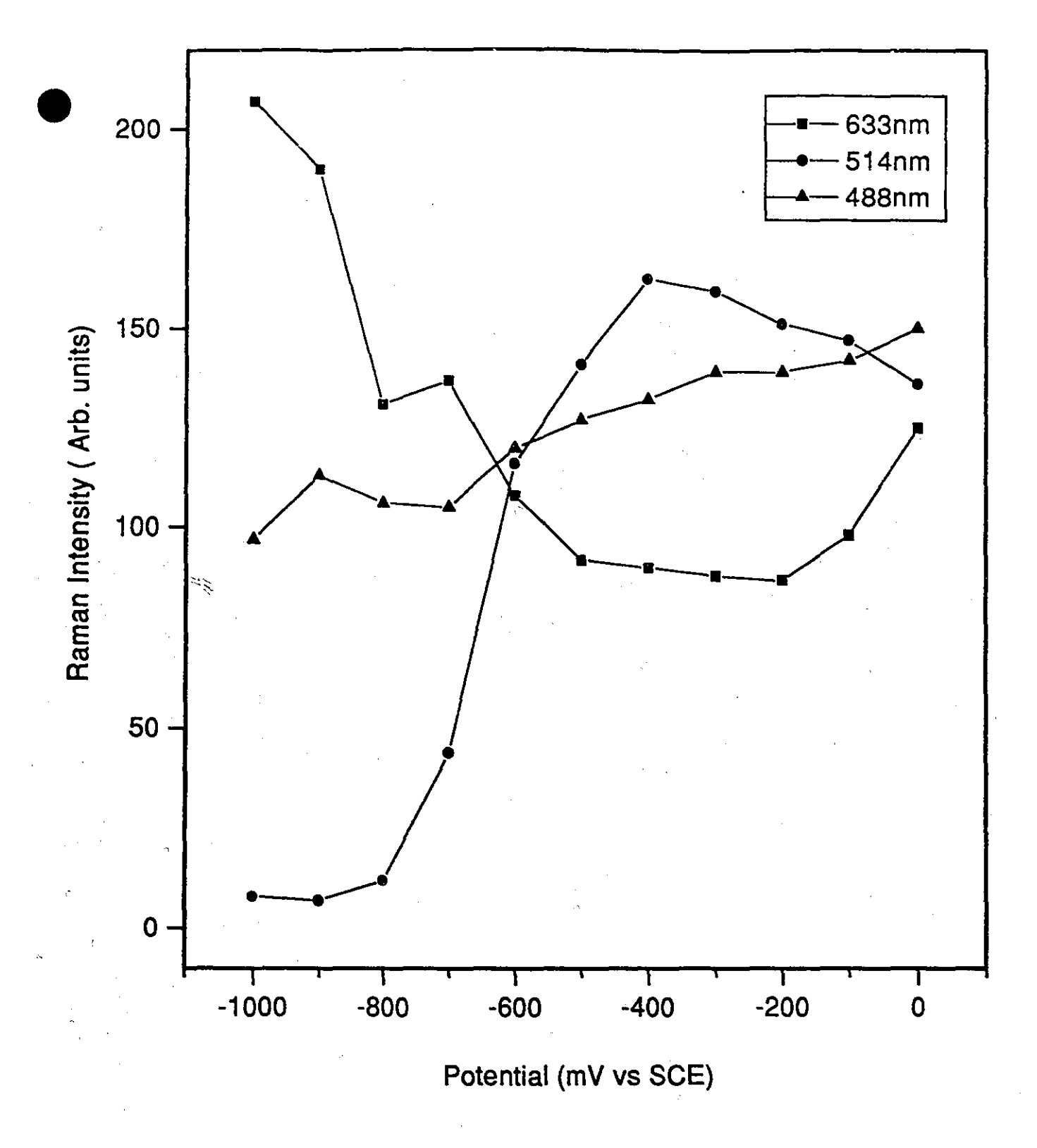


FIGURE 5.8 Normalized SERS intensities of the  $\upsilon_1$  ring breathing mode of 4-MPy for: 633.47 nm (a); 514.5 nm (b); and 488 nm excitations (c), plotted as a function of applied electrode potential (vs. SCE).

experiments, the Fermi level (Ef) of the electrode can be changed relative to electronic level of the adsorbed molecule by changing the applied potential. The SERS intensity becomes large at certain potentials where the energy gap between E_f and a molecular electronic level becomes equal to the excitation energy of the incident radiation. According to the theoretical CT model of SERS, the intensity-potential profile should be symmetric if the affinity level involved in CT is symmetric.⁴ However, the observed profile for all excitation wavelengths appears asymmetric since the I_{max} for 488 and 633.47 nm excitation seems to lie on the edge of the potential range covered. The intensity-potential profiles (Figure 5.5) for each wavelength intersect near -600 mV and, with increasing negative potential, the curve points become scattered. The appearence of the Type  $II v_1$  band near -600 mV, attributed to 4-MPy species adsorbed via the nitrogen atom, may be correlated with the asymmetry of the intensity-potential profile. The remaining a₁ or b₂ ring modes do not display CT-like intensity-potential profiles with excitation. The effect of vibronic coupling⁴⁸ in substituted pyridines, e.g., in 4-MPy where the C-S bond modes are mixed with a₁ ring modes, ⁴⁹ must be taken into account when considering the contribution of a CT mechanism to the enhancement profile. This observation is in contrast to the SERS of pyridine, where a number of a1 modes benefit from a CT mechanism and show symmetric intensity-potential profiles.⁸ We conclude that although a CT mechanism appears to contribute to the enhancement profile of 4-MPy, perturbations to this intensity-potential profile are manifested by spectral changes such as the appearence of an additional v₁ band, attributed to the Type II species.

As discussed above, the contributions of CT and EM mechanisms are known to influence the SERS intensities of adsorbates. These effects are not easily resolved from the changes in intensity brought about by reorientation. Some observations, suggest that reorientation from a perpendicular to a flat  $\pi$ -bonded conformation on the surface does not occur. A potential-dependent reorientation of the 4-MPy ring on the surface from a normal to a flat ring  $\pi$ -adsorbate interaction is not expected to yield a  $v_1$  mode shifted to higher

wavenumbers. A shift in  $v_1$  to lower energy is anticipated since bonding through  $\pi$ orbitals is expected to weaken the C=C ring bonds.⁵⁰ In addition, the out-of-plane modes
in the lower wavenumber region, which would be expected to increase in intensity for a flat
orientation, remained unchanged.

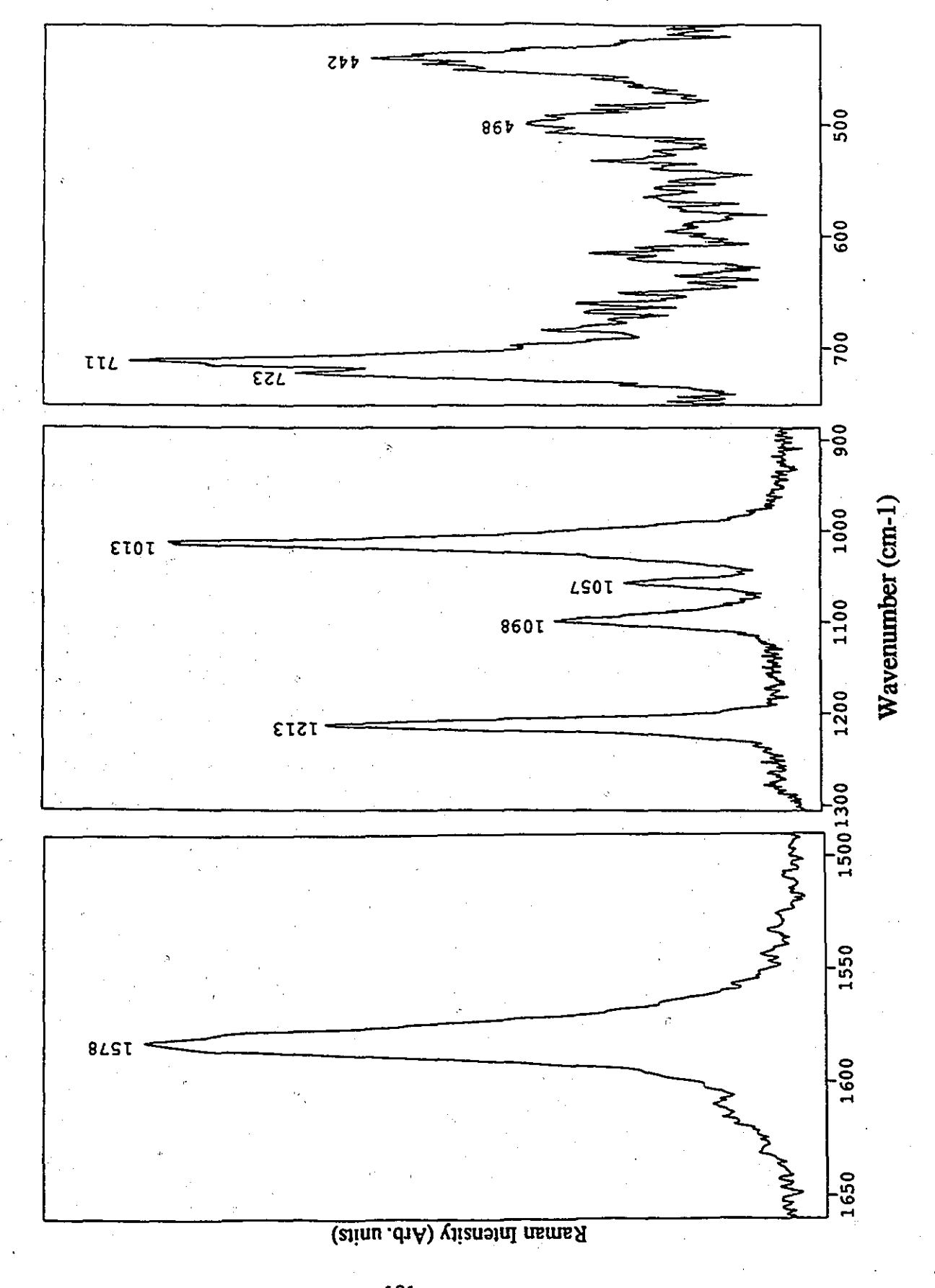
To summarize, the spectral changes observed at higher negative potentials are manifested by a change in bonding conformation at the electrode surface, namely, 4-MPy adsorbed *via* the pyridine nitrogen. The proposed "free" uncoordinated nitrogen of surface-confined 4-MPy is stabilized at more positive potentials on the electrode surface and should be available to bind probe ions such as Cu²⁺ at the solution interface at open potential. Spectral changes associated with a Cu-pyridine nitrogen interaction would be expected to have some similarities with the SERS spectra of 4-MPy observed at higher negative potentials where a Ag-pyridine nitrogen interaction occurs.

# 5.4.4. Immersion of a 4-MPy-Modified Ag Electrode in Aqueous Cu(NO₃)₂ Solution

Following the potential- and wavelength-dependent experiments, another ORC was applied to the 4-MPy derivatized Ag electrode using 514.5 nm excitation. The spectral profile of the adsorbed 4-MPy collected at open circuit (-358 mV) was comparable to that shown in Figure 5.1 (d). A 10 mL (2 mM) solution of  $Cu(NO_3)_2$  was then introduced into the electrochemical cell containing 0.1M KCl after which the open potential was changed to +81 mV. The SERS spectrum collected 5 min after addition of  $Cu(NO_3)_2$  is shown in Figure 5.9. The most dramatic intensity changes are observed for the ring breathing modes,  $v_1$  and  $v_{12}$ , and the  $\beta(CH)/\delta(NH)$  band at 1213 cm⁻¹ as compared to the SERS spectrum of 4-MPy in the absence of  $Cu^{2+}$  (at a similar potential). The relative intensity ratios for  $Iv_1/Iv_{12}$  and  $Iv_1/I\beta(CH)/\delta(NH)$  decrease from 2.8 to 0.67 and from 1.95 to 1.3, respectively, after  $Cu^{2+}$  ion addition. The spectral changes observed upon  $Cu^{2+}$  addition (see Table 4.1) are similar to those observed for Type II species in the potential

FIGURE 5.9 SERS spectrum of adsorbed 4-MPy on Ag electrode at open potential after the addition of 10 mL (2 mM) Cu(NO₃)₂ solution to the electrolyte solution.





range -700 to -1000 mV in the absence of  $Cu^{2+}$  i.e., where the Ag-pyridine nitrogen interaction occurs at the electrode surface. Other spectral changes noted were: a  $v_1$  shift to higher energy (1013 cm⁻¹), the absence of the  $v_8a_1$  band, an additional  $\beta(CC)/v(C-S)$  band at 723 cm⁻¹, and a  $\delta(C-S)/\gamma(CCC)$  band shift to higher frequency (442 cm⁻¹). By analogy to the spectral interpretation presented for 4-MPy Type II species, the spectral changes observed upon  $Cu^{2+}$  addition, which have similar spectral counterparts to the Type II bands, can be associated with a metal-pyridine nitrogen interaction. The  $v_1$  band shift (1003 to 1013 cm⁻¹) is similar to the  $v_1$  band shift reported for pyridine adsorbed on an Ag electrode (1007 to 1012 cm⁻¹) after submonolayer underpotential deposition of  $Cu^{2+}$  ions (-700 mV  $v_S$ . SCE and 0.1M NaCl electrolyte). Only low copper concentrations (submonolayer coverage) deposited on the electrode surface exhibit a Cu-pyridine nitrogen interaction, which retains SERS activity using 514.5 nm excitation. In our study, SERS activity was retained in the presence of  $Cu^{2+}$  ions at open potential.

For both  $\upsilon(\text{C-S})$  bands at 711 and 723 cm⁻¹, the former is associated with 4-MPy adsorbed to the electrode surface via the thiolate sulfur (compared to 706 cm⁻¹ in the absence of Cu²⁺) while the latter band is attributable to a Cu-4-MPy complex, which has a weaker Ag-sulfur electrode interaction. Perturbation of the Ag-sulfur interaction is also accompanied by the  $\upsilon_{12}$  band intensity decrease. The  $\upsilon_{12}$  band, similar to that for benzenethiol, is mixed with a  $\upsilon(\text{C-S})$  mode (see Table 4.1). The intensity increase displayed by  $\beta(\text{CH})/\delta(\text{NH})$  band, together with the shift in  $\upsilon_1$ , suggest that the perturbation experienced by the delocalized  $\pi$ -electrons of the ring is accompanied by a change in the pyridine nitrogen environment. The intensity changes are unlikely to result from a change in orientation on the surface as the out-of-plane modes remain unenhanced and the  $\upsilon_8 \upsilon_2$  band intensity is enhanced after Cu²⁺ addition (as is also observed for Type II species).

Spectral changes observed with Cu²⁺ addition, namely changes to bands in the 1650-1000 cm⁻¹ region, are comparable to the IOEW-SERS study of 4-MPy after

immersion in Cu²⁺ ion solution, discussed in Chapter 4. Bands associated with (C-S) modes in the lower frequency region were obscured by scattering from the waveguide interface in the IOEW-SERS spectrum. Thus, SERS from 4-MPy modified Ag electrode can provide complementary information with respect to the sulfur-Ag interaction.

On the basis of SERS data alone, the structure of the surface  $Cu^{2+}$ -complex cannot be discerned. Few systematic changes have been observed for the vibrational fundamentals of pyridine (upon metal complexation) associated with changes in complex stoichiometry, stereochemistry, or valency of the complexing metal.^{42,52} The unenhanced FT-Raman spectra of  $Cu(Py)_n(NO_3)_2$  complexes (n = 2, 4, 6) are very similar⁵³ and the SERS spectra of pyridine adsorbed at various copper interfaces show only slight differences.⁵⁴

A progressive loss in SERS activity was observed upon exposure to Cu²⁺ ions at open potential and, after 25 min, the SERS spectrum was not observed. Although the underpotential deposition (UPD) of Cu on Ag electrodes does not occur at open potential (+81 mV),⁵¹ it is possible that quenching of SERS activity may arise from Cu²⁺ ions which penetrate through the 4-MPy layer to the electrode surface. A non-compact coverage of 4-MPy on the electrode surface would allow for ion penetration destroying SERS-active sites and/or changing the optical/electronic properties responsible for the SERS activity. These effects have been correlated for UPD of foreign metals on SERS-active electrodes.^{55,56} Alternatively, changes in the surface adsorbate coverage on Cu²⁺-modified Ag electrodes may contribute to the SERS quenching. An ORC was applied in the range +200 to -200 mV in an attempt to regenerate the SERS spectrum. In addition to the UPD of copper on the electrode surface, the same SERS spectrum was recovered, but at ca. 10% of the initial SERS intensity.

3

#### 5.5 CONCLUSIONS

The SERS of 4-MPy adsorbed on an Ag electrode has been examined as a function of potential (-1000 to 0 mV vs.SCE) and laser excitation using 488, 514.5, 633.47 and 651.5 nm wavelengths. The spectral profiles of the SERS spectra in the potential range 0 to -500 mV are similar to those of other SERS spectra reported for 4-MPy on a variety of metal substrates. Analysis of the spectral features reveals that 4-MPy adsorbs on the Ag electrode through the thiolate sulfur with the ring plane perpendicular to the surface (Type I). With increasing negative potentials (E > -600 mV), additional bands associated with  $v_1$ ring breathing and v(C-S) modes appear. The former band is shifted to higher and the latter to lower energies relative to the band positions observed at more positive potentials. These changes suggest that a new 4-MPy species (Type II) is adsorbed on the electrode surface, in addition to the 4-MPy species adsorbed via the sulfur atom. This Type II species is assigned to 4-MPy which is adsorbed via the pyridine nitrogen. Spectral changes similar to those observed for Type II species were noted when the 4-MPyderivatized electrode was exposed to a Cu²⁺ ion solution at open potential. In this case, 4-MPy remains adsorbed on the electrode via the sulfur atom and the "free" uncoordinated pyridine nitrogen is available to interact with the Cu²⁺ probe ions. The spectral changes associated with Cu2+ exposure are manifested by a metal-pyridine interaction and are similar to the spectral shifts observed for pyridine adsorbed on Ag electrodes with submonolayer Cu coverages.

Potential-dependent band intensity changes were observed and, to evaluate the possible contribution of a CT process to the band enhancement profile of 4-MPy, the relative band intensities were plotted as a function of applied potential and excitation wavelength. The wavelength-dependent, intensity-potential curves are similar to the CT profile previously observed for pyridine on metal electrodes.

#### REFERENCES

- (1) Otto, A.; Mrozek, I.; Grabhorn, H.; Akeman, W. Phys. Rev. Lett. 1992, 43, 147.
- (2) Moskovits, M. Review. Mod. Phys. 1985, 57, 783.
- (3) Chang, R. K.; Furtak, T. E. Surface Enhanced Raman Scattering; Plenum Press: New York, 1982.
- (4) Lombardi, J. R.; Birle, R. L.; Lu, T.; Xu, J. J. Phys. Chem. 1986, 84, 4174.
- (5) Furtak, T. E.; Roy, D. Phys. Rev. Lett. 1983, 50, 1301.
- (6) Furtak, T. E.; Roy, D. Surf. Sci. 1985, 158, 126.
- (7) Lombardi, J. R.; Birke, R. L.; Snachez, L. A.; Bernard, I.; S., S. Chem. Phys. Lett. 1984, 104, 240.
- (8) creighton, J. A. Surf. Sci. 1986, 173, 665.
- (9) Bunding, K. A.; Bell, M. I. Surf. Sci. 1983, 118, 329.
- (10) Busby, C. C. Surf. Sci 1984, 140, 294.
- (11) Gale, R. J. Spectroelectrochemistry: Theory and Practice; Plenum: New York, 1988.
- (12) Taniguichi, I.; Iseki, M.; Yamaguchi, H.; Yasukouchi, K. J. Electroanal. Chem 1985, 186, 299.
- (13) Brolo, A. G.; Temperini, M. L. A. in *Proceedings of the XVII International Conference on Raman Spectroscopy*; Wurzberg, Germany, Eds.; Keifer, W.; Cardona, M.; Schaack, G.; Scheider, F. W.; Schotter, H. W.; Wiley: 1992.
- (14) Sabatani, E.; Cohen-Boulakia, J.; Bruening, M.; Rubeinstein, I. Langmuir 1993, 9, 2974.
- (15) Joo, H. T.; Kim, M. S.; Kim, K. J. Raman Spectrosc. 1987, 18, 57.
- (16) Garrell, R. L.; Szafranski, C.; Tanner, W. SPIE Proceedings: Raman and Luminescence Spectrosc. in Tech. 1990, 1336, 264.
- (17) Carron, K.; Hurley, L. G. J. Phys. Chem. 1991, 95, 9979.
- (18) Joo, T. H.; Yim, Y. H.; Kim, K.; Kim, M. S. J. Phys. Chem. 1989, 93, 1422.
- (19) Swalen, J. O.; Allara, D. L.; Andrade, J. B.; Chandross, E. A.; Garoff, S.; Israelachvilli, J.; Mc Carthy, T. J.; Murray, R.; Pease, R. F.; Rabolt, J. F.; Wymnne, K. L.; Yu, H. Langmuir 1987, 3, 932.
- (20) Jones, T. A.; Perez, G. P.; Johnson, B. J.; Crooks, R. M. Langmuir 1995, 11, 1318.
- (21) Chadwick, J. E.; Myles, D. C.; Garrell, R. L. J. Am. Chem. Soc. 1993, 115, 10364.
- (22) Bryant, M. A.; Joa, S. L.; Pemberton, J. E. Langmuir 1992, 8, 753.

- (23) Gui, J. Y.; Lu, F.; Stern, D. A.; Hubbard, A. T. J. Electroanal. Chem. 1990, 292, 245.
- (24) Xu, H.; Tseng, C. H.; Vickers, T. J.; Mann, C. K.; Schelenoff, J. B. Surf. Sci. 1994, 311, L707.
- (25) Baldwin, J. A.; Schühler, N.; Andrews, M. A.; Butler, I. S. Manuscript in preparation.
- (26) Irish, D. E.; Guzonas, D. A.; Atkinson, G. F. Surf. Sci. 1985, 158, 314.
- (27) Cermakova, K.; Sestak, O.; Matejka, P.; Baumruk, V.; Vlckova, B. Collect. Czech. Chem. Commun. 1993, 58, 2682.
- (28) Spinner, E. J. Chem. Soc. 1963, 3860.
- (29) Green, J. H. S.; Kynaston, W.; Paisley, H. M. Spectrochim. Acta 1963, 19, 549.
- (30) Lautie, A.; Hervieu, J.; Beloc, J. Spectrochim. Acta 1983, 39A, 367.
- (31) Dollish, F. R.; Fateley, W. G.; Bentley, F. F. Characteristic Raman Frequencies of Organic Compounds; Wiley: New York, 1974.
- (32) Cotton, T. M.; Vavra, M. Chem. Phys. Lett. 1984, 106, 491.
- (33) Cotton, T. M.; Dwarakannath, K.; Iorga, D. J. Am. Chem. Soc. 1983, 105, 7462.
- (34) Moskovits, M.; Suh, J. S. J. Phys. Chem. 1984, 88, 5526.
- (35) Creighton, J. A. in *Spectroscopy of Surfaces*; Clark, R. J. H.; Hester, R. E., Eds.; Wiley: New York, 1988; Vol. 16, Ch. 2, p37
- (36) Stoyanov, S.; Petkov, I.; Antonov, L.; Stoyanova, T.; Karagiannidis, P.; Aslanidis, P. Can. J. Chem. 1989, 68, 1482.
- (37) Beak, P.; Fry, F. S.; Lee, J. J.; Steele, F. J. Am. Chem. Soc. 1976, 98, 171.
- (38) Kennedy, B. P.; Lever, A. B. P. Can. J. Chem. 1972, 50, 3489.
- (39) Owen, J. F.; Chen, T. T.; Chang, R. K. Surf. Sci. 1983, 131, 195.
- (40) Thornton, D. A. Coord. Chem. Rev. 1990, 104, 251.
- (41) Akyuz, S.; Dempster, B.; Morehouse, R. L.; Suzuchi, S. J. Mol. Struct. 1973, 17, 105.
- (42) Akyuz, S.; Davies, J. E. D.; Holmes, K. T. J. Mol. Struct. 1977, 42, 59.
- (43) Hendra, P. J.; Horder, J. R.; Loader, E. J. J. Chem. Soc. A 1971, 1766.
- (44) Fleischmann, M.; Hill, I. R. J. Electroanal. Chem. 1983, 146, 353.
- (45) Perkin, R. S.; Andersen, T. N. Mod. Aspects Electrochem. 1969, 2, 203.
- (46) Sun, S. C.; Bernard, I.; Birke, R. L.; Lombardi, J. R. J. Electroanal. Chem. 1985, 196, 359.
- (47) Osawa, M.; Matsuda, N.; Yoshii, K.; Uchida, I. J. Phys. Chem. 1994, 98, 12707.

- (48) Kobayashi, M.; Imai, M. Surf. Sci. 1985, 158, 275.
- (49) Lin-Vien, D.; Colthrop, N. B.; Fateley, W. G.; Grasselli, J. G. Handbook of Characteristic Infrared and Raman Frequencies of Inorganic Compounds; Academic Press: San Diego, 1991.
- (50) Moskovits, M.; DiLella, D. P.; Maynard, K. J. Langmuir 1988, 4, 67.
- (51) Moerl, L.; Pettinger, B. Solid State Commun. 1982, 43, 315.
- (52) Gill, N. S.; Nuttal, R. H.; Scraife, D. E.; Sharp, D. W. A. J. Inorg. Nucl. Chem. 1961, 18, 79.
- (53) Baldwin, J. A. Unpublished results.
- (54) Rubim, J. C.; Gutz, G. R.; Sala, O. Chem. Phys. Lett. 1984, 111, 117.
- (55) Guy, A. L.; Pemberton, J. E. Langmuir 1987, 125.
- (56) Gao, Y.; Lopez-Rios, T. J. Phys. Chem. 1987, 87, 2327.

CHAPTER 6

SUMMARY

#### 6.1 CONCLUSIONS

The research undertaken in this thesis describes the surface enhanced Raman spectroscopic analysis of pyrazinamide, 2- and 4- mercaptopyridine. A variety of SERS substrates were used to study these adsorbates, namely, silver colloidal sols, silver metal liquid-like films (MELLFs), and roughened silver electrodes. In addition to these more classical methods, a novel SERS technique was developed which combines both waveguide Raman spectroscopy (WRS) and SERS, known as Integrated Optics, Evanescent Wave, Surface Enhanced Raman Scattering (IOEW-SERS). The potential application of surface-confined 4-mercaptopyridine as a chemical sensor was demonstrated using IOEW-SERS.

Chapter 2 described the preparation of interfacial Ag colloid-adsorbate films between an aqueous Ag colloid and a solution of an adsorbate in dichloromethane. The internal structures of the resulting films were substantially influenced by the chemical nature of the adsorbate. Pyrazinamide (pza) and 2-mercaptopyridine (2-MPy) formed lustrous metallic interfacial films under the conditions routinely used for the preparation of Ag colloid-adsorbate interfacial films. On the other hand, 4-mercaptopyridine (4-MPy) is the only adsorbate for which an interphase transfer of adsorbate-covered particles from the aqueous to the organic phase, forming an organosol, was observed. This particular chemical specificity of 4-MPy was attributed to the sterically unhindered position of the para -substituted pyridine nitrogen resulting in 3-D polymer-like, colloid-adsorbate aggregates. By comparison, 2-MPy provides 2-D monolayers of colloid-adsorbate interfacial films. TEM photographs of deposited films show 3-D clusters from the Ag colloid-4-MPy organosol sample and a 2-D monolayer from the Ag colloid-2-MPy interfacial film sample. Furthermore, we showed that for a particular adsorbate, the process of film formation (e.g., rate of interphase transfer) as well as the microstructure of the film is substantially influenced by the Ag content of the parent Ag colloid. In the case of Ag-pza film, the difference between the Ag content of Ag colloid I and II leads to distinctly different structures of the resulting films. The Ag-pza I films form continuous layer(s) of pza covered particles, while the Ag-pza II film shows an SPA similar to a fractal-like system. Spectral changes observed for the SERS spectra of Ag-pza I and II films suggest that the pza molecules assume flat and perpendicular orientations, respectively. Similarly, upon deposition the Ag-4-MPy I organosol aggregates readily assemble into a continuous film, while the compact 3-D Ag-4-MPy II aggregates remain unperturbed. The SERS spectrum of the Ag-4-MPy II sample is comparable to a monolayer of 4-MPy chemisorbed via thiolate moiety, whereas additional bands observed in the SERS spectrum of Ag-4-MPy I organosol are attributed to a bidentate coordination complex (using both S and N atoms) of 4-MPy. In the case of 2-MPy, no aggregation occurred with Ag colloid II. The Ag particle:adsorbate concentration ratio was thus varied by altering the adsorbate concentration. The SERS spectra show that for high adsorbate concentration, the 2-MPy molecules are packed perpendicular to the surface while at low concentration the molecules lie flat.

Chapter 3 describes the fabrication of a waveguide heterostructure on nano-scale dimensions by grafting silver colloid particles onto thin glass slides using a molecular adhesive, 3-MPT. This assembly combines the unique optical properties of both SERS and WRS systems by allowing optically guided light to propagate into the thin colloid film as an evanescent wave. An IOEW- SERS spectrum of 4,4'-bipyridine adsorbed on the colloidal superstrate surface demonstrates the SERS-activity of this waveguide, even though nearly 98% of the incident field is within the waveguide itself. In addition, spectral bands associated with the adsorbate layer are enhanced considerably compared to spectral features from the waveguide interface. The IOEW-SERS spectrum of 4,4'-bipyridine was shown to be comparable to the SERS spectrum of 4,4'-bipyridine colloidal sol. To

demonstrate the efficiency of optically guiding the light into the waveguide, a classical 90^o scattering geometry resulted in carbonization of the waveguide surface.

The IOEW-SERS of 2- and 4-MPy have been compared with other SERS substrates such as MELLFs and Ag colloidal sols in Chapter 4. It was concluded from the analysis of relative intensity changes and frequency shifts that 2- and 4-MPy adsorb onto the colloidal surface through the thiolate sulfur in which the pyridine ring plane has an orientation perpendicular to the surface. The "free" uncoordinated pyridine nitrogen of surface-confined 4-MPy was used as a sensing layer and exposed to H+ and Cu²⁺ probe ions. Perturbations to the vibrational structure of 4-MPy indicated that quarternization with protons was reversible, whereas Cu²⁺ was bound irreversibly. X-ray photoelectron spectroscopy provided insight into the layer-by layer assembly of the waveguide heterostructure, from the substrate to the Cu²⁺ ion. The XPS data showed surface-confined 4-MPy had two nitrogen environments, attributed to both physisorbed and chemisorbed species. Both N 1s peaks shifted to lower binding energies upon exposure to Cu²⁺ which adds further support to the interpretation of the IOEW-SERS data.

In Chapter 5, the SERS of 4-MPy adsorbed onto an Ag electrode was collected as a function of potential (-1000 to 0 mV vs.SCE) and laser excitation using 488, 514.5, 633.47 and 651.5 nm wavelengths. With increasing negative potentials (E < -600 mV), additional bands appear, namely bands associated with the ring breathing and C-S bond modes of 4-MPy. These changes were attributed to a new 4-MPy species (Type II) adsorbed via the pyridine nitrogen on the electrode surface. This species is stabilized relative to the thiolate bonded species (Type I) at higher negative potentials. Spectral changes similar to those observed for Type II species were noted when the 4-MPy derivatized electrode was exposed to a Cu²⁺ ion solution at open potential. In this case, 4-MPy remained adsorbed on the electrode via the sulfur atom and the "free" uncoordinated

pyridine nitrogen was available to interact with the  $Cu^{2+}$  probe ions. Spectral changes observed for the  $\upsilon_1$  and  $\upsilon_{12}$  ring breathing modes on  $Cu^{2+}$  exposure had similar spectral counterparts observed for the IOEW-SERS study of 4-MPy with  $Cu^{2+}$  exposure providing further evidence of a Cu-pyridine nitrogen interaction on the waveguide substrate.

#### 6.2 CONTRIBUTIONS TO ORIGINAL KNOWLEDGE

- (1) The rate of formation, adsorbate orientation and the macrostructure of interfacial Ag colloid-adsorbate films (MELLFs) formed between an aqueous Ag colloid and a solution of an adsorbate in dichloromethane were shown to be substantially influenced by the chemical nature of the adsorbate and the Ag content of the parent colloidal sol. Ambidentate ligands such as pyrazinamide, and 2- and 4-mercaptopyridine were used in this thesis study and were shown to influence the above processes.
- (2) The work described in this thesis demonstrates a novel technique for combining waveguide Raman spectroscopy (WRS) and surface enhanced Raman scattering (SERS), i.e., Integrated Optics, Evanescent Wave, Surface Enhanced Raman Spectroscopy, (IOEW-SERS). The fabrication of a heterogenous waveguide assembly by grafting silver colloidal particles onto a glass waveguide was described. The propagation of optically guided light which can propagate into the colloidal layer as an evanescent wave and couple with the surface plasmon modes was shown to support conditions necessary for SERS. The IOEW-SERS spectra from the waveguide interfacial structure and from an adsorbed layer of 4,4'-bipyridine were measured.
- (3) The IOEW-SERS of 4-mercaptopyridine (4-MPy) was shown to be coextensive with other SERS techniques studied in this work i.e., silver colloidal sols, MELLFs and roughened silver electrodes. A comparative study of all the SERS substrates using 4-MPy was undertaken where relative intensities and band shifts associated with surface-confined 4-MPy were shown to be similar. Analysis of the spectral profile confirmed that 4-MPy is adsorbed *via* the thiolate sulfur with the plane of pyridine ring being perpendicular to the silver surface.

- (4) The surface-confined 4-MPy layer was shown to have the ability to behave as a proton and copper-ion sensor by IOEW-SERS. A layer-by-layer interrogation of the waveguide heterostructure using XPS provided complementary evidence regarding the interfacial structure of the waveguide and the Cu-4-MPy interaction *via* the pyridine nitrogen moiety.
- (5) The potential and wavelength dependence of the SERS of 4-MPy using roughened silver electrodes was demonstrated for the first time. The ambidentate properties of 4-MPy were exploited and the spectral changes observed with changes in surface potential were attributed to both thiolate- and nitrogen-bonded surface-confined 4-MPy species. In a manner similar to the IOEW-SERS study, exposure to Cu²⁺ probe ions produced spectral changes consistent with a Cu-nitrogen interaction.

#### 6.3 SUGGESTIONS FOR FUTURE WORK.

**(1)** The persistence of the SERS effect using near infrared (NIR) excitation has been clearly demonstrated for gold substrates. 1,2 The wavelength and potential dependence of SERS extends to the NIR region even though classic cross sections for Raman scattering would predict a decrease in going from visible to near infrared the actual intensities increase. The extension of WRS into the FT-Raman regime using NIR (1.064 µm) excitation requires the same waveguiding requirements such as prisms, substrates and coupling optics and refractive indexes conditions.³ There are, however, two experimental problems using NIR which can be overcome. The first involves using invisible radiation at 1.064 µm which can be coupled in the waveguide using the red line of a He:Ne laser colinear with the Nd:YAG beam. When coupling is complete the He:Ne can be turned off, leaving the Nd:YAG as the propagating beam in the waveguide. Secondly, the geometrical mismatch of the waveguide streak and the circular entrance aperture of the FT-IR can compensated for by using a fiber optic for collection that has a line geometrical arrangement on one end that can be used for collecting the scattered light from the streak and a circular arrangement at the other end for alignment with the FT-IR aperture.

Since the above aspects demonstrate that both WRS and SERS are accessible to NIR excitation, the IOEW-SERS substrate can also be adapted for NIR excitation by using a Au colloid derivatized waveguide. The benefits of operating at this wavelength include minimization of photochemical effects such as fluorescence and the lack of thermal heating. The IOEW-SERS experiment using visible excitation suffers periodically from an apparent background fluorescence in the higher energy regions 2000-4000 cm⁻¹. Although the SERS effect is known to quench fluorescence, this background could evolve from the glass\siloxane layers of the waveguide. Fluorescence from bonded phase materials e.g., siloxane/silica have been reported previously.³ Exposure of materials to laboratory

atmosphere is known to result in fluorescence which is thought to arise from adsorption of organic vapors and subsequent photolysis under laser irradiation.

encompass a number of substrates besides glass. Colloid films grafted to indium tin oxide (ITO) surfaces using 3-MPT can also function as an electrode.⁴ The self assembly of redox-active monolayers onto the colloid surface e.g., alkylthiols, can be used to estimate the effectiveness of monolayers in inhibiting electrode kinetics and the extent to which surface redox reactions are suppressed can be used to evaluate the quality of the monolayer.⁵ Defects in the chemical association of the monolayer to the colloid and/or structural defects in the attachment of the colloid to the ITO surface and/or colloid particle size distribution could lead to the incomplete coverage of a monolayer detected by residual electroactivity in cyclic voltammogram experiments.

Quartz and silica based fiber optics can also avail of the self assembly process of Ag colloid particles by 3-MPT adhesive. The waveguide geometry can thus be extended from asymmetric planar slabs to cylindrical fiber optics.

(3) The topography of the Ag colloid surface of the waveguide such as the lateral distribution and sizes of metal particles can be probed by TEM, SEM, AFM and STM techniques. For all of these techniques except TEM, the Ag colloid derivatized waveguide substrate does not require any modification in order to be probed i.e., substrate is electrically conducting. Surfaces for TEM analysis are usually placed on carbon covered copper or copper grids. In order to retain the original integrity of the glass/3-MPT/Ag colloid assembly for TEM analysis, this multilayer arrangement can be assembled on SiO covered copper grids (Ernest F. Fullam, Inc.).

- (5) The XPS analysis of the derivatized waveguide in Chapter 5 requires references for the S 2p and N 1s regions of free (uncoordinated) 4-MPy. The references can be acquired by spin coating a layer of 4-MPy from solvent onto a silicon wafer. These results can be used to identify the contributions from free 4-MPy and from 4-MPy adsorbed onto the colloid surface. The same procedure can be applied to Cu(NO₃)₂ to clarify the shift associated to copper binding on the 4-MPy layer.
- (6) A study can be done to investigate the optical effect and IOEW-SERS of the incident beam polarization (TE vs. TM) in the waveguide. Perturbations to the optical behaviour of the waveguide may arise from changes to the radiative dielectric constant.
- (7) The waveguide can be heterogenized by grafting 3-MPT to the colloid surface of the waveguide. The terminal thiol group of 3-MPT will react with colloidal particles leaving the methoxy groups available for subsequent hydrolysis and condensation reaction. This glass layer can then be reacted with R-Si(Cl)₃, exposing the terminal R group allowing for a chemically modified surface.

## REFERENCES

- (1) Chase, B.; Parkinson, P. J. Phys. Chem. 1991, 95, 7810.
- (2) Ingram, J. C.; Pemberton, J. E. Langmuir 1992, 8, 2034.
- (3) Chase, D. B.; Rabolt, J. F. Fourier Transform Raman Spectroscopy: From Concept to Experiment, Academic Press: New York, 1994.
- (4) Doron, A.; Katz, E.; Willner, I. Langmuir 1995, 11, 1313.
- (5) Sabatani, E.; Cohen-Boulakia, J.; Bruening, M.; Rubeinstein, I. *Langmuir* 1993, 9, 2974 and refs. therein.